UNIVERSITÄTSKLINIKUM HAMBURG-EPPENDORF

Klinik und Poliklinik für Neurologie

Klinikdirektor: Prof. Dr. Christian Gerloff

Analysis of brain-derived extracellular vesicles in steady-state conditions and after ischemic stroke

Dissertation

zur Erlangung des Doktorgrades Dr. rer. biol. hum. / PhD
an der Medizinischen Fakultät der Universität Hamburg.

vorgelegt von:

Santra Brenna
aus Como, Italien

Hamburg 2021

Angenommen von der
Medizinischen Fakultät der Universität Hamburg am: 05.09.2022

Veröffentlicht mit Genehmigung der
Medizinischen Fakultät der Universität Hamburg.

Prüfungsausschuss, der/die Vorsitzende: PD Dr. Berta Puig-Martorell

Prüfungsausschuss, zweite/r Gutachter/in: Prof. Dr. Markus Glatzel

1. Synopsis

1.1 Introduction

Extracellular vesicles (EVs) are double-membrane structures released from possibly all types of cells. In the past years, a wide variety of subgroups of EVs have been identified and classified, based on their cellular biogenesis, size, cellular source, or function (1). EVs range in diameter from 50 nm to 5 µm and they can carry a cargo composed of lipids, metabolites, nucleic acids, and proteins (1-3).

For several decades, EVs have been successfully isolated from cell culture media and body fluids (e.g., CSF, blood, urine)(4, 5) and, only recently, protocols to isolate EVs from tissue have been published (6-8).

EVs are involved in several biological processes, both physiological and pathological, such as angiogenesis, the transfer of genetic material into recipient cells, the activation of immune cells, inflammation, and cancer invasion (9-13).

This introduction intends to give a detailed overview of EVs' biogenesis, characteristics, cargo content, and their involvement in physiological and pathological processes in the central nervous system (CNS), specifically in ischemic stroke. The pathophysiology of ischemic stroke will be analyzed, together with the contribution of EVs and the prion protein (PrP). The mentioned topics (EVs, ischemic stroke, and PrP) are fundamental to understand the results and data of the papers that contributed to this thesis.

1.1.1 EVs: background

In 1946, Chargaff and West observed that after ultracentrifugation plasma was losing its capacity to coagulate, deducing that there was a factor in the resulting pellet that was necessary for this process (14). Later in 1967, Wolf *et al.* reported minute lipid particles with "platelet-like" activity recovered after ultracentrifugation from serum and plasma (15). The lipidic material was first referred to as "platelet dust", and later as "microparticles". In 1971 the term "extracellular vesicles" was first used by Aaronson and colleagues to describe the different-sized secreted membranous structures they observed with electron microscopy in the golden alga, *Ochronomas Danica* (16).

In 1981, Trams and colleagues proposed the term "exosomes" to describe shed vesicles isolated from conditioned media of glioblastoma cell lines. These vesicles had a particular membrane composition and a function, as they were able to dephosphorylate surface constituents in the recipient cells (17). A few years later, two different labs studying the maturation of reticulocytes to erythrocytes reported in parallel that the transferrin receptor was eliminated via "exosomes", particles formed at the endocytic compartment and then released by fusion of multivesicular bodies (MVB) with the plasma membrane (18-20).

During those years, EVs were described by many names ("shedding vesicles", "microparticles", "microvesicles", "exosomes"), often even in the same manuscript. Moreover, scientists were skeptical about specific EVs functions. In fact many of them considered exosomes as mere garbage bags, produced and released by cells to eliminate old or superfluous proteins, such as during the maturation of reticulocytes to erythrocytes (21).

It was only later in 1996 that Raposo and colleagues could prove an actual active role of exosomes in a more complex biological process. They were able to show that antigen-presenting exosomes derived from B lymphocytes specifically stimulated T cells (11). Moreover, it was also shown that the co-receptors CCR5 and CXCR4 (key players in HIV infection) could be transferred via EVs released from platelets and blood peripheral monocytes from a susceptible to a refractory cell, making the latter susceptible to the infection (22, 23).

In the early 2000s, different studies reported that EVs carry genetic material that can be transferred and translated on a recipient cell (10, 24). In addition to reticulocytes, lymphocytes, and platelets, the release of exosomes was soon proved to be a mechanism employed also by mast, dendritic, intestinal epithelial, and several other cells (1, 25-27).

In the following years, the interest for EVs grew exponentially and different protocols for their isolation from conditioned media, body fluids, and, more recently, from tissue have been published (6-8). This growing attention urged for more rigorous guidelines, allowing to compare the studies. In 2011 the International Society for Extracellular Vesicles (ISEV) was founded, with the mission to increase interaction between researchers in the EVs field and with the attempt to standardize the isolation, purification, and characterization protocols, among other goals. Since then, ISEV is releasing position papers intending to update the guidelines not only for the isolation and characterization, but also for the storage, handling, and nomenclature of EVs (28).

1.1.2 EVs: nomenclature

EVs have been grouped according to size and biogenesis in **microvesicles/ectosomes** (with a size of 100-1000 nm), which are vesicles released directly from the plasma membrane and **exosomes** (with a size of 50-150 nm), released vesicles of endosomal origin. Additionally, when cells are undergoing apoptosis, they release **apoptotic EVs (ApoEVs)** (100-5000 nm), which are also shed from the plasma membrane and comprise large vesicles named "apoptotic bodies" and smaller apoptotic microvesicles (Figure 1).

Recently, a new type of particles has been observed, the **exomeres** (30-50 nm), but their function is still unclear and are not considered EVs (29, 30).

Currently, since exosomes and microvesicles have overlapping sizes, their classification only based on size is not recommended, and current protocols and markers used for their isolation and characterization cannot specifically differentiate between them. Therefore, if no specific proof of the cellular origin is available (e.g. electron microscopy pictures of the fusion of MVB with the plasma membrane releasing exosomes), the agreement is to name them "extracellular vesicles (EVs)" (28, 31), which can be further categorized by size (i.e., small EVs (≤200 nm) or medium/large EVs (≥200 nm); density (low, middle, high); composition (presence/absence of markers such as CD81, CD9, Annexin 5…) and origin/conditions of origin (primary neural EVs, hypoxic EVs…).
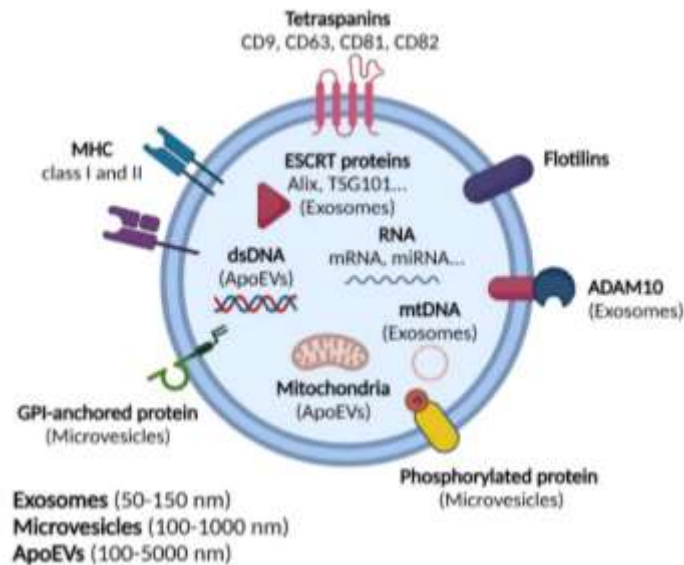
Figure 1: Schematic representation of a generic EV. EVs are double-membrane vesicles that carry proteins, nucleic acids, metabolites and lipids. In the figure are represented protein markers common for all types of EVs, such as tetraspanins, flotilin, MHC class I and II, and protein markers typical of exosomes, such as Alix, TSG101, and mature (m) ADAM10. Phosphorylated proteins and GPI-anchored proteins are enriched in microvesicles but present in all EVs. EVs can carry RNA (mRNA, miRNA, lncRNA…). Exosomes have been shown to carry mtDNA and ApoEVs to carry dsDNA and mitochondria. Image created with Biorender.

1.1.3 EVs: formation and release

Generally, EVs are formed either via the endocytic pathway (exosomes) or by direct shedding at the plasma membrane (ectosomes/microvesicles) (Figure 2).

-Exosomes

Exosomes are intraluminal vesicles (ILVs) that are released to the extracellular space upon fusion of the multivesicular endosome (MVEs)/multivesicular bodies (MVBs) with the plasma membrane. Thus, they are formed at the endocytic pathway. This pathway consists of a series of dynamic membrane compartments that internalize extracellular material or cellular components from the plasma membrane directing them either to degradation or recycling.

In the first endocytic pathway step, primary vesicles budding off the plasma membrane, together with the material that has to be internalized, pinch off inside the cell, forming a primary vesicle which fuses and delivers the cargo to the early endosomes (EEs). In there, molecules that have to be degraded at the lysosome are sorted by invaginations of the endosomal membrane. These invaginations pinch off during the maturation process of the EEs to late endosomes (LE) and, once free, they are known as ILVs. The carriers of these ILVs are the MVEs which are an intermediate compartment between EEs and late endosomes (LEs) (32). Very important for the ILVs biogenesis (although not fundamental, as ESCRT-independent mechanisms have also been described) is the Endosomal Sorting Complex Required for Transport (ESCRT), a machinery composed of cytosolic proteins assembled into four complexes (ESCRT-0, ESCRT-I, ESCRT-II, and

ESCRT-III) together with associated proteins (ALIX, VPS4, VTA1)(33, 34). This process starts in specific domains of the endosomal membrane, where ubiquitin-tagged proteins are recognized by the ubiquitin-binding subunits of ESCRT-0. ESCRT-I clusters the ubiquitinated proteins and together with ESCRT-II, drives the membrane deformation that leads to the formation of the ILVs (35). ESCRT-0, -I, and -II combine with ESCRT-III, which promotes the final budding process and vesicles scission (35).

Segregation of proteins to ILVs imply that they can follow three possible pathways: (i) degradation at the lysosomes, acidic organelles containing hydrolytic enzymes that can degrade several types of biomolecules (36), (ii) back-fusion with the endosome, or (iii) fusion of the endosomes with the plasma membrane and release of the vesicles, now renamed as "exosomes", into the extracellular space (37). The mechanisms involved in the selection of the pathways are currently unknown (32). During their biogenesis, there is selective incorporation of proteins into the membrane of the exosomes together with cytosolic components. However, the mechanisms responsible for this sorting are still unknown. Exosomes also carry proteins that are involved in their biogenesis, such as the ESCRT accessory protein ALIX and TSG101, which is part of the ESCRT-I complex. Both have been found to play a key role in the biogenesis of exosomes, as silencing them either decreases the number of released exosomes or modifies their cargo (38). It has been also shown that ALIX binds syntenin, a soluble multifunctional adapter protein, facilitating ILVs formation, in a partially ESCRT-independent fashion (39). Other ESCRT proteins found to affect the release of exosomes are STAM1 and Hrs (40, 41). However, the precise mechanisms and the role of each protein of the complexes in the biogenesis of exosomes, and their cargo loading is not yet well understood. It has been shown that exosome biogenesis could occur via ESCRT-independent mechanisms (34). For example, even after silencing key proteins of all ESCRT complexes, vesicles were still formed in MVBs (42). Tetraspanins, transmembrane proteins enriched in exosomes, such as Tspan8, CD9, CD82, and CD63 are involved in the biogenesis of exosomes (43-45).

-Microvesicles

As mentioned above, EVs released by outward budding at the plasma membrane are defined as "ectosomes" or "microvesicles". The biogenesis of microvesicles is far less characterized than exosomes. It is known that the budding of microvesicles occurs in specific cholesterol-rich and detergent-resistant microdomains, known as lipid rafts (46), and that this process involves the redistribution of phospholipids on the plasma membrane and the contraction of cytoskeletal proteins. Particularly, when calcium increases in the cytosol, enzymes like floppase and scramblase are activated, allowing the movement of lipids from the inner to the outer membrane, enhancing bi-directional lipid movements. Enzymes like flippases, which move lipids from the extracellular to the cytoplasmic face, are inactivated, causing the flipping of negatively charged phosphatidylserine (PS) to the outer leaflet of the membrane bilayer (47). Nevertheless, since this modification does not always take place, not all microvesicles expose PS on the outer leaflet (48).

Together with the redistribution of the membrane lipids, a contractile machinery at the cell surface pulls opposite membranes together and then cuts off the connection, allowing the newly formed vesicles to be released into the extracellular milieu (49). The microvesicles' shedding depends on the interaction between actin and myosin and the subsequent ATP-dependent contraction (50). ARF6 has been shown to play a key role in microvesicles shedding, as it promotes the downstream phosphorylation of the myosin light chain and therefore the activation of the contractile machinery responsible for the budding of microvesicles (51).

During the shedding, specific proteins in the membrane and the cytosol are selectively included or excluded in the vesicles (52, 53). However, the sorting mechanism, as for exosomes, is still unknown.

-Apoptotic EVs

During apoptosis or programmed death, cells release apoptotic EVs (ApoEVs), which include large vesicles like apoptotic bodies and smaller apoptotic microvesicles. Apoptosis occurs in multicellular organisms and it is a type of energy-dependent cell death that activates intrinsic mechanisms characterized by chromatin condensation and nuclear fragmentation, followed by blebbing of the cell and its shrinkage, leading to the division of the cellular component into the apoptotic bodies (54). Apoptotic bodies are quite large (up till 5 μm) and they can carry cell organelles such as mitochondria (55-57). Studies have pointed out that membrane blebbing is partially mediated by the interaction between actin and myosin (58, 59). Specifically, the Rho effector protein ROCK I contributes to the increase of the phosphorylation of the myosin light chains (MLC), to the myosin ATPase activity, and the increase of actin-myosin filaments coupling to the membrane. All these steps, allow the dynamic membrane blebbing typical of apoptosis (58, 59).
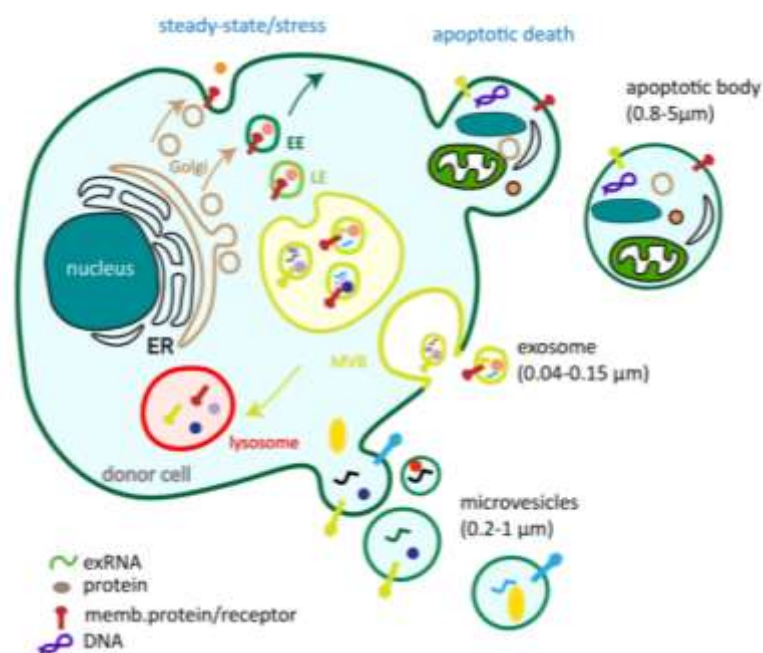
Figure 2: Schematic representation of the biogenesis of EVs. In steady-state conditions and during stress, cells release exosomes via the endocytic pathway. First, the plasma membrane invaginates

forming primary vesicles that will fuse with the EEs, delivering their cargo. EEs mature then into MVBs and LEs, gathering ILVs in their lumen by inward budding of the endosomal membrane. The MVBs can either fuse with the lysosomes, back-fuse with the endosome, or fuse with the plasma membrane, releasing ILVs (now called exosomes) into the extracellular space. In steady-state conditions and during stress, the cell can also release microvesicles by direct budding of the plasma membrane. During apoptosis, the cell releases apoptotic bodies, along with other ApoEVs, by budding at the plasma membrane.

1.1.4 EVs: uptake

Generally, the biogenesis and release of EVs are far more studied and understood than their uptake. Many pieces of evidence are suggesting that after their release in the extracellular space, EVs reach and are taken up by a target/recipient cell, in proximity or distance (60). Thus, when EV membranes are stained with fluorescent lipid dyes, fluorescence could be measured in recipient cells by confocal microscopy or by flow cytometry after uptake (61, 62). Moreover, indirect proofs of EVs internalization are the downstream effects of their cargo on the recipient cells. Thus, when EVs were loaded with GAPDH siRNA and delivered specifically to neurons, microglia, oligodendrocytes in the brain, this resulted in a specific gene knockdown (63).

So far, different pathways have been suggested for EVs uptake, which can be grouped into two main routes: endocytosis and fusion (64)(Figure 3). However, the exact mechanism of uptake has been proven elusive.

-Endocytosis

Several studies suggested that EVs can be taken up via endocytosis, a term that includes different types of molecular internalization pathways, among them clathrin-mediated endocytosis, macropinocytosis, phagocytosis, and specific protein-protein interaction-induced endocytosis (65).

In clathrin-mediated endocytosis, proteins from the cytosol assemble at the plasma membrane, bending it and forming a vesicular bud (clathrin-coated pit), which after scission from the plasma membrane is released as a vesicle, gets un-coated, and fuses with the endosome. It was shown that inhibiting the formation of clathrin-coated pits significantly decreased the uptake of EVs by cancer cells (66). Moreover, a negative mutant of the Epidermal Growth Factor Receptor Pathway Substrate clone 15 (EPS15), a component of clathrin-coated pits, was shown to induce a reduction in the uptake of EVs by macrophages (67).

Macropinocytosis in most cell types occurs when a change in actin dynamics forms protrusions at the plasma membrane, the so-called "ruffles", that enclose fluid and small particles from the extracellular space, the macropinosome, which then pinches-off forming an internal vesicle. The maturation and fate of these vesicles are very much cell-dependent, some of them will become late endosomes and fuse with the lysosome, while others will fuse back with the plasma membrane (68). This process seems to be triggered by specific substances, such as growth factors, apoptotic cell debris, and some viruses. Several players are involved, such as the protein Rac1 and the Na $+$/H+ exchanger. Hence, it was shown that both the inhibition of Rac1 and the Na+/H+ exchanger, reduced EVs uptake by microglia (69). However, it seems that macropinocytosis might be a pathway less used by cells for

EVs uptake, or used only by specific cell types, as other studies also inhibiting this pathway did not observe changes in EVs uptake (67, 70).

Phagocytosis is a receptor-mediated pathway that involves rearrangements of the actin cytoskeleton and the formation of infoldings (phagosomes) around opsonized particulate matter, such as bacteria and fragments of apoptotic cells, larger particles compared to EVs. The size difference might speak against the uptake of EVs via this route, yet EVs were found to co-localize with phagosomes, and the inhibition of PI3K, which plays an important role in the formation of phagosomes, decreased EVs uptake (67). Moreover, many EVs present PS in the outer leaflet, similarly to apoptotic cells and contrary to the physiological orientation in healthy cells, which is a crucial feature for triggering phagocytosis. Blocking TIM4, a receptor involved in PS-dependent phagocytosis, reduced EVs uptake in macrophages (67). When dendritic cells were treated with a soluble PS-analogue that competed for the binding with αv/β3 integrin on the cell surface, they lowered the EVs uptake (61) and, similarly, when EVs were pre-treated with Annexin V, which binds PS with high affinity, they were less taken up by natural killer cells (71) and macrophages (72).

Several studies, especially on cells of the immune system, have pointed out an uptake mechanism dependent on the interaction between proteins on the surface of the recipient cell and proteins on the surface of EVs that would facilitate subsequent endocytosis. It is proposed that tetraspanins, integrins, immunoglobulins, and proteoglycans play a role in protein-interaction mediated endocytosis. Tetraspanins, known to have a role in cell adhesion and motility, are highly enriched on the EVs surface (73). Particularly, CD63, CD9, and CD81 are considered typical markers of EVs (74). It has been shown that dendritic cells reduced the uptake of EVs after treatment with antibodies against CD9 and CD81 (61). It was observed that the tetraspanin complex Tspan8-CD49d was important for the EVs' uptake by endothelial cells, a process mediated by Immunoglobulin Intercellular Adhesion Molecule 1 (ICAM-1 or CD54) (75). Moreover, the EVs' uptake by dendritic cells can be decreased with antibodies that block ICAM-1 receptor, or one of its ligands (61). EVs from Antigen Presenting Cells (APCs) can trigger a proliferative and differentiation response in naïve T-cells after three different receptor/ligand interactions which lead to EVs' internalization: the T cell receptor (TCR) with the major histocompatibility complex (MHC), the lymphocyte function-associated antigen 1 (LFA-1) with ICAM-1 and CD28 with membrane protein B7 (76). CD4+ cells take up EVs isolated from dendritic cells via the interactions between LFA-1 and ICAM-1 (77). Proteoglycans (PG), such as the family of heparin sulphate proteoglycans (HSPGs), are proteins with a high carbohydrate component, used by viral particles to entry into target cells (78). Cell-surface proteoglycans also have been suggested to have a role in the uptake of EVs. For instance, the uptake of EVs was lowered both in WT cells treated with a drug to stop the normal production of HSPGs and in mutant cells lacking PGs (70).
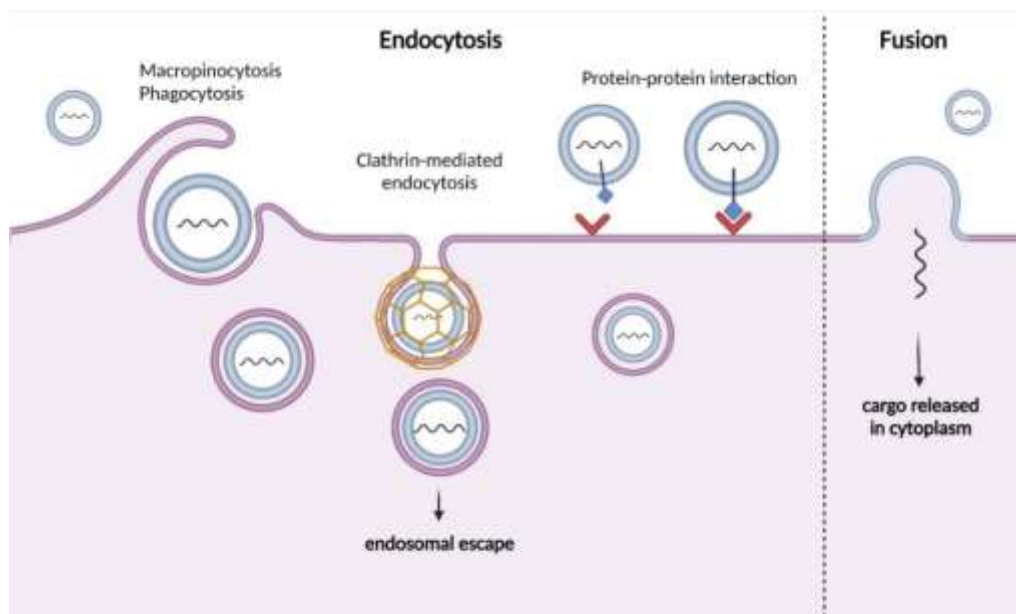
-Fusion

Fusion occurs when two separate membranes merge in an aqueous environment, exposing the hydrophilic and keeping the hydrophobic part protected. Different

proteins are involved in this process, such as the SNAREs and Rab proteins, and Sec1/Munc-18-related proteins (SM-proteins) (79).

It has been shown that in acidic conditions cancer cells increase the EVs uptake via fusion, as they contain increased amounts of the monosialodihexosylgangliosid GM3 and sphingomyelin (SM), which alter the EVs' membrane rigidity, increasing their ability to fuse. This study also showed that lipidic vesicles depleted of proteins do not fuse, suggesting that not only the type of lipids but also proteins exert a key role in the fusion process (80). The fusion pathway might be facilitated by the lipid raft-like composition of the EVs membrane (81).

After reaching the target, the EV's cargo should be delivered. By direct fusion with the plasma membrane, EVs could directly release their cargo into the cytoplasm of the recipient cell, while with endocytosis the EVs' cargo can only reach the cell cytoplasm by "escaping" the endosomal compartments, as observed for viruses. Several studies pointed out minimal successful transfer of cargo in the recipient cell, suggesting "endosomal escape" as a limiting step in EVs' cargo transfer (82-84).

However, EVs from dendritic cells were shown to be able to deliver miRNAs and luciferin in the cytoplasm of recipient cells, proving fusion of EVs membrane with either the plasma membrane or the endosomal membrane (85).

Figure 3: Schematic representation of EVs' uptake routes. EVs are endocytosed through protrusions of the cell plasma membrane (macropinocytosis, phagocytosis), via the formation of clathrin-coated pits (clathrin-mediated endocytosis), or after specific protein-protein interaction. After being encapsulated, EVs enter the endosomal membrane compartments. The EVs' cargo can reach the cytoplasm only by "escaping" the endosomal compartments. EVs can also be taken up via fusion at the plasma membrane of the recipient cell, where the cargo is directly delivered in the cytoplasm. The image was created using Biorender.

1.1.5 EVs: cargo and composition

EVs' cargo can be composed of proteins, nucleic acids, lipids, and metabolites, which vary according to the cell of origin and its status.

-Proteins

Exosomes, which originate from the endocytic pathway, are enriched in proteins of the ESCRT complexes, such as TSG101 and Alix (86), while microvesicles, originating directly at the plasma membrane, are enriched in proteins with post-translational modifications, such as glycoproteins, phosphoproteins, and integrins (87, 88). While first considered exosome markers, tetraspanins (CD9, CD63, CD81, and CD82) have been also found in microvesicles (89-91). MHC proteins and Flotilin-1 and 2 are common EVs markers (89, 92), with the latest also being involved in their biogenesis (93-95).

In contrast, resident proteins of the Golgi apparatus and the endoplasmic reticulum, such as GM130 and calnexin, have been reported to be absent in EVs, and are therefore commonly used as a confirmation for the purity of EVs preparations (28, 96).

The disintegrin and metalloproteinase ADAM10 is considered a specific marker for small extracellular vesicles (97) and it has been found on the surface of EVs isolated from cell culture in its cleaved and activated form (98).

EVs carry protein markers specific to the cell of origin. For instance, in the case of brain cells, PLP and CNPase, specific oligodendrocytes markers, have been found on oligodendrocyte-derived EVs (99). Excitatory amino acid transporter EAAT-1 and EAAT-2, characteristic of astrocytes, have been found in EVs derived from astrocytes (100).

EVs' cargo reflects the status of the cell of origin. For example, it has been shown that after stimulation with ATP, the proteome of microglia-derived EVs changes, influencing the response of recipient cells (101).

-Nucleic acids

RNA, and to a lesser extend DNA, have been reported to be present in EVs. The presence of DNA in EVs has been documented for apoptotic bodies (102) and for large EVs, where the entire genome of the parental tumor cell was detected (103). Exosomes, on the other hand, have been shown to carry mitochondrial DNA (mtDNA) (104, 105). The presence of double-stranded DNA (dsDNA) in exosomes raises a debate, as some studies were able to detect dsDNA in exosomes while others ruled this possibility out (106, 107).

Most of the genetic information found in EVs correspond primarily to RNA, such as small non-coding RNAs (e.g., miRNA), mRNA, ribosomal RNA (rRNA), and long non-coding RNA (lncRNA). As with proteins, the RNA contained in EVs is related to the type and the status of the cell of origin, but at the same time, it differs substantially from the cellular RNA, indicating selective incorporation in EVs (108-110). Generally, cellular RNAs form ribonucleoprotein (RNP) complexes by associating with RNA-binding proteins (RBPs), which are highly expressed in EVs (108, 111). Mechanisms for RNA sorting into EVs include the association with RBPs and the presence of specific RNA sequence motifs (112). Specifically, it has been shown that several members of the heterogeneous nuclear RNP (hnRNPs) family are involved in the sorting of RNA into EVs. hnRNPA2B1 sorts miR-17 and miR-93 containing AGG and UAG motifs into EVs, which also requires the interaction of

caveolin-1 (113). Y-box binding protein 1 (YBX1), another RBP, is involved in the packaging of miR-223 into exosomes released from HEK293T cells, possibly recognizing specific secondary RNA structures, such as hairpins in the 3'-UTR region (114, 115). YBX1 is also implicated in the sorting of miR-133 in hypoxic conditions into human endothelial progenitor cell (EPC)-derived exosomes, leading to increased angiogenesis (116). ALIX also seems to be involved in the packaging of miRNAs with antitumor and regenerative activities in EVs released by human liver stem-like cells (117).

As for functional studies (although it seems that the RNA copies per EV are very low (118, 119)), it has been shown that miR-26a-5p present in astrocytic EVs modulates dendritic complexity in neurons (120) and that during inflammation, microglia deliver microRNA 146-a-5p via EVs to neurons, affecting negatively synaptic density and strength (12). Moreover, translation of mRNA delivered by EVs in recipient cells has been observed (10), and, more recently, gene silencing in recipient cells was possible by delivering the mRNA of endonuclease CRISPR associated protein 9 (Cas9), loaded by electroporation into EVs (121). These experiments point out that translation of mRNA delivered by EVs in recipient cells is possible, yet it remains unclear its relevance in physiological and pathological conditions.

-Lipids

The lipid composition of EVs has been extensively studied (122, 123) and, as for proteins and genetic material, reflects the cell of origin, although some lipids might be specifically enriched in EVs.

EVs are enriched in cholesterol, sphingomyelin, phosphatidylserine ganglioside, and ceramide, among others (123), while phosphatidylcholine and diacyl-glycerol are significantly less present when compared to the membrane of the cell of origin (124). The lipid composition of EVs might play a fundamental role in binding and uptake, as it has been shown that the enrichment of "reversed" PS (facing the extracellular space) may facilitate their uptake by recipient cells (69).

Exosomes are particularly enriched in disaturated phospholipids (123, 124), which causes increased membrane rigidity compared to the membrane of the cell of origin. The rigidity is also increased by the high ratio of protein/lipid in exosomes (125) and might be relevant to ensure a longer half-life when circulating in body fluids. When treated with detergents, exosomes are more resistant than microvesicles (125). When injected intravenously in mice, exosomes showed a half-life of 4 min, with 10% detectable after 4h (126), while microvesicles were faster degraded in the circulation, probably because the lipids on their membrane tend to be hydrolyzed by circulating phospholipases (127, 128).

1.1.6 EVs isolation

To study and analyze EVs and their cargo, it is necessary to isolate them from the biological source. EVs have been successfully purified from cell culture media, body fluids, and more recently from tissue. Several isolation approaches are used. Each method takes advantage of different EVs' characteristics, such as density, size, and

affinity to specific ligands, and each approach has its degree of EVs' recovery and contamination.

For instance, differential ultracentrifugation (UC) is the most popular technique for EVs' isolation and it uses centrifugal force to separate substances according to the sedimentation principle: larger and more dense particles pellet at the bottom, while smaller and less dense particles remain in the supernatant (89, 129). UC is often accompanied by density gradients, which isolate particles solely based on their density, to further purify the sample from contaminants, especially when the isolation is done on tissue such as brain (6, 7). EVs have a size of 50-5000 nm and a density in the range of 1.06–1.23 g/mL, which distinguish them from molecules such as chylomicrons, very low-density lipoprotein (VLDL), intermediate-density lipoprotein (IDL), and low-density lipoprotein (LDL), since these particles have a lower density than EVs. On the other hand, high-density lipoproteins (HDL) have a similar density to EVs, but different sizes. Samples such as blood are enriched in lipoproteins, representing a problem when it comes to EVs isolation.

Size exclusion chromatography (SEC) has also been used for EVs' isolation (130-132). A typical SEC column is composed of a mobile phase, a solvent that carries the sample down the column, and a porous stationary phase. SEC separates particles according to their size, as larger particles are eluted first and the porous stationary phase captures the smaller particles, which are eluted later. Contrarily to UC, SEC is effective in removing HDLs, but not chylomicrons, VLDL, IDL, and LDL, as they have the same size range of EVs.

Other techniques that exploit the size of EVs for their isolation are ultrafiltration (UF) and tangential flow filtration (TFF)(133, 134). UF utilizes pressure or centrifugation to pass the sample through a membrane with a defined molecular weight cut-off (MWCO), that allows the passage of particles with the size of interest. UF is widely used for diluted samples and cell cultures. It is a relatively simple technique and the isolation of EVs is faster when compared to, for example, UC, which is more time consuming and needs a trained operator (134). UF does not eliminate contaminating particles having the same size as EVs and protein contaminants (135).

TFF is also based on the passage through a membrane with a cut-off, but the fluids flow tangentially across the membrane and therefore the smaller particles passing through it are discarded, while particles larger than the cut-off level stay on the membrane and are recovered. The samples with TFF at the end are more concentrated, while SEC on the contrary dilutes the sample (136).

Apart from density and size, EVs can also be purified using selective affinity to proteins present at their surface with their specific ligands, which are immobilized or conjugated on solid material, such as beads or columns. For instance, a common affinity-based approach used for EVs' isolation consists of the use of magnetic beads covalently coupled with antibodies against molecules such as CD9, CD63, and CD81, which are highly enriched in EVs (73, 137).

More recently, microfluidic technologies, chambers able to manipulate fluids on the microscale, have also been used for the isolation of EVs, based either on their size or on their affinity with specific molecules (138).

As of today, more and more techniques are being employed for EVs' isolation, but the gold standard is still considered to be UC (139). When choosing the technique to

isolate EVs, is fundamental to consider the type of sample. For instance, when isolating EVs from conditioned cell culture media the volume of the sample is the limiting factor. When isolating EVs from body fluids, the critical factor is their viscosity, as they carry several non-EV structures, such as lipidic components in the plasma and serum, fat-containing vesicles in milk, and surfactant in bronchoalveolar lavage, that can be isolated together with EVs (5, 28).

More complex is the purification process on tissue, such as brain, which has first to be mechanically disrupted and enzymatically digested to liberate the EVs from the extracellular matrix (ECM) (6, 7). During this procedure, the risk of isolating contaminants together with EVs is high, therefore the sample undergoes several rounds of centrifugation, including UC in the presence of a density gradient of sucrose, percoll, or iodixanol (28).

1.1.7 EVs and the central nervous system

The isolation of EVs from cerebral spinal fluid (CSF), from cell culture, and, more recently, directly from brain tissue has allowed the characterization and functional studies of EVs from the CNS (140, 141).

The CNS is composed mainly of neurons and glial cells. Neurons are electrically excitable cells composed of a cell body (soma), dendrites, and a single axon that extrude from the soma. At the axon terminal, the neuron can transmit a signal to another cell across a structure called synapse.

Glial cells (or glia), comprising -among others- astrocytes, oligodendrocytes, and microglia, provide metabolic and structural support to neurons, contribute to neurotransmission and synaptic plasticity and are involved in the immunological response in the brain.

Astrocytes are the most abundant type. They are star-shaped cells that during development secrete growth-promoting and inhibiting molecules important for axon guidance, and they are also involved in the homeostasis of synapses, by removing excess of glutamate, the major CNS excitatory transmitter (142, 143). Astrocytes also play a role in neuronal signaling, the so-called tripartite synapse (144), as they modulate synaptic transmission by the release of chemical transmitters, such as glutamate and γ-aminobutyric acid (GABA)(143, 145). The astrocytic end feet form part of the blood-brain barrier (BBB), a semipermeable barrier that selects the solutes allowed to pass from the circulating blood to the extracellular fluid of the CNS (146). The BBB allows the passage of hydrophobic molecules (oxygen, CO_2, and hormones) and small non-polar molecules (147). Interestingly, EVs can also cross the BBB (148).

In response to harmful stimuli, astrocytes proliferate, progressively becoming hypertrophic, and change their molecular expression towards a pro-inflammatory phenotype. Proliferating reactive astrocytes are essential for scar formation, which reduces the spread of inflammatory signals to the healthy tissue after inflammation or severe tissue damage (149, 150). Astrocytes are in close communication with microglia, playing an important role in CNS inflammation (151).

Microglia cells are the resident immune cells of the CNS. They are specialized macrophages with phagocytic ability that in normal conditions have long branching processes and are mobile ("resting" microglia). Following exposure to pathogen-

associated molecular patterns (PAMPs) or endogenous damage-associated molecular patterns (DAMPs) change their phenotype to "reactive"/"activated", with phagocytic activity. Microglia can also release substances such as hydrogen peroxide and proinflammatory cytokines such as IL-1, to eliminate infected cells, viruses, and bacteria. This cytotoxic secretion can also cause collateral damages, such as neural cell death and demyelination of neuronal axons (152, 153). Post-inflammation microglia can also secrete anti-inflammatory cytokines and recruit astrocytes and oligodendrocyte progenitor cells (OPCs) to the damaged area, promoting tissue repair (154).

Microglial cells are also involved in normal physiological processes, such as synaptic pruning. During development, unwanted synapses are tagged with C1q, triggering the complement cascade and microglial phagocytosis via recognition of activated complement molecule C3 by its receptor CR3 (155, 156). Recent studies have proposed that aberrant synaptic pruning by microglia is a mechanism underlying several neurodegenerative diseases, such as Alzheimer's disease (AD), Multiple Sclerosis (MS), Parkinson's disease (PD), or schizophrenia (157-159).

Oligodendrocytes cover the neuronal axons of the CNS, forming the so-called myelin, which provides insulation and permits the electrical signal transmission. They provide trophic support by producing the brain-derived neurotrophic factor (BDNF), the glial cell-derived neurotrophic factor (GDNF), and the insulin-like growth factor-1 (IGF-1)(160). In both, physiological and pathological conditions, the communication and the interplay between these different cell types are pivotal. Although the study of the communication between brain cells through EVs is a very young field, they probably play an important role in the activity and coordination of cells in healthy and diseased brain.

-Role of the EVs in the CNS under physiological conditions

Neurons (161), astrocytes (162, 163), oligodendrocytes (99), and microglia (162) release EVs. Neuronal EVs have been linked to synaptic transmission, as their release is induced by KCl-induced depolarization (164), and to neuronal excitation, as they carry the AMPA receptor subunits GluR2/3, which might alter the excitability of recipient cells (165).

Neuronal EVs may be important for the development of neuronal circuits, as human primary neurons showed increased neurogenesis and neuronal differentiation when incubated with EVs isolated from human-induced pluripotential stem cells (hiPSC). In the same study, when rat neuronal primary cultures-derived EVs were injected into the lateral ventricle of P4 mice, they led to neurogenesis (166). EVs isolated from primary neurons can deliver miR-132 to endothelial cells, regulating the expression of Cdh5, a vascular junction protein, highlighting a possible role in neurovascular communication for neuronal EVs (167). Neurons regulate the release of oligodendrocytes-derived EVs with an autoinhibitory effect on oligodendrocyte surface expansion, modulating myelin sheath formation (168).

Astrocytic EVs carrying miR-26a-5p modulate dendritic complexity in neurons (169). Additionally, EVs secreted by astrocytes deliver Apolipoprotein D (ApoD) to neurons, modulating their survival after oxidative stress (170).

Lastly, microglia-derived EVs can either stimulate neuronal synaptic activity via enhanced sphingolipid metabolism or can inhibit it via endocannabinoid signaling activated by N-arachidonoylethanolamine (AEA) exposed on the EVs' surface (171, 172).

-EVs' involvement in CNS pathologies

The role of EVs in CNS pathologies has been best studied in the context of neurodegenerative diseases (NDs) and brain tumors.

NDs are disorders of the CNS that can be classified by the aggregation and deposit of specific misfolded proteins in the brain, such as Aβ and Tau for AD and α-synuclein for PD.

In AD, the Aβ peptides, derived from the cleavage of the amyloid precursor protein (APP), aggregate to form oligomers, which accumulate extracellularly as amyloid plaques, one of the characteristic hallmarks of AD. Tau becomes abnormally hyperphosphorylated and it polymerizes into filaments which aggregate in neurofibrillary tangles (NFTs), the other typical hallmark of the disease. Several studies point to a role of EVs in the development of the disease, as ALIX is found in amyloid plaques, thus suggesting a possible role of EVs in plaque formation (92). Moreover, BDEVs isolated from a mouse model of AD contain tau, that can propagate in a prion-like fashion to primary neurons (173). EVs carry Aβ, APP, and other APP-derived proteolytic fragments (174), acting as vehicles for intercellular transmission (175, 176). Interestingly, EVs bind Aβ via PrP^c, accelerating the fibrillization of Aβ, thus reducing the neurotoxic effects caused by oligomeric Aβ (177). Recent studies also suggested that EVs may contribute to the accumulation in the brain of certain APP fragments, which might be the at the origin of the neurodegenerative process (6, 178).

In PD, abnormal isoforms of α-synuclein, a cytosolic protein physiologically involved in the regulation of the synaptic transmission, aggregate in oligomers forming the characteristic structures, Lewy bodies, and Lewy neurites. EVs carrying α-synuclein and EVs carrying its oligomers are toxic to primary neurons (179-181). Moreover, EVs isolated both from the CSF and brains of PD patients induced the formation of α-synuclein aggregates in recipient cells, implying participation in the disease progression (182, 183).

However, in humans, where NDs last for years, it is unclear whether EVs are promoting the spread of the disease, or they are trying -unsuccessfully- to clear the misfolded proteins, or both (184).

In Multiple Sclerosis (MS), an inflammatory autoimmune disease where the myelin sheet on the axons is damaged, myeloid microvesicles are increased in the CSF of patients. When incubated with primary glia cells or injected into a mouse model of MS these EVs could spread inflammatory signals, suggesting their involvement in the disease progression (185). Interestingly, plasma EVs from naïve WT mice delivered to mice at the clinical peak of the disease induced a spontaneous phenotype of a relapsing−remitting disease. This effect was hypothesized to be caused by the fibrinogen contained in the EVs, which influence the activity of CD8+ T cells (186). Finally, let-7i miRNA is increased in EVs of MS patients and could play a

crucial role in the development of the disease as they suppress the differentiation of CD4+T cells into Treg cells, a hallmark of MS (187).

Lastly, EVs have been extensively studied in the context of brain tumors. Glioblastoma (GBM), a tumor of glial origin, is one of the most aggressive. It has been shown that EVs isolated from the serum of GBM patients polarize monocytes to the anti-inflammatory phenotype M2, favouring the growth of the tumor in vitro (188). Moreover, EVs released by GBM cells are enriched in miR-451 and miR-21, which downregulate the expression of c-myc in recipient cells, increasing the activation of glial cells, and supporting the tumor growth (189, 190). GBM-EVs influence astrocytes, increasing their migratory capacity and their cytokine production, promoting tumor cell growth (191).

It is worthy to note that EVs have been studied as potential biomarkers not only for all of the previously mentioned diseases (140, 184, 192) but also for other neurological disorders such as traumatic brain injury and ischemic stroke (193, 194).
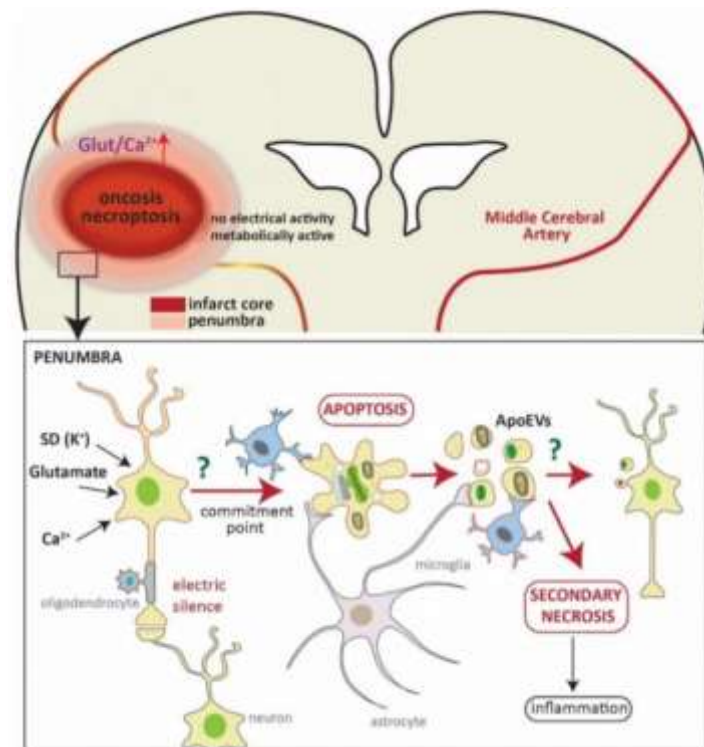
1.1.8 Ischemic stroke

Stroke is globally one of the primary causes of mortality and long-term disability. Ischemic stroke accounts for 87% of the cases, being the other type haemorrhagic stroke (195). Ischemic stroke occurs when a brain artery is occluded by a blood clot (thrombus). The thrombus can originate in the arteries supplying the brain (thrombotic stroke); or the blood clot can form in a different organ, such as the heart, and travel through the bloodstream to the brain (embolic stroke). This leads to a lack of blood flow and thus, a lack of nutrients and oxygen supply in the affected brain area. Cells at the core of the lesion will die rapidly by oncosis (cellular swelling) and necroptosis (programmed necrosis, or inflammatory cell death), while cells in the surrounding area, the so-called "penumbra", enter into a state of electrical silence (although still metabolically active) and either die by programmed death (apoptosis) or survive in the following hours, depending on several factors (Figure 4).

-Pathophysiology of ischemic stroke

Within minutes, the hypoxia caused by the lack of blood flow leads to ATP depletion. In the infarct core, this leads to the failure of the Na+/K+ pump, neuronal depolarization, and the release of glutamate. Since at that point, neither neurons nor astrocytes can take up the glutamate (196), its levels in the extracellular space rise rapidly, hyperactivating the N-Methyl-D-Aspartate Receptors (NMDAR).

Once activated, there is a rise of intracellular entry of Ca2+, which activates calpains and phospholipases, causing excitotoxic cell death. Neurons in the peri-infarct area also receive glutamate from the necrotic core, triggering their depolarization.

Figure 4: Schematic representation of the infarct core and the penumbra after ischemic stroke. In the upper part, a blocked brain artery (yellow) causes the hypoperfusion of the brain, leading to the formation of the core infarct area (where cells die by oncosis/necroptosis) and of the penumbra (where cells are electrically silent but metabolically active). The lower part depicts what happens in the penumbra. Here, neurons receive an influx of glutamate, Ca2+, and spreading depolarizations (SD) originated at the core of the stroke. If a neuron in the penumbra reaches the commitment point, it will die by apoptosis generating apoptotic bodies and ApoEVs, which will be engulfed by phagocytic cells, without triggering inflammation. This step is critical to avoid secondary necrosis and inflammatory response. Whether ApoEVs influence other cells such neurons is unknown. Originally published in (197).

These repetitive cycles of depolarization/repolarization (spreading depolarization, SD) can last for hours, further depleting neurons of energy (198). In the ischemic core, the dying cells release DAMPs such as adenosine triphosphate (ATP) and heat shock proteins (HSPs), triggering inflammation (199), and rapidly activating microglia, which proliferate and migrate to the stroke area. The BBB is disrupted due to the activation of matrix metalloproteinases, which degrade the basal lamina and the tight junctions of endothelial cells. As a consequence, macrophages and other immune cells from the blood, such as neutrophils, lymphocytes, and dendritic cells can now infiltrate to the brain, aggravating the inflammatory process.

In the early phase of stroke, microglia contribute to the ischemic damage by releasing pro-inflammatory cytokines, such as TNFα, IL-1β, C1q, or IL-6, which activate astrocytes, that can either further exacerbate neuronal death or can be neuroprotective by promoting the formation of the glial scar, limiting inflammation and protecting the surrounding healthy tissue (149, 200-203). After the acute phase of stroke, microglia turn beneficial. It has been shown that 72h after stroke, microglia release important neuroprotective factors (204). Hence, the environment and its stimuli are crucial for the activation state of both microglia and astrocytes.

In the penumbra, cells undergoing apoptosis release ApoEVs, which are cleared by microglia (205). If not properly removed, ApoEVs lead to secondary necrosis, resulting in inflammation (206), however, they can also have a decisive role in communication (207). It has been shown that they can transfer DNA to recipient cells (102) and that, through ApoEVs, aggressive cancer cells can transfer therapy resistance to other cells (208, 209). Lastly, oligodendrocytes are very sensitive to ischemic damage, and many die after stroke. However, in the recovery phase, OPCs migrate to the affected area to remyelinate the sprouting axons, an action promoted by microglia (154).

-EVs and ischemic stroke

The communication among the resident cells of the brain, and between them and the infiltrating ones, is pivotal for the fate of neurons in the penumbra and EVs may play a role in this process (Figure 5). For instance, oligodendrocyte release EVs that rescue neurons under *in vitro* ischemic or stress conditions, and stimulate microglial phagocytosis (210-212). When microglia are activated by extracellular ATP, they release EVs with a modified proteome compared to steady-state conditions, that activates astrocytes (101); and vice versa, astrocytes release ATP that induces shedding of microglial EVs containing the pro-inflammatory cytokine IL-1β (213, 214). Moreover, microglia exposed to inflammatory stimuli release EVs containing miR-146a-5p, which decrease the synaptic stability (12), and EVs containing IL6 and TNFα, which exacerbate inflammation (215). Neuronal EVs deliver miRNA 124a to astrocytes, leading to an increased expression of glutamate transporter 1 (GLT-1) (216). Furthermore, neuronal EVs can support the functionality of the neurovascular unit (NVU) and the endothelial integrity after stroke, by releasing EVs containing miR132 (167). Interestingly, EVs from astrocytes containing mitochondria lead to increased neuronal survival in both conditions, *in vitro* (after Oxygen Glucose Deprivation (OGD), a model of stroke) and *in vivo* (in mice subjected to transient middle cerebral artery occlusion (tMCAO), a mouse model of stroke) (55).
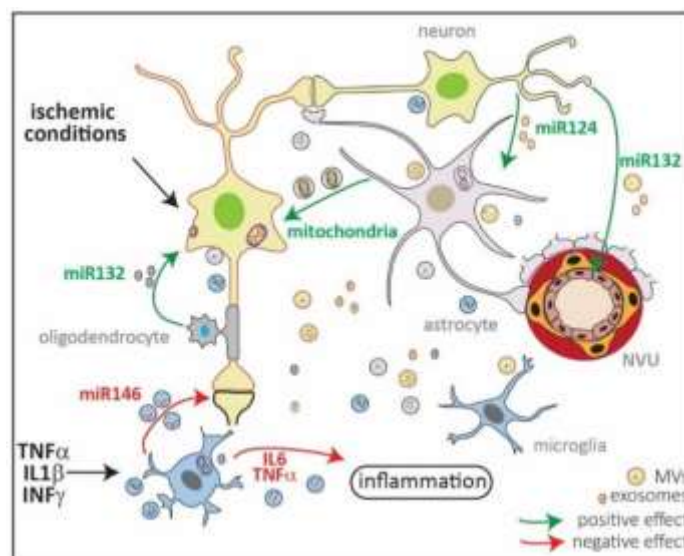
Figure 5: Schematic representation of some of the positive (green arrows) and negative (red arrows) effects of EVs (exosomes and microvesicles) in ischemic stroke. After ischemia, oligodendrocytes

release EVs containing miR132, which are taken up by neurons and promote their survival. By contrast, microglia exposed to inflammatory stimuli release EVs containing miR146, which decrease the synaptic stability, and cytokines that exacerbate inflammation. Neurons contribute to the NVU functionality by releasing EVs containing miR132. Neurons also regulate the expression of GLT1 in astrocytes through miR124. Lastly, astrocytes can release EVs carrying mitochondria, which promote neuronal survival. Originally published in (197).
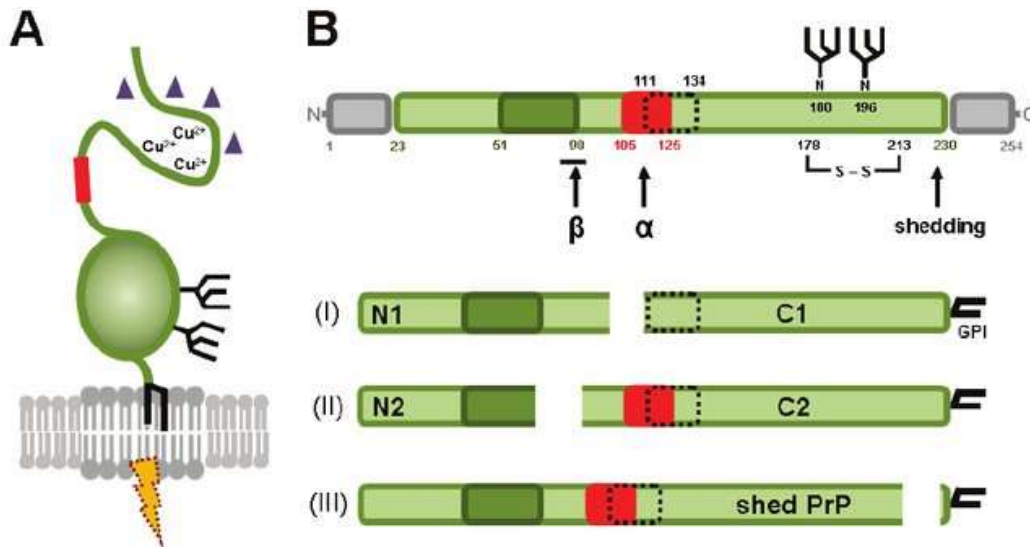
1.1.9 The prion protein

A protein that is protective against ischemic stroke is the cellular prion protein (PrP^C). PrP^C is a cell surface glycoprotein, encoded by the PRNP gene, highly expressed in the brain, but also in other tissues (217). Mature PrP^C is mainly located in lipid rafts, and its structure consists of a flexible N-terminal tail, which includes an octapeptide repeat region, a charged and a hydrophobic domain, and a globular C-terminal domain, which includes two N-glycosylation sites. It is attached to the outer leaflet of the plasma membrane by a GPI anchor (218, 219) (Figure 6).

PrP^C is highly conserved in mammals, and some domains such as the C-terminal are even preserved from fishes, pointing to an important physiological function. Nevertheless, the exact physiological role of PrP^C is still not fully clarified, as mice knock-out for PrP^c do not present major deficiencies (220).

Several functions have been attributed to PrP^C, such as being a regulator of neuritogenesis and being involved in peripheral myelination. PrP^C is also a modulator of synaptic activity and a receptor for toxic oligomers, such as Aβ (221). This wide range of functions might be explained by the various ligands and binding partners of PrP^C (222), and by its post-translational modifications giving rise to several biologically active fragments (223).

PrP^C can go through several types of cleavages (Figure 6). The major cleavage event in physiological conditions is the α-cleavage, performed by a yet-to-be-identified protease(s), at position 111. The α-cleavage produces the soluble N1 fragment and the C1 fragment which remains attached to the membrane. The C1 fragment exposes N-terminally a hydrophobic domain, which reminds of some viral surface glycoproteins critical for host cell attachment and membrane fusion (224, 225).

β-cleavage occurs around position 90 and produces a soluble N2 fragment and a membrane-attached C2 fragment, and it is mainly generated under pathological conditions (226, 227). γ-cleavage takes place presumably between residues 176 and 200 and produces a large, soluble, non-glycosylated N3 fragment and a short, membrane-attached, C3 fragment (228). Finally, shed PrP (sPrP) is generated by the action of the metalloprotease ADAM10 which cuts the protein near the GPI-anchor (229-231). N1, N2, N3 and shed PrP can be un-, mono- and di-glycosilated. PrP is mostly known because of its misfolded and pathogenic form, PrP^{Sc}, the causative agent of prion diseases (PrD), such as Creutzfeldt-Jakob disease (CJD) and the bovine spongiform encephalopathy (BSE), which are fatal transmissible neurodegenerative diseases (232). Both PrP^C and PrP^{Sc} are released via EVs (233, 234). PrP is enriched in EVs and involved in the biogenesis of exosomes through the interaction with Caveolin-1 (CAV-1).

Figure 6: Schematic representation of murine PrP. (A) The prion protein is attached to the outer leaflet of the cellular membrane via a GPI-anchor. The flexible N-terminal has a neurotoxic domain (red box) and binds copper ions and oligomeric amyloid β (purple triangles). The globular C-terminal has two N-glycan side chains. PrP^c is involved in protective or toxic signaling (dotted thunderbolt). (B) The N-terminal signal sequence (1-22) is removed by signal peptidases in the endoplasmic reticulum. At the C-terminal part (aa 231-254) there is the sequence for attachment of the GPI-anchor. The octameric repeat region (aa 51-90), the neurotoxic domain (aa 105-125), and the hydrophobic core (aa 111-134) are present in the mature protein. PrP presents also a disulfide bridge (between aa 178 and 213) and two N-glycosylation sites (aa 180 and 196). Below are represented the three most important cleavage events of PrP. (I) α-cleavage (aa 111) produces a soluble N1 fragment of 11 kDa and a membrane-bound C1 fragment of 18 kDa, destroying the neurotoxic domain. (II) β-cleavage (around aa 90) produces N2 (9 kDa) and C2 (20 kDa) fragments. (III) Shedding close to the GPI-anchor causes the release of -nearly- full-length PrP from the membrane. Originally published in (224).

Thus, PrP modulates CAV-1 distribution between the plasma membrane and the cytosol, where CAV-1 can inhibit the autophagy, allowing the MVBs to release exosomes instead of fusing with the lysosomes for degradation (235).

-PrP and stroke

Several studies have pointed out that PrP^C (and its fragments) have a protective role in stroke. Thus, cells lacking PrP^C are more vulnerable to oxidative stress than wild-type (WT) cells. PrP knock-out mice (*Prnp$^{0/0}$*) subjected to permanent middle cerebral artery occlusion (pMCAO), a mouse model of stroke, had a larger infarct volume compared to WT mice. The effect was dependent on the amount of PrP^C, as the heterozygous mice showed a rescued phenotype (236). Moreover, mice infected with PrP^{Sc} increase oxidative stress, probably as a consequence of a loss of function of PrP (237). Interestingly, PrP^C was found increased in the penumbra of mice subjected to pMCAO (236). The analysis of human brain samples with stroke showed similar results, coinciding with neuronal survival and with higher PrP^C levels in plasma 24h after stroke (238). However, another study suggested that the upregulation of PrP^C is a survival mechanism only used in the early time-points of severe stroke damage, as it was only observed in pMCAO between 4 and 8h after stroke/reperfusion (and back at normal levels 24h after), whereas in tMCAO (which

usually leads to a milder stroke), PrP^C was not upregulated (239). Lastly, PrP could have a function in the long-term recovery effects. Mice overexpressing PrP (Tga20) one month after tMCAO had decreased infarct volume and neurological improvement when compared to WT and PrP KO mice (240).

Different mechanisms have been proposed for the neuroprotective function of PrP (241). For example, PrP is involved in neural precursor cells (NPCs) recruitment (homing) to the site of injury, and their differentiation and neurogenesis (240). PrP^C fragments were reported to modulate the quiescence of neural stem cells (242), suggesting a potential role in adult neurogenesis. PrP^C and its fragments appear to also have a role in the recruitment of bone marrow-derived cells (BMDC) from the periphery to the affected brain area (243, 244), probably supporting angiogenesis. The docking of BMDC to endothelial cells and their migration through the vessel seem to be dependent on the presence of PrP^C at the recipient cell's surface and therefore on homophilic ligand–receptor interaction. Moreover, the N1 fragment showed to be protective for neurons after ischemic damage and able to regulate the interaction of microglia with other brain cells (245, 246). Lastly, EVs released by astrocytes contain PrP^C which showed to be protective when delivered to primary neurons under ischemic conditions (247).

1.2 Aims of the thesis

Much of the basic knowledge of EVs' functions in the healthy and diseased brain is lacking and there are still many unanswered questions regarding their biology. In CNS' pathologies, EVs are regarded as attractive biomarkers and as potential therapeutic tools due to their ability to cross the blood-brain barrier (BBB). EVs have been successfully purified from conditioned media of neural cell lines, primary brain cells and CSF, but protocols for the isolation of EVs directly from brain tissue have only recently been published. The analysis of BDEVs can help to understand complex and multicellular physiological and pathological processes of the CNS, which is simply not possible with *in vitro* studies.

The main aim of the present thesis was to isolate EVs from murine brain to study the variations of their content at different time points after stroke. We hypothesized that with this approach we could shed light on their role in neuronal death/survival at the penumbra.

To pursue this goal, we wanted:

a) to establish a reliable protocol to isolate brain-derived EVs (BDEVs) from murine tissue and to characterize their proteomic content in steady-state conditions and after stroke;

b) to further characterize BDEVs from stroke mice from a transcriptional point of view;

c) to assess possible changes in PrP content and composition (fragments) in BDEVs after stroke and its function;

d) to study the role of immune cell-derived EVs in the control of immune responses;

e) to assess the efficiency and the influence of different published protocols for EVs' isolation from brain tissue on BDEVs' protein cargo.

The papers included in this thesis are:

1) **Characterization of brain-derived extracellular vesicles reveals changes in cellular origin after stroke and enrichment of the prion protein with a potential role in cellular uptake** (2020, *Journal of Extracellular Vesicles*)

2) **Multiplexed mRNA analysis of brain-derived extracellular vesicles upon experimental stroke in mice reveals increased mRNA content related to inflammation and recovery processes** (2021, *bioRxiv*)

3) **Brain-Derived Extracellular Vesicles in Health and Disease: A Methodological Perspective** (2021, *International Journal of Molecular Sciences*)

4) **CD73-mediated adenosine production by CD8 T cell-derived extracellular vesicles constitutes an intrinsic mechanism of immune suppression** (2021*, Nature Communications*)

1.3 Material and methods

1.3.1 Methods performed by the doctoral candidate

- "*Characterization of brain-derived extracellular vesicles reveals changes in cellular origin after stroke and enrichment of the prion protein with a potential role in cellular uptake*": isolation of EVs from murine brain tissue; isolation of EVs from conditioned cell culture media; Nanoparticle Tracking Analysis (NTA); fluorescence labeling of EVs; primary neuronal culture; mixed glia culture; immunocytochemistry (ICC); flow cytometry (labelling); western blot (WB); PNGase F assay.

- "*Multiplexed mRNA analysis of brain-derived extracellular vesicles upon experimental stroke in mice reveals increased mRNA content related to inflammation and recovery processes*": isolation of EVs from murine brain tissue; NTA; WB; PCR.

- "*CD73-mediated adenosine production by CD8 T cell-derived extracellular vesicles constitutes an intrinsic mechanism of immune suppression*": WB.

1.3.2 WB antibodies list

14--3-3- Santa Cruz, sc-16-57

Alix- Cell Signaling, #2171S

CD40- Novusbio, NB100-56127SS

CD73- Cell Signaling, #13160

CD81- Cell Signaling, #10037

CD81- Cell Signaling, #56039

CNP- Sigma, C5922

EAAT1- Novusbio, NB100-1869SS

EAAT2- Novusbio, NBP1-20136SS,

Flotilin-1- BD biosciences, #610820

GM130- BD biosciences, #610822

NCAM- Cell Signaling, #99746

PLP- Novusbio, NB100-74503

P2Y12- LSBio, LS-C209714

P2Y12- Proteintech, #11976-1-AP

PrP (POM1) (248)

PSD95- Millipore, MABN68

SNAP-25- Cell Signaling, #3926

Synapsin1- Synaptic Systems, #106103

TMEM119- Proteintech, #66948-1-Ig

anti-rabbit-HRP conjugated secondary antibody- Cell Signaling

anti-mouse-HRP conjugated secondary antibody- Cell Signaling

1.3.3 ICC antibodies and dyes list

Phalloidin-iFluor 488- Abcam, ab176753

Alexa Fluor donkey antirat 488- Life Technologies, A21208

Alexa Fluor donkey anti-rabbit 555- Life Technologies, A31572

Alexa Fluor donkey anti-rat 555- Abcam, ab150154

IBA1- Wako, 019–19,741

LAMP-1- Invitrogen, 4–1071-82

MAP2- Sigma, M9942

mCLING- Synaptic Systems

1.3.4 Flow cytometry antibodies list

CD11b-FITC- Biolegend, Clone M 1/70

GLAST-PE- MiltenyiBiotec

1.3.5 PCR primers

C1qa:
5´ATGGAGACCTCTCAGGGATGG3´(sense),
3´TCAGGCCGAGGGGAAAATGA5´(antisense);

C1qb:
5´TGAAGACACAGTGGGGTGAGG3´(sense),
3´TACGCATCCATGTCAGGGAAAA5´(antisense);

C1qc:
5´ATGGTCGTTGGACCCAGTTG3´(sense),
3´CTAGTCGGGAAACAGTAGGAAAC5´(antisense);

Gfap:
5´ATGGAGCGGAGACGCATCA3´(sense),

3´ACATCACCACGTCCTTGTGC5´(antisense);

Cd44:
5´GTTTTGGTGGCACACAGCTT3´(sense),
3´CAGATTCCGGGTCTCGTCAG5´(antisense)

1.3.6 qPCR probes (Thermo Fischer):

Hmox1 #Mm00516005_m1

Fcrls #Mm00472833_m1

Cd44 #Mm01277161_m1

C1qb #Mm01179619_m1

Gfap # Mm01253033_m1

Asb7 #Mm01318985_m1

Fam104a   #Mm01245127_g1

1.4 Results

Paper 1: *"Characterization of brain-derived extracellular vesicles reveals changes in cellular origin after stroke and enrichment of the prion protein with a potential role in cellular uptake"*
- small BDEVs (diameter <200 nm) are highly enriched in ribosomal proteins when compared to large BDEVs (diameter >200 nm);
- in steady-state conditions, microglia are the main contributors to the BDEVs' pool;
- 24h after stroke/reperfusion, the BDEVs released from astrocytes are significantly increased in stroke mice compared to shams;
- BDEVs are enriched in PrP^C and its C1 fragment;
- 24h after stroke, PrP^C is significantly increased in BDEVs;
- the presence of PrP^C on the surface of BDEVs influences the uptake route of the recipient cells.

Paper 2: "*Multiplexed mRNA analysis of brain-derived extracellular vesicles upon experimental stroke in mice reveals increased mRNA content related to inflammation and recovery processes*"
- 72h after stroke/reperfusion, BDEVs released by oligodendrocytes are significantly increased in stroke mice compared to shams;
- 72h after stroke, BDEVs increase their content of mRNA related to inflammatory and recovery processes;
- the mRNA of the top 5 most upregulated genes in BDEVs after stroke are present as full-length;
- in BDEVs, the mRNA analysis with the Nanostring nCounter panels is feasible even bypassing the RNA extraction from the EVs, thus eliminating steps from the protocol.

Paper 3: "*Brain-Derived Extracellular Vesicles in Health and Disease: A Methodological Perspective*"
- although all published protocols considered in our study were successful in BDEVs isolation, the total number of proteins detected (and so, the performance of each protocol) was different;
- differences are also reflected when GO pathways are compared between the studies, as specific protein enrichment were differently distributed.

Paper 4: "*CD73-mediated adenosine production by CD8 T cell-derived extracellular vesicles constitutes an intrinsic mechanism of immune suppression*"
- human activated CD8 T cells release EVs expressing CD73 with high AMPase activity;
- the AMPase activity of CD8 T cells-derived EVs is sufficient to degrade the AMP produced by the high ATPase activity of human Tregs;
- the interplay between CD8 T cells-derived EVs and Tregs lowers T cell proliferation and function, controlling the immune response.

1.5 Discussion

The studies included in this thesis focus on the characterization and the analysis of BDEVs in steady-state conditions and at different time-points after stroke, and the role of EVs in inflammation.
In this chapter, the results obtained from each study (summarized in chapter 1.4) will be discussed as a whole and put into their scientific context and current knowledge. Moreover, an outlook including ongoing and future directions of EVs research will be provided.

-Proteomic characterization of BDEVs in steady-state conditions

Until recently, most of the studies related to EVs in the CNS have been performed on vesicles isolated from cell culture media and body fluids. The purification of EVs from brain tissue has been increasingly used only in the last years, after 2012, when the first protocol for isolation was published (6).
Isolating EVs from brain is challenging, as the first necessary step is to liberate them from the network of glycosaminoglycans, proteoglycans, glycoproteins, and fibrous proteins forming the ECM. This is generally achieved by mechanical disruption (i.e., the tissue being cut into small pieces) and enzymatic digestion. For the latter, the two enzymes widely reported are papain (6), a cysteine protease found in papaya, and collagenase (7), which breaks the collagen peptide bonds of the ECM. However, due to the mechanical disruption, it is very difficult that after this step there is no contamination with intracellular vesicles and membrane debris or the creation of artifacts, such as synaptosome-like vesicles. Therefore several steps of centrifugation, filtration, and gradient ultracentrifugation (among other approaches) have to be introduced.
For our studies, we decided to use a recently (at that moment) published protocol that used collagenase III as the enzyme of choice, several centrifugation steps, and a final ultracentrifugation with a sucrose gradient (7). We introduced some modifications, such as a filtering step through a 0.2 µm porous membrane to isolate small BDEVs (sBDEVs). Because we wanted to know whether this modification was leading to the isolation of different BDEVs populations, we performed quantitative proteomic analysis. We found that, indeed, sBDEVs were particularly enriched in ribosomal proteins, while the non-filtered larger BDEVs were enriched in proteins associated with metabolic pathways (249). By searching recently published literature, we found some studies that used our protocol with modifications, or a completely different protocol using a precipitation method to isolate BDEVs (250). As in these studies also proteomic data was published, we decided to address the question of how the protocol influenced (if so) the protein cargo identified in BDEVs. Thus, we compared the available proteomic raw data from three human and three mouse studies, including our publication (249, 251)(Figure 7).
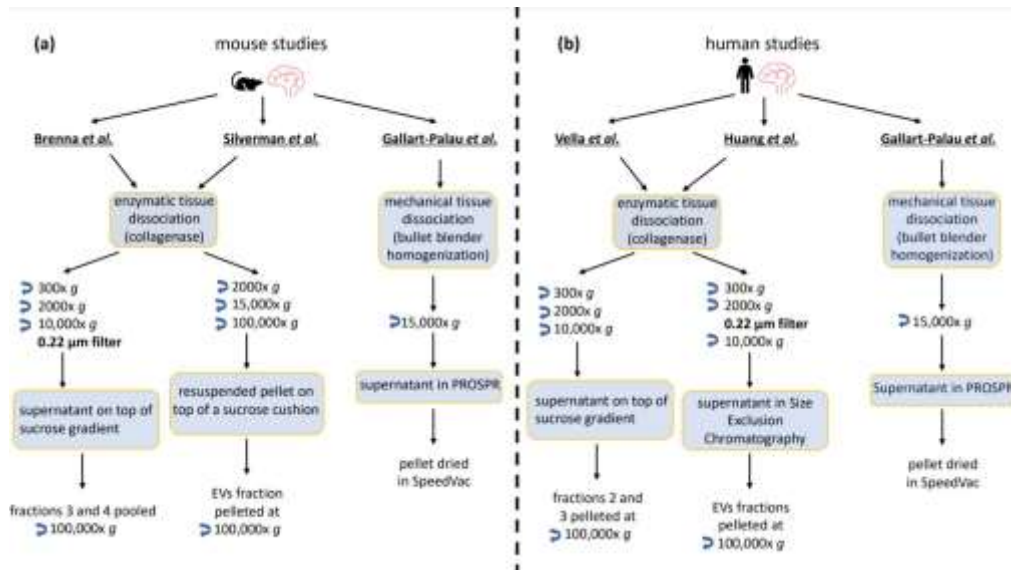
Figure 7: Summarizing scheme of the protocols used for isolation of brain EVs in the studies considered for proteomics comparison. (a) Schematic workflow in the mouse studies. (b) Schematic workflow in human studies. Originally published in (251).

In general, collagenase was the chosen enzyme in all of the protocols (7, 249, 252, 253), except for one, where the tissue dissociation was performed only mechanically, with a bullet blender homogenization (250). The following purification steps included a series of centrifugations, membrane pore filtration through a 0.22 µm filter, either sucrose cushion or density gradients, size exclusion chromatography, or the PROSPR method, which precipitate EVs using organic solvents. A summary of the protocols is shown in Figure 7.

After re-analysis and comparison of the proteomic data from each study, we observed some differences in both, the absolute numbers of proteins detected in each study, and the enrichment of specific gene ontology pathways (GO terms). Specifically, from the six studies, four (among them our study introducing the filtration step) detected an enrichment of ribosomal-related proteins (Figure 8).

We observed that the studies showing an enriched presence of ribosomal proteins shared major steps in the protocols, including ultracentrifugation with sucrose gradients, suggesting that this step isolates BDEVs with similar characteristics and/or contaminants. However, as not all the protocols were completely detailed, differences among the six proteomic data sets could have also depended on other aspects, such as the amount and area (especially in human samples) of tissue used for EVs purification, the mass spectrometric strategy for the analysis, and the mass spectrometer itself. Despite the massive advancement in the last few years in terms of isolation techniques, the characterization and categorization of EVs is still a challenge (28).

- Main cell contributors to the BDEVs' pool in steady-state conditions and after stroke

The cargo of EVs is cell type-dependent and reflects their cellular origin, but it is not an easy issue to assess the cell contribution to the pool of EVs isolated from tissue.
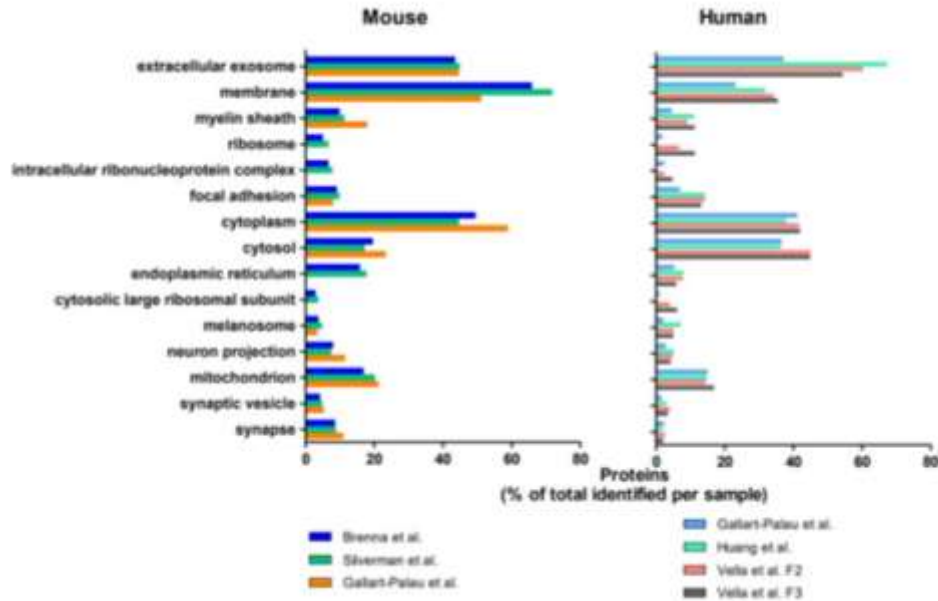
Figure 8: Bar charts showing the 15 most enriched GO Cellular Components (GOCCs) in studies on mice (on the left) and humans (on the right). The gene enrichment analysis was performed with DAVID. Originally published in (251).

Only in a previous study by Silverman et al. (252), also considered in our proteomic comparison study (251), the relative proportion of EVs derived from different brain cell populations was assessed by flow cytometry (FCM). We decided to undertake a different approach, by performing western of 2 specific membrane-bound protein markers and analyze their relative enrichment in BDEVs compared to total murine brain homogenates (249). The G-protein coupled P2Y receptor (P2Y12) and the Transmembrane protein 119 (TMEM119) were used as microglial markers (254, 255), synapsin1 and the Synaptosomal Nerve-Associated Protein 25 (SNAP25) as neuronal markers (256, 257), PLP and 2′-3′-Cyclicnucleotide 3′-phosphodiesterase (CNP) as oligodendrocytes' markers (160, 258) and EAAT-1 and EAAT-2 as astrocytic markers (259). We assessed that, in steady-state conditions, microglia were the main contributor to the whole pool of BDEVs, as P2Y12 and TMEM119 were the most enriched in this fraction compared to the total homogenates. Contrary to us, Silverman et al. detected enrichment of astrocytic and neuronal markers in their pool of BDEVs in steady-state conditions. This difference could depend on the isolation protocol used, as we included a further filtration step which probably enriched for a different subpopulation of EVs. However, because of the detection limit of FCM (400 nm for conventional FCM (260)), it is also plausible that this technique might have excluded sBDEVs from the analysis, which were considered debris. Unlike FCM, western blot analysis includes all the EVs. In our assessment, we also considered that one of the proteins used as cell markers (e.g., P2Y12) could be, per se, more loaded into EVs, without implying the presence of more EVs of microglial origin in the pool of BDEVs. Therefore, we reasoned that by only using one cell marker, this could be the case, but that the probabilities were reduced when two specific cell markers significantly presented the same trend.

Ischemic stroke has different phases (acute, subacute, and chronic) and the molecular mechanisms that are detrimental in the acute phase can turn beneficial in the recovery (subacute/chronic) phase of the disease (261). Moreover, different brain cell types and infiltrating ones are involved, differently contributing to the progression of the pathology over time (262). Interpreting how neurons and glial cells communicate is of utmost importance for understanding the pathophysiology of ischemic stroke and the inner mechanisms of recovery. By using the same methodology as in steady-state conditions, we studied the cellular contribution to the BDEVs pool 24h after stroke/reperfusion. By comparing EVs isolated from sham controls to mice subjected to tMCAO, we observed that 24h after stroke, astrocytes significantly increased their release of EVs. Additionally, we observed that 72h after stroke/reperfusion, oligodendrocytes significantly increased their EVs release.

Astrocytes have several important functions in steady-state and pathological conditions. They regulate synapses and synaptic transmission, immune response, modulation of neuronal excitability, and BBB formation, among others (150, 151). In early time points after stroke, they proliferate, become hypertrophic, and form the glial scar (149, 150). But through EVs, they may also contribute to recovery processes, as neurons exposed to reactive oxygen species (ROS) and hypoxic conditions increased their survival after being incubated with EVs derived from astrocytes (170). Moreover, it was shown that EVs released by astrocytes conferred protection to neurons after OGD treatment, and this property was dependent on the presence of PrP (247). After brain injury, astrocytes and microglia are in close communication with each other, as it was shown that microglia activate astrocytes by releasing inflammatory cytokines and in turn, activated astrocytes contribute to the activation of distant microglia (101, 201, 203, 213, 214). Whether the astrocytic BDEVs increase that we detected in brain 24h after stroke is related to the formation of the glial scar, neuronal survival, or microglial activation, clearly needs further investigations.

Oligodendrocytes are the myelinating cells of the CNS and, besides that after ischemic damage, oligodendrocytes progenitor cells (OPCs) migrate into the penumbra to proliferate and start the remyelination process (154), not much is known about their role after stroke. However, it has been shown that after OGD treatment, neurons can be rescued by oligodendrocyte-derived EVs (210). Oligodendrocytes are also in close communication with microglia, as microglial phagocytosis can be promoted by chemokines and other factors (possibly EVs) released by oligodendrocytes (211). 72h after stroke is a time when recovery processes start to take place, so the increase of EVs derived from oligodendrocytes that we observed at this time-point in brain might be related not only to the neuronal remyelination, but also to neuronal survival and removal of debris, probably via interaction with microglia.

Overall, our results show that there is a high dynamism among brain cell populations after stroke and that BDEVs clearly contribute to the communication among them.

- Transcriptomic analysis of BDEVs after stroke

The pivotal role of microglia 72h after stroke is suggested also by our analysis of the RNA content of BDEVs at this time-point, as we detected that most of the upregulated mRNA in tMCAO mice could be ascribed to microglia.

In this study, we focused on the analysis of the mRNA content of brain EVs 72h after stroke, comparing BDEVs isolated from tMCAO mice to BDEVs isolated from sham mice. We applied a targeted approach using the nCounter© Neuropathology Panel, which allows the simultaneous analysis of 770 genes related to neurotransmission, neuron-glia interaction, and neuroinflammation, among others. We observed that the most upregulated mRNAs in EVs 72h after stroke were related to inflammatory response, stress defense, and recovery processes, and that 13 out of the 20 most upregulated mRNAs that could be ascribed to a cell type, belonged to microglia. The upregulation of the highest top hits, Hmox1, Cd44, C1q, and Gfap, was further confirmed via qPCR and, interestingly, the mRNA was present in full-length in BDEVs, as we could assess by PCR of their open reading frames (ORFs). A few studies reported that the mRNA in EVs is mainly fragmented (263, 264), yet another study performing RNAseq identified full length mRNA (up to 19.000 bp) in EVs isolated from human blood (265). Another study showed that most full-length mRNAs are less than 1 kb (264), even though, similarly to viruses, longer sequences could be packed if condensed (266). In our case Gfap, with approximately 1.5 kb, was present in BDEVs in full-length.

From a methodological point of view, since these panels can also work bypassing the prior step of mRNA isolation, we wanted to investigate if this was also applicable to BDEVs samples, as it has been used so far only in cellular approaches. And indeed, even when incubating the nCounter panels circumventing the mRNA extraction, we obtained similar results to the panels incubated with isolated mRNA, proving the effectiveness of the panel in these settings. This represents a technical advantage as it eliminates non-necessary steps from the protocol, decreasing variability and increasing the chances to detect species that otherwise would be lost. Recent studies using these panels to analyze EVs isolated from human plasma samples and cell cultures supernatants reported the need for intermediate steps, such as RNA retro-transcription and cDNA amplification, as the amount of EVs obtained was too low (267, 268). Since the analysis of RNA from EVs is still a problem in the EVs' research field (269), our results by studying mRNA from EVs obtained from complex tissues represent an important advance for the field, as we gain more knowledge about available tools and techniques to analyze EVs' mRNA.

As already discussed in the previous paragraph, we showed that small BDEVs were enriched in ribosomal proteins when compared to not filtered (larger) BDEVs (249). In the transcriptomic analysis, when comparing small EVs (≤200 nm) and larger EVs (≥200), we did not detect differences in amounts of mRNA. Although we cannot rule out the possibility of technical issues (i.e. the increased amounts of proteins due to the inclusion of larger BDEVs could partially impair mRNA binding to their targets), this could imply that small EVs carry the majority of mRNAs. In this line, a study investigating EVs from cell lines demonstrated that RNA was mainly carried by exosomes, included in the category of small EVs, thus confirming our data (90).

Since BDEVs have been found to carry tRNA (270), it could be hypothesized that BDEVs, unlike EVs isolated from cell lines (10), can deliver most of the translation machinery plus the full-length mRNA to the recipient cells.

Full-length mRNAs in EVs could potentially be translated in the recipient cells and therefore be a source of new proteins. However, to be functional, the mRNA in the EVs must reach the cytoplasm of the recipient cell, which is feasible when the vesicle enters via fusion, but more challenging when the EVs enter via the endocytic pathway, as an "endosomal escape" is then necessary. The transfer of EVs' RNA (and their cargo in general) is difficult to assess, as there is a lack of stoichiometry in experiments and reliable assays to determine cargo's activity (271). Moreover, EVs isolated with different protocols and techniques carry different types of contaminants (e.g RNA-protein complexes) that can bias the experiments. EVs usually carry both, the mRNA and its translated protein, complicating the assessment of direct translation in the recipient cells (272). Thus, studying the biological relevance and proving the functionality of the EVs' mRNA (and other RNA) content is still a major challenge in the field, and while some studies reported the translation in recipient cell of mRNA transferred via EVs (10, 273), other studies point out that this process is minor, if not undetectable (82, 274). We tried to make a rough estimation of the ratio mRNA per EVs in our study, by using the full-length mRNA with the highest counts (Gfap) and the amount of EVs used to load the panel. This resulted in a ratio of approximately 1 mRNA copy every 19.000.000 EVs. Another study estimated from 1 copy every 1000 EVs for the most abundant mRNA, to 1 copy in a million EVs for some RNA species (264). Thus, the possible biological relevance of full-length mRNAs present in these relatively low amounts is difficult to assess, considering our current knowledge and the available tools for analysis.

*-Role of EVs in the immune response*

As discussed in chapter 1.1.8, the dying cells in the ischemic core release ATP, which activates microglia, triggering inflammation (199). The release of extracellular ATP during inflammation is favoured by immune cell activation, cellular stress, or metabolic changes and, to avoid unnecessary damage to healthy tissue, it is of utmost importance that it is rapidly metabolized and degraded by specific enzymes (275). CD39 is an ecto-nucleotidase that dephosphorylates ATP and ADP to AMP(275). CD73, an ecto-5′-nucleotidase, then converts AMP to adenosine, which limits inflammation (275). Regulatory T cells (Tregs) can suppress the immune response by inhibiting T cell proliferation and cytokine production (276). While mouse Tregs express both CD39 and CD73, human Tregs almost do not express CD73 (277, 278). Therefore, it is not known how Tregs in humans perform their immunosuppressive function. In our study, we demonstrated that the amounts of CD73 contained in EVs released upon activation of CD8 T cells, are sufficient to degrade the AMP produced by the high ATPase activity of Tregs (279). The interplay between these cells warrants sufficient immune suppression, as it lowers T cell proliferation and function. We hypothesized that, even though CD73 has a higher enzymatic activity in its soluble form, the EVs-bound form could be an advantage, as it has an extended half-life and presumably a better distribution through body fluids.

Moreover, we analyzed EVs isolated from the synovial fluid (SF) of patients with juvenile idiopathic arthritis (JIA)) to assess the above-mentioned results in the frame of human inflammation. We found that EVs isolated from the SF also carried CD73. These EVs were mainly released by T cells (as they also carried CD8), endothelial, and mesenchymal stem cells. When incubated *in vitro*, they promoted T cell activation and proliferation, probably due to their cargo of cytokines and growth factors (280). However, after the addition of an inhibitor of adenosine deaminase (ADA), which degrades adenosine, and ATP to enhance the purinergic signaling cascade, these EVs showed immunosuppressive activity (279), similarly to CD73-containing EVs released by tumor cells (281). Thus, in sites of inflammation and ischemia, an environment enriched in ATP, the purinergic signaling cascade is pivotal for immune regulation, and EVs play a key role in this process.

-The function of PrP in EVs

Since PrP is a known resident of EVs and is neuroprotective in ischemic conditions, we investigated the presence and the role of PrP in BDEVs from healthy mice and mice subjected to tMCAO (249). Western blot analyses of BDEVs isolated from healthy WT mice revealed enrichment of PrP in the EVs' fractions when compared to total brain homogenates. Interestingly, the pattern of PrP in EVs was different compared to the total homogenates when using a specific antibody against the C-terminal part of the protein (248). A previous study reported that PrP present in EVs was largely not recognized by antibodies against the N-terminal of the protein, suggesting cleavage (234). After treatment with PNGase to remove N-linked glycans, we could observe that the prominent band detected at 34 kDa in BDEVs was the C1 fragment. Thus, we concluded that BDEVs carry mainly PrP-C1 and full-length PrP, both in their di-glycosylated form. The hydrophobic domain N-terminally exposed by C1 after α-cleavage reminds of some fusion peptides of viral surface proteins (224), which allow viruses to dock and fuse with the host cells. The comparison between EVs and viruses traces back to 1975 (282), as it was already observed that they share many similarities (266, 283). Thus, we hypothesized that a possible role for C1 on BDEVs could be the tethering of EVs to recipient cells and/or facilitating their uptake, similarly to what is observed for viral proteins. We incubated labeled BDEVs with primary neurons and we observed that already one hour after incubation BDEVs isolated from PrP$^{0/0}$ mice were readily taken up by neurons and glial cells in higher amounts than BDEVs isolated from WT mice. The WT EVs presented a rather diffuse staining surrounding the plasma membrane, while PrP-KO EVs were rapidly colocalizing with lysosomes. Our data suggest that the presence of PrP and/or PrP-C1 indeed influences fusion events. On the one hand, we observed a more diffuse staining at the plasma membrane when primary neurons were incubated with WT BDEVs. On the other hand, PrP-KO BDEVs were delivered to late endosomes/lysosomes. This indicates that PrP is either enhancing the fusion of EVs at the plasma membrane, or the fusion at endocytic compartments (i.e. endosomal escape), and that only when PrP is missing, EVs end up in the lysosomes (Figure 9). However, it is worth mentioning that WT BDEVs were found (at later time points) also colocalizing with lysosomes, indicating that most likely the balance between

fusion/endocytosis is not only dependent on PrP/PrP-C1, but also on other proteins/ligands.
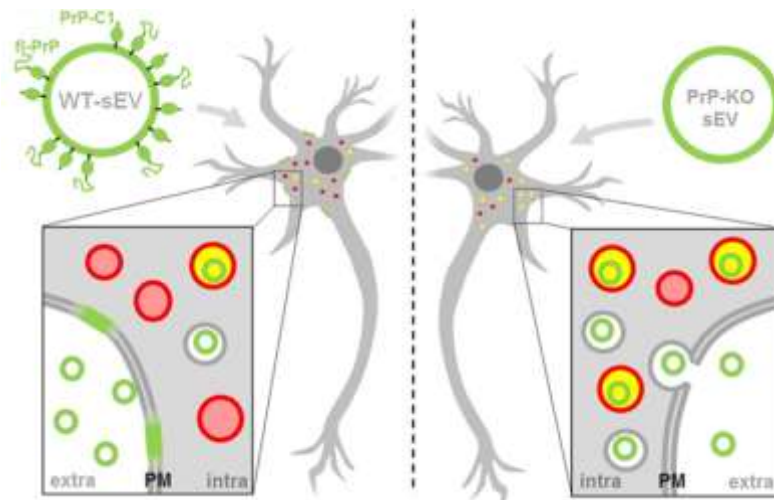
Figure 9: Schematic representation of the differential uptake of WT BDEVs and PrPKO BDEVs, probably influenced by PrP. WT-sEVs (small EVs, on the left) carry both fl-PrP and its C1 fragment. These EVs seemingly fuse with the plasma membrane (PM). PrP-KO EVs (on the right) are rather endocytosed and transported to lysosomes (red circles). Lysosomes containing EVs are coloured in yellow. Originally published in and modified from (249).

Likewise, we cannot rule out that an altered EVs' lipid composition can be responsible for the differential uptake, as it has been shown in vitro that membrane detergent-resistant domains can be modified by the presence of GPI-anchored proteins, such as PrP (284). Therefore, the lack of PrP could influence the type of lipids present in the BDEVs. A previous study reported that for EVs' fusion with purified membrane sheets in a cell-free system, both, the presence of proteins on both surfaces and an acidic pH were necessary (285). As discussed above, how the EVs are taken up by recipient cells is still poorly understood (271), and further studies are clearly necessary to define the possible role of PrP in the EVs' uptake process.

We observed that 24 h after stroke, the amount of PrP is further increased in stroke BDEVs compared to shams. Interestingly, another study showed that EVs released by astrocytes were protective when delivered to primary neurons under ischemic conditions and that this protective effect was dependent on the presence of PrP on EVs. In the same study, the authors also found that after OGD, the amounts of PrP in astrocyte-derived EVs were increased. Apart from the increase of BDEVs-associated PrP after stroke, we also observed an increase in EVs released by astrocytes (249). Due to technical limitations, we could not assess the cell origin of the BDEVs that presented PrP increase, however, the fact that (i) astrocytic EVs are increased and (ii) PrP is increased in BDEVs after stroke, could represent a protective mechanism in the acute phase after stroke and it may have functional consequences in intercellular communication, as it influences the BDEVs uptake. Nevertheless, further studies are necessary to clarify the role of BDEVs-associated PrP.

-Conclusions and future perspectives

Since the publication of the first isolation protocol (6), BDEVs have become important tools for studying intercellular communication in both, healthy and diseased brain. Being the EVs' research field relatively young and rapidly growing, there is a major need for protocol and experimental standardization. As highlighted by our proteomic comparison study, it is important for the sake of reproducibility, to report the exact experiment parameters, such as protein amounts, tissue brain regions, etc., for reliable and reproducible results.

In our studies, we have analyzed BDEVs from WT brains by proteomics, and BDEVs from stroke and sham mice with a transcriptomic approach. Proteomic, lipidomic, and metabolomic analyses at different time points after stroke (from the acute to recovery phase) are still necessary to picture a full overview of the EVs' content. We expect that this kind of study will help us in the understanding of brain communication after ischemic injury, increasing the knowledge of underlying processes in stroke, but also leading to the discovery of new potential therapeutic targets.

However, there are still a lot of open questions about the basic EVs' biology. To bestow them a clear function, one of the main questions to be solved is where does the cargo go, and how it is taken up by recipient cells (271). Since EVs and viruses share similarities (266), and in the latter the entry cell mechanism has been extensively studied for years, it seems logical to learn from the virology field when trying to find answers for EVs' research.

As the study of EVs is so young and there are so many unexplored territories, it represents a fantastic opportunity to bring together different research fields with their specific background and expertise. Only with a highly collaborative spirit this promising field will advance in the exploration of new biomarkers and future therapies.

2. List of abbreviations

Aβ	Amyloid β peptide
AD	Alzheimer's disease
ADAM10	A disintegrin and metalloproteinase 10
AEA	N-arachidonoylethanolamine
ApoEVs	Apoptotic cell-derived extracellular vesicles
APP	Amyloid precursor protein
ATP	Adenosine triphosphate
BBB	Blood-brain barrier
BDEVs	Brain-derived extracellular vesicles
BDNF	Brain-derived neurotrophic factor
BMDC	Bone marrow-derived dendritic cell
BSE	Bovine spongiform encephalopathy
Cas9	CRISPR associated protein 9
CAV-1	Caveolin-1
CJD	Creutzfeldt-Jakob disease
CNS	Central nervous system
CSF	Cerebrospinal fluid
DAMPS	Damage-associated molecular patterns
dsDNA	Double strand DNA
EAAT	Excitatory amino acid transporter
ECM	Extracellular matrix
EE	Early endosomes
EPC	Endothelial progenitor cell
EVs	Extracellular vesicles
GABA	γ-aminobutyric acid
GBM	Glioblastoma
GDNF	Glial cell-derived neurotrophic factor
GLT-1	Glutamate transporter 1
HDL	High-density-lipoprotein

hiPSC	human-induced pluripotential stem cell
hnRNPs	heterogeneous nuclear ribonucleoproteins
HSPs	heat shock proteins
HSPGs	heparan sulphate proteoglycans
ICAM-1	immunoglobulin Intercellular adhesion molecule 1
IDL	Intermediate density lipoprotein
IGF-1	Insulin-like growth factor-1
IGF1R	Insulin-like growth factor-1 receptor
ILVs	Intraluminal vesicles
IS	Ischemic stroke
ISEV	International society for extracellular vesicles
LDL	Low density lipoprotein
LE	Late endosomes
LFA-1	Lymphocyte function-associated antigen 1
lncRNA	Long non-coding RNA
MHC	Major histocompatibility complex
MLC	Myosin light chain
miRNA	microRNA
MS	Multiple sclerosis
mtRNA	Mitochondrial RNA
MVB	Multivesicular bodies
MVE	Multivesicular endosomes
NDs	Neurodegenerative diseases
NMDARs	N-Methyl-D-Aspartate Receptors
NPCs	Neural progenitors cells
NVU	Neurovascular unit
OGD	Oxygen-glucose deprivation
OPCs	Oligodendrocytes progenitors cells
PAMPS	Pathogen-associated molecular patterns

PD	Parkinson's disease
pMCAO	Permanent middle cerebral artery occlusion
PNS	Peripheral nervous system
PrP	Prion protein
PS	Phosphatidylserine
RBPs	RNA-binding proteins
SD	Spreading depolarizations
SEC	Size exclusion chromatography
SM	Sphingomyelin
TCR	T cell receptor
TFF	Tangential flow filtration
TGFBR1	Transforming growth factor beta receptor 1
tMCAO	Transient middle cerebral artery occlusion
UC	Ultracentifugation
UF	Ultrafiltration
VLDL	Very low density lipoprotein
YBX1	Y-box binding protein 1

3. Bibliography

1. Colombo M, Raposo G and Théry C: Biogenesis, secretion, and intercellular interactions of exosomes and other extracellular vesicles. Annu Rev Cell Dev Biol 30: 255-289, 2014.
2. Williams C, Palviainen M, Reichardt NC, Siljander PR and Falcón-Pérez JM: Metabolomics Applied to the Study of Extracellular Vesicles. Metabolites 9, 2019.
3. Vassileff N, Cheng L and Hill AF: Extracellular vesicles - propagators of neuropathology and sources of potential biomarkers and therapeutics for neurodegenerative diseases. J Cell Sci 133, 2020.
4. Street JM, Barran PE, Mackay CL, et al.: Identification and proteomic profiling of exosomes in human cerebrospinal fluid. J Transl Med 10: 5, 2012.
5. Witwer KW, Buzás EI, Bemis LT, et al.: Standardization of sample collection, isolation and analysis methods in extracellular vesicle research. J Extracell Vesicles 2, 2013.
6. Perez-Gonzalez R, Gauthier SA, Kumar A and Levy E: The exosome secretory pathway transports amyloid precursor protein carboxyl-terminal fragments from the cell into the brain extracellular space. J Biol Chem 287: 43108-43115, 2012.
7. Vella LJ, Scicluna BJ, Cheng L, et al.: A rigorous method to enrich for exosomes from brain tissue. J Extracell Vesicles 6: 1348885, 2017.
8. Crescitelli R, Lässer C and Lötvall J: Isolation and characterization of extracellular vesicle subpopulations from tissues. Nat Protoc 16: 1548-1580, 2021.
9. Kim HK, Song KS, Chung JH, Lee KR and Lee SN: Platelet microparticles induce angiogenesis in vitro. Br J Haematol 124: 376-384, 2004.
10. Valadi H, Ekström K, Bossios A, Sjöstrand M, Lee JJ and Lötvall JO: Exosome-mediated transfer of mRNAs and microRNAs is a novel mechanism of genetic exchange between cells. Nat Cell Biol 9: 654-659, 2007.
11. Raposo G, Nijman HW, Stoorvogel W, et al.: B lymphocytes secrete antigen-presenting vesicles. J Exp Med 183: 1161-1172, 1996.
12. Prada I, Gabrielli M, Turola E, et al.: Glia-to-neuron transfer of miRNAs via extracellular vesicles: a new mechanism underlying inflammation-induced synaptic alterations. Acta Neuropathol 135: 529-550, 2018.
13. Janowska-Wieczorek A, Marquez-Curtis LA, Wysoczynski M and Ratajczak MZ: Enhancing effect of platelet-derived microvesicles on the invasive potential of breast cancer cells. Transfusion 46: 1199-1209, 2006.
14. CHARGAFF E and WEST R: The biological significance of the thromboplastic protein of blood. J Biol Chem 166: 189-197, 1946.
15. Wolf P: The nature and significance of platelet products in human plasma. Br J Haematol 13: 269-288, 1967.
16. Aaronson S, Behrens U, Orner R and Haines TH: Ultrastructure of intracellular and extracellular vesicles, membranes, and myelin figures produced by Ochromonas danica. J Ultrastruct Res 35: 418-430, 1971.
17. Trams EG, Lauter CJ, Salem N and Heine U: Exfoliation of membrane ecto-enzymes in the form of micro-vesicles. Biochim Biophys Acta 645: 63-70, 1981.
18. Pan BT and Johnstone RM: Fate of the transferrin receptor during maturation of sheep reticulocytes in vitro: selective externalization of the receptor. Cell 33: 967-978, 1983.
19. Harding C, Heuser J and Stahl P: Receptor-mediated endocytosis of transferrin and recycling of the transferrin receptor in rat reticulocytes. J Cell Biol 97: 329-339, 1983.
20. Johnstone RM, Adam M, Hammond JR, Orr L and Turbide C: Vesicle formation during reticulocyte maturation. Association of plasma membrane activities with released vesicles (exosomes). J Biol Chem 262: 9412-9420, 1987.
21. Johnstone RM, Mathew A, Mason AB and Teng K: Exosome formation during maturation of mammalian and avian reticulocytes: evidence that exosome release is a major route for externalization of obsolete membrane proteins. J Cell Physiol 147: 27-36, 1991.

22. Mack M, Kleinschmidt A, Brühl H, et al.: Transfer of the chemokine receptor CCR5 between cells by membrane-derived microparticles: a mechanism for cellular human immunodeficiency virus 1 infection. Nat Med 6: 769-775, 2000.

23. Rozmyslowicz T, Majka M, Kijowski J, et al.: Platelet- and megakaryocyte-derived microparticles transfer CXCR4 receptor to CXCR4-null cells and make them susceptible to infection by X4-HIV. AIDS 17: 33-42, 2003.

24. Lotvall J and Valadi H: Cell to cell signalling via exosomes through esRNA. Cell Adh Migr 1: 156-158, 2007.

25. Raposo G, Tenza D, Mecheri S, Peronet R, Bonnerot C and Desaymard C: Accumulation of major histocompatibility complex class II molecules in mast cell secretory granules and their release upon degranulation. Mol Biol Cell 8: 2631-2645, 1997.

26. Zitvogel L, Regnault A, Lozier A, et al.: Eradication of established murine tumors using a novel cell-free vaccine: dendritic cell-derived exosomes. Nat Med 4: 594-600, 1998.

27. van Niel G, Raposo G, Candalh C, et al.: Intestinal epithelial cells secrete exosome-like vesicles. Gastroenterology 121: 337-349, 2001.

28. Théry C, Witwer KW, Aikawa E, et al.: Minimal information for studies of extracellular vesicles 2018 (MISEV2018): a position statement of the International Society for Extracellular Vesicles and update of the MISEV2014 guidelines. J Extracell Vesicles 7: 1535750, 2018.

29. Zhang H, Freitas D, Kim HS, et al.: Identification of distinct nanoparticles and subsets of extracellular vesicles by asymmetric flow field-flow fractionation. Nat Cell Biol 20: 332-343, 2018.

30. Anand S, Samuel M and Mathivanan S: Exomeres: A New Member of Extracellular Vesicles Family. Subcell Biochem 97: 89-97, 2021.

31. Witwer KW and Théry C: Extracellular vesicles or exosomes? On primacy, precision, and popularity influencing a choice of nomenclature. J Extracell Vesicles 8: 1648167, 2019.

32. Gruenberg J: Life in the lumen: The multivesicular endosome. Traffic 21: 76-93, 2020.

33. Schmidt O and Teis D: The ESCRT machinery. Curr Biol 22: R116-120, 2012.

34. Babst M: MVB vesicle formation: ESCRT-dependent, ESCRT-independent and everything in between. Curr Opin Cell Biol 23: 452-457, 2011.

35. Wollert T and Hurley JH: Molecular mechanism of multivesicular body biogenesis by ESCRT complexes. Nature 464: 864-869, 2010.

36. Luzio JP, Rous BA, Bright NA, Pryor PR, Mullock BM and Piper RC: Lysosome-endosome fusion and lysosome biogenesis. J Cell Sci 113 (Pt 9): 1515-1524, 2000.

37. Hessvik NP and Llorente A: Current knowledge on exosome biogenesis and release. Cell Mol Life Sci 75: 193-208, 2018.

38. Colombo M, Moita C, van Niel G, et al.: Analysis of ESCRT functions in exosome biogenesis, composition and secretion highlights the heterogeneity of extracellular vesicles. J Cell Sci 126: 5553-5565, 2013.

39. Baietti MF, Zhang Z, Mortier E, et al.: Syndecan-syntenin-ALIX regulates the biogenesis of exosomes. Nat Cell Biol 14: 677-685, 2012.

40. Tamai K, Tanaka N, Nakano T, et al.: Exosome secretion of dendritic cells is regulated by Hrs, an ESCRT-0 protein. Biochem Biophys Res Commun 399: 384-390, 2010.

41. Gross JC, Chaudhary V, Bartscherer K and Boutros M: Active Wnt proteins are secreted on exosomes. Nat Cell Biol 14: 1036-1045, 2012.

42. Stuffers S, Sem Wegner C, Stenmark H and Brech A: Multivesicular endosome biogenesis in the absence of ESCRTs. Traffic 10: 925-937, 2009.

43. Nazarenko I, Rana S, Baumann A, et al.: Cell surface tetraspanin Tspan8 contributes to molecular pathways of exosome-induced endothelial cell activation. Cancer Res 70: 1668-1678, 2010.

44. Chairoungdua A, Smith DL, Pochard P, Hull M and Caplan MJ: Exosome release of β-catenin: a novel mechanism that antagonizes

Wnt signaling. J Cell Biol 190: 1079-1091, 2010.

45. Hurwitz SN, Conlon MM, Rider MA, Brownstein NC and Meckes DG: Nanoparticle analysis sheds budding insights into genetic drivers of extracellular vesicle biogenesis. J Extracell Vesicles 5: 31295, 2016.

46. Del Conde I, Shrimpton CN, Thiagarajan P and López JA: Tissue-factor-bearing microvesicles arise from lipid rafts and fuse with activated platelets to initiate coagulation. Blood 106: 1604-1611, 2005.

47. Hugel B, Martínez MC, Kunzelmann C and Freyssinet JM: Membrane microparticles: two sides of the coin. Physiology (Bethesda) 20: 22-27, 2005.

48. Connor DE, Exner T, Ma DD and Joseph JE: The majority of circulating platelet-derived microparticles fail to bind annexin V, lack phospholipid-dependent procoagulant activity and demonstrate greater expression of glycoprotein Ib. Thromb Haemost 103: 1044-1052, 2010.

49. Cocucci E, Racchetti G and Meldolesi J: Shedding microvesicles: artefacts no more. Trends Cell Biol 19: 43-51, 2009.

50. D'Souza-Schorey C and Clancy JW: Tumor-derived microvesicles: shedding light on novel microenvironment modulators and prospective cancer biomarkers. Genes Dev 26: 1287-1299, 2012.

51. Muralidharan-Chari V, Clancy J, Plou C, et al.: ARF6-regulated shedding of tumor cell-derived plasma membrane microvesicles. Curr Biol 19: 1875-1885, 2009.

52. Cocucci E, Racchetti G, Podini P and Meldolesi J: Enlargeosome traffic: exocytosis triggered by various signals is followed by endocytosis, membrane shedding or both. Traffic 8: 742-757, 2007.

53. Moskovich O and Fishelson Z: Live cell imaging of outward and inward vesiculation induced by the complement c5b-9 complex. J Biol Chem 282: 29977-29986, 2007.

54. Kerr JF, Wyllie AH and Currie AR: Apoptosis: a basic biological phenomenon with wide-ranging implications in tissue kinetics. Br J Cancer 26: 239-257, 1972.

55. Hayakawa K, Esposito E, Wang X, et al.: Transfer of mitochondria from astrocytes to neurons after stroke. Nature 535: 551-555, 2016.

56. Jiang L, Paone S, Caruso S, et al.: Determining the contents and cell origins of apoptotic bodies by flow cytometry. Sci Rep 7: 14444, 2017.

57. Taylor RC, Cullen SP and Martin SJ: Apoptosis: controlled demolition at the cellular level. Nat Rev Mol Cell Biol 9: 231-241, 2008.

58. Coleman ML, Sahai EA, Yeo M, Bosch M, Dewar A and Olson MF: Membrane blebbing during apoptosis results from caspase-mediated activation of ROCK I. Nat Cell Biol 3: 339-345, 2001.

59. Sebbagh M, Renvoizé C, Hamelin J, Riché N, Bertoglio J and Bréard J: Caspase-3-mediated cleavage of ROCK I induces MLC phosphorylation and apoptotic membrane blebbing. Nat Cell Biol 3: 346-352, 2001.

60. Krämer-Albers EM and Hill AF: Extracellular vesicles: interneural shuttles of complex messages. Curr Opin Neurobiol 39: 101-107, 2016.

61. Morelli AE, Larregina AT, Shufesky WJ, et al.: Endocytosis, intracellular sorting, and processing of exosomes by dendritic cells. Blood 104: 3257-3266, 2004.

62. Tian T, Zhu YL, Hu FH, Wang YY, Huang NP and Xiao ZD: Dynamics of exosome internalization and trafficking. J Cell Physiol 228: 1487-1495, 2013.

63. Alvarez-Erviti L, Seow Y, Yin H, Betts C, Lakhal S and Wood MJ: Delivery of siRNA to the mouse brain by systemic injection of targeted exosomes. Nat Biotechnol 29: 341-345, 2011.

64. Mulcahy LA, Pink RC and Carter DR: Routes and mechanisms of extracellular vesicle uptake. J Extracell Vesicles 3, 2014.

65. Kumari S, Mg S and Mayor S: Endocytosis unplugged: multiple ways to enter the cell. Cell Res 20: 256-275, 2010.

66. Escrevente C, Keller S, Altevogt P and Costa J: Interaction and uptake of exosomes by ovarian cancer cells. BMC Cancer 11: 108, 2011.

67. Feng D, Zhao WL, Ye YY, et al.: Cellular internalization of exosomes occurs through phagocytosis. Traffic 11: 675-687, 2010.

68. Lim JP and Gleeson PA: Macropinocytosis: an endocytic pathway for internalising large gulps. Immunol Cell Biol 89: 836-843, 2011.

69. Fitzner D, Schnaars M, van Rossum D, et al.: Selective transfer of exosomes from oligodendrocytes to microglia by macropinocytosis. J Cell Sci 124: 447-458, 2011.

70. Christianson HC, Svensson KJ, van Kuppevelt TH, Li JP and Belting M: Cancer cell exosomes depend on cell-surface heparan sulfate proteoglycans for their internalization and functional activity. Proc Natl Acad Sci U S A 110: 17380-17385, 2013.

71. Nolte-'t Hoen EN, Buschow SI, Anderton SM, Stoorvogel W and Wauben MH: Activated T cells recruit exosomes secreted by dendritic cells via LFA-1. Blood 113: 1977-1981, 2009.

72. Yuyama K, Sun H, Mitsutake S and Igarashi Y: Sphingolipid-modulated exosome secretion promotes clearance of amyloid-β by microglia. J Biol Chem 287: 10977-10989, 2012.

73. Andreu Z and Yáñez-Mó M: Tetraspanins in extracellular vesicle formation and function. Front Immunol 5: 442, 2014.

74. Escola JM, Kleijmeer MJ, Stoorvogel W, Griffith JM, Yoshie O and Geuze HJ: Selective enrichment of tetraspan proteins on the internal vesicles of multivesicular endosomes and on exosomes secreted by human B-lymphocytes. J Biol Chem 273: 20121-20127, 1998.

75. Rana S, Yue S, Stadel D and Zöller M: Toward tailored exosomes: the exosomal tetraspanin web contributes to target cell selection. Int J Biochem Cell Biol 44: 1574-1584, 2012.

76. Hwang I, Shen X and Sprent J: Direct stimulation of naive T cells by membrane vesicles from antigen-presenting cells: distinct roles for CD54 and B7 molecules. Proc Natl Acad Sci U S A 100: 6670-6675, 2003.

77. Hao S, Bai O, Li F, Yuan J, Laferte S and Xiang J: Mature dendritic cells pulsed with exosomes stimulate efficient cytotoxic T-lymphocyte responses and antitumour immunity. Immunology 120: 90-102, 2007.

78. Shukla D, Liu J, Blaiklock P, et al.: A novel role for 3-O-sulfated heparan sulfate in herpes simplex virus 1 entry. Cell 99: 13-22, 1999.

79. Jahn R and Südhof TC: Membrane fusion and exocytosis. Annu Rev Biochem 68: 863-911, 1999.

80. Parolini I, Federici C, Raggi C, et al.: Microenvironmental pH is a key factor for exosome traffic in tumor cells. J Biol Chem 284: 34211-34222, 2009.

81. Valapala M and Vishwanatha JK: Lipid raft endocytosis and exosomal transport facilitate extracellular trafficking of annexin A2. J Biol Chem 286: 30911-30925, 2011.

82. Hung ME and Leonard JN: A platform for actively loading cargo RNA to elucidate limiting steps in EV-mediated delivery. J Extracell Vesicles 5: 31027, 2016.

83. Kanada M, Bachmann MH, Hardy JW, et al.: Differential fates of biomolecules delivered to target cells via extracellular vesicles. Proc Natl Acad Sci U S A 112: E1433-1442, 2015.

84. Sutaria DS, Jiang J, Elgamal OA, et al.: Low active loading of cargo into engineered extracellular vesicles results in inefficient miRNA mimic delivery. J Extracell Vesicles 6: 1333882, 2017.

85. Montecalvo A, Larregina AT, Shufesky WJ, et al.: Mechanism of transfer of functional microRNAs between mouse dendritic cells via exosomes. Blood 119: 756-766, 2012.

86. Théry C, Boussac M, Véron P, et al.: Proteomic analysis of dendritic cell-derived exosomes: a secreted subcellular compartment distinct from apoptotic vesicles. J Immunol 166: 7309-7318, 2001.

87. Palmisano G, Jensen SS, Le Bihan MC, et al.: Characterization of membrane-shed microvesicles from cytokine-stimulated β-cells using proteomics strategies. Mol Cell Proteomics 11: 230-243, 2012.

88. Heijnen HF, Schiel AE, Fijnheer R, Geuze HJ and Sixma JJ: Activated platelets release two types of membrane vesicles: microvesicles by surface shedding and exosomes derived from exocytosis of multivesicular bodies and alpha-granules. Blood 94: 3791-3799, 1999.

89.	Tauro BJ, Greening DW, Mathias RA, et al.: Comparison of ultracentrifugation, density gradient separation, and immunoaffinity capture methods for isolating human colon cancer cell line LIM1863-derived exosomes. Methods 56: 293-304, 2012.

90.	Crescitelli R, Lässer C, Szabó TG, et al.: Distinct RNA profiles in subpopulations of extracellular vesicles: apoptotic bodies, microvesicles and exosomes. J Extracell Vesicles 2, 2013.

91.	Tauro BJ, Greening DW, Mathias RA, Mathivanan S, Ji H and Simpson RJ: Two distinct populations of exosomes are released from LIM1863 colon carcinoma cell-derived organoids. Mol Cell Proteomics 12: 587-598, 2013.

92.	Rajendran L, Honsho M, Zahn TR, et al.: Alzheimer's disease beta-amyloid peptides are released in association with exosomes. Proc Natl Acad Sci U S A 103: 11172-11177, 2006.

93.	de Gassart A, Geminard C, Fevrier B, Raposo G and Vidal M: Lipid raft-associated protein sorting in exosomes. Blood 102: 4336-4344, 2003.

94.	Staubach S, Razawi H and Hanisch FG: Proteomics of MUC1-containing lipid rafts from plasma membranes and exosomes of human breast carcinoma cells MCF-7. Proteomics 9: 2820-2835, 2009.

95.	Phuyal S, Hessvik NP, Skotland T, Sandvig K and Llorente A: Regulation of exosome release by glycosphingolipids and flotillins. FEBS J 281: 2214-2227, 2014.

96.	Sinha A, Ignatchenko V, Ignatchenko A, Mejia-Guerrero S and Kislinger T: In-depth proteomic analyses of ovarian cancer cell line exosomes reveals differential enrichment of functional categories compared to the NCI 60 proteome. Biochem Biophys Res Commun 445: 694-701, 2014.

97.	Kowal J, Arras G, Colombo M, et al.: Proteomic comparison defines novel markers to characterize heterogeneous populations of extracellular vesicle subtypes. Proc Natl Acad Sci U S A 113: E968-977, 2016.

98.	Stoeck A, Keller S, Riedle S, et al.: A role for exosomes in the constitutive and stimulus-induced ectodomain cleavage of L1 and CD44. Biochem J 393: 609-618, 2006.

99.	Krämer-Albers EM, Bretz N, Tenzer S, et al.: Oligodendrocytes secrete exosomes containing major myelin and stress-protective proteins: Trophic support for axons? Proteomics Clin Appl 1: 1446-1461, 2007.

100.	Gosselin RD, Meylan P and Decosterd I: Extracellular microvesicles from astrocytes contain functional glutamate transporters: regulation by protein kinase C and cell activation. Front Cell Neurosci 7: 251, 2013.

101.	Drago F, Lombardi M, Prada I, et al.: ATP Modifies the Proteome of Extracellular Vesicles Released by Microglia and Influences Their Action on Astrocytes. Front Pharmacol 8: 910, 2017.

102.	Holmgren L, Szeles A, Rajnavölgyi E, et al.: Horizontal transfer of DNA by the uptake of apoptotic bodies. Blood 93: 3956-3963, 1999.

103.	Vagner T, Spinelli C, Minciacchi VR, et al.: Large extracellular vesicles carry most of the tumour DNA circulating in prostate cancer patient plasma. J Extracell Vesicles 7: 1505403, 2018.

104.	Guescini M, Genedani S, Stocchi V and Agnati LF: Astrocytes and Glioblastoma cells release exosomes carrying mtDNA. J Neural Transm (Vienna) 117: 1-4, 2010.

105.	Sansone P, Savini C, Kurelac I, et al.: Packaging and transfer of mitochondrial DNA via exosomes regulate escape from dormancy in hormonal therapy-resistant breast cancer. Proc Natl Acad Sci U S A 114: E9066-E9075, 2017.

106.	Thakur BK, Zhang H, Becker A, et al.: Double-stranded DNA in exosomes: a novel biomarker in cancer detection. Cell Res 24: 766-769, 2014.

107.	Jeppesen DK, Fenix AM, Franklin JL, et al.: Reassessment of Exosome Composition. Cell 177: 428-445.e418, 2019.

108.	Sork H, Corso G, Krjutskov K, et al.: Heterogeneity and interplay of the extracellular vesicle small RNA transcriptome and proteome. Sci Rep 8: 10813, 2018.

109.	Mittelbrunn M, Gutiérrez-Vázquez C, Villarroya-Beltri C, et al.: Unidirectional transfer of microRNA-loaded exosomes from T cells to antigen-presenting cells. Nat Commun 2: 282, 2011.

110. Guduric-Fuchs J, O'Connor A, Camp B, O'Neill CL, Medina RJ and Simpson DA: Selective extracellular vesicle-mediated export of an overlapping set of microRNAs from multiple cell types. BMC Genomics 13: 357, 2012.

111. Di Liegro CM, Schiera G and Di Liegro I: Regulation of mRNA transport, localization and translation in the nervous system of mammals (Review). Int J Mol Med 33: 747-762, 2014.

112. Bolukbasi MF, Mizrak A, Ozdener GB, et al.: miR-1289 and "Zipcode"-like Sequence Enrich mRNAs in Microvesicles. Mol Ther Nucleic Acids 1: e10, 2012.

113. Lee H, Li C, Zhang Y, Zhang D, Otterbein LE and Jin Y: Caveolin-1 selectively regulates microRNA sorting into microvesicles after noxious stimuli. J Exp Med 216: 2202-2220, 2019.

114. Shurtleff MJ, Temoche-Diaz MM, Karfilis KV, Ri S and Schekman R: Y-box protein 1 is required to sort microRNAs into exosomes in cells and in a cell-free reaction. Elife 5, 2016.

115. Yanshina DD, Kossinova OA, Gopanenko AV, et al.: Structural features of the interaction of the 3'-untranslated region of mRNA containing exosomal RNA-specific motifs with YB-1, a potential mediator of mRNA sorting. Biochimie 144: 134-143, 2018.

116. Lin F, Zeng Z, Song Y, et al.: YBX-1 mediated sorting of miR-133 into hypoxia/reoxygenation-induced EPC-derived exosomes to increase fibroblast angiogenesis and MEndoT. Stem Cell Res Ther 10: 263, 2019.

117. Iavello A, Frech VS, Gai C, Deregibus MC, Quesenberry PJ and Camussi G: Role of Alix in miRNA packaging during extracellular vesicle biogenesis. Int J Mol Med 37: 958-966, 2016.

118. Chevillet JR, Kang Q, Ruf IK, et al.: Quantitative and stoichiometric analysis of the microRNA content of exosomes. Proc Natl Acad Sci U S A 111: 14888-14893, 2014.

119. He D, Wang H, Ho SL, et al.: Total internal reflection-based single-vesicle in situ quantitative and stoichiometric analysis of tumor-derived exosomal microRNAs for diagnosis and treatment monitoring. Theranostics 9: 4494-4507, 2019.

120. Polanco JC, Scicluna BJ, Hill AF and Götz J: Extracellular Vesicles Isolated from the Brains of rTg4510 Mice Seed Tau Protein Aggregation in a Threshold-dependent Manner. J Biol Chem 291: 12445-12466, 2016.

121. Usman WM, Pham TC, Kwok YY, et al.: Efficient RNA drug delivery using red blood cell extracellular vesicles. Nat Commun 9: 2359, 2018.

122. Carayon K, Chaoui K, Ronzier E, et al.: Proteolipidic composition of exosomes changes during reticulocyte maturation. J Biol Chem 286: 34426-34439, 2011.

123. Llorente A, Skotland T, Sylvänne T, et al.: Molecular lipidomics of exosomes released by PC-3 prostate cancer cells. Biochim Biophys Acta 1831: 1302-1309, 2013.

124. Laulagnier K, Motta C, Hamdi S, et al.: Mast cell- and dendritic cell-derived exosomes display a specific lipid composition and an unusual membrane organization. Biochem J 380: 161-171, 2004.

125. Osteikoetxea X, Balogh A, Szabó-Taylor K, et al.: Improved characterization of EV preparations based on protein to lipid ratio and lipid properties. PLoS One 10: e0121184, 2015.

126. Charoenviriyakul C, Takahashi Y, Morishita M, Matsumoto A, Nishikawa M and Takakura Y: Cell type-specific and common characteristics of exosomes derived from mouse cell lines: Yield, physicochemical properties, and pharmacokinetics. Eur J Pharm Sci 96: 316-322, 2017.

127. Lhermusier T, Chap H and Payrastre B: Platelet membrane phospholipid asymmetry: from the characterization of a scramblase activity to the identification of an essential protein mutated in Scott syndrome. J Thromb Haemost 9: 1883-1891, 2011.

128. Fourcade O, Simon MF, Viodé C, et al.: Secretory phospholipase A2 generates the novel lipid mediator lysophosphatidic acid in membrane microvesicles shed from activated cells. Cell 80: 919-927, 1995.

129. Théry C, Amigorena S, Raposo G and Clayton A: Isolation and characterization of exosomes from cell culture supernatants and

biological fluids. Curr Protoc Cell Biol Chapter 3: Unit 3.22, 2006.

130. Vaswani K, Mitchell MD, Holland OJ, et al.: A Method for the Isolation of Exosomes from Human and Bovine Milk. J Nutr Metab 2019: 5764740, 2019.

131. Prieto-Fernández E, Aransay AM, Royo F, et al.: A Comprehensive Study of Vesicular and Non-Vesicular miRNAs from a Volume of Cerebrospinal Fluid Compatible with Clinical Practice. Theranostics 9: 4567-4579, 2019.

132. Zheng H, Guan S, Wang X, Zhao J, Gao M and Zhang X: Deconstruction of Heterogeneity of Size-Dependent Exosome Subpopulations from Human Urine by Profiling N-Glycoproteomics and Phosphoproteomics Simultaneously. Anal Chem 92: 9239-9246, 2020.

133. Busatto S, Vilanilam G, Ticer T, et al.: Tangential Flow Filtration for Highly Efficient Concentration of Extracellular Vesicles from Large Volumes of Fluid. Cells 7, 2018.

134. Merchant ML, Powell DW, Wilkey DW, et al.: Microfiltration isolation of human urinary exosomes for characterization by MS. Proteomics Clin Appl 4: 84-96, 2010.

135. Rood IM, Deegens JK, Merchant ML, et al.: Comparison of three methods for isolation of urinary microvesicles to identify biomarkers of nephrotic syndrome. Kidney Int 78: 810-816, 2010.

136. McNamara RP, Caro-Vegas CP, Costantini LM, et al.: Large-scale, cross-flow based isolation of highly pure and endocytosis-competent extracellular vesicles. J Extracell Vesicles 7: 1541396, 2018.

137. Sharma S, LeClaire M, Wohlschlegel J and Gimzewski J: Impact of isolation methods on the biophysical heterogeneity of single extracellular vesicles. Sci Rep 10: 13327, 2020.

138. Cheng S, Li Y, Yan H, et al.: Advances in microfluidic extracellular vesicle analysis for cancer diagnostics. Lab Chip 21: 3219-3243, 2021.

139. Royo F, Théry C, Falcón-Pérez JM, Nieuwland R and Witwer KW: Methods for Separation and Characterization of Extracellular Vesicles: Results of a Worldwide Survey Performed by the ISEV Rigor and Standardization Subcommittee. Cells 9, 2020.

140. Gassama Y and Favereaux A: Emerging Roles of Extracellular Vesicles in the Central Nervous System: Physiology, Pathology, and Therapeutic Perspectives. Front Cell Neurosci 15: 626043, 2021.

141. Levy E: Exosomes in the Diseased Brain: First Insights from. Front Neurosci 11: 142, 2017.

142. Anderson CM and Swanson RA: Astrocyte glutamate transport: review of properties, regulation, and physiological functions. Glia 32: 1-14, 2000.

143. Eulenburg V and Gomeza J: Neurotransmitter transporters expressed in glial cells as regulators of synapse function. Brain Res Rev 63: 103-112, 2010.

144. Perea G, Navarrete M and Araque A: Tripartite synapses: astrocytes process and control synaptic information. Trends Neurosci 32: 421-431, 2009.

145. Fields RD and Stevens-Graham B: New insights into neuron-glia communication. Science 298: 556-562, 2002.

146. Ballabh P, Braun A and Nedergaard M: The blood-brain barrier: an overview: structure, regulation, and clinical implications. Neurobiol Dis 16: 1-13, 2004.

147. Drewes LR: What is the blood-brain barrier? A molecular perspective. Cerebral vascular biology. Adv Exp Med Biol 474: 111-122, 1999.

148. Wood MJ, O'Loughlin AJ and Samira L: Exosomes and the blood-brain barrier: implications for neurological diseases. Ther Deliv 2: 1095-1099, 2011.

149. Sofroniew MV: Astrogliosis. Cold Spring Harb Perspect Biol 7: a020420, 2014.

150. Sofroniew MV: Reactive astrocytes in neural repair and protection. Neuroscientist 11: 400-407, 2005.

151. Farina C, Aloisi F and Meinl E: Astrocytes are active players in cerebral innate immunity. Trends Immunol 28: 138-145, 2007.

152. Aloisi F: Immune function of microglia. Glia 36: 165-179, 2001.

153. Gehrmann J, Matsumoto Y and Kreutzberg GW: Microglia: intrinsic immuneffector cell of the brain. Brain Res Brain Res Rev 20: 269-287, 1995.

154. Miron VE, Boyd A, Zhao JW, et al.: M2 microglia and macrophages drive oligodendrocyte differentiation during CNS remyelination. Nat Neurosci 16: 1211-1218, 2013.

155. Schafer DP, Lehrman EK, Kautzman AG, et al.: Microglia sculpt postnatal neural circuits in an activity and complement-dependent manner. Neuron 74: 691-705, 2012.

156. Paolicelli RC, Bolasco G, Pagani F, et al.: Synaptic pruning by microglia is necessary for normal brain development. Science 333: 1456-1458, 2011.

157. Hong S, Dissing-Olesen L and Stevens B: New insights on the role of microglia in synaptic pruning in health and disease. Curr Opin Neurobiol 36: 128-134, 2016.

158. Aono H, Choudhury ME, Higaki H, et al.: Microglia may compensate for dopaminergic neuron loss in experimental Parkinsonism through selective elimination of glutamatergic synapses from the subthalamic nucleus. Glia 65: 1833-1847, 2017.

159. Michailidou I, Willems JG, Kooi EJ, et al.: Complement C1q-C3-associated synaptic changes in multiple sclerosis hippocampus. Ann Neurol 77: 1007-1026, 2015.

160. Bradl M and Lassmann H: Oligodendrocytes: biology and pathology. Acta Neuropathol 119: 37-53, 2010.

161. Fauré J, Lachenal G, Court M, et al.: Exosomes are released by cultured cortical neurones. Mol Cell Neurosci 31: 642-648, 2006.

162. Potolicchio I, Carven GJ, Xu X, et al.: Proteomic analysis of microglia-derived exosomes: metabolic role of the aminopeptidase CD13 in neuropeptide catabolism. J Immunol 175: 2237-2243, 2005.

163. Tytell M: Release of heat shock proteins (Hsps) and the effects of extracellular Hsps on neural cells and tissues. Int J Hyperthermia 21: 445-455, 2005.

164. Chivet M, Javalet C, Laulagnier K, Blot B, Hemming FJ and Sadoul R: Exosomes secreted by cortical neurons upon glutamatergic synapse activation specifically interact with neurons. J Extracell Vesicles 3: 24722, 2014.

165. Lachenal G, Pernet-Gallay K, Chivet M, et al.: Release of exosomes from differentiated neurons and its regulation by synaptic glutamatergic activity. Mol Cell Neurosci 46: 409-418, 2011.

166. Sharma P, Mesci P, Carromeu C, et al.: Exosomes regulate neurogenesis and circuit assembly. Proc Natl Acad Sci U S A 116: 16086-16094, 2019.

167. Xu B, Zhang Y, Du XF, et al.: Neurons secrete miR-132-containing exosomes to regulate brain vascular integrity. Cell Res 27: 882-897, 2017.

168. Bakhti M, Winter C and Simons M: Inhibition of myelin membrane sheath formation by oligodendrocyte-derived exosome-like vesicles. J Biol Chem 286: 787-796, 2011.

169. Luarte A, Henzi R, Fernández A, et al.: Astrocyte-Derived Small Extracellular Vesicles Regulate Dendritic Complexity through miR-26a-5p Activity. Cells 9, 2020.

170. Pascua-Maestro R, González E, Lillo C, Ganfornina MD, Falcón-Pérez JM and Sanchez D: Extracellular Vesicles Secreted by Astroglial Cells Transport Apolipoprotein D to Neurons and Mediate Neuronal Survival Upon Oxidative Stress. Front Cell Neurosci 12: 526, 2018.

171. Antonucci F, Turola E, Riganti L, et al.: Microvesicles released from microglia stimulate synaptic activity via enhanced sphingolipid metabolism. EMBO J 31: 1231-1240, 2012.

172. Gabrielli M, Battista N, Riganti L, et al.: Active endocannabinoids are secreted on extracellular membrane vesicles. EMBO Rep 16: 213-220, 2015.

173. Asai H, Ikezu S, Tsunoda S, et al.: Depletion of microglia and inhibition of exosome synthesis halt tau propagation. Nat Neurosci 18: 1584-1593, 2015.

174. Vingtdeux V, Hamdane M, Loyens A, et al.: Alkalizing drugs induce accumulation of amyloid precursor protein by-products in luminal vesicles of multivesicular bodies. J Biol Chem 282: 18197-18205, 2007.

175. Sardar Sinha M, Ansell-Schultz A, Civitelli L, et al.: Alzheimer's disease pathology propagation by exosomes containing toxic

amyloid-beta oligomers. Acta Neuropathol 136: 41-56, 2018.

176.   Laulagnier K, Javalet C, Hemming FJ, et al.: Amyloid precursor protein products concentrate in a subset of exosomes specifically endocytosed by neurons. Cell Mol Life Sci 75: 757-773, 2018.

177.   Falker C, Hartmann A, Guett I, et al.: Exosomal cellular prion protein drives fibrillization of amyloid beta and counteracts amyloid beta-mediated neurotoxicity. J Neurochem 137: 88-100, 2016.

178.   Pérez-González R, Kim Y, Miller C, Pacheco-Quinto J, Eckman EA and Levy E: Extracellular vesicles: where the amyloid precursor protein carboxyl-terminal fragments accumulate and amyloid-β oligomerizes. FASEB J, 2020.

179.   Saman S, Kim W, Raya M, et al.: Exosome-associated tau is secreted in tauopathy models and is selectively phosphorylated in cerebrospinal fluid in early Alzheimer disease. J Biol Chem 287: 3842-3849, 2012.

180.   Emmanouilidou E, Melachroinou K, Roumeliotis T, et al.: Cell-produced alpha-synuclein is secreted in a calcium-dependent manner by exosomes and impacts neuronal survival. J Neurosci 30: 6838-6851, 2010.

181.   Danzer KM, Kranich LR, Ruf WP, et al.: Exosomal cell-to-cell transmission of alpha synuclein oligomers. Mol Neurodegener 7: 42, 2012.

182.   Ngolab J, Trinh I, Rockenstein E, et al.: Brain-derived exosomes from dementia with Lewy bodies propagate α-synuclein pathology. Acta Neuropathol Commun 5: 46, 2017.

183.   Stuendl A, Kunadt M, Kruse N, et al.: Induction of α-synuclein aggregate formation by CSF exosomes from patients with Parkinson's disease and dementia with Lewy bodies. Brain 139: 481-494, 2016.

184.   Hill AF: Extracellular Vesicles and Neurodegenerative Diseases. J Neurosci 39: 9269-9273, 2019.

185.   Verderio C, Muzio L, Turola E, et al.: Myeloid microvesicles are a marker and therapeutic target for neuroinflammation. Ann Neurol 72: 610-624, 2012.

186.   Willis CM, Nicaise AM, Menoret A, et al.: Extracellular vesicle fibrinogen induces encephalitogenic CD8+ T cells in a mouse model of multiple sclerosis. Proc Natl Acad Sci U S A 116: 10488-10493, 2019.

187.   Kimura K, Hohjoh H, Fukuoka M, et al.: Circulating exosomes suppress the induction of regulatory T cells via let-7i in multiple sclerosis. Nat Commun 9: 17, 2018.

188.   Harshyne LA, Nasca BJ, Kenyon LC, Andrews DW and Hooper DC: Serum exosomes and cytokines promote a T-helper cell type 2 environment in the peripheral blood of glioblastoma patients. Neuro Oncol 18: 206-215, 2016.

189.   Akers JC, Ramakrishnan V, Kim R, et al.: MiR-21 in the extracellular vesicles (EVs) of cerebrospinal fluid (CSF): a platform for glioblastoma biomarker development. PLoS One 8: e78115, 2013.

190.   van der Vos KE, Abels ER, Zhang X, et al.: Directly visualized glioblastoma-derived extracellular vesicles transfer RNA to microglia/macrophages in the brain. Neuro Oncol 18: 58-69, 2016.

191.   Oushy S, Hellwinkel JE, Wang M, et al.: Glioblastoma multiforme-derived extracellular vesicles drive normal astrocytes towards a tumour-enhancing phenotype. Philos Trans R Soc Lond B Biol Sci 373, 2018.

192.   Ciregia F, Urbani A and Palmisano G: Extracellular Vesicles in Brain Tumors and Neurodegenerative Diseases. Front Mol Neurosci 10: 276, 2017.

193.   Guedes VA, Devoto C, Leete J, et al.: Extracellular Vesicle Proteins and MicroRNAs as Biomarkers for Traumatic Brain Injury. Front Neurol 11: 663, 2020.

194.   Zhang ZG and Chopp M: Exosomes in stroke pathogenesis and therapy. J Clin Invest 126: 1190-1197, 2016.

195.   Feigin VL, Norrving B and Mensah GA: Global Burden of Stroke. Circ Res 120: 439-448, 2017.

196.   Rossi DJ, Oshima T and Attwell D: Glutamate release in severe brain ischaemia is mainly by reversed uptake. Nature 403: 316-321, 2000.

197.   Puig B, Brenna S and Magnus T: Molecular Communication of a Dying Neuron in Stroke. Int J Mol Sci 19, 2018.

198.   Hartings JA, Rolli ML, Lu XC and Tortella FC: Delayed secondary phase of peri-

infarct depolarizations after focal cerebral ischemia: relation to infarct growth and neuroprotection. J Neurosci 23: 11602-11610, 2003.

199. Gelderblom M, Sobey CG, Kleinschnitz C and Magnus T: Danger signals in stroke. Ageing Res Rev 24: 77-82, 2015.

200. Buscemi L, Price M, Bezzi P and Hirt L: Spatio-temporal overview of neuroinflammation in an experimental mouse stroke model. Sci Rep 9: 507, 2019.

201. Liddelow SA, Guttenplan KA, Clarke LE, et al.: Neurotoxic reactive astrocytes are induced by activated microglia. Nature 541: 481-487, 2017.

202. Rothhammer V, Borucki DM, Tjon EC, et al.: Microglial control of astrocytes in response to microbial metabolites. Nature 557: 724-728, 2018.

203. Shinozaki Y, Shibata K, Yoshida K, et al.: Transformation of Astrocytes to a Neuroprotective Phenotype by Microglia via P2Y. Cell Rep 19: 1151-1164, 2017.

204. Lalancette-Hébert M, Gowing G, Simard A, Weng YC and Kriz J: Selective ablation of proliferating microglial cells exacerbates ischemic injury in the brain. J Neurosci 27: 2596-2605, 2007.

205. Stolzing A and Grune T: Neuronal apoptotic bodies: phagocytosis and degradation by primary microglial cells. FASEB J 18: 743-745, 2004.

206. Berda-Haddad Y, Robert S, Salers P, et al.: Sterile inflammation of endothelial cell-derived apoptotic bodies is mediated by interleukin-1α. Proc Natl Acad Sci U S A 108: 20684-20689, 2011.

207. Caruso S and Poon IKH: Apoptotic Cell-Derived Extracellular Vesicles: More Than Just Debris. Front Immunol 9: 1486, 2018.

208. Gregory CD and Dransfield I: Apoptotic Tumor Cell-Derived Extracellular Vesicles as Important Regulators of the Onco-Regenerative Niche. Front Immunol 9: 1111, 2018.

209. Bergsmedh A, Szeles A, Henriksson M, et al.: Horizontal transfer of oncogenes by uptake of apoptotic bodies. Proc Natl Acad Sci U S A 98: 6407-6411, 2001.

210. Frühbeis C, Fröhlich D, Kuo WP, et al.: Neurotransmitter-triggered transfer of exosomes mediates oligodendrocyte-neuron communication. PLoS Biol 11: e1001604, 2013.

211. Peferoen L, Kipp M, van der Valk P, van Noort JM and Amor S: Oligodendrocyte-microglia cross-talk in the central nervous system. Immunology 141: 302-313, 2014.

212. Fröhlich D, Kuo WP, Frühbeis C, et al.: Multifaceted effects of oligodendroglial exosomes on neurons: impact on neuronal firing rate, signal transduction and gene regulation. Philos Trans R Soc Lond B Biol Sci 369, 2014.

213. Bianco F, Pravettoni E, Colombo A, et al.: Astrocyte-derived ATP induces vesicle shedding and IL-1 beta release from microglia. J Immunol 174: 7268-7277, 2005.

214. Turola E, Furlan R, Bianco F, Matteoli M and Verderio C: Microglial microvesicle secretion and intercellular signaling. Front Physiol 3: 149, 2012.

215. Yang Y, Boza-Serrano A, Dunning CJR, Clausen BH, Lambertsen KL and Deierborg T: Inflammation leads to distinct populations of extracellular vesicles from microglia. J Neuroinflammation 15: 168, 2018.

216. Morel L, Regan M, Higashimori H, et al.: Neuronal exosomal miRNA-dependent translational regulation of astroglial glutamate transporter GLT1. J Biol Chem 288: 7105-7116, 2013.

217. Bendheim PE, Brown HR, Rudelli RD, et al.: Nearly ubiquitous tissue distribution of the scrapie agent precursor protein. Neurology 42: 149-156, 1992.

218. Puig B, Altmeppen H and Glatzel M: The GPI-anchoring of PrP: implications in sorting and pathogenesis. Prion 8: 11-18, 2014.

219. Biasini E, Turnbaugh JA, Unterberger U and Harris DA: Prion protein at the crossroads of physiology and disease. Trends Neurosci 35: 92-103, 2012.

220. Büeler H, Fischer M, Lang Y, et al.: Normal development and behaviour of mice lacking the neuronal cell-surface PrP protein. Nature 356: 577-582, 1992.

221. Wulf MA, Senatore A and Aguzzi A: The biological function of the cellular prion protein: an update. BMC Biol 15: 34, 2017.

222. Linden R, Martins VR, Prado MA, Cammarota M, Izquierdo I and Brentani RR: Physiology of the prion protein. Physiol Rev 88: 673-728, 2008.

223. Linsenmeier L, Altmeppen HC, Wetzel S, Mohammadi B, Saftig P and Glatzel M: Diverse functions of the prion protein - Does proteolytic processing hold the key? Biochim Biophys Acta Mol Cell Res 1864: 2128-2137, 2017.

224. Altmeppen HC, Puig B, Dohler F, et al.: Proteolytic processing of the prion protein in health and disease. Am J Neurodegener Dis 1: 15-31, 2012.

225. Mohammadi B, Linsenmeier L, Shafiq M, et al.: Transgenic Overexpression of the Disordered Prion Protein N1 Fragment in Mice Does Not Protect Against Neurodegenerative Diseases Due to Impaired ER Translocation. Mol Neurobiol 57: 2812-2829, 2020.

226. Caughey B, Raymond GJ, Ernst D and Race RE: N-terminal truncation of the scrapie-associated form of PrP by lysosomal protease(s): implications regarding the site of conversion of PrP to the protease-resistant state. J Virol 65: 6597-6603, 1991.

227. Chen SG, Teplow DB, Parchi P, Teller JK, Gambetti P and Autilio-Gambetti L: Truncated forms of the human prion protein in normal brain and in prion diseases. J Biol Chem 270: 19173-19180, 1995.

228. Lewis V, Johanssen VA, Crouch PJ, Klug GM, Hooper NM and Collins SJ: Prion protein "gamma-cleavage": characterizing a novel endoproteolytic processing event. Cell Mol Life Sci 73: 667-683, 2016.

229. Taylor DR, Parkin ET, Cocklin SL, et al.: Role of ADAMs in the ectodomain shedding and conformational conversion of the prion protein. J Biol Chem 284: 22590-22600, 2009.

230. Altmeppen HC, Prox J, Puig B, et al.: Lack of a-disintegrin-and-metalloproteinase ADAM10 leads to intracellular accumulation and loss of shedding of the cellular prion protein in vivo. Mol Neurodegener 6: 36, 2011.

231. Linsenmeier L, Mohammadi B, Wetzel S, et al.: Structural and mechanistic aspects influencing the ADAM10-mediated shedding of the prion protein. Mol Neurodegener 13: 18, 2018.

232. Dugger BN and Dickson DW: Pathology of Neurodegenerative Diseases. Cold Spring Harb Perspect Biol 9, 2017.

233. Fevrier B, Vilette D, Archer F, et al.: Cells release prions in association with exosomes. Proc Natl Acad Sci U S A 101: 9683-9688, 2004.

234. Vella LJ, Sharples RA, Lawson VA, Masters CL, Cappai R and Hill AF: Packaging of prions into exosomes is associated with a novel pathway of PrP processing. J Pathol 211: 582-590, 2007.

235. Dias MV, Teixeira BL, Rodrigues BR, et al.: PRNP/prion protein regulates the secretion of exosomes modulating CAV1/caveolin-1-suppressed autophagy. Autophagy 12: 2113-2128, 2016.

236. McLennan NF, Brennan PM, McNeill A, et al.: Prion protein accumulation and neuroprotection in hypoxic brain damage. Am J Pathol 165: 227-235, 2004.

237. Guentchev M, Voigtländer T, Haberler C, Groschup MH and Budka H: Evidence for oxidative stress in experimental prion disease. Neurobiol Dis 7: 270-273, 2000.

238. Mitsios N, Saka M, Krupinski J, et al.: Cellular prion protein is increased in the plasma and peri-infarcted brain tissue after acute stroke. J Neurosci Res 85: 602-611, 2007.

239. Weise J, Crome O, Sandau R, Schulz-Schaeffer W, Bähr M and Zerr I: Upregulation of cellular prion protein (PrPc) after focal cerebral ischemia and influence of lesion severity. Neurosci Lett 372: 146-150, 2004.

240. Doeppner TR, Kaltwasser B, Schlechter J, et al.: Cellular prion protein promotes post-ischemic neuronal survival, angioneurogenesis and enhances neural progenitor cell homing via proteasome inhibition. Cell Death Dis 6: e2024, 2015.

241. Puig B, Yang D, Brenna S, Altmeppen HC and Magnus T: Show Me Your Friends and I Tell You Who You Are: The Many Facets of Prion Protein in Stroke. Cells 9, 2020.

242. Collins SJ, Tumpach C, Groveman BR, Drew SC and Haigh CL: Prion protein cleavage fragments regulate adult neural stem cell quiescence through redox modulation of mitochondrial fission and SOD2 expression. Cell Mol Life Sci 75: 3231-3249, 2018.

243. Lee YJ and Baskakov IV: The cellular form of the prion protein is involved in controlling cell cycle dynamics, self-renewal, and the fate of human embryonic stem cell differentiation. J Neurochem 124: 310-322, 2013.

244. Lin CH, Chiu L, Lee HT, et al.: PACAP38/PAC1 signaling induces bone marrow-derived cells homing to ischemic brain. Stem Cells 33: 1153-1172, 2015.

245. Guillot-Sestier MV, Sunyach C, Druon C, Scarzello S and Checler F: The alpha-secretase-derived N-terminal product of cellular prion, N1, displays neuroprotective function in vitro and in vivo. J Biol Chem 284: 35973-35986, 2009.

246. Carroll JA, Groveman BR, Williams K, Moore R, Race B and Haigh CL: Prion protein N1 cleavage peptides stimulate microglial interaction with surrounding cells. Sci Rep 10: 6654, 2020.

247. Guitart K, Loers G, Buck F, Bork U, Schachner M and Kleene R: Improvement of neuronal cell survival by astrocyte-derived exosomes under hypoxic and ischemic conditions depends on prion protein. Glia 64: 896-910, 2016.

248. Polymenidou M, Moos R, Scott M, et al.: The POM monoclonals: a comprehensive set of antibodies to non-overlapping prion protein epitopes. PLoS One 3: e3872, 2008.

249. Brenna S, Altmeppen HC, Mohammadi B, et al.: Characterization of brain-derived extracellular vesicles reveals changes in cellular origin after stroke and enrichment of the prion protein with a potential role in cellular uptake. J Extracell Vesicles 9: 1809065, 2020.

250. Gallart-Palau X, Serra A and Sze SK: Enrichment of extracellular vesicles from tissues of the central nervous system by PROSPR. Mol Neurodegener 11: 41, 2016.

251. Brenna S, Krisp C, Altmeppen HC, Magnus T and Puig B: Brain-Derived Extracellular Vesicles in Health and Disease: A Methodological Perspective. Int J Mol Sci 22, 2021.

252. Silverman JM, Christy D, Shyu CC, et al.: CNS-derived extracellular vesicles from superoxide dismutase 1 (SOD1). J Biol Chem 294: 3744-3759, 2019.

253. Huang Y, Cheng L, Turchinovich A, et al.: Influence of species and processing parameters on recovery and content of brain tissue-derived extracellular vesicles. J Extracell Vesicles 9: 1785746, 2020.

254. Sasaki Y, Hoshi M, Akazawa C, et al.: Selective expression of Gi/o-coupled ATP receptor P2Y12 in microglia in rat brain. Glia 44: 242-250, 2003.

255. Bennett ML, Bennett FC, Liddelow SA, et al.: New tools for studying microglia in the mouse and human CNS. Proc Natl Acad Sci U S A 113: E1738-1746, 2016.

256. Agliardi C, Guerini FR, Zanzottera M, Bianchi A, Nemni R and Clerici M: SNAP-25 in Serum Is Carried by Exosomes of Neuronal Origin and Is a Potential Biomarker of Alzheimer's Disease. Mol Neurobiol 56: 5792-5798, 2019.

257. Thiel G: Synapsin I, synapsin II, and synaptophysin: marker proteins of synaptic vesicles. Brain Pathol 3: 87-95, 1993.

258. Lappe-Siefke C, Goebbels S, Gravel M, et al.: Disruption of Cnp1 uncouples oligodendroglial functions in axonal support and myelination. Nat Genet 33: 366-374, 2003.

259. Kanai Y, Smith CP and Hediger MA: A new family of neurotransmitter transporters: the high-affinity glutamate transporters. FASEB J 7: 1450-1459, 1993.

260. Erdbrügger U and Lannigan J: Analytical challenges of extracellular vesicle detection: A comparison of different techniques. Cytometry A 89: 123-134, 2016.

261. Lo EH: A new penumbra: transitioning from injury into repair after stroke. Nat Med 14: 497-500, 2008.

262. Gelderblom M, Leypoldt F, Steinbach K, et al.: Temporal and spatial dynamics of cerebral immune cell accumulation in stroke. Stroke 40: 1849-1857, 2009.

263. Batagov AO and Kurochkin IV: Exosomes secreted by human cells transport largely mRNA fragments that are enriched in the 3'-untranslated regions. Biol Direct 8: 12-12, 2013.

264. Wei Z, Batagov AO, Schinelli S, et al.: Coding and noncoding landscape of extracellular RNA released by human glioma stem cells. Nat Commun 8: 1145, 2017.

265. Li Y, Zhao J, Yu S, et al.: Extracellular Vesicles Long RNA Sequencing Reveals Abundant mRNA, circRNA, and lncRNA in Human Blood as Potential Biomarkers for Cancer Diagnosis. Clin Chem 65: 798-808, 2019.

266. Nolte-'t Hoen E, Cremer T, Gallo RC and Margolis LB: Extracellular vesicles and viruses: Are they close relatives? Proc Natl Acad Sci U S A 113: 9155-9161, 2016.

267. Dong L, Huang CY, Johnson EJ, et al.: High-Throughput Simultaneous mRNA Profiling Using nCounter Technology Demonstrates That Extracellular Vesicles Contain Different mRNA Transcripts Than Their Parental Prostate Cancer Cells. Anal Chem 93: 3717-3725, 2021.

268. Bracht JWP, Gimenez-Capitan A, Huang CY, et al.: Analysis of extracellular vesicle mRNA derived from plasma using the nCounter platform. Sci Rep 11: 3712, 2021.

269. Van Deun J, Mestdagh P, Sormunen R, et al.: The impact of disparate isolation methods for extracellular vesicles on downstream RNA profiling. J Extracell Vesicles 3, 2014.

270. Cheng L, Vella LJ, Barnham KJ, McLean C, Masters CL and Hill AF: Small RNA fingerprinting of Alzheimer's disease frontal cortex extracellular vesicles and their comparison with peripheral extracellular vesicles. J Extracell Vesicles 9: 1766822, 2020.

271. Somiya M: Where does the cargo go?: Solutions to provide experimental support for the "extracellular vesicle cargo transfer hypothesis". J Cell Commun Signal 14: 135-146, 2020.

272. Arroyo JD, Chevillet JR, Kroh EM, et al.: Argonaute2 complexes carry a population of circulating microRNAs independent of vesicles in human plasma. Proc Natl Acad Sci U S A 108: 5003-5008, 2011.

273. Skog J, Würdinger T, van Rijn S, et al.: Glioblastoma microvesicles transport RNA and proteins that promote tumour growth and provide diagnostic biomarkers. Nat Cell Biol 10: 1470-1476, 2008.

274. Zomer A, Maynard C, Verweij FJ, et al.: In Vivo imaging reveals extracellular vesicle-mediated phenocopying of metastatic behavior. Cell 161: 1046-1057, 2015.

275. Zimmermann H, Zebisch M and Sträter N: Cellular function and molecular structure of ecto-nucleotidases. Purinergic Signal 8: 437-502, 2012.

276. Sakaguchi S, Miyara M, Costantino CM and Hafler DA: FOXP3+ regulatory T cells in the human immune system. Nat Rev Immunol 10: 490-500, 2010.

277. Deaglio S, Dwyer KM, Gao W, et al.: Adenosine generation catalyzed by CD39 and CD73 expressed on regulatory T cells mediates immune suppression. J Exp Med 204: 1257-1265, 2007.

278. Rissiek A, Baumann I, Cuapio A, et al.: The expression of CD39 on regulatory T cells is genetically driven and further upregulated at sites of inflammation. J Autoimmun 58: 12-20, 2015.

279. Schneider E, Winzer R, Rissiek A, et al.: CD73-mediated adenosine production by CD8 T cell-derived extracellular vesicles constitutes an intrinsic mechanism of immune suppression. Nat Commun 12: 5911, 2021.

280. Fitzgerald W, Freeman ML, Lederman MM, Vasilieva E, Romero R and Margolis L: A System of Cytokines Encapsulated in ExtraCellular Vesicles. Sci Rep 8: 8973, 2018.

281. Clayton A, Al-Taei S, Webber J, Mason MD and Tabi Z: Cancer exosomes express CD39 and CD73, which suppress T cells through adenosine production. J Immunol 187: 676-683, 2011.

282. Dalton AJ: Microvesicles and vesicles of multivesicular bodies versus "virus-like" particles. J Natl Cancer Inst 54: 1137-1148, 1975.

283. van Dongen HM, Masoumi N, Witwer KW and Pegtel DM: Extracellular Vesicles Exploit Viral Entry Routes for Cargo Delivery. Microbiol Mol Biol Rev 80: 369-386, 2016.

284. Morandat S, Bortolato M and Roux B: Role of GPI-anchored enzyme in liposome detergent-resistance. J Membr Biol 191: 215-221, 2003.

285. Bonsergent E and Lavieu G: Content release of extracellular vesicles in a cell-free extract. FEBS Lett 593: 1983-1992, 2019.
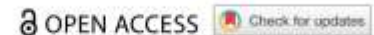
Taylor & Francis
Taylor & Francis Group

RESEARCH ARTICLE

∂ OPEN ACCESS [Check for updates]

Characterization of brain-derived extracellular vesicles reveals changes in cellular origin after stroke and enrichment of the prion protein with a potential role in cellular uptake

Santra Brenna [a], Hermann C. Altmeppen [2], Behnam Mohammadi [2], Björn Rissiek [a], Florence Schlink[a], Peter Ludewig [a], Christoph Krisp[c], Hartmut Schlüter [c], Antonio Virgilio Failla [4], Carola Schneider[e], Markus Glatzel [2], Berta Puig [a] and Tim Magnus [a]

[a]Neurology Department, Experimental Research in Stroke and Inflammation, University Medical Center Hamburg-Eppendorf, Hamburg, Germany; [2]Institute of Neuropathology, University Medical Center Hamburg-Eppendorf, Hamburg, Germany; [c]Institute of Clinical Chemistry and Laboratory Medicine, Mass Spectrometric Proteomics University Medical Center Hamburg-Eppendorf, Hamburg, Germany; [4]UKE Microscopy Imaging Facility, University Medical Center Hamburg-Eppendorf, Hamburg, Germany; [e]Heinrich Pette Institute, Leibniz Institute for Experimental Virology, Hamburg, Germany

ABSTRACT

Extracellular vesicles (EVs) are important means of intercellular communication and a potent tool for regenerative therapy. In ischaemic stroke, transient blockage of a brain artery leads to a lack of glucose and oxygen in the affected brain tissue, provoking neuronal death by necrosis in the core of the ischaemic region. The fate of neurons in the surrounding penumbra region depends on the stimuli, including EVs, received during the following hours. A detailed characterization of such stimuli is crucial not only for understanding stroke pathophysiology but also for new therapeutic interventions. In the present study, we characterize the EVs in mouse brain under physiological conditions and 24 h after induction of transient ischaemia in mice. We show that, in steady-state conditions, microglia are the main source of small EVs (sEVs), whereas after ischaemia the main sEV population originates from astrocytes. Brain sEVs presented high amounts of the prion protein (PrP), which were further increased after stroke. Moreover, EVs were enriched in a proteolytically truncated PrP fragment (PrP-C1). Because of similarities between PrP-C1 and certain viral surface proteins, we studied the cellular uptake of brain-derived sEVs from mice lacking (PrP-KO) or expressing PrP (WT). We show that PrP-KO-sEVs are taken up significantly faster and more efficiently than WT-EVs by primary neurons. Furthermore, microglia and astrocytes engulf PrP-KO-sEVs more readily than WT-sEVs. Our results provide novel information on the relative contribution of brain cell types to the sEV pool in murine brain and indicate that increased release of sEVs by astrocytes together with elevated levels of PrP in sEVs may play a role in intercellular communication at early stages after stroke. In addition, amounts of PrP (and probably PrP-C1) in brain sEVs seem to contribute to regulating their cellular uptake.

Introduction

Extracellular vesicles (EVs) are lipid bilayer structures released from probably almost all types of cells, that carry biologically active molecules, such as proteins, lipids, and extracellular RNAs (e.g. mRNA, miRNA, tRNA and YRNA), and are capable to elicit responses in the receptor cells [1,2]. Although once considered as "platelet dust" or "trash cans", EVs are currently regarded as potent means of intercellular communication and currently represent an intense field of research [3–6]. Exosomes (with a size of 40–150 nm; originating from multivesicular bodies), microvesicles (150–1,000 nm; shed from the plasma membrane) and apoptotic vesicles (ApoEVs; 1,000–5,000 nm; released from cells undergoing apoptosis) are subtypes of EVs. An increasing amount of evidence shows that EVs play important roles in physiological and in pathological conditions [7–9]. Moreover, they are considered as potential disease biomarkers and, given their ability to cross the blood-brain barrier (BBB), are also investigated as tools for tissue- or cell-specific delivery of a therapeutic cargo [10–14].

Stroke is the second most common cause of death and the main cause of disability worldwide, being responsible for ~6 million deaths in 2016 (http://www.who.int/en/news-room/fact-sheets/detail/the-top-10-causes-of-death). Ischaemic stroke accounts for 87%

of cases and is caused by an occluded brain artery, which leads to a temporary lack of glucose and oxygen supply in the affected brain region. Neurons – the most susceptible brain cell population – that are at the core of the stroke will die by necrosis, whereas neurons located in the periphery (penumbra) will enter into electrical silence and, depending on many factors, will either die or survive within the following hours and days [15,16]. The pathophysiology of stroke is very complex and involves several mechanisms such as excitotoxicity and neuroinflammation [17–19]. At present, the only therapeutic approach is recanalization and treatment with recombinant tissue plasminogen activator (rtPA). The latter has a very limited time window of 4.5–6 h after stroke and, thus, only 20% of the stroke patients can benefit from it [20]. Hence, there is an urgent need for novel therapeutic options to be used after this time period. At present, EVs are regarded as tools for regenerative therapy after stroke [21,22].

The cellular prion protein (PrP) is enriched in EVs isolated from cerebral spinal fluid (CSF) and neuronal cells [23–25]. PrP is a cell surface N-glycosylated, GPI-anchored protein mainly located in detergent-resistant domains (also known as lipid rafts) [26], which are important for the biogenesis of EVs [27,28]. Although PrP is highly conserved through evolution and many functions have been suggested, the exact physiological role of PrP is still not well-defined, mainly because knock-out mice for PrP do not present major deficiencies [29,30]. However, under ischaemic conditions, it has been shown that PrP has a protective role. Thus, in mouse models of stroke, PrP-deficient (PrP-KO) mice present an increased stroke volume compared to wild-type (WT) mice [30,31], which can be rescued by PrP overexpression [32,33]. Moreover, mice overexpressing PrP showed improved long-term neuronal recovery after stroke, which was associated with increased neuro- and angiogenesis [34]. Interestingly, in mouse models of ischaemia, but also in brains from patients suffering from stroke, an increase of PrP has been observed at the penumbra area, probably as an attempt to decrease the oxidative stress [35–37]. Last but not least, exosomal PrP secreted by astrocytes under ischaemic conditions had a protective effect on ischaemic neuronal cerebellar cells, but this protection was eliminated when exosomes were exempt from PrP [38]. PrP undergoes several physiological cleavages that are highly conserved in mammals, including the α- and β-cleavage, and shedding near the GPI anchor, which may account for the myriad of functions attributed to PrP [39–41]. The fact that α-cleavage, leading to the formation of a released neuroprotective N1 fragment and a membrane-attached C1 fragment, seems to be performed and ensured by several (yet-to-be-identified) proteases, provides an idea of its biological importance [39,42].

Because of the potential of EVs in stroke therapy [21,43], further understanding and characterization of brain-derived EVs in physiological and under stroke conditions becomes necessary. With this aim, and taking advantage of the recently developed protocols to isolate EVs from brain tissue [44], we show here that (i) microglia are the main cell population to release small EVs (i.e. EVs ≤ 200 nm; sEVs) in steady-state conditions, (ii) brain-derived sEVs are enriched in PrP and, seemingly, in its truncated C1 fragment, and (iii) this may influence the cellular uptake of EVs. Moreover, (iv) lack of PrP on sEVs is a possible factor that increases their uptake by neurons, microglia, and astrocytes. Finally, (v) in a mouse model of stroke, astrocytic contribution to the sEV pool as well as levels of PrP on brain sEVs are significantly increased after 24 h of reperfusion. We hypothesize that regulating the amounts of PrP, and particularly PrP-C1, is a mechanism to modulate EVs uptake and cargo destination by brain cells that may be employed therapeutically in the future. Moreover, a deeper understanding of the increased astrocytic release of EVs in reaction to stroke could lead to a targeted therapy.

Material and methods

Ethics statement

All animal experiments have been conducted after the approval of the local animal care committees (*Behörde für Lebensmittelsicherheit und Veterinärwesen Hamburg*, project number: N45/2018) and in accordance with the guidelines of the animal facility of the University Medical Center Hamburg-Eppendorf (UKE).

Transient middle cerebral artery occlusion (tMCAO)

The tMCAO was performed as previously described in detail [19]. Three-month-old male mice were used for the procedure. tMCAO was achieved by using a 6–0 nylon monofilament to stop the blood supply for 40 min. In the control group ("sham"), animals were also anesthetized, and the arteries were visualized but not disturbed.

Isolation and purification of brain EVs

EVs were isolated from brain as previously described [44] with some modifications. Briefly, frozen brains (either full brain without cerebellum (between 0.31

and 0.33 g) or half of an hemisphere, ipsilateral to tMCAO (between 0.16 and 0.18 g)), stored for not more than one month) from C57BL/6 WT or *Prnp*$^{0/0}$ (PrP-KO) mice [45] (aged between 12–18 weeks) were gently chopped in few drops of Hibernate-E (Gibco) and transferred to a 15 mL tube containing 75 U/mL of collagenase type III (Worthington) in Hibernate-E at a ratio of 800 μL buffer per 100 mg of brain, and incubated in a water bath at 37°C for 20 min. Alternatively, some samples were incubated with 75 U/mL of collagenase type IV (Worthington). During this time, the tube was mixed by inversion every 5 min and pipetted up and down using a 10 mL pipette. Immediately after, the tube was returned on ice and proteinase inhibitors (Complete Protease Inhibitor Tablets, Roche) were added. The sample was then centrifuged at 300xg for 5 min at 4°C and the supernatant collected and further centrifuged at 2,000xg for 10 min at 4°C.

The 2000xg supernatant was again collected and centrifuged at 10,000xg for 30 min at 4°C. To isolate small extracellular vesicles (sEVs), the supernatant was passed through a 0.22 μm sodium acetate filter (GE Healthcare). The resulting flow-through (filtered) or supernatants that were not passed through the filter (non-filtered) was layered on top of a sucrose gradient (0.6 M, 1.3 M, 2.5 M). The gradient was centrifuged at 180,000xg (31,800 rpm in SW40Ti rotor) for 3 h at 4°C and six fractions of 2 mL each were collected, diluted in PBS, and further centrifuged at 100,000xg (24,000 rpm in SW40Ti rotor) at 4°C for 70 min. The final pellet was then resuspended in PBS (for NTA measurements and labelling) or RIPA buffer (for western blots), containing protease and phosphatase inhibitors (PhosSTOP Tablets, Roche). For some experiments, the 300xg pellet (P1) was also collected and further homogenized with RIPA buffer (50 mM Tris-HCl pH = 7.4, 150 mM NaCl, 1% NP40, 0.5% Na-Deoxycholate and 0.1% SDS) containing protease inhibitors, and either non-centrifuged or centrifuged at 10,000xg.

To calculate the density of the sucrose gradient, the six fractions obtained after ultracentrifugation were analysed with an Abbemat 550 refractometer (Anton Paar).

For EVs isolation from media supernatants of mouse neuroblastoma (N2a) cells and a murine hippocampal cell line (mHippoE-14), 15 cm dishes with 80% confluent cells were incubated 24 h with serum-free Opti-MEM (Gibco). After collecting the conditioned media and addition of protease inhibitors, serial centrifugations at 300xg, 2,000xg and 10,000xg were performed with the corresponding supernatants as previously described [46]. After a final centrifugation at 100,000xg (24,000 rpm in SW40Ti rotor) for 70 min, pellets were collected in RIPA buffer and further processed for PNGase digestion and SDS-PAGE and western blot (see below).

Nanoparticle tracking analysis (NTA)

Resuspended pellets resulting from the 100,000xg centrifugation step were used for NTA. Briefly, 1 μL of the final pellet suspension was diluted at 1:5,000 for non-filtered EVs and 1:1,000 for filtered EVs in PBS and 500 μL were loaded into the sample chamber of an LM10 unit (Nanosight, Amesbury, UK). Ten videos of ten seconds were recorded for each sample. Data analysis was performed with NTA 3.0 software (Nanosight). Software settings for analysis were as follows: detection threshold = 6, screen gain = 2.

Fluorescence labelling of EVs

EVs from pooled fractions 3 and 4, in a concentration of 10^{12}/ml, were incubated with 5 nM of mCLING (Synaptic Systems) on ice and in the dark for 5 min. After incubation, the reaction was stopped by adding 1% BSA in PBS. The unincorporated dye was then removed from labelled EVs by centrifugation at 100,000xg at 4°C for 70 min. The final pellet was resuspended in PBS and immediately used for the experiments. As a control, 5 nM of mCLING incubated in PBS without EVs followed the same procedure as described above.

Primary neuronal culture

Primary hippocampal neurons were prepared at P0-P2 as previously described [47]. Briefly, animals were decapitated, the brain was rapidly excised and cleaned from meninges and choroid plexus. Hippocampi were isolated and digested for 30 min at 37°C in 10 mM glucose (500 μL/brain) containing 25 U of papain (Sigma) and 20 μg/mL DNAse (Sigma). Cells were washed several times with plating medium (MEM (Gibco), 10 mM glucose and 10% horse serum) and, after the last wash, cells were mechanically dissociated. 100,000 cells were plated in 12-well plates containing plating medium and poly-L-lysine-coated 13 mm diameter coverslips. After 5 h, the media was changed to Neurobasal-A medium (Gibco) supplemented with 1% B27 (Thermo Fisher), 0.5% Glutamax (Gibco) and 0.1% Gentamicin (Gibco). After 24 h, arabinoside-C (ARA-C, Tocris) was added at a concentration of 15 μM to prevent mitotic proliferation of non-neuronal

cells. Neuronal cultures were kept at 37°C in 5% CO_2 for 14 days and half of the medium was replaced every 3 days.

Co-culturing of neurons with an astrocytic feeder layer

For the co-culture, an astrocyte feeder layer was prepared 21 days in advance from P0/P1 WT mouse pups. Briefly, after isolating the brain and cleaning meninges and choroid plexus, the cortex was removed and put in GGM (Glial Growth Medium: DMEM (Gibco) supplemented with 1.35% glucose, 1% pen/strep and 10% FCS). After addition of pre-warmed 0.25% trypsin (Sigma), the tissue was digested for 15 min at 37°C in a water bath while shaking (300 rpm). After that, 50 µg/mL of DNAse I (Sigma) was added for 1 min and the enzymatic reaction was stopped by adding 4 volumes of GMM. Cells were then washed twice with GGM by centrifuging 5 min at 180xg, the cell suspension was passed through a 70 µm cell strainer and the final cell suspension was plated in T75 flasks with GMM.

For neuronal preparation, P0 mice pups were used as previously described [48]. Briefly, after extracting the brain and cleaning from meninges and choroid plexus, the isolated hippocampi were digested at 37°C for 15 min in dissection media (1× HBSS (Gibco), 1% pen/strep, 10 mM HEPES (Gibco) and 0.6% glucose) containing pre-warmed 0.25% trypsin (Gibco). After the enzymatic digestion, DNAse I (20 µg/mL) was added and incubated at RT for 1 min. GMM was added to quench the enzymatic reaction. Cells were then centrifuged for 5 min at 180xg. The resulting pellet was gently triturated in Neuronal Maintenance Medium (NMM, Neurobasal medium (Gibco) containing 1% glutamax (Gibco), 2% B27 (Gibco) and 1% pen/strep) using a 5 mL pipette followed by a 1 mL pipette. Cells were then centrifuged again for 5 min at 180xg. The pellet was resuspended in NMM and passed through a 70 µm cell strainer. About 40,000 cells were plated in 24-well plates containing pre-coated poly-L-lysin coverslips and NMM. After 2 h, the coverslips were inverted on the top of the pre-cultured feeder layer with a wax-dot spacer in between. After 24 h, the mitotic inhibitor FUDR (2′-Deoxy-5-fluorouridine; Sigma) was added in a concentration of 10 µM. Neuronal cultures were kept at 37°C in 5% CO_2 for 14 days and half of the medium was replaced every 3 days.

Mixed glia culture

Mixed glia cultures were prepared from P0-P2 mice pups. Briefly, animals were decapitated, the brain excised and cleaned from meninges. The cortex was isolated and washed twice with HBSS (Gibco) containing 10 mM HEPES by centrifuging at 310xg for 5 min at 4°C. The tissue was then incubated in digestion solution (HBSS-HEPES 10 mM containing 25 U of papain (Sigma) and 10 µg/mL DNAse) at 37°C for 30 min. Plating media (BME (Gibco) with 10% FCS and 0.1% gentamycin (Gibco)) was added to stop the digestion reaction. Cells were then further centrifuged for 5 min at 310xg, the pellet resuspended in the plating media using a Pasteur pipette and passed through a 70 µm cell strainer. Cells were then plated in T25 flasks or in 12-well plates.

Immunocytochemistry, confocal and STED microscopy

Neurons were incubated for 1, 3, or 6 h with 5 µL (containing about 2.6×10^8 particles as measured with NTA) of sEVs isolated either from WT or PrP-KO brains, previously labelled with mCLING as described above. For the co-culture system, coverslips containing neurons were transferred to another well where the incubation with EVs was taking place without potential influence by the astrocytic feeder layer. After incubation, neurons were fixed with 4% PFA and 0.2% glutaraldehyde in PBS for 10 min, permeabilized for 10 min with 0.5% saponin in PBS, blocked for 30 min with 1% BSA in PBS-Tween (0.1%) and then incubated for 1 h with the primary antibodies (the lysosomal marker LAMP-1 (Invitrogen, 4–1071-82, 1:500), the microglia marker IBA1 (Wako, 019–19,741, 1:500), or the neuronal marker MAP2 (Sigma, M9942, 1:500) diluted in PBS-0.1% BSA. The coverslips were then washed three times with PBS and incubated either with the secondary antibody Alexa Fluor donkey anti-rat 488 (Life Technologies, A21208), Alexa Fluor donkey anti-rabbit 555 (Life Technologies, A31572) or Alexa Fluor donkey anti-rat 555 (Abcam, ab150154, 1:500). Actin labelling was performed by adding at this step Phalloidin-iFluor 488 (Abcam, ab176753, 1:500) diluted in BSA 0.1% in PBS. The coverslips were washed three times with PBS and mounted with DAPI Fluoromount-G (SouthernBiotech, 0100–20). Between 15 and 20 pictures of randomly chosen single neurons per experiment were taken with the 63× immersion oil objective and at a magnification of 3×

with a Leica TCS SP8 confocal microscope. The signal of the 633 nm wavelength corresponding to EVs was quantified and referred to the neuronal cell body area using ImageJ Fiji. Experiments were repeated three times for each time point.

For STED microscopy 15 μL of sEVs labeled with mCLING as previously described, were placed on a coverslip and then mounted with solid mounting medium (Abberior).

STED and corresponding confocal microscopy were carried out in sequential line scanning mode using an Abberior STED expert line microscope. This setup was based on a Nikon Ti-E microscope body and employed for excitation and detection of the fluorescence signal at 60× (NA 1.4) P-Apo oil immersion objective. One pulsed laser was used for excitation at 640 nm and near-infrared pulsed laser (775 nm) for depletion. The detected fluorescence signal was directed through a variable-sized pinhole (set to match 1 Airy at 640 nm) and detected by novel state of the art avalanche photo diodes APDs with appropriate filter settings Cy5 (615–755 nm). Images were recorded with a dwell time of 3 μs and the pixel size was set to be 20 nm. The acquisitions were carried out in time gating mode, i.e. with a time gating width of 8 ns and a delay of 781 ps. After acquisition images were displayed and analysed by the freeware ImageJ Fiji.

Flow cytometry

Mixed culture glia cells were incubated with 5μL (containing about 2.6×10^8 particles as measured with NTA) of WT or PrP-KO sEVs labelled with mCLING for 3 h. Cells were then trypsinized and transferred to FACS tubes containing FACS buffer (PBS with 1 mM EDTA and 0.2% BSA). Cells were centrifuged for 5 min at 4°C at 310xg, washed in FACS buffer and centrifuged again. Cells were stained for 30 min on ice with anti-CD11b–FITC (1:100; Clone M 1/70, Biolegend) and anti-GLAST-PE (1:100; MiltenyiBiotec) in the presence of Fc Block (1:100; Bio X Cell) in FACS buffer, washed two times with FACS buffer and finally resuspended in 200 μL of FACS buffer. Measurements were done with a BD FACSCanto™ II and analysed with FlowJo.

Western blot

The total protein content in total homogenates (TH), 300xg pellets and cell lysates (CL) was assessed with the Pierce BCA Protein assay kit (Thermo Scientific) following the instructions of the supplier. For brain-derived EVs, brain-derived sEVs and N2a and mHippo E-14 EVs the total protein content was

assessed with Micro BCA Protein assay kit (Thermo Scientific) following the instructions of the supplier. Samples were then denatured at 70°C for 10 min with NuPage LDS Sample Buffer (Invitrogen) and NuPage sample reducing agent (Invitrogen) and equal amounts of protein were then loaded on precast NuPage 10% Bis-Tris protein gels (Invitrogen). After electrophoretic separation, proteins were transferred onto nitrocellulose membranes (LI-COR) by wet-blotting. The membranes were then stained with Revert Total Protein Stain (LI-COR) following the manufacturer´s protocol to detect total amounts of protein. Membranes were subsequently blocked for 1 h with Rotiblock (Roth) and incubated with primary antibody overnight at 4°C on a shaking platform. The antibodies used were: rabbit antibody against Alix (1:500; #ABC40, Millipore; for some experiments on the Suppl. Fig. another antibody (#2171 CST) was used at 1:400), mouse monoclonal against CNP (1:1000; #C5922, Sigma), rabbit monoclonal against CD81 (1:1000; #10037, Cell Signalling), rabbit antibody against EAAT1 (1:1000; #NB100-1869SS, Novusbio), rabbit antibody against EAAT2 (1:500; #NBP1-20136SS, Novusbio), mouse antibody against flotillin-1 (1:1000; #610820, BD Biosciences), mouse antibody against GM130 (1:1000; #610822, BD Biosciences), rabbit antibody against PLP (1:1000; #NB100-74503, Novusbio), rabbit antibody against P2Y12 (1:500; #LS-C209714, LSBio), mouse monoclonal antibody against PrP (POM1; 1:2000 [49]), rabbit antibody against SNAP-25 (1:1000; #3926, Cell Signalling), rabbit antibody against synapsin1 (1:1000; #106103, Synaptic Systems), mouse monoclonal antibody against PSD95 (1:1000; # MABN68, Millipore), and mouse monoclonal antibody against TMEM119 (1:1000; #66948-1-Ig, Proteintech). After washing with TBST, membranes were incubated for 1 h with the respective HRP-conjugated secondary antibodies (1:1000, Cell Signalling) and subsequently washed 6× with TBST. After incubation with Pierce ECL Pico or Super Signal West Femto substrate (Thermo Fisher Scientific), chemiluminescence was detected with a ChemiDoc imaging station (BioRad) and quantified densitometrically using Image Studio software (LI-COR).

PNGase F assay

For removal of the N-linked glycans attached to PrP and its C1 fragment, sEV samples and total homogenates (TH) were digested with PNGase F (New England Biolabs) according to the manufacturer´s protocol.

Electron microscopy

Pellets from the 100.000xg centrifugation step were fixed with 4% PFA containing 2.5% glutaraldehyde in PBS and adsorbed in cellulose capillary tubes. Subsequently, the pellets were washed with PBS, post-fixed for 30 min with 1% OsO_4 in PBS, washed with ddH_2O, and stained with 1% uranyl acetate in water. The samples were gradually dehydrated with ethanol and embedded in Epon resins (Carl Roth) for sectioning. Ultrathin 50 nm sections were prepared using an Ultracut Microtome (Leica Microsystems). The sections were poststained with 2% uranyl acetate. Electron micrographs were obtained with a 2 K wide-angle CCD camera (Veleta, Olympus Soft Imaging Solutions GmbH) attached to a FEI Tecnai G 20 Twin transmission electron microscope (FEI) at 80kv.

Differential quantitative mass spectrometric proteomics

For proteomics, the final pellet containing either non-filtered or filtered (sEVs) EVs was resuspended in 10 mM of HEPES buffer pH 7.8. Twenty µg of protein per sample were diluted in 100 mM triethaylammonium bicarbonate (TEAB, Thermo Fisher) and 1% (w/v) sodium deoxycholate (SDC, Sigma Aldrich) buffer to a total volume of 100 µL. Subsequently, samples were incubated for 30 min at 60°C in the presence of 10 mM Dithiotreitol (DTT, Sigma Aldrich) to reduce disulphate bonds and 20 mM iodoacetamide (IAA, Sigma Aldrich) was added to alkylate cysteine residues. Proteins were subjected to tryptic digestion (1:50 protein to enzyme ratio, sequencing grade, Promega) over night at 37°C. SDC was precipitated by the addition of 1% formic acid (FA, Fluka), removed by centrifugation, and the supernatant was then dried in a vacuum centrifuge.

Per sample, 1 µg of peptides were separated on a 50 cm C18 reversed phase column (Acclaim PepMap100 C18, 3 µm, 100 Å, 75 µm × 50 cm) within a 60 min gradient from 2% to 30% acetonitrile (equilibration buffer: 0.1% formic acid; elution buffer: 99.9% acetonitrile and 0.1% formic acid) at a flow rate of 300 nL/min using a nano-UPLC system (DionexUltiMate 3000, Thermo Fisher Scientific), coupled via electrospray ionization (ESI) to a tribid mass spectrometer equipped with a quadrupole, an orbitrap, and an ion trap (Fusion, Thermo Fisher Scientific), using data dependent acquisition (DDA) mode in quadrupole-orbitrap-iontrap mode. Here, after a survey scan (orbitrap 400–1300 m/z, 2×10^5 ions, 120 ms max fill time, 120,000 resolution), the most intense ions (charge stages 2^+-5^+, dynamic exclusion of 30 s) were fragmented and resulting fragment ions analysed by MS/MS within a cycle time of 3s (iontrap 28 normalised collision energy, HCD, 1×10^4 ions, 60 ms max. fill time, 1.6 m/z isolation window).

The obtained peptide spectra were searched with the search engine Andromeda (integrated in MaxQuant software version 1.6.3, Max Planck Institute of Biochemistry, Munich, Germany) using the mouse Uniprot protein database (EMBL; Hinxton Cambridge, UK, release October 2019, 17,013 entries), with carbamidomethylation on cysteine residues as fixed modification and the oxidation of methionine as well as the protein N-terminal acetylation as variable modifications. The error tolerance for the first precursor search was 20 ppm, for the following main search 4.5 ppm. Fragment spectra were matched with a 20 ppm error tolerance. Label-free quantification and match between runs was enabled. False discovery rate for proteins and peptides was set to 1%.

Protein-protein interactions (PPI) network construction

Protein sets that were statistically significantly up/downregulated between filtered (sEVs) and non-filtered brain-derived EVs were analysed with the online database STRING (v11.0, https://string-db.org/) using a high-confidence score (cut-off ≥0.9) and the evidence mode in the settings [50]. We further analysed the data using the FunRich 3.1.1 analysis tool for graphical representation of functional enrichment analyses [51].

Statistical analysis

For statistical analysis of mass spectrometry results, the MaxQuant Protein Group output files were imported into the Perseus software (Max Planck Institute of Biochemistry, Munich, Germany). Proteins which had at least three valid values in at least one of the groups were kept for further analysis. Therefore, missing values were imputed by a downwards shifted normal distribution. Each sample was then normalized by the median protein area per sample and Student's *t*-test, principal component analysis and hierarchical clustering was performed. Proteins were considered to be significantly different in abundance if the Student's *t*-test based *p* value was ≤ 0.05 and at least a 1.5-fold change in either direction was observed.

The GraphPad Prism 8 statistic software program was used for statistical analysis of western blot, NTA and immunohistochemistry results. To assess differences between the THs and the corresponding sEVs,

as well as between sEVs from sham and strokes in western blot, after passing a normality test, either a paired or unpaired t-test was used, respectively. NTA measurements were assessed by unpaired t-test. Statistical significance was considered when p values were as follows: $^*p < 0.05$, $^{**}p < 0.005$ and $^{***}p < 0.001$. Values are given as mean ± SEM. The exact p value is given in the text.

Results

Characterization of brain-derived EVs

Recently, the isolation of EVs from brain has become an important tool to study crucial events in the propagation of misfolded proteins in neurodegenerative diseases [52]. We took advantage of a recently published protocol [44] to study the expression of PrP in brain-derived EVs, and to assess the cell populations that mainly release EVs in both, steady-state conditions and after experimental stroke. Since the guidelines of the *International Society for Extracellular Vesicles* recommend to rather differentiate between small EVs (sEVs; ≤200 nm) and medium/large EVs (≥ 200 nm) instead of exosomes and microvesicles/ectosomes [53], we introduced in the above-mentioned protocol an extra filtration step with a 0.22 μm filter before the samples were loaded in the sucrose gradient to differentiate between these two EVs pools (see Material and Methods). As shown in Figure 1A, six fractions from either non-filtered or filtered samples were collected and analysed by western blot. In the non-filtered samples, a higher amount of total protein (as shown with the total staining, TS) was detected in all fractions compared to the respective filtered ones, but in both cases fractions 3 to 5 (corresponding to a density of 1.11 to 1.25 g/mL as measured with the refractometer) were enriched in known markers of EVs such as the cytosolic protein Alix (96 kDa), the membrane-bound flotillin-1 (49 kDa), and the tetraspanin CD81 (26 kDa) [53,54]. GM130 (130 kDa), a resident protein of the cis-Golgi, was used as 'proof of no contamination' marker. The total brain homogenate (TH) is shown for comparison. Fractions 3 (density 1.11 g/mL) and 4 (density 1.16 g/mL) were pooled for all further experiments. When assessed with transmission electron microscopy (TEM), non-filtered samples showed a combination of small and large vesicles, whereas in filtered samples the population appeared more homogeneous (Figure 1B). To confirm that the EVs could be marked and visualized by microscopy for further experiments, we labelled them using the mCLING dye, which has the capacity to emit fluorescence only

when intercalated into the lipid bilayer [55]. When isolated EVs were stained, fixed and mounted on coverslips, we compared the signal obtained by confocal microscopy with the one obtained by *Stimulated Emission Depletion* (STED) microscopy (Figure 1C). Due to the higher resolution, the blurred signal obtained with confocal microscopy (in green) was transformed to single dots corresponding to individual EVs in STED (in red), although some aggregates (probably corresponding to clustered EVs) were also present.

Finally, *Nanoparticle Tracking Analysis* (NTA, Figure 1D) revealed a decrease in the number of events counted in the filtered $(1.5 \times 10^{12} \pm 5.8 \times 10^{10})$ compared to the non-filtered samples $(4.5 \times 10^{12} \pm 3.5 \times 10^{11})$; $p = 0.0002$), together with a confirmatory decrease in mean EV size (211.7 ±1.9 nm in non-filtered vs 188.3 ±2 nm in filtered samples; $p = 0.0004$). Note that the filtered samples still contained some vesicles of more than 200 nm, suggesting that some larger EVs may squeeze through the 0.2 μm filter or representing clustered sEVs.

To assess whether the filtration step was helping to differentiate EV populations by their protein composition, we performed quantitative mass spectrometric proteome analysis of brain EVs isolated from WT mice with ($n = 4$) or without ($n = 4$) the 0.2 μm filtration step. A total of 1531 proteins were identified across all samples. Figure 2A shows the heat map corresponding to the proteins found to be relatively increased in non-filtered EVs (106 proteins; $p \leq 0.05$) compared to filtered EVs and vice versa (121 proteins were significantly increased in filtered EVs compared to non-filtered, $p \leq 0.05$). A list of all identified proteins is shown in Suppl. Table 1. The volcano plot in Figure 2B depicts the distribution of the proteins' fold-increase related to their p value. The names of proteins with a fold change either higher than a $\log_2$ value of 1, lower than a $\log_2$ value of −1, or with a minor $\log_2$ fold change but a $\log_{10}$ (p value) above 3 (highly significant) are provided in the volcano plot. Principal Component Analysis (PCA) shows separate clustering of both populations, filtered and non-filtered EVs (Suppl. Fig. 1). We next analysed proteins not found in filtered EVs in contrast to non-filtered EVs (and vice versa) considering proteins quantified in at least 3 out of 4 replicates per group and found that only 6 proteins were exclusively present in filtered EVs, whereas 34 proteins were exclusively present in non-filtered EVs (Suppl. Table 2).

The list of proteins being present in significantly different amounts in the compared samples were further analysed with FunRich 3.1.1. Gene Ontology of Molecular Function of the enriched proteins. In
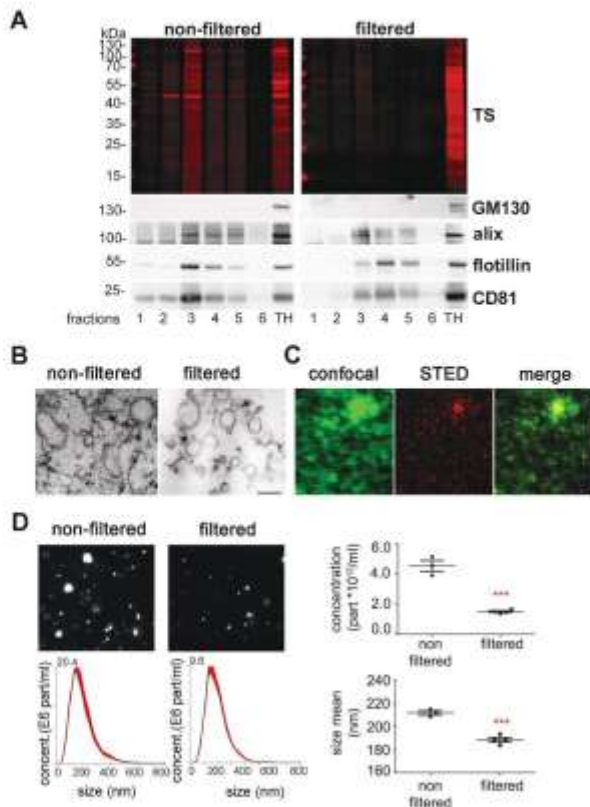
Figure 1. Characterization of brain EVs. (A) Representative western blots of the six fractions obtained after sucrose gradient centrifugation, from samples that were either passed through a 0.22 μm filter (filtered, sEVs) or not (non-filtered EVs). The total protein staining (TS, used as a loading control) shows a decrease in the total protein amount for the filtered samples. The cytosolic protein alix (96 kDa) and the membrane-bound proteins flotillin-1 (49 kDa) and CD81 (26 kDa), all considered as markers of EVs, were found in both cases mainly in fractions 3 and 4. The Golgi resident protein GM130 was used as a marker of non-EVs (negative control). (B) Representative transmission electron microscopy (TEM) images of pooled fractions 3 and 4 from non-filtered and filtered EVs. As seen for the TS in the western blot, the filtered fraction shows a decrease in EVs and a more uniform population. Scale bar represents 0.2 μm. (C) Confocal (green signal) and STED (red signal) images from pooled sEVs labeled with mCLING and the merge of both showing that, with high-resolution STED imaging, the blurry dots in the confocal correspond to single (or clusters of) EV particles. (D) Representative frames and concentration/size graphs from Nanoparticle Tracking Analysis (NTA) of pooled non-filtered and filtered EVs. Concentration (in particles/mL) and mean size (in nm) analysis of non-filtered pooled EVs (n = 3 preparations) and filtered pooled EVs (n = 4) show a significant reduction in concentration and mean size of EVs after filtration. Values are reported in the main text.

filtered EVs analysis showed an increase of proteins related to translation (gene ontology term (GO) "structural constituent of ribosome" GO:0003735), whereas
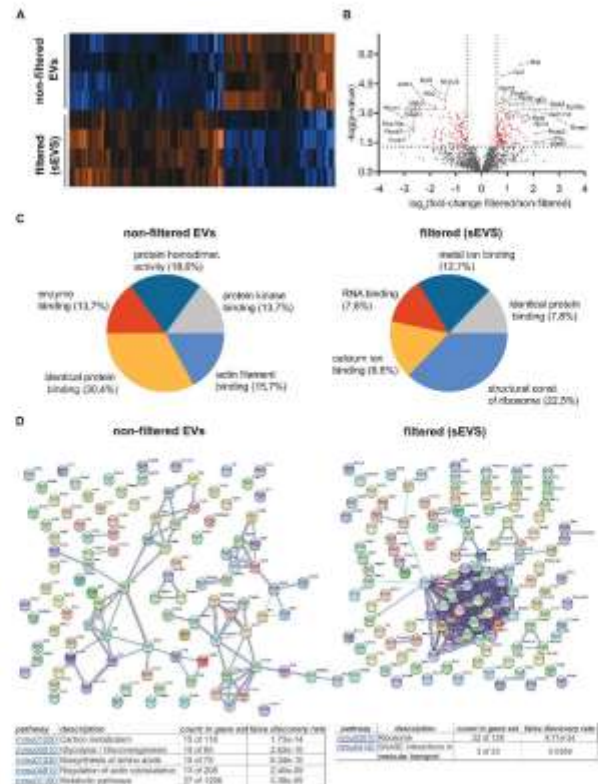
Figure 2. Differential quantitative proteome analysis of non-filtered versus filtered brain-derived EVs. (A) Heat map of the proteins identified by proteomics that were significantly different from non-filtered compared to filtered brain EVs. (B) Volcano plot showing the log2 fold-change on the x-axis and the statistical significance on the y-axis for proteins that were significantly differently abundant in filtered versus non-filtered brain EVs. The names of proteins that had a fold-change ≥ 2 are shown in the plot. (C) Pie charts showing the gene ontology analysis (GO) of Molecular Function for the proteins that were found to be significantly increased more than 1.5-fold (log2 more than 0.58) using the FunRich analysis tool. The five most representative pathways showing the percentage of proteins belonging to these pathways are shown. (D) Protein–protein interaction analysis (STRING database) of the proteins that were significantly upregulated in non-filtered and in filtered EVs (log2 more than 0.58). In order to create the network, a confidence score threshold of 0.9 (very high) and no text-mining options were selected. KEGG pathways obtained by this analysis are shown for each group.

in non-filtered EVs we found a relative increase in proteins that interact selectively with identical proteins (GO:0042802, "identical protein binding") Figure 2C. In order to visualize how these proteins are related, we also performed STRING analysis (Figure 2D). By using evidence settings and the highest stringency (0.09), we confirmed that many proteins related to ribosomal function were clustered together in filtered EVs. KEGG (Kyoto Encyclopaedia of Genes and Genomes)

pathways analysis also show an enrichment of proteins related to ribosomal and SNAREs vesicular transport pathways for filtered EVs (see tables in Figure 2D).

Assessment of the relative contribution of major brain cell types to the sEV pool indicates microglia as a dominant source of sEVs under physiological conditions

To study the relative contribution of different brain cell populations to the whole pool of brain sEVs in physiological conditions, we assessed enrichment of known cell type-specific markers in sEVs relative to their signal in total brain homogenate (TH) by western blot analysis (Figure 3A). Each sample's signal was first referred to the respective signal of the total staining (TS) as a loading control and then, the mean value obtained in sEVs samples ($n = 4$) was compared to the mean value obtained in the corresponding TH ($n = 4$). Since it could be that a given marker protein is more strongly sorted into sEVs than others (and thus not directly indicating the relative contribution of this cell population to the total pool of sEVs), we decided to assess two (exclusively membrane-bound) marker proteins per cell type in order to reduce the risk of misinterpretation. The G-protein coupled P2Y receptor (P2Y12) and the Transmembrane protein 119 (TMEM119) were chosen as microglial markers [56,57]; PLP (proteolipid protein, a major component of the myelin sheath) and 2'-3'-Cyclicnucleotide 3'-phosphodiesterase (CNP) were used as oligodendrocyte markers [58,59]; synapsin1 and the Synaptosomal Nerve-Associated Protein 25 (SNAP25), present at the membrane of synaptic vesicles and at the pre/post-synaptic membrane respectively, were assessed as neuronal markers [60–65], and the Excitatory Amino Acid Transporters 1 and 2 (EAAT-1 and EAAT-2) were used as astrocytic markers [66]. Quantifications are shown in Figure 3B. We observed that, in steady-state conditions, markers for microglia were mainly contributing to the pool of brain sEVs, as P2Y12 (2.5-fold increased; TH set to 100%±3.9%; sEVs: 247.5 ±12.4%; $p = 0.0073$) and TMEM119 (1.7-fold increased; TH set to 100% ±5.5%; sEVs: 168.7 ±8.6%; $p = 0.0119$) were most drastically enriched in the sEVs fractions compared to the TH. Interestingly, TMEM119 presented a band at around 55 kDa in the TH, whereas in the sEV-enriched fractions, a main band was observed around 20 kDa. Because four isoforms have been described for TMEM119, this lower band could correspond either to a truncated version of TMEM119 or to one of the four isoforms, probably also lacking the O-glycan modification [67]. The oligodendrocyte marker PLP showed

a slight yet non-significant relative increase (TH was set to 100% ±4.7%; sEVs: 138.9% ±11%;$p = 0.1$), whereas the other oligodendrocyte marker CNP1 revealed no differences (TH set to 100% ±15.3%; sEVs: 97.2% ±12.4%). In contrast, the neuronal marker synapsin 1 (syn-1; TH set to 100% ±12.9%; sEVs: 78.1% ±4.9%;$p = 0.050$) and SNAP25 (TH set to 100% ±3.7%; sEVs: 22.4% ±4.3%;$p = 0.0018$) were significantly decreased in the sEVs in comparison to the TH, thus implying that neuronal sEVs rather represent a minor fraction in the brain sEV pool under normal conditions. The presence of SNAP25 and synapsin 1 could indicate synaptosomal contamination due to the EVs isolation procedure. However, another protein highly enriched in synaptosomes, the post-synaptic density protein 95 (PSD95), was not detectable in EVs by western blot, thus excluding a major synaptosomal contamination (Suppl. Fig 2). Lastly, the astrocytic markers EAAT-1 and EAAT-2 showed no significant differences in sEVs compared to the TH (for EAAT-1: TH set to 100% ±4.6%; sEVs: 95.9% ±6.7%/for EAAT-2: TH set to 100% ±14.8%;sEVs: 48% ±14.8%), indicating presence but no relative enrichment of astrocytic sEVs in the total pool (Figure 3B). Thus, neurons and astrocytes only show a moderate contribution to the total sEVs pool in brain, whereas oligodendrocytic and, significantly, microglial sEVs are relatively enriched.

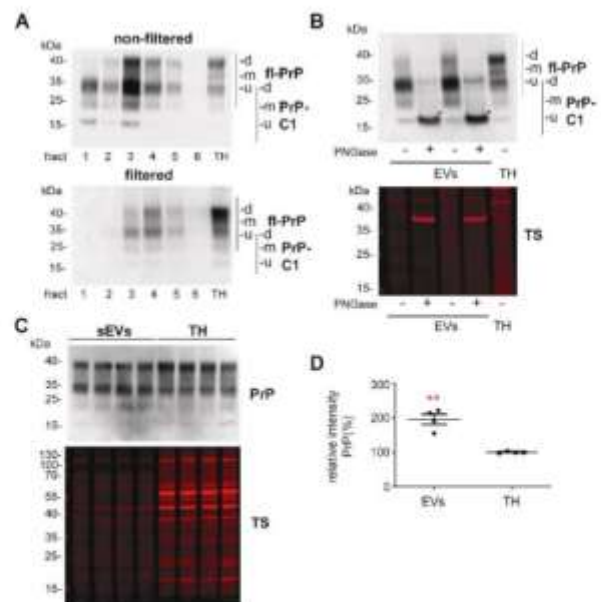## Brain-derived EVs are enriched in the cellular prion protein

Since we were also interested in PrP as both, a known resident of EVs and a protein that was shown to act neuroprotective in ischaemic insults, we performed western blot analyses of filtered and non-filtered EV-enriched fractions. As expected, and shown in Figure 4A, PrP is present in both, non-filtered and filtered EVs. Interestingly, in both cases, the pattern of PrP in EVs is different compared to the TH when visualized with the POM1 antibody raised against the C-terminal part of PrP [49]. It should be noted that the combination of gels and protein ladder used here resulted in bands running at higher molecular weight than expected. Hence, for the TH we could observe the typical banding pattern of PrP with a prominent diglycosylated band at around 40 kDa (commonly running at ~35 kDa) followed by two lower and less conspicuous bands corresponding to mono- and unglycosylated full-length (fl) PrP. In the EV fractions, apart from a diglycosylated fl-PrP band, a major band at 34 kDa was present, which could either represent unglycosylated fl-PrP or its diglycosylated C1 fragment (usually running at ~25 kDa) [41]. In order to
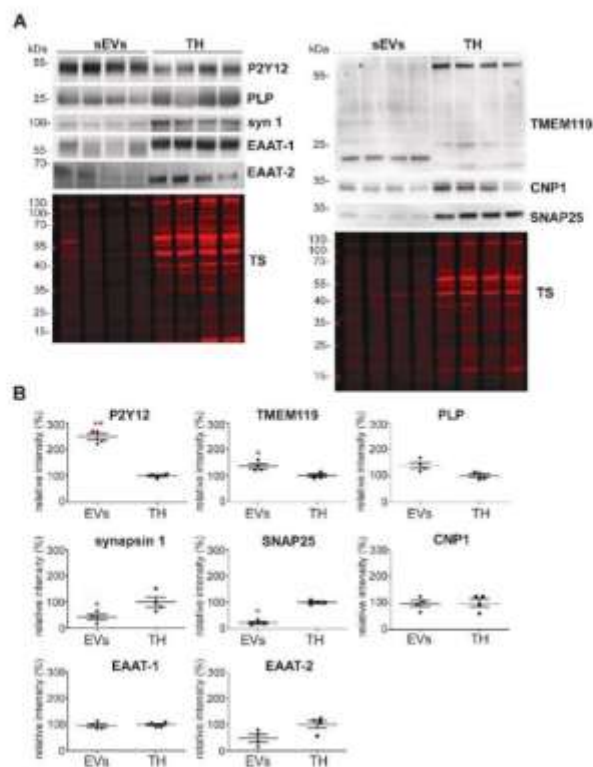
Figure 3. **Microglia cells are the main contributor to the physiological brain sEV pool.** (A) Representative western blots of pooled fractions 3 and 4 of filtered EVs (sEVs; n = 4) compared to their respective total brain homogenates (TH). P2Y12 and TMEM119 were chosen as markers of microglia, PLP and CNP as markers of oligodendrocytes, synapsin1 and SNAP-25 as neuronal markers, and EAAT1 (GLAST) and EAAT2 (GLT-1) as markers of astrocytes. Of note, TMEM119 presented a lower band (at around 20 kDa) in the sEVs-enriched fractions instead of the reported 60 kDa band (approx.) observed in the TH. This could correspond to an isoform or a truncated version of TMEM119. (B) Scatter plots showing relative intensity quantifications of each cell type marker. Each lane was first referred to its total protein staining (TS) signal and the means of each group (sEVs vs. TH) were then compared in order to check for relative enrichment (with TH set to 100%). P2Y12 and TMEM119 are approximately 2.5 and 1.5 times enriched in sEVs compared to the TH, indicating a dominant contribution from microglia to the whole pool of brain sEVs. Synapsin1 and SNAP-25 are significantly decreased compared to the TH, suggesting a low contribution of neuronal sEVs to the total pool. PLP, CNP, EAAT1 and EAAT2 did not show any significant differences compared to the TH. Exact mean, SEM and p-values are given in the main text.

Figure 4. **Brain EVs are enriched in PrP and its C1 fragment.** (A) Representative western blots of the six fractions obtained after sucrose gradient centrifugation of non-filtered (EVs) and filtered EVs (sEVs) probed with POM1 antibody. A total homogenate (TH) was loaded for comparison. Note that PrP in the TH presents with a prominent diglycosylated full-length band (fl-PrP) at 43 kDa followed by two lowerbands, corresponding to mono- and unglycosylated PrP, respectively. In EVs, a major band at 34 kDa is presented which could either correspond to unglycosylated fl-PrP or to its diglycosylated truncated C1 fragment (PrP-C1). (B) Representative Western blots of EV fractions 3 and 4 treated (+) or not (-) with PNGase F and probed with POM1 and total protein staining (TS). The PNGase digestion reveals that the major band at 34 kDa present in the EVs corresponds to the C1 fragment (marked with an asterisk). (C) Representative Western blots of pooled sEVs (n = 4) compared to their respective total brain homogenates (TH) probed with POM1 and total protein staining (TS). (D) Scatter plot showing the quantification of the comparison between total PrP in the TH versus sEVs. PrP shows a significant twofold increase in sEVs relative to the TH. Each lane was first referred to its total protein staining and then the means for total PrP in sEVs and TH were compared. The mean, SEM and p-values are stated in the main text.

discriminate between these two forms, we treated the sEVs and the TH fractions with PNGase to enzymatically remove the N-linked glycans (Figure 4B). This revealed that the dominant band in the EVs fractions indeed represents the C1 fragment of PrP (here running at ~18 kDa-corresponding to ~15 kDa in other systems upon deglycosylation). When amounts of total PrP in sEVs were compared to the respective levels in TH (Figures 4C,D), we found that PrP is significantly enriched in brain-derived sEVs (PrP in TH set to 100% ±21.8%; sEVs: 195.5% ±14.9%; p = 0.0073).

Since the identity of the protease(s) responsible for the α-cleavage of PrP is still unknown [40,68], it could be that the enrichment in PrP-C1 is an artefact caused by the collagenase III treatment used for EVs isolation. Therefore, we also examined isolated sEVs with collagenase IV (which has a lower tryptic activity), and we assessed the 300xg pellet, which also underwent the enzymatic treatment but is theoretically devoid of

EVs. As shown in Suppl. Fig. 3A, we observed that, in fact, the PrP-C1 fragment was present in the 300xg pellets, indicating a partial cleavage due to the enzymatic treatment. As TMEM119 was another protein showing a cleavage (or a spliced form) in EVs, we also checked the influence of collagenase III treatment in this instance, but we could not see this fragment in the 300xg pellet (Suppl. Fig. 3B) concluding that the fragment (or spliced form) of TMEM119 is sEVs specific. Since we consistently observed that the amounts of PrP-C1 in the 300xg pellets were still lower than in the EV fraction, we decided to study EVs isolated from cell culture supernatants, which do not require enzymatic treatment. As shown in Suppl. Fig. 4, we observed that in two different mouse cell lines (N2a (neuroblastoma) and mHippoE-14 (embryonic hippocampal)), PrP-C1 is indeed enriched in EVs relative to the corresponding cell lysates, as shown after the PNGase treatment (for N2A cells: 35.8%±1.6% (EVs) vs 16.1%±0.9% (TH), $p = 0.0004$, $n = 3$; for mHippoE-14: 45% (EVs) vs 31% (TH) $n = 1$ pooling 4 dishes). Thus, although we here refrain from quantifying PrP-C1 levels in brain-derived EVs (due to a seemingly partial artificial contribution of the collagenase treatment), our experimental data from murine brain and neuroblastoma/embryonic hippocampal cell lines clearly point to a physiological enrichment of PrP-C1 in EVs.

Increased release of sEVs by astrocytes and elevated levels of PrP in brain-derived sEVs after experimental stroke (tMCAO)

To study changes in the relative contribution of different cell populations to the sEV pool in brain at 24 h after tMCAO, we performed western blot analyses with the brain cell markers described above, comparing sEVs isolated either from sham ($n = 8$) or from tMCAO-operated mice ($n = 8$) (Figure 5A). We observed that only the levels of the astrocytic marker EAAT1 were significantly increased in sEVs after tMCAO (shams were set to 100% ±5.6% vs tMCAO, 134.2% ±11.1%; $p = 0.0158$), indicating that at 24 h after stroke reperfusion injury there is an increased release of sEVs by astrocytes. Although there was a slight tendency of increase for oligodendrocytic PLP (shams set to 100% ±4.2% vs tMCAO, 158.4% ±34.1) and microglial P2Y12 (shams set to 100% ±4.3% vs tMCAO, 110.8% ±16.8%), these changes were not significant. The neuronal marker synapsin1 was not changed between shams and tMCAO samples (shams set to 100% ±8.7% vs tMCAO, 102% ±10%).

Notably, a significant increase was also seen for total PrP (Figure 5B), which was enriched in sEVs from tMCAO samples compared to sham brains (shams set to 100% ±4.4% versus strokes: 121.47% ±7.6%; $p = 0.0284$).

As shown in Suppl. Fig. 5, neither levels of PrP nor the proteins used as cellular markers were altered in the TH from stroked (tMCAO) compared to sham-treated mice, demonstrating that the observed changes were exclusive for the brain-derived sEVs. Of note, no differences were observed in the overall amounts of sEVs isolated (as assessed by NTA) between shams and tMCAO-operated mice or in the distribution of EVs marker proteins in tMCAO-operated mice, as shown in Suppl. Figures 6C and 6D.

PrP influences uptake of brain-derived sEVs by primary neurons and glia cells

Isolated brain-derived EVs are enriched in PrP and PrP-C1. The C1 fragment, resulting from the α-cleavage in the middle of the PrP sequence, exposes a hydrophobic domain at its N-terminus [41]. Both, the structural aspect with an exposed stretch of hydrophobic amino acids and its dependence on proteolytic "activation" are strikingly reminiscent of some viral surface glycoproteins critical for host cell attachment and membrane fusion (for instance those of some paramyxoviruses). In these viruses, the viral envelope fuses with the host cell membrane with the help of two glycoproteins, one that initially attaches the virus and another one that, after an endoproteolytic cleavage, exposes the highly hydrophobic fusion peptide, which integrates into the host cell membrane and mediates the fusion process [69,70]. Because of the similarities between PrP-C1 and the fusogenic viral surface proteins, and given the relative enrichment of PrP-C1 in EVs, we hypothesized that the C1 fragment might act as a tethering factor and play a role in the uptake of EVs by cells [41]. To assess this potential role of PrP in EVs, we incubated primary neuronal cultures from WT mice with labelled sEVs isolated from either WT or PrP-KO mouse brain (Suppl. Fig. 6A) and fixed them after 1, 3, or 6 h of incubation. Of note, PrP-KO sEVs were isolated from the same density fraction as WT-PrP sEVs they did not present differences in the expression of EVs marker proteins (Suppl. Fig. 5B). Moreover, no differences were detected in the amount of isolated brain-derived sEVs between PrP-WT and PrP-KO mouse brain samples after measuring the number of particles with NTA (Suppl. Fig. 6 C).

As shown in Suppl. Fig. 7, the sEVs labelling with mCling was specific as incubation with a dye that has
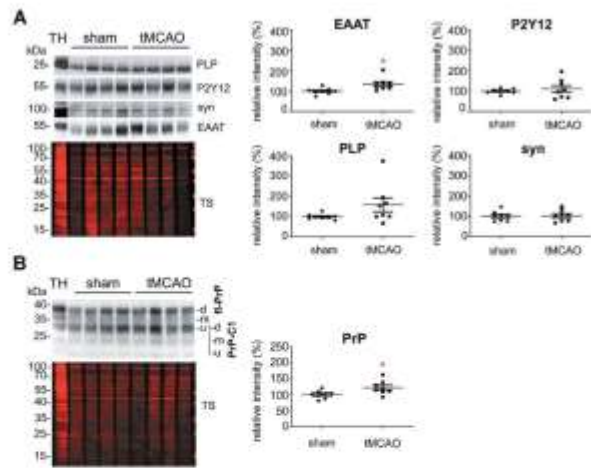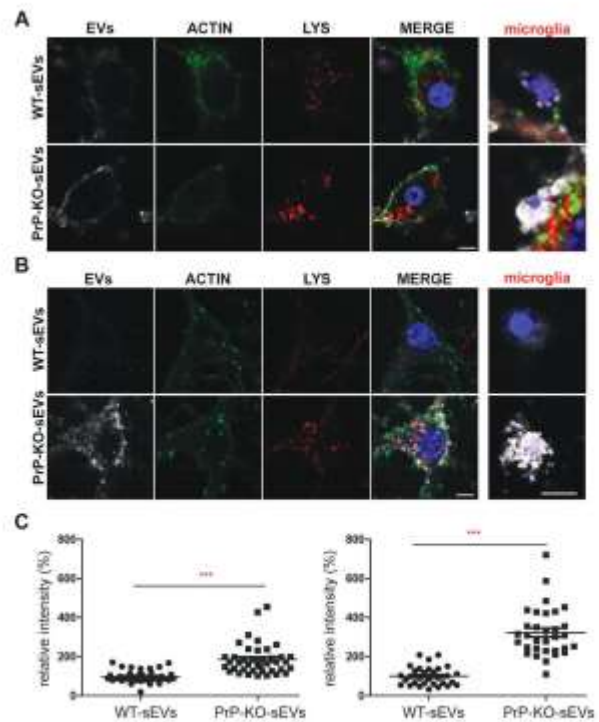
Figure 5. Contribution of astrocytes to the brain sEV pool is upregulated and PrP levels on brain sEVs are increased 24 h after tMCAO. (A) Representative western blots of sEVs from sham mice (n = 8) and mice that underwent the tMCAO procedure (n = 8). Blots show the total protein staining (TS) and cell type-specific surface markers: PLP for oligodendrocytes, P2Y12 for microglia, synapsin1 for neurons, and EAAT1 for astrocytes. On the right, scatter plots of relative intensity quantifications show a significant increase of the astrocytic marker EAAT1 in tMCAO sEVs compared to sham sEVs. PLP, P2Y12 and synapsin1 were not significantly changed. For quantification each lane was first referred to the TS and then the mean values of the two experimental groups were compared. (B) Representative western blots of sEVs from sham (n = 8) and tMCAO mice (n = 8) probed with POM1 antibody and total protein staining (TS). On the right side, scatter plot of relative intensity quantifications showing an increase in total PrP in tMCAO sEVs compared to sham sEVs. The mean, SEM and p-values are reported in the main text.

Figure 6. PrP influences brain sEVs uptake by primary neurons. (A) Representative confocal microscopy images of primary neurons from WT mice in high-density culture (HDC) incubated for 1 h with sEVs isolated from either WT (WT-sEVs) or $Prnp^{0/0}$ mouse brains (PrP-KO-sEVs) and labelled with mCLING dye. Small EVs signals are shown in white. Neurons were stained with phalloidin (green; to visualize F-actin), the lysosomal marker LAMP-1 (red), and with DAPI (blue; to visualize the nucleus). Note that after 1 h of incubation, WT-sEVs present with a weak and rather diffuse staining at the neuronal plasma membrane, whereas PrP-KO-sEVs show a dotty staining at the neuronal plasma membrane with some PrP-KO-sEVs being present inside the neuronal cell body (yellow arrow). In this HDC condition, other cell types (apparently microglia based on their morphology in culture) were observed to take up a few WT-sEVs, yet conspicuously much higher amounts of PrP-KO-sEVs. (B) Representative confocal images of low-density culture (LDC) primary neurons from WT mice incubated for 1 h with sEVs isolated from WT (WT-sEVs) or PrP-KO mouse brains (PrP-KO-sEVs) labelled with mCLING as in (A). Here again, PrP-KO-sEVs (showing a distinct dotty pattern inside neurons) are taken up more readily than WT-sEVs. Cells presumed to be microglia cells (see also Figure 7A) showed a similarly strong engulfment pattern for sEVs from PrP-KO brain as in (A). Scale bar is 5 μm. (C) Scatter plot showing intensity of sEVs quantification in high-density (HDC, on the left) and low-density primary neuronal cultures (LDC, on the right). PrP-KO-sEVs are significantly more taken up by neurons after 1 h than WT-sEVs. The mean, SEM and p-values are given in the main text.

went through the same preparation procedure but without presence of sEVs, showed no staining when incubated with primary neurons.

As shown in Figure 6A, after 1 h of incubation, labelled sEVs from WT (shown in white) presented as a rather diffuse staining surrounding the neuronal cell body (marked by phalloidin-based staining of the actin cytoskeleton in green), whereas the PrP-KO-sEVs showed a dotty staining at the plasma membrane and, to some extent, inside cells, indicating that some of the particles had already been internalized at this early time point. Surprisingly, we also observed that our primary neuronal cultures (which presented staining for MAP2 as shown in Suppl. Fig. 8) contained some microglia, despite having been treated with Arabinoside C to eradicate proliferating cells. In several instances, these microglia were found to contain high amounts of PrP-KO-derived sEVs, a feature that we could not observe for WT-derived sEVs (Figure 6A, Figure 7A). We then established another protocol for

primary neuronal cultures from WT mice (low-density culture, LDC), where neurons grow in co-culture with (yet spatially separated from) astrocytes [48]. On the one hand, this approach allows for lower seeding
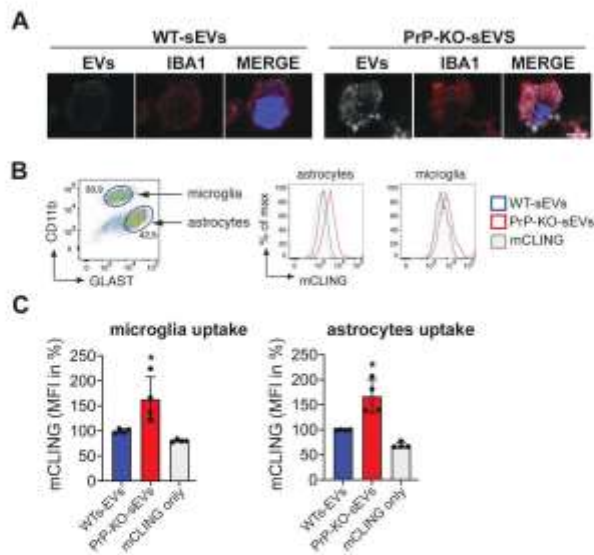
Figure 7. PrP also affects the uptake of brain-derived sEVs by microglia and astrocytes. (A)Confocal microscopy images confirming that the non-neuronal cells observed in our HDC and LDC neuronal cultures from WT mice (Figure 6) are indeed microglia, as they stain positive for IBA1. As in Figure 5, sEVs are labelled with mCLING and shown in white. DAPI (in blue) is used as a nuclear staining. (B) Representative FACS plot of astrocytes (GLAST+) and microglia (CD11b+) from mixed cultured primary glia cells (n = 4). Mixed glia cells from WT mice were incubated for 3 h with equal amounts of either WT-sEVs or PrP-KO-sEVs labelled with mCLING and analysed for sEVs uptake using flow cytometry. On the right side, histograms showing the intensity of the sEVs fluorescence measured from astrocytes or microglia. Note that in both cases the intensity (mCLING mean fluorescence intensity (MFI) shown in %, WT is set to 100%) is higher for PrP-KO-sEVs. (C) Bar scatter plots of normalized fluorescence intensity show that both, microglia and astrocytes, take up PrP-KO-sEVs more efficiently than WT-sEVs. The exact means, SEM and p-values are reported in the main text.

density and, therefore, improved microscopic analysis, while on the other hand, contamination by other brain cell types is sensibly lower. As shown in Figure 6B, we could again confirm a strong difference in the neuronal uptake behaviour, with PrP-KO-derived sEVs being efficiently taken up in contrast to sEVs from WT brain (which at 1 h of incubation were hardly detectable in the culture). Moreover, although microglia were much less and therefore more difficult to find in this type of culture, the few microglia cells that could be identified were also highly decorated with PrP-KO-sEVs, whereas microglia showed less positive sEV-associated labelling when treated with WT-derived sEVs.

The quantification in Figure 6C shows that the neuronal uptake in the primary culture with higher amounts of microglia (HDC; Figure 6A) was almost twofold increased for the PrP-KO-derived sEVs than

for WT-derived sEVs (WT-sEVs: set to 100%±5.3%; PrP-KO-sEVs: 185.8%±12.5%; $p \leq 0.0001$), while in the LDC with low microglia content (Figure 6B), neuronal uptake of sEVs from PrP-KO brain was about three times higher compared to WT-sEVs (WT-sEVs: set to 100%±8.6%; PrP-KO-sEVs: 323.3%±22.1%; $p \leq 0.0001$). We hypothesize that this difference between the culture conditions could either be a consequence of the lower number of neurons or the reduction in microglia in the LDC, both resulting in a higher sEV-to-neuron ratio.

In order to confirm that microglia efficiently take up PrP-KO-sEVs, we established mixed glial cell cultures (containing microglia and astrocytes) and incubated them with either WT-sEVs or PrP-KO-sEVs for 3 h (Figure 7). This type of culture allowed us to measure the sEVs uptake not only by microglia but also by astrocytes (which were absent in our previous primary neuronal cultures). After incubation with sEVs we labelled the two populations with cell type-specific markers (GLAST-1 for astrocytes and CD11b for microglia) and performed flow cytometric analysis (Figure 7B). As quantified in Figure 7C, we could confirm that microglia take up significantly more PrP-KO-sEVs than WT-sEVs (WT-sEVset to 100% ±2.5% vs PrP-KO-sEVs: 163.2% ±22.3%; $p = 0.035$). In addition, similar to what we observed for neurons and microglia, PrP-KO-sEVS were also taken up more efficiently by astrocytes (WT-sEVs set to 100% ±2.6% vs PrP-KO-sEVs: 166.9% ±16.6%; $p = 0.0068$).

Regarding the neuronal uptake after 3 h (Figure 8A), treatment with WT-sEVs in the HDC again revealed a diffuse staining of the sEV-labelling at the plasma membrane, although seemingly more intense than after 1 h (Figure 6A). In addition, some sEVs could now be detected as vesicle-like structures at the plasma membrane or even internalized and colocalizing with the lysosomal marker LAMP-1, fitting to lysosomes being described as one of the major targets of internalized EVs [71,72]. In the case of PrP-KO-sEVs, although some signal was still detected at the plasma membrane, the vast majority at this time point was observed inside the neurons and colocalizing with LAMP-1. Quantification of sEVs signal intensity inside neurons (Figure 8C) showed that at 3 h still about the double amount of PrP-KO-sEVs was taken up compared to WT-sEVs (WT-sEVs set to 100% ±7.45% vs PrP-KO-sEVs: 219% ±16.3%; $p \leq 0.0001$).

At the latest time point assessed in this study (6 h of incubation), the majority of both, WT- and PrP-KO-sEVs, were found inside neurons and colocalizing with LAMP-1 (Figure 8B). Again, quantification of the sEVs-associated fluorescence signal present inside the neurons
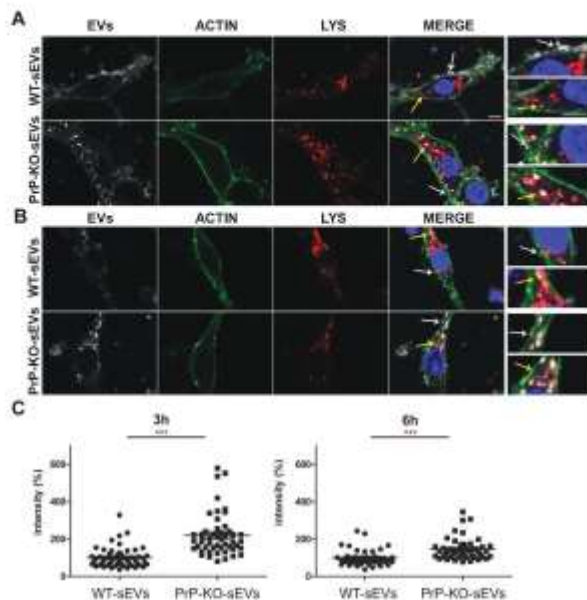
Figure 8. Brain-derived sEVs are found in lysosomes after 3 and 6 h of incubation. (A) Representative confocal microscopy images of primary neurons from WT mice (labelled with phalloidin, in green) in high-density culture (HDC) incubated for 3 h with WT-sEVs or PrP-KO-sEVs labeled with mCLING (white signal). The lysosomal marker LAMP-1 is shown in red and nuclei are stained with DAPI (in blue). Note that both, WT- and PrP-KO-sEVs, co-localize with LAMP-1, although we consistently observed a much higher level of colocalization for PrP-KO-sEVs. Instead, a rather diffuse mCLING staining at the membrane is found for cells treated with WT-sEVs. White arrows highlight sEVs located at the plasma membrane (PM), whereas yellow arrows indicate colocalization of sEVs with LAMP-1. Note that for WT-sEVs there are many sEVs found at the plasma membrane, whereas PrP-KO-sEVs much stronger colocalize with LAMP-1. (B) Representative confocal microscopy images showing primary neurons as in (A) but incubated with sEVs for 6 h. sEV identity and stainings as in (A). Note that after 6 h sEV-associated signals are mainly found in colocalization with lysosomes. Scale bar is 5 µm. (C) Scatter plots showing intensity quantifications of WT-sEVs and PrP-KO-sEVs in primary neurons at 3 h (on the left) and 6 h (on the right) of incubation in the HDC. As for 1 h (Figure 5), PrP-KO-sEVs are significantly more taken up by neurons than WT-sEVs. Mean, SEM and p-values are reported in the main text.

still revealed a higher amount of uptaken sEVs from PrP-KO compared to those derived from WT brain (WT-sEVs set to 100% ±6.6% vs PrP-KO-sEVs: 145.37% ±8.56%; $p \leq 0.0001$). For the LDC condition (Suppl. Fig. 9), results obtained at 3 h and 6 h were similar to the ones mentioned above for the HDC (for 3 h incubation: WT-sEVs set to 100% ±3.46% vs PrP-KO-sEVs: 214% ±17.58%; $p \leq 0.0001$/for 6 h incubation: WT-sEVs set to 100% ±5.6% vs PrP-KO-sEVs: 187% ±14%; $p \leq 0.0001$).

Discussion

In the present study, we have characterized sEVs in the murine brain in steady-state conditions and after 24 h of stroke-reperfusion. We show that, under physiological conditions, microglia are the main sEVs source in brain. This situation changed at 24 h after induced stroke-reperfusion, where a significant increase of astrocytic sEVs was observed. Furthermore, we show that EVs isolated from murine brain and brain-derived cell lines are enriched in PrP and its C1 fragment, with consequences in the regulation of vesicle uptake by recipient cells. Accordingly, when sEVs lack PrP, their uptake by neurons is increased and, conspicuously, they are also more readily taken up by microglia and astrocytes. Moreover, PrP-KO-sEVs were found to colocalize with lysosomes much faster than WT-sEVs. We also demonstrate that, 24 h after stroke, the amount of PrP in brain sEVs is even further increased, which may have functional consequences in intercellular communication after stroke (a graphical summary of the principal findings is depicted in Figure 9).

EVs have become an intense field of research, not only because they represent a novel form of cell-to-cell communication able to bridge wide distances, but also by their potential applicability as therapeutic tools. In the case of brain disorders, they are very attractive because of their property to cross the BBB when genetically modified to target the brain [73]. A protective role of EVs derived from mesenchymal cells in a variety of brain insults and disorders [74], including stroke [34,75–77], has also been shown. Until recently, most of the EVs assessed in various studies were isolated from cell culture supernatants or body fluids. Isolation of EVs from complex tissue such as the brain parenchyma has been increasingly reported in the last few years only [44,78,79].

Despite enormous progress in recent years, isolation, characterization and categorization of EVs remains a challenge. One of the aims of our study was to characterize the differential contribution of the brain cell populations to the EVs pool in normal conditions and to assess potential changes 24 h after ischemia-reperfusion in the tMCAO mouse model of stroke. We modified a published protocol of EV isolation from brain [44] by including a filtration step (frequently used in other brain-derived EVs isolation protocols [78,80–85]) to differentiate between small EVs (≤200 nm) and EVs larger than 200 nm, because NTA measurements showed that the non-filtered population was, in average, bigger than 200 nm. We
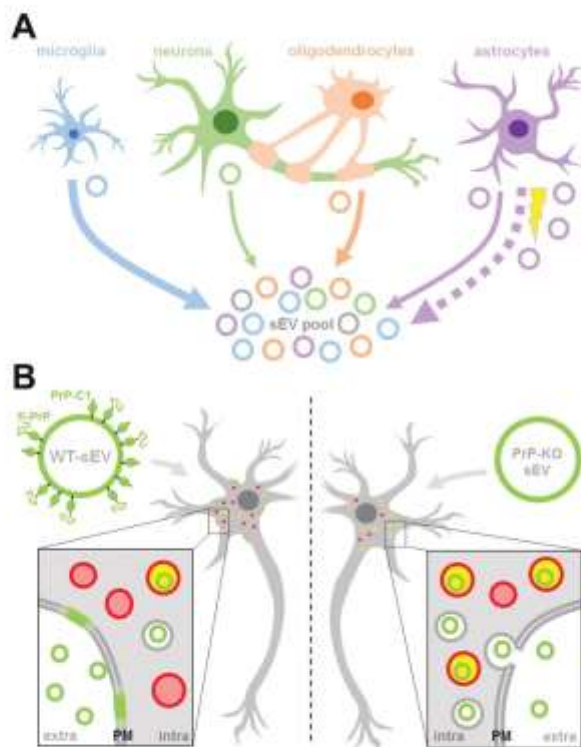
Figure 9. Summarizing scheme. (A) Schematic representation of the relative contribution of different brain cell types to the sEV pool in murine brain. Under physiological conditions, microglia appear to be the main contributor to the sEV pool, followed by oligodendrocytes and astrocytes, while neurons contribute relatively little (contribution indicated by thickness of solid arrows). Upon experimental stroke (indicated by the yellow thunderbolt), astrocytic release of sEVs is upregulated and astrocytes appear to be the main contributor 24 h after reperfusion (indicated by the bold dotted arrow). sEVs are depicted as circles and the color refers to their cellular origin. Note that a fraction of sEVs (grey) may also be released by other cell types not assessed here, such as pericytes or endothelial cells. (B) Differential uptake of WT-sEVs and PrP-KO-sEVs may be influenced by PrP. WT-sEVs (on the left) are packed with fl-PrP and its truncated C1 fragment ending with a stretch of hydrophobic amino acids. These sEVs are relatively slowly taken up by neurons and rather seem to fuse with the plasma membrane (PM). In contrast, sEVs lacking PrP (PrP-KO-sEV; on the right) are rapidly endocytosed and transported to lysosomes (red circles). Colocalization (i.e. lysosomes containing sEVs) is indicated in yellow. Similar observations have been made with microglia or astrocytes as recipient cells. Note that other surface proteins and cargo of sEVs, as well as the lipid bilayer of vesicles, lysosomes, and sEVs, are not depicted here to simplify matters.

performed this step to yield, at least by size, a homogeneous population for our downstream analyses (sEVs) [86]. Our proteome analysis revealed that in both, filtered and unfiltered EVs, proteins defined as markers of exosomes and EVs (CD9, Rab11, VSP4T, V-ATPases, CD81, tau, flotillins, Alix, Thy-1, 14.3.3),

and proteins that have been described to be present in microvesicles only (Annexin 1) [87,88], were present as expected. In addition, as supported by the volcano plot and the PCA analysis, we observed two differentiated populations, with the filtered sEVs being particularly enriched in proteins related to ribosomes, whereas the non-filtered EVs (though also including the sEV pool) were enriched in proteins associated with metabolic pathways. Thus, our brain-derived sEVs likely represent a mixture of bona fide exosomes and small microvesicles [53], but the additional filtration step further concentrates a population (enriched in SNARE, ribosomal proteins and ribosomal-binding proteins) that differs from the non-filtered population. Since categorization and definitions of EVs are increasing in complexity [53,88], our present findings with brain-derived EVs deserve further studies to pinpoint the exact nature of these EVs.

Because the cargo of EVs is cell type-dependent and includes proteins that reflect their cellular origin, we sought to investigate the relative contribution of different cell types to the total brain sEVs pool by assessing the relative enrichment (compared to TH) of certain brain cell markers by western blot. We show that, in steady-state conditions, P2Y12 and TMEM-119, two known markers of microglia, are significantly enriched in the pool of mouse brain sEVs.On the contrary, the neuronal markers synapsin1 and SNAP-25 showed a relative decrease, indicating a rather minor contribution to the total sEVs brain pool. The fact that SNAP-25 is enriched at the pre- and post-synaptic terminal and synapsin1 is a protein marker of synaptic vesicles, could potentially indicate synaptosomal contamination as an artefact produced during tissue preparation. However, since these two proteins are also found in EVs isolated from cerebrospinal fluid (CSF), this rather suggest them as being de facto components of neuronal EVs [62,63,65]. Oligodendrocytes (assessed with PLP and CNP1) and astrocytes (detected with EAAT-1 and EAAT-2 as exclusive markers) showed no enrichment in sEVs when compared to the TH and, therefore, we concluded they are not the major populations that contribute to the brain sEVs pool in steady-state conditions. We cannot rule out the possibility that certain (marker) proteins are more heavily packed into EVs than others, but we are confident that the use of two markers for each cell type and the fact that they were behaving similarly, reduces the risk of misinterpretation and ensures more reliable results regarding the relative contribution of different cells. Relative quantification of EVs in brain is not an easy issue. In a recent paper, Silverman et al. [89] have also characterized the relative proportion of EVs derived from different brain

cell populations. By means of flow cytometry and in contrast to our findings, they observed an increased proportion of astrocytic and neuronal markers in both, brain- and spinal cord-derived samples. The discrepancy with our results could well be a consequence of (i) the investigation of different subpopulations of EVs (note that we included a 0.2 μm filtration step) and (ii) the detection limit of flow cytometry possibly excluding some small vesicles that were considered as debris (yet were included in the western blot analyses of our study). It has been calculated that sEVs are at least one order of magnitude more frequent than medium/large EVs [90,91] and this pool may have been lost by flow cytometry measurements.

What we observed, under the same settings used for the study of sEVs in the steady-state condition is that, 24 h after stroke-reperfusion, the brain sEV pool was altered as sEVs containing the astrocytic marker EAAT-1 were significantly increased. Astrocytes have multiple important functions in the brain, ranging from regulation of synaptic transmission, modulation of neuronal excitability, BBB formation, and regulation of blood flow. Since they are relatively resistant to glucose and oxygen deprivation, they cope better than neurons with ischemic insults and, at present, they are raising attention as potential targets in stroke therapy [92]. At earlier times points after ischaemia, astrocytes proliferate, become hypertrophic (reactive astrogliosis) and, after a few days, start to form the glial scar with both, potential benefits but also detrimental effects [93,94]. Likewise, microglia are significantly increased at 24 h in a mouse model of stroke [19]. Since there is close communication between astrocytes and microglia after brain injury, and given that activated astrocytes can in turn contribute to the activation of distant microglia after ischaemia [95], it may be that an elevated release of EVs from astrocytes at 24 h is a factor facilitating the recruitment of reactive microglia. Moreover, astrocytes present neuroprotective features after stroke [96] and, fittingly, neurons exposed to reactive oxygen species (ROS) showed increased survival when treated with astrocytic EVs [97]. Whether the relative increase in astrocytic sEVs is related to microglia proliferation, the formation of the glial scar, or protection against ROS, clearly deserves further studies. Interestingly, Guitart et al. [38] showed that exosomes released by astrocytes under hypoxic conditions (using the in vitro model of oxygen-glucose deprivation, OGD) conferred protection to neurons. Of note, this activity was dependent on the presence of PrP, which they also found increased in exosomes derived from stressed astrocytes. Contrarily, exosomes from stressed astrocytes devoid of PrP were not protective [38]. In

our experiments, apart from the increase in astrocytic sEV release, we also observed an increase in sEV-associated PrP levels after stroke. It should be noted that, due to technical limitations, we could not assess whether these changes in sEV-associated PrP are caused by the alterations in the relative contribution of cell types to the sEV pool. However, in view of the reported neuroprotective effects of PrP after ischaemia [31,34,37] this increase in both, astrocytic sEVs and sEV-associated PrP amounts, could represent a protective feedback mechanism to counteract the oxidative stress present in the first hours after stroke. Although an increase in PrP levels has been observed in animal models of stroke and in humans after ischaemic insult [35,36,98,99], the present study is the first to report elevated levels of this protein in brain-derived sEVs. However, further studies are clearly required to elucidate its consequences.

We also observed that the proteolytically generated PrP-C1 fragment is enriched in sEVs. Although part of the presence of PrP-C1 is provoked by the collagenase treatment, the study of two neuronal cell lines further confirmed that PrP-C1 is enriched in EVs. Interestingly, Vella et al. [100] already described that EV-associated PrP was largely not recognized with antibodies against the N-terminal part of the protein, indicating truncation. In agreement with that, we show here that the main PrP forms packed onto sEVs in the brain are PrP-C1 together with fl-PrP (with both primarily being in their diglycosylated state). We had already suggested a parallelism between the hydrophobic domain, which is N-terminally exposed in C1 after the α-cleavage of PrP, and the fusion peptides of certain viral surface proteins [41]. Because the latter allows viruses to dock to and fuse with the host cells, we hypothesized that PrP-C1 on EVs could perform a similar function, such as tethering EVs to recipient cells and/or facilitating their uptake. The fact that EVs also share many similarities with viruses [101,102] would reinforce our hypothesis. Surprisingly, we found that, as early as 1 h after incubation, labelled brain-derived sEVs lacking PrP are readily taken up and present inside neurons (and glia cells), whereas sEVs from WT mice are poorly taken up, but rather present as diffuse staining surrounding the neuronal body. At later time points, although WT-sEVs are also engulfed and start to colocalize with lysosomes, there are still significant differences compared with PrP-KO sEVs, with the latter being more massively taken up and colocalizing with lysosomes [103]. This seems counterintuitive with our initial hypothesis since our findings rather indicate that a lack of PrP leads to more efficient uptake. However,

it has been shown that EVs can either fuse with the plasma membrane, thereby releasing their content into the cytoplasm, or they can be taken up by clathrin/caveolin-dependent mechanisms or by phagocytosis and macropinocytosis [104]. Since we always treated cells with the same amount of sEVs yet consistently detected more endocytosed PrP-KO sEVs, this could indicate that presence of PrP and/or PrP-C1 (in WT-sEVs) indeed influences fusion events. This may also be supported by the diffuse sEV-associated staining at the plasma membrane observed for cells incubated with WT-sEVs. In contrast, in the absence of PrP it seems that vesicles are taken up more quickly by other mechanisms and delivered to certain organelles (in this case lysosomes). Thus, modulation of PrP composition could regulate EV fusion versus uptake and, consequently, influence whether EV cargo is released to the cytoplasm or intracellular compartments, respectively. Nevertheless, we cannot completely rule out the possibility that other gene products (e.g. flanking genes) possibly affected by the knock-out strategy [29]or PrP binding partners altered in $Prnp^{0/0}$ mice could potentially influence this aspect. Moreover, as detergent-resistant domains in the membrane can be modified (at least in vitro) by the presence of GPI-anchored proteins [105], we can likewise not exclude that an altered lipid composition of EVs is partially responsible for the differential uptake. Further studies including lipidomic profiling would clarify this point.

It has been reported that fusion of EVs with purified membrane sheets in a cell-free system requires the presence of proteins at the surface of both entities and an acidic pH [106]. Our data suggest that PrP and PrP-C1 may be relevant EVs residents in this initial EV-to-target cell interaction. However, given that, at a later time-point, we observed both, WT- and PrP-KO-sEVs, to colocalize with LAMP-1, final subcellular targeting of at least a fraction of sEVs rather seems to be PrP-independent. In general, intracellular cargo delivery of EVs is still poorly understood and further studies, as for the potential role of PrP in these processes, are clearly needed to clarify this important point in EV biology and intercellular communication.

It has been shown that EVs derived from cortical neurons are taken up preferentially by hippocampal neurons, whereas EVs from other origins are generally taken up by microglia [107]. In our study, we have a mixture of brain EVs and further analyses are needed to assess which type of EVs are internalized by neurons. However, we observed that the uptake of sEVs lacking PrP by microglia and astrocytes was likewise highly increased. This result could point out to a role of PrP in EV recognition by the immune system. It is striking that PrP is highly abundant in organs that possess immune privilege, such as brain, placenta and testicles [108]. Fittingly, in several inflammatory processes, such as ischaemia, brain trauma, and experimental autoimmune encephalomyelitis (EAE; as a model for multiple sclerosis), the inflammatory damage is exacerbated when PrP is absent, supporting a role of this protein in immunological quiescence [108].

In conclusion, the present study describes that microglia are the main contributors to the sEV pool in murine brain under physiological conditions and that brain sEVs are enriched in PrP and PrP-C1, which may modulate EV uptake in recipient cells. After experimental stroke, astrocytes increasingly contribute to the sEV pool and levels of sEV-associated PrP are further enhanced. These findings add novel insight to previous studies indicating a major role of both, PrP and EVs, in the brain under physiological and ischaemic conditions.

ORCID

Santra Brenna http://orcid.org/0000-0001-8233-2110
Hermann C. Altmeppen http://orcid.org/0000-0001-9439-6533
Behnam Mohammadi http://orcid.org/0000-0002-9178-3949
Björn Rissiek http://orcid.org/0000-0001-5327-5479
Peter Ludewig http://orcid.org/0000-0001-9025-6402
Hartmut Schlüter http://orcid.org/0000-0002-9358-7036
Antonio Virgilio Failla http://orcid.org/0000-0002-7137-0506
Markus Glatzel http://orcid.org/0000-0002-7720-8817
Berta Puig http://orcid.org/0000-0002-2255-8393
Tim Magnus http://orcid.org/0000-0001-6232-9555

References

[1] Valadi H, Ekström K, Bossios A, et al. Exosome-mediated transfer of mRNAs and microRNAs is a

novel mechanism of genetic exchange between cells. Nat Cell Biol. 2007;9(6):654.

[2] Eldh M, Ekström K, Valadi H, et al. Exosomes communicate protective messages during oxidative stress; possible role of exosomal shuttle RNA. PloS One. 2010;5(12):e15353–e15353.

[3] Cocucci E, Racchetti G, Meldolesi J. Shedding microvesicles: artefacts no more. Trends Cell Biol. 2009;19(2):43–51.

[4] Simons M, Raposo G. Exosomes – vesicular carriers for intercellular communication. Curr Opin Cell Biol. 2009;21(4):575–581.

[5] Lo Cicero A, Stahl PD, Raposo G. Extracellular vesicles shuffling intercellular messages: for good or for bad. Curr Opin Cell Biol. 2015;35:69–77.

[6] Tkach M, Kowal J, Théry C. Why the need and how to approach the functional diversity of extracellular vesicles. Philos Trans R Soc B. 2018;373(1737):20160479.

[7] Yáñez-Mó M, Siljander PR-M, Andreu Z, et al. Biological properties of extracellular vesicles and their physiological functions. J Extracell Vesicles. 2015;4(1):27066.

[8] Krämer-Albers EM, Hill AF. Extracellular vesicles: interneural shuttles of complex messages. Curr Opin Neurobiol. 2016;39:101–107.

[9] Candelario KM, Steindler DA. The role of extracellular vesicles in the progression of neurodegenerative disease and cancer. Trends Mol Med. 2014;20(7):368–374.

[10] Cooper JM, Wiklander PBO, Nordin JZ, et al. Systemic exosomal siRNA delivery reduced alpha-synuclein aggregates in brains of transgenic mice. Mov Disord. 2014;29(12):1476–1485.

[11] Armstrong JPK, Holme MN, Stevens MM. Re-engineering extracellular vesicles as smart nanoscale therapeutics. ACS Nano. 2017;11(1):69–83.

[12] Wiklander OPB, Nordin JZ, O'Loughlin A, et al. Extracellular vesicle in vivo biodistribution is determined by cell source, route of administration and targeting. J Extracell Vesicles. 2015;4(1):26316.

[13] Mentkowski KI, Snitzer JD, Rusnak S, et al. Therapeutic potential of engineered extracellular vesicles. Aaps J. 2018;20(3):50.

[14] Kanninen KM, Bister N, Koistinaho J, et al. Exosomes as new diagnostic tools in CNS diseases. Biochim Biophys Acta (BBA) - Mol Basis Dis. 2016;1862(3):403–410.

[15] Puig B, Brenna S, Magnus T. Molecular communication of a dying neuron in stroke. Int J Mol Sci. 2018;19(9):2834.

[16] Marchal G, Beaudouin V, Rioux P, et al. Prolonged persistence of substantial volumes of potentially viable brain tissue after stroke: a correlative PET-CT study with voxel-based data analysis. Stroke. 1996;27(4):599–606.

[17] Dirnagl U, Iadecola C, Moskowitz MA. Pathobiology of ischaemic stroke: an integrated view. Trends Neurosci. 1999;22(9):391–397.

[18] George PM, Steinberg GK. Novel stroke therapeutics: unraveling stroke pathophysiology and its impact on clinical treatments. Neuron. 2015;87(2):297–309.

[19] Gelderblom M, Leypoldt F, Steinbach K, et al. Temporal and spatial dynamics of cerebral immune cell accumulation in stroke. Stroke. 2009;40(5):1849–1857.

[20] Cheng NT, Kim AS. Intravenous thrombolysis for acute ischemic stroke within 3 hours versus between 3 and 4.5 hours of symptom onset. Neurohospitalist. 2015;5(3):101–109.

[21] Zhang ZG, Buller B, Chopp M. Exosomes — beyond stem cells for restorative therapy in stroke and neurological injury. Nat Rev Neurol. 2019;15(4):193–203.

[22] Doeppner TR, Bähr M, Hermann DM, et al. Concise review: extracellular vesicles overcoming limitations of cell therapies in ischemic stroke. Stem Cells Transl Med. 2017;6(11):2044–2052.

[23] Vella LJ, Greenwood DLV, Cappai R, et al. Enrichment of prion protein in exosomes derived from ovine cerebral spinal fluid. Vet Immunol Immunopathol. 2008;124(3–4):385–393.

[24] Falker C, Hartmann A, Guett I, et al. Exosomal cellular prion protein drives fibrillization of amyloid beta and counteracts amyloid beta-mediated neurotoxicity. J Neurochem. 2016;137(1):88–100.

[25] Fauré J, Lachenal G, Court M, et al. Exosomes are released by cultured cortical neurones. Mol Cell Neurosci. 2006;31(4):642–648.

[26] Puig B, Altmeppen HC, Glatzel M. The GPI-anchoring of PrP: implications in sorting and pathogenesis. Prion. 2014;8(1):11–18.

[27] Record M, Silvente-Poirot S, Poirot M, et al. Extracellular vesicles: lipids as key components of their biogenesis and functions. J Lipid Res. 2018;59(8):1316–1324.

[28] de Gassart A, Géminard C, Février B, et al. Lipid raft-associated protein sorting in exosomes. Blood. 2003;102(13):4336–4344.

[29] Wulf MA, Senatore A, Aguzzi A. The biological function of the cellular prion protein: an update. BMC Biol. 2017;15(3):34.

[30] Steele AD, Lindquist S, Aguzzi A. The prion protein knockout mouse: a phenotype under challenge. Prion. 2007;1(2):83–93.

[31] Spudich A, Frigg R, Kilic E, et al. Aggravation of ischemic brain injury by prion protein deficiency: role of ERK-1/-2 and STAT-1. Neurobiol Dis. 2005;20(2):442–449.

[32] Doeppner TR, Kaltwasser B, Schlechter J, et al. Cellular prion protein promotes post-ischemic neuronal survival, angioneurogenesis and enhances neural progenitor cell homing via proteasome inhibition. Cell Death Dis. 2015;6(12):e2024–e2024.

[33] Shyu WC, Lin SZ, Chiang MF, et al. Overexpression of PrP^C by adenovirus-mediated gene targeting reduces ischemic injury in a stroke rat model. J Neurosci. 2005;25(39):8967–8977.

[34] Doeppner TR, Herz J, Görgens A, et al. Extracellular vesicles improve post-stroke neuroregeneration and prevent postischemic immunosuppression. Stem Cells Transl Med. 2015;4(10):1131–1143.

[35] Weise J, Crome O, Sandau R, et al. Upregulation of cellular prion protein (PrPc) after focal cerebral ischemia and influence of lesion severity. Neurosci Lett. 2004;372(1–2):146–150.

[36] Mitsios N, Saka M, Krupinski J, et al. Cellular prion protein is increased in the plasma and peri-infarcted brain tissue after acute stroke. J Neurosci Res. 2007;85(3):602–611.

[37] Weise J, Doeppner TR, Müller T, et al. Overexpression of cellular prion protein alters postischemic Erk1/2 phosphorylation but not Akt phosphorylation and protects against focal cerebral ischemia. Restor Neurol Neurosci. 2008;26(1):57–64.

[38] Guitart K, Loers G, Buck F, et al. Improvement of neuronal cell survival by astrocyte-derived exosomes under hypoxic and ischemic conditions depends on prion protein. Glia. 2016;64(6):896–910.

[39] Linsenmeier L, Altmeppen HC, Wetzel S, et al. Diverse functions of the prion protein – does proteolytic processing hold the key? Biochim Biophys Acta, Mol Cell Res. 2017;1864(11):2128–2137.

[40] Altmeppen HC, Prox J, Puig B, et al. Roles of endoproteolytic alpha-cleavage and shedding of the prion protein in neurodegeneration. Febs J. 2013;280 (18):4338–4347.

[41] Altmeppen HC, Puig B, Dohler F, et al. Proteolytic processing of the prion protein in health and disease. Am J Neurodegener Dis. 2012;1(1):15–31.

[42] McDonald AJ, Millhauser GL. PrP overdrive: does inhibition of α-cleavage contribute to PrP(C) toxicity and prion disease? Prion. 2014;8(2):183–191.

[43] Doeppner TR, Bahr M, Giebel B, et al. Immunological and non-immunological effects of stem cell-derived extracellular vesicles on the ischaemic brain. Ther Adv Neurol Disord. 2018;11:1756286418789326.

[44] Vella LJ, Scicluna BJ, Cheng L, et al. A rigorous method to enrich for exosomes from brain tissue. J Extracell Vesicles. 2017;6(1):1348885.

[45] Büeler H, Fischer M, Lang Y, et al. Normal development and behaviour of mice lacking the neuronal cell-surface PrP protein. Nature. 1992;356(6370):577.

[46] Théry C, Amigorena S, Raposo G, et al. Isolation and characterization of exosomes from cell culture supernatants and biological fluids. Curr Protoc Cell Biol. 2006;30(1):3. 22.21–23.22.29.

[47] Puig B, Altmeppen HC, Ulbrich S, et al. Secretory pathway retention of mutant prion protein induces p38-MAPK activation and lethal disease in mice. Sci Rep. 2016;6(1):24970.

[48] Kaech S, Banker G. Culturing hippocampal neurons. Nat Protoc. 2006;1(5):2406–2415.

[49] Polymenidou M, Moos R, Scott M, et al. The POM monoclonals: a comprehensive set of antibodies to non-overlapping prion protein epitopes. PLoS One. 2008;3(12):e3872.

[50] Szklarczyk D, Gable AL, Lyon D, et al. STRING v11: protein–protein association networks with increased coverage, supporting functional discovery in genome-wide experimental datasets. Nucleic Acids Res. 2018;47 (D1):D607–D613.

[51] Pathan M, Keerthikumar S, Ang C-S, et al. FunRich: an open access standalone functional enrichment and interaction network analysis tool. PROTEOMICS. 2015;15(15):2597–2601.

[52] Levy E. Exosomes in the diseased brain: first insights from in vivo studies. Front Neurosci. 2017;11. DOI:10.3389/fnins.2017.00142.

[53] Théry C, Witwer KW, Aikawa E, et al. Minimal information for studies of extracellular vesicles 2018 (MISEV2018): a position statement of the international society for extracellular vesicles and update of the MISEV2014 guidelines. J Extracell Vesicles. 2018;7 (1):1535750.

[54] Lötvall J, Hill AF, Hochberg F, et al. Minimal experimental requirements for definition of extracellular vesicles and their functions: a position statement from the international society for extracellular vesicles. J Extracell Vesicles. 2014;3(1):26913.

[55] Revelo NH, Kamin D, Truckenbrodt S, et al. A new probe for super-resolution imaging of membranes elucidates trafficking pathways. J Cell Biol. 2014;205(4):591–606.

[56] Sasaki Y, Hoshi M, Akazawa C, et al. Selective expression of Gi/o-coupled ATP receptor P2Y12 in microglia in rat brain. Glia. 2003;44(3):242–250.

[57] Bennett ML, Bennett FC, Liddelow SA, et al. New tools for studying microglia in the mouse and human CNS. Proc Natl Acad Sci U S A. 2016;113(12):E1738–E1746.

[58] Bradl M, Lassmann H. Oligodendrocytes: biology and pathology. Acta Neuropathol. 2010;119(1):37–53.

[59] Lappe-Siefke C, Goebbels S, Gravel M, et al. Disruption of Cnp1 uncouples oligodendroglial functions in axonal support and myelination. Nat Genet. 2003;33(3):366–374.

[60] Thiel G. Synapsin I, Synapsin II, and Synaptophysin: marker proteins of synaptic vesicles. Brain Pathol. 1993;3(1):87–95.

[61] Antonucci F, Corradini I, Fossati G, et al. SNAP-25, a known presynaptic protein with emerging postsynaptic functions. Front Synaptic Neurosci. 2016;8. DOI:10.3389/fnsyn.2016.00007.

[62] Agliardi C, Guerini FR, Zanzottera M, et al. SNAP-25 in serum is carried by exosomes of neuronal origin and is a potential biomarker of alzheimer's disease. Mol Neurobiol. 2019;56(8):5792–5798.

[63] Guha D, Lorenz DR, Misra V, et al. Proteomic analysis of cerebrospinal fluid extracellular vesicles reveals synaptic injury, inflammation, and stress response markers in HIV patients with cognitive impairment. J Neuroinflammation. 2019;16(1):254.

[64] Gallart-Palau X, Serra A, Sze SK. Enrichment of extracellular vesicles from tissues of the central nervous system by PROSPR. Mol Neurodegener. 2016;11(1):41.

[65] Goetzl EJ, Kapogiannis D, Schwartz JB, et al. Decreased synaptic proteins in neuronal exosomes of frontotemporal dementia and Alzheimer's disease. Faseb J. 2016;30(12):4141–4148.

[66] Kanai Y, Smith CP, Hediger MA. A new family of neurotransmitter transporters: the high-affinity glutamate transporters. Faseb J. 1993;7(15):1450–1459.

[67] Kanamoto T, Mizuhashi K, Terada K, et al. Isolation and characterization of a novel plasma membrane protein, osteoblast induction factor (obif), associated with osteoblast differentiation. BMC Dev Biol. 2009;9(1):70.

[68] Liang J, Kong Q. α-Cleavage of cellular prion protein. Prion. 2012;6(5):453–460.

[69] Pager CT, Craft WW, Patch J, et al. A mature and fusogenic form of the Nipah virus fusion protein requires proteolytic processing by cathepsin L. Virology. 2006;346(2):251–257.

[70] Diederich S, Sauerhering L, Weis M, et al. Activation of the Nipah virus fusion protein in MDCK cells is mediated by cathepsin B within the endosome-recycling compartment. J Virol. 2012;86(7):3736–3745.

[71] Polanco JC, Li C, Durisic N, et al. Exosomes taken up by neurons hijack the endosomal pathway to spread to interconnected neurons. Acta Neuropathol Commun. 2018;6(1):10.

[72] Heusermann W, Hean J, Trojer D, et al. Exosomes surf on filopodia to enter cells at endocytic hot spots, traffic within endosomes, and are targeted to the ER. J Cell Biol. 2016;213(2):173–184.

[73] Alvarez-Erviti L, Seow Y, Yin H, et al. Delivery of siRNA to the mouse brain by systemic injection of targeted exosomes. Nat Biotechnol. 2011;29(4):341.

[74] Galieva LR, James V, Mukhamedshina YO, et al. Therapeutic potential of extracellular vesicles for the treatment of nerve disorders. Front Neurosci. 2019;13:163.

[75] Bang OY, Kim EH. Mesenchymal stem cell-derived extracellular vesicle therapy for stroke: challenges and progress. Front Neurol. 2019;10:211.

[76] Lee JY, Kim E, Choi S-M, et al. Microvesicles from brain-extract-treated mesenchymal stem cells improve neurological functions in a rat model of ischemic stroke. Sci Rep. 2016;6(1):33038.

[77] Webb RL, Kaiser EE, Jurgielewicz BJ, et al. Human neural stem cell extracellular vesicles improve recovery in a porcine model of ischemic stroke. Stroke. 2018;49 (5):1248–1256.

[78] Perez-Gonzalez R, Gauthier SA, Kumar A, et al. The exosome secretory pathway transports amyloid precursor protein carboxyl-terminal fragments from the cell into the brain extracellular space. J Biol Chem. 2012;287(51):43108–43115.

[79] Levy E. Exosomes in the Diseased Brain: first Insights from In vivo Studies. Front Neurosci. 2017;11:142.

[80] Baker S, Polanco JC, Götz J. Extracellular Vesicles Containing P301L mutant tau accelerate pathological tau phosphorylation and oligomer formation but do not seed mature neurofibrillary tangles in ALZ17 mice. J Alzheimers Dis. 2016;54(3):1207–1217.

[81] Dinkins MB, Dasgupta S, Wang G, et al. The 5XFAD mouse model of alzheimer's disease exhibits an age-dependent increase in anti-ceramide igg and exogenous administration of ceramide further increases anti-ceramide titers and amyloid plaque burden. J Alzheimers Dis. 2015;46(1):55–61.

[82] Iguchi Y, Eid L, Parent M, et al. Exosome secretion is a key pathway for clearance of pathological TDP-43. Brain. 2016;139(12):3187–3201.

[83] Polanco JC, Scicluna BJ, Hill AF, et al. Extracellular vesicles isolated from the brains of rTg4510 mice seed tau protein aggregation in a threshold-dependent manner. J Biol Chem. 2016;291(24):12445–12466.

[84] Spencer B, Kim C, Gonzalez T, et al. α-Synuclein interferes with the ESCRT-III complex contributing to the pathogenesis of Lewy body disease. Hum Mol Genet. 2016;25(6):1100–1115.

[85] Wang B, Han S. Exosome-associated tau exacerbates brain functional impairments induced by traumatic brain injury in mice. Mol Cell Neurosci. 2018;88:158–166.

[86] Mateescu B, Kowal EJK, van Balkom BWM, et al. Obstacles and opportunities in the functional analysis of extracellular vesicle RNA – an ISEV position paper. J Extracell Vesicles. 2017;6(1):1286095.

[87] Kowal J, Arras G, Colombo M, et al. Proteomic comparison defines novel markers to characterize heterogeneous populations of extracellular vesicle subtypes. Proc Nat Acad Sci. 2016;113(8):E968–E977.

[88] Jeppesen DK, Fenix AM, Franklin JL, et al. Reassessment of exosome composition. Cell. 2019;177 (2):428–445.e418.

[89] Silverman JM, Christy D, Shyu CC, et al. CNS-derived extracellular vesicles from superoxide dismutase 1 (SOD1) G93A ALS mice originate from astrocytes and neurons and carry misfolded SOD1. J Biol Chem. 2019;294(10):3744–3759.

[90] van der Pol E, Coumans FAW, Grootemaat AE, et al. Particle size distribution of exosomes and microvesicles determined by transmission electron microscopy, flow cytometry, nanoparticle tracking analysis, and resistive pulse sensing. J Thromb Haemost. 2014;12 (7):1182–1192.

[91] van der Pol E, Sturk A, van Leeuwen T, et al. Standardization of extracellular vesicle measurements by flow cytometry through vesicle diameter approximation. J Thromb Haemost. 2018;16(6):1236–1245.

[92] Liu Z, Chopp M. Astrocytes, therapeutic targets for neuroprotection and neurorestoration in ischemic stroke. Prog Neurobiol. 2016;144:103–120.

[93] Adams KL, Gallo V. The diversity and disparity of the glial scar. Nat Neurosci. 2018;21(1):9–15.

[94] Susarla BTS, Villapol S, Yi J-H, et al. Temporal patterns of cortical proliferation of glial cell populations after traumatic brain injury in mice. ASN Neuro. 2014;6(3):159–170.

[95] Liu W, Tang Y, Feng J. Cross talk between activation of microglia and astrocytes in pathological conditions in the central nervous system. Life Sci. 2011;89(5–6):141–146.

[96] Becerra-Calixto A, Cardona-Gómez GP. The role of astrocytes in neuroprotection after brain stroke: potential in cell therapy. Front Mol Neurosci. 2017;10:88.

[97] Pascua-Maestro R, González E, Lillo C, et al. Extracellular vesicles secreted by astroglial cells transport apolipoprotein d to neurons and mediate neuronal survival upon oxidative stress. Front Cell Neurosci. 2019;12. DOI:10.3389/fncel.2018.00526.

[98] McLennan NF, Brennan PM, McNeill A, et al. Prion protein accumulation and neuroprotection in hypoxic brain damage. Am J Pathol. 2004;165(1):227–235.

[99] Beraldo FH, Soares IN, Goncalves DF, et al. Stress-inducible phosphoprotein 1 has unique cochaperone activity during development and regulates cellular response to ischemia via the prion protein. Faseb J. 2013;27(9):3594–3607.

[100] Vella L, Sharples RA, Lawson VA, et al. Packaging of prions into exosomes is associated with a novel pathway of PrP processing. J Pathol. 2007;211(5):582–590.

[101] van Dongen HM, Masoumi N, Witwer KW, et al. Extracellular vesicles exploit viral entry routes for cargo delivery. Microbiol Mol Biol Rev. 2016;80 (2):369–386.

[102] Nolte-'t Hoen E, Cremer T, Gallo RC, et al. Extracellular vesicles and viruses: are they close relatives? Proc Natl Acad Sci U S A. 2016;113(33):9155–9161.

[103] Tian T, Wang Y, Wang H, et al. Visualizing of the cellular uptake and intracellular trafficking of exosomes by live-cell microscopy. J Cell Biochem. 2010;111(2):488–496.

[104] Mulcahy LA, Pink RC, Carter DRF. Routes and mechanisms of extracellular vesicle uptake. J Extracell Vesicles. 2014;3(1):24641.

[105] Morandat S, Bortolato M, Roux B. Role of GPI-anchored enzyme in liposome detergent-resistance. J Membr Biol. 2003;191(3):215–221.

[106] Bonsergent E, Lavieu G. Content release of extracellular vesicles in a cell-free extract. FEBS Lett. 2019;593 (15):1983–1992.

[107] Chivet M, Javalet C, Laulagnier K, et al. Exosomes secreted by cortical neurons upon glutamatergic synapse activation specifically interact with neurons. J Extracell Vesicles. 2014;3(1):24722.

[108] Bakkebo MK, Mouillet-Richard S, Espenes A, et al. The cellular prion protein: a player in immunological quiescence. Front Immunol. 2015;6:450.

Multiplexed mRNA analysis of brain-derived extracellular vesicles upon experimental stroke in mice reveals increased mRNA content related to inflammation and recovery processes

Annika Bub[1]*, Santra Brenna[1]*, Malik Alawi[2], Paul Kügler[1], Yuqi Gui[1], Oliver Kretz[3], Hermann Altmeppen[4], Tim Magnus[1], Berta Puig[1‡]

[1] Neurology Department, Experimental Research in Stroke and Inflammation (ERSI). University Medical Center Hamburg-Eppendorf, Hamburg, Germany.

[2] Bioinformatics Core, University Medical Center Hamburg-Eppendorf, Hamburg, Germany.

[3] III Department of Medicine, University Medical Center Hamburg-Eppendorf, Hamburg, Germany.

[4] Institute of Neuropathology, University Medical Center Hamburg-Eppendorf, Hamburg, Germany.

*shared first authorship

‡ to whom correspondence should be addressed: b.puig-martorell@uke.de

ABSTRACT

Extracellular vesicles (EVs) are lipid bilayer enclosed structures that not only represent a newly discovered means for cell-to-cell communication but may also serve as promising disease biomarkers and therapeutic tools. Apart from proteins, lipids, and metabolites, EVs can deliver genetic information such as mRNA eliciting a response in the recipient cells. In the present study, we have analyzed the mRNA content of brain-derived EVs (BDEVs) isolated 72 hours after experimental stroke in mice and compared them to controls (shams) using the nCounter® Nanostring panels, with or without prior RNA isolation from BDEVs. We found that both panels show similar results when comparing upregulated mRNA in stroke. Notably, the higher upregulated mRNAs were related to processes of stress and immune system responses, but also to anatomical structure development, cell differentiation, and extracellular matrix organization, indicating that regenerative mechanisms are already taking place at this time-point. The five top overexpressed mRNAs in stroke mice compared to shams were confirmed by RT-qPCR and, interestingly, were found to be present as full-length open-reading frame in BDEVs. We could reveal that the majority of the mRNA cargo in BDEVs was of microglial origin and probably predominantly present in small BDEVs (≤ 200 nm in diameter). However, the EV population with the highest increase in the total BDEVs pool at 72 h after stroke was of oligodendrocytic origin. Our study shows that nCounter® panels are a good tool to study mRNA content in tissue-derived EVs as they can be carried out even without previous mRNA isolation and that the mRNA cargo of BDEVs indicates their participation in inflammatory but also recovery processes after stroke.

74

INTRODUCTION

Extracellular vesicles (EVs) are lipid bilayer particles secreted by all types of cells that play an important role in communication among cells as they can transfer proteins, lipids, and genetic material to recipient cells, even over long distances[1,2]. Among the genetic information contained in EVs, different types of RNA cargoes have been identified such as non-coding RNAs (miRNA, tRNA, siRNA, YRNA, lncRNA, circRNA), and fragmented as well as intact mRNAs[3,4]. The loading of RNAs into EVs is not random as earlier studies support selective incorporation, reflecting the type and the physiological state of the parent cells[5,6]. Moreover, several studies have reported that different types of EVs originating from the same cell type contain differentially sorted miRNAs and mRNAs[7-9].

The mRNAs in EVs are transferred to and translated into protein in recipient cells[10-14]. Other types of RNAs such as fragmented non-coding RNAs and miRNAs have been shown to play an important role in cancer development[14-18]. However, many of the physiological consequences of mRNA and non-coding RNAs contained in EVs once taken up by recipient cells are still unclear.

Ischemic stroke is the world-leading cause of sustained disability. It has a complex pathophysiology involving the reaction of both, brain and infiltrating immune cells, the latter due to the breakdown of the blood-brain barrier (BBB)[19]. After the blockage of an artery, a transient lack of glucose and oxygen at the core of the stroke triggers necrotic cell death in neurons which release their content to the extracellular space, generating Danger Associated Molecular Patterns (DAMPs, such as ATP). DAMPs activate microglia and astrocytes, triggering an immune response. Surrounding the ischemic core, there is a hypoperfused area, the penumbra, where cells are still metabolically active and could potentially be rescued within a critical timeframe[20,21], probably implying a better outcome for the patient[22,23].

Several studies support the idea that EVs play an important role in deciding the neuronal fate under stress conditions and probably the same applies to the neuronal outcome in the penumbra after stroke. On the one hand, *in vitro* studies showed that extracellular ATP stimulates microglia to release EVs containing an altered proteome compared to steady-state conditions, triggering an inflammatory phenotype in astrocytes[24]. ATP released by astrocytes also stimulates the release of microglial EVs containing the proinflammatory cytokine IL-1β[25,26]. On the other hand, EVs derived from non-stimulated astrocytes can rescue neurons under ischemic conditions, a function that depends on the cellular prion protein (PrP^C)[27]. Furthermore, EVs derived from oligodendrocytes increase the viability of neurons subjected to nutrient deprivation[28-30]. Interestingly, a recent study proposed that neurons release "help-me" signals through EVs[31]. The authors showed that EVs containing miRNA-98 released by neurons were taken up by microglia *in vitro* and *in vivo* and, consequently, microglial phagocytosis of stressed but still salvageable neurons was decreased in the penumbra after stroke. Thus, to study the intercellular communication after stroke through EVs is of utmost importance to (i) understand the underlying pathophysiological mechanisms, (ii) identify novel biomarkers, and (iii) develop new therapeutic approaches.

Our present study aimed to investigate if and how the mRNA content in BDEVs changes after stroke compared to sham. To this end, we applied a targeted approach using the nCounter® Neuropathology Panel allowing for the simultaneous assessment of 770 genes related to diverse aspects of neurodegeneration such as neurotransmission, neuron-glia interaction, and neuroinflammation, among others. As these panels can also be used without previous mRNA extraction, another aim was to investigate if this was also applicable to the study of tissue-derived EVs, which would represent a technical advantage as it would eliminate steps in the protocol, thus reducing sample loss and decreasing variability. We subjected mice to transient Middle Cerebral Artery Occlusion (tMCAO), a widely stablished mouse model of stroke, and explored the mRNA content of BDEVs at 72 h after reperfusion, when recovery processes may start to take place. We show that (i) the nCounter® panels

can be used for EVs analysis bypassing the mRNA isolation, obtaining similar results to the panels incubated with previously isolated mRNA; (ii) the highest increase in BDEVs from tMCAO mice was observed for mRNAs related to inflammatory and recovery processes with (iii) mRNA top hits being present as full-length and mostly contained in small EVs (≤200nm); (iv) the majority of highly upregulated mRNAs in BDEVs are released by microglia at this time point even though (v), the most upregulated contributors to the whole BDEV pool at 72 h after stroke are oligodendrocytes.

To the best of our knowledge, this is the first report of mRNA analysis from BDEVs. From a technical point, the present study shows that nCounter® panels are a convenient and reliable method to study EVs as they can perform without prior mRNA isolation. We also show that full-length mRNAs with possible implications in inflammatory and regenerative processes are increasingly shuttled in EVs after stroke, revealing conceivable regulatory roles in stroke pathophysiology.

MATERIAL AND METHODS

Ethics statement

All animal experiments were approved by the local animal care committee (*Behörde für Gesundheit und Verbraucherschutz, Veterinärwesen und Lebensmittelsicherheit of the Freie und Hansestadt Hamburg*, project number N045/2018), and performed following the guidelines of the animal facility of the University Medical Center Hamburg-Eppendorf.

Mice used for this study were kept under a 12h dark-light cycle with *ad libitum* access to food and water.

Transient middle cerebral artery occlusion (tMCAO) procedure

12-18 weeks old male C57BL/6 mice were used for the experiments. Mice were anesthetized and tMCAO was performed as described previously[19]. Briefly, the temporary occlusion of the middle cerebral artery was achieved by inserting a 6.0 nylon filament (602312PK10, Doccol) for 40 min. Control (sham) animals were also anesthetized, and their arteries were exposed but not occluded.

Mice were euthanized 72 h after the tMCAO procedure. Ipsilateral and contralateral hemispheres were stored separately at −80 °C. For the present study, only the ipsilateral hemispheres were used.

EVs isolation

EVs were isolated from the ipsilateral hemisphere of mice from the stroke or sham group as described previously[32]. Briefly, frozen brains were slightly thawed in Hibernate E media (Gibco), finely chopped, and digested with 75U/mL of Collagenase type III (Worthington) in Hibernate E (800µL/ 100mg tissue) for 20 min in a shaking water bath at 37°C. Digestion was stopped using protease inhibitors (Roche). Samples were centrifuged at 300×*g* for 5 min at 4°C, the supernatant was collected and further centrifuged at 2,000×*g* for 10 min at 4°C. The resultant supernatant was further centrifuged at 10.000×*g* for 30 min at 4°C. For some experiments ("filtered samples", F), the resultant supernatant was passed through a 0.22µm cellulose-acetate filter (Whatman) or directly used in the next step ("non-filtered samples", NF). The supernatant was layered on top of a sucrose gradient (2.5M, 1.3M, 0.6M) and centrifuged at 180,000 ×*g* (corresponding to 31,800 rpm in a SW40Ti rotor) for 3h at 4°C. Six fractions were collected, diluted in PBS (Gibco), and further centrifuged at 100,000×*g* (24,000 rpm in SW40Ti rotor) for 1h at 4°C. After the initial characterization, fractions 2,3, and 4 were pooled before dilution in PBS. The pellet was stored at -20°C for further RNA isolation or resuspended in RIPA buffer (50 mM Tris-HCl pH=7.4, 150 mM NaCl, 1% NP40, 0.5% Na-Deoxycholate and 0.1% SDS) or PBS with protease and phosphatase inhibitors (Roche) to be used for western blot or NTA analysis, respectively.

SDS-PAGE and western blot

EVs samples in RIPA were mixed with 4× NuPage LDS Sample buffer (Invitrogen) and 10× NuPage Sample reducing agent (Invitrogen) and heated at 70°C for 10 min. For EVs characterization, the same volume for the 6 fractions was loaded (15 µL) in NuPage 10% Bis-Tris precast gels and run at 150V. Proteins were then transferred onto nitrocellulose membrane (LI-COR) at 400 mA for 1h. Total protein content was visualized by staining the membranes with Revert Total Protein Stain Kit (LI-COR), as described by the manufacturer's instructions. To block unspecific binding, membranes were incubated with 1× RotiBlock (Roth) in TBS for 1h at room temperature while shaking and incubated overnight at 4°C with the following primary antibodies: ADAM10 (1:1,000; EPR5622), Alix (1:500; #2171;CST), CD81 (1:1,000; #10037; Cell Signaling), Flotilin-1 (1:1,000; #610820; BD Biosciences), or GM130 (1:1,000; #61082; BD Biosciences). After incubation, membranes were washed with TBST, incubated for 1h with the corresponding secondary antibody (1:1,000 Anti-mouse IgG,#7076/Anti-rabbit IgG, #7074; both from Cell Signaling), washed again with TBST, and developed with Super Signal West Femto Substrate (ThermoFisher). The chemiluminescence reaction was detected with a ChemiDoc Imaging Station (BioRad).

For cellular markers characterization, 3 µg of proteins measured with the Micro BCA Protein Assay Kit (Thermo Scientific) following the instructions of the supplier, were mixed with 4× loading buffer (250mM Tris-HCl, 8% SDS, 40% glycerol, 20% β-mercaptoethanol, 0.008% Bromophenol Blue, pH 6.8), boiled for 5 min at 95°C, loaded onto a 10% Bis/Tris acrylamide gel and subjected to electrophoresis as described above. The following antibodies were used: CD40 (1:500, NB100-56127SS; Novusbio), CNP(1:1,000, C5922; Sigma), EAAT1 (1:500, NB100-1869SS; Novusbio), EAAT2 (1:500, NBP1-20136SS; Novusbio), NCAM (1:1,000, #99746; Cell Signaling), P2Y12 (1:500, #11976-1-AP; Proteintech), PLP (1:1,000, NB100-74503; Novusbio), Synapsin-1 (1:1,000, #106103; Synaptic Systems). After overnight incubation while shaking at 4°C, the detection was performed as described above.

RNA isolation

RNA was isolated from the EVs using the Qiagen RNeasy Plus Micro Kit (Qiagen). Briefly, EV pellets from fractions 2, 3, and 4 were resuspended each in 117 µL of Lysis Buffer RLT Plus (Qiagen), vortexed, and pooled together (total of 350 µL as recommended by the supplier) and RNA was isolated following the manufacturer's instructions. The quality and purity of the isolated RNA were checked using the Agilent 2100 Bioanalyzer following the instructions of the supplier.

Gene expression analysis with nCounter® panels

Gene expression analysis was performed by using the NanoString nCounter® Neuropathology panel (#XT-CSO-MNROP1-12, NanoString Technologies). Two panels were used: one loaded with RNA isolated from BDEVs (that were filtered during the preparation of EVs); and another one where all the samples bypassed the RNA isolation ("non-isolated", NI) but some were filtered during the BDEVs preparation (F) and the others were not filtered (NF) during preparation.

To run the first panel, 50 ng of previously isolated RNA measured by Qubit™ RNA High Sensitivity Assay Kit (Thermo Fisher) using the 3.0 QuBit Fluorometer, were mixed with RNAse–free water (Qiagen) up to 5 µL. Samples were hybridized for 18 h and mixed with 15 µL of RNAse-free water to be loaded on the nCounter® Sprint Cartridge (#LBL-10038-01, NanoStringTechnologies), following the instructions of the company. The analysis was run for 6 h.

For direct loading of EV lysates (i.e., no previous RNA isolation, NI), frozen EVs were resuspended in RLT lysis buffer and RNAse-free water in a ratio of 1:3 and loaded based on protein concentration measured by Micro BCA Protein Assay Kit (Thermo Scientific). 2,8 µg of proteins were loaded.

Reverse Transcription and quantitative PCR (RT-qPCR)

The cDNA was synthesized from the BDEVs' isolated RNA using Maxima First Strand cDNA Synthesis Kit for RT-qPCR (Thermo Scientific), following the supplier's instructions. The resulting cDNA was loaded in a 1:15 dilution with a master mix (Probe qPCR MM No ROX; Thermo Scientific) with the following TaqMan Probes: Hmox1 (#Mm00516005_m1), Fcrls (#Mm00472833_m1), Cd44 (#Mm01277161_m1), C1qb (#Mm01179619_m1), Gfap (#Mm01253033_m1) all from Thermo Scientific. Asb7 (#Mm01318985_m1) and Fam104a (#Mm01245127_g1), both from Thermo Scientific, were used as housekeeping genes based on the nCounter® analysis. The reaction was performed using LightCycler 96 (Roche) with the following conditions: 50°C for 120 s, 95°C for 600 s, followed by 45 cycles of 95°C for 10 s, and 60°C for 30 s and further cooling of 37°C for 30 s. Samples were run in triplicates. Differential expression was analyzed using the $2^{-\Delta\Delta CT}$ method. ΔCT was calculated by subtracting the arithmetic means of the CT values of our two housekeeping genes from the CT values of the mRNA of interest. $\Delta\Delta CT$ was calculated by subtracting the average ΔCT of the sham samples from the ΔCT of the stroke samples. The fold change (FC) was calculated as $2^{-\Delta\Delta CT}$.

PCR

cDNA was synthesized as above and 5µL of the resulting EVs cDNA (concentration not measured as the PCR was only intended to be qualitative) or 1 µL of total WT brain cDNA (positive control) or 1 µL of water (negative control) were mixed with 1× Master Mix: dNTPs 0.4 mM, primers 0.4 µM, Dream Taq polymerase 1U, 1× Dream Taq Green Buffer (all from Thermo Fischer) and water. The following primers were used:

Hmox1: 5′ATGGAGCGTCCACAGCC 3′(sense), 3′ GGCATAAATTCCCACTGCCAC 5′(antisense)
C1qa: 5′ATGGAGACCTCTCAGGGATGG 3′(sense), 3′TCAGGCCGAGGGGAAAATGA 5′(antisense);
C1qb:5′TGAAGACACAGTGGGGTGAGG 3′(sense), 3′TACGCATCCATGTCAGGGAAAA 5′(antisense);
C1qc: 5′ATGGTCGTTGGACCCAGTTG 3′(sense), 3′CTAGTCGGGAAACAGTAGGAAAC 5′(antisense);
Gfap: 5′ATGGAGCGGAGACGCATCA 3′(sense), 3′ACATCACCACGTCCTTGTGC 5′(antisense); and
Cd44: 5′GTTTTGGTGGCACACAGCTT 3′(sense), 3′CAGATTCCGGGTCTCGTCAG 5′(antisense).
The PCR reaction was performed as follows: 95°C for 5 min; 95°C for 45 s and 61°C for 45 s, and 72°C for 1 min (×35 cycles); 72°C for 5 min. The samples were loaded in a 1.5% Agarose gel mixed with Roti-GelStain (Roth) and run at 120 V for 40 min. The gel was then stained with ethidium bromide (Fluka) and imaged with UVP UVsolo touch (Analytik Jena).

Nanoparticle Tracking Analysis (NTA)

Pellets resulting from the EVs isolation were resuspended in 30 µL PBS and 1 µL of this suspension was diluted in PBS at 1:500, and the resulting 500 µL were then loaded into the sample chamber of the LM10 unit (Nanosight, Amesbury, UK). Samples were recorded with ten videos, each 10 s long. Data analysis was performed by NTA 3.0 software (Nanosight) with the following software settings: detection threshold = 6, screen gain = 2.

Transmission Electron Microscopy

For TEM, extracellular vesicle pellets were re-suspended in 0.1M PBS. Drops of these suspensions were placed on parafilm. Carbon-coated copper meshed grids (Plano, Germany) were placed on the drops for 5 minutes for probe adsorption. After five minutes of fixation on drops of 1% glutaraldehyde (Roth, Germany) grids were washed 4 times for 30 seconds and negative contrasted using 1% uranyl acetate. Grids were air-dried and analyzed using a Philips CM 100 transmission electron microscope.

Analysis of the nCounter® panel data, GO terms enrichment, and cell types of origin

For each of the three datasets, genes with raw expression scores not exceeding the average plus two standard deviations of all corresponding negative control probes, in at least one sham and one stroke sample, were removed from the analysis. Normalization was based on the ten housekeeping mRNAs present on the panel. Differential expression analysis was carried out with DESeq2[33]. A mRNA was considered differentially expressed if the corresponding absolute log2-fold change (log2FC) was larger or equal to 1 and the False Discovery Rate (FDR) was smaller or equal to 0.1.

To perform overrepresentation analysis, clusterProfiler[34] was used in combination with GOslim terms[35].

A gene expression matrix for the data set 'Whole Cortex & Hippocampus - 10X Genomics (2020) was obtained from the Allen Mouse Brain Atlas[36]. To generate this matrix we used the mRNA values corresponding to log2FCs greater or equal to 2 and FDRs smaller or equal than 0.1 in the panel with samples I+F.

Statistical analysis

To analyze the differences between sham and strokes in the western blot and for the NTA we used GraphPad Prism 8, applying non-parametric Mann-Whitney U test in both cases. Statistical significance was considered for $*p < 0.05$, $**p < 0.005$, and $***p < 0.001$. Values are given as a mean± standard error of the mean (SEM). The exact p-values are given in the main text.

RESULTS

Characterization of BDEVs and mRNA isolation

An overview of our experimental strategy and workflow concerning the respective data in the main figures is shown in Fig. 1A. EVs from mouse brains were isolated as described before[32] and characterized by western blot (WB), nanoparticle tracking analysis (NTA), and electron microscopy (EM) following the MISEV 2018 guidelines[37]. As shown in Fig. 1B, six fractions were obtained after sucrose gradient centrifugation. Fractions 2, and 3 were enriched in common EV markers such as flotillin, CD81, mature ADAM10, 14-3-3, and Alix (with the latter two being cytosolic proteins, indicating EV integrity). GM130, a membrane protein of the cis-Golgi apparatus was used here as a marker of contamination with intracellular organelles and was not present in any of the six fractions. For subsequent experiments, we pooled fractions 2, 3, and 4 (as in the latter fraction flotillin and CD81 were also present) as the "EVs fraction". NTA measurements of this EV fraction revealed that the number of EVs was not significantly elevated in the tMCAO brains compared to shams, although there was a clear tendency towards an increase (mean value shams: $5.5 \times 10^{11} \pm 1.77 \times 10^{11}$; mean value tMCAOs: $1.07 \times 10^{12} \pm .,82 \times 10^{11}$; Fig. 1C; n=6 for each group). EM pictures showed that EVs of different sizes were enriched in the pooled pellets (Fig. 1D, black arrowheads). Some structures with a more squared profile were also identified (white asterisks) probably indicating some degree of contamination, yet no major differences were observed between EVs isolated from tMCAO brains compared to shams). We then proceeded to isolate RNA from the EVs fraction and analyzed it with Bioanalyzer. Most of the RNA contained in the EVs from shams or stroke brains corresponded to small RNAs of less than 1,000 nucleotides (nt), although some bands appeared between 1,000 and 4,000 nt as well. Very low amounts of the ribosomal RNA (rRNA) subunit 18S and no detectable levels of the 28S rRNA subunit were observed (Fig. 1E). A representative RNA electropherogram is shown in Fig. 1F confirming that the majority of RNA is less than 1,000 nt with only a few ranging between 1,000 and 4,000 nt. The mean RNA concentration for shams was 23.06 ± 2.053 ng/µL) whereas for strokes this was 22.06 ± 3.64 ng/µL (n=3 per condition) as measured with QuBit™ RNA High Sensitivity Assay.

Similar BDEVs` mRNA profiles are obtained with the nCounter® panels with and without previous mRNA extraction, and with and without a filtration step during preparation of BDEVs

Isolated mRNA from EVs purified from the ipsilateral hemisphere of either sham (n=3) or tMCAO (n=3) mice were hybridized with the nCounter® Neuropathology panel from Nanostring which allows for multiplexed detection and quantification of 770 genes related to several aspects of neurodegeneration. Of interest for the studies of EVs´ mRNA, this method can detect low abundant mRNA[38]. To analyze the data, we used two criteria, a stringent one, focusing on those mRNAs that showed an absolute log2 fold-change (log2FC) larger or equal to 2 (i.e., increase/decrease), and a broader criteria also considering mRNAs increased/decreased with an absolute log2FC larger or equal to 1, respectively. The false discovery rate (FDR) in each case was required to be below or equal to 0.1.

Out of the 770 genes present in the panel, 94 genes were significantly upregulated (log2FC≥1) and 3 were significantly downregulated (log2FC≤-1) in the tMCAO BDEVs compared to shams (Fig. 2A; Suppl. Table 1). A log2FC≥2 cut-off resulted in 31 mRNAs showing upregulation with Hmox1 being the highest hit with a log2FC of 3.73 (i.e., about 13-fold upregulated). However, the mRNA with the highest counts significantly upregulated in tMCAO (indicating a strong presence in BDEVs), was for Gfap (Fig.2B, Suppl. Table 1). No downregulated mRNA presented a log2FC≤-2. Principal component analysis (PCA) showed that samples of either sham or tMCAO cluster together, respectively, indicating differential mRNA expression between the two experimental groups (Suppl. Fig. 1).

One of the advantages offered by the nCounter® panels is their sensitivity, as they can be used without prior mRNA extraction. This is intended for cells and, to our knowledge, it has not been employed for EV analyses yet. Considering that EV isolation from tissue already is a multistep process (with the risk of losing material and information at every step of the protocol, we thought it could be of great advantage to bypass the mRNA isolation step, as the latter may result in mRNA loss. Hence, as a proof of concept, we ran a second nCounter® Mouse Neuropathology panel for which the mRNA was not isolated before (from now onwards termed "NI (non-isolated) samples" versus "I (isolated) samples"). The heat map and volcano plot in Fig. 2C and 2D show that from the "NI"-samples, we obtained several significantly upregulated mRNAs for the tMCAO BDEVs compared to shams (88 mRNAs upregulated with a log2FC ≥1 and 11 mRNAs downregulated with log2FC ≤-1; Fig. 2C, Table 1 and Suppl. Table 2). With some differences in the fold-change, "I" and "NI" samples shared most of the highly upregulated mRNAs. Thus, out of the significantly upregulated mRNAs (log2FC≥2) in tMCAO (31 in the "I"-samples panel, and 29 in the NI-samples panel), 23 were common (Table 1 and Venn diagram in Fig. 2E). Eight mRNAs (Tgfb1, Tspo, Cxcl16, Grn, Ccr2, Hpgds, Itga5, and Spi1) present in the isolated samples panel with a log2FC≥2 showed a lower fold-change in the "NI" samples panel, although still showing upregulation (log2FC≥1). Vice-versa, five mRNAs (Lrrc25, Tnfrsf1b, Bcas1, Tnfrsf1a, and Irf8) showed a log2FC≥2 in the "NI" samples, which was lower (although still upregulated with a log2FC≥ 1) in the "I" samples (Table 1). "I" and "NI" samples also shared most of the differentially expressed mRNAs (76 mRNAs), meaning that 81% of the absolute log2FC≥1 mRNA significantly differentially expressed in the "I"-samples are likewise significantly differentially expressed in the "NI"-samples. Because differences between the panels could be attributed to panel batches or sample variation in the tMCAO model, we conclude that overall the nCounter® panels are suitable for the study of BDEVs mRNA cargo without the need for prior mRNA extraction.

In a previous study, we have shown that introducing a filtration step with a 0.2µm membrane leads to the differentiation between two EV populations harboring different protein content, with the population with a diameter ≤ 200 µm (i.e., small BDEVs, sBDEVs) being relatively enriched in ribosomal proteins[32]. The results presented above were generated with samples undergoing this filtration step. However, we were also interested in knowing whether the relative mRNAs in BDEV populations would change by skipping this filtration step and including larger EVs as well. Therefore, in the same panel

(all "NI"-samples), we also added BDEVs samples that were lacking the 0.2 μm filtration step ("NF" samples) and compared them to the filtrated ("F") samples described above. As shown in the heat map and the volcano plot (Fig. 3A and 3B) and Table 1, the most upregulated mRNAs (log2FC≥2) present in the "NF" samples were also among the most upregulated present in the filtrated samples, although the relative fold-change slightly varied. In the "NI"+"NF" samples, we found 22 mRNAs upregulated with a log2FC≥2, and 60 mRNAs upregulated when the cut-off was set to log2FC≥1. In these samples, no significantly downregulated mRNA species with a log2FC≤-1 were found (Table 1 and Suppl. Table 3). As shown in the Venn diagrams in Fig. 3C and 3D, no mRNA was exclusively detected when the samples were not filtered. These findings could indicate that the majority of mRNAs are contained in small EVs (≤ 200 μm). Alternatively, our observations may suggest that because bigger EVs have a relatively higher protein content, the background of the panels is increased thereby relatively lowering mRNA detection, which could explain the generally low fold-change detection in 2 out of the 3 samples shown in the heat map (Fig. 3A).

Upregulated mRNAs in BDEVs after tMCAO are (i) related to inflammatory responses, stress defense, and recovery processes, (ii) are mainly released by microglia, and (iii) top hits present in full-length.

To validate the data obtained with the nCounter® panels, we next performed RT-qPCR for 5 of the top mRNAs found upregulated in the tMCAO samples. As shown in Fig.4A, the amount of mRNA extracted from BDEVs was sufficient to perform reverse transcription to cDNA and RT-qPCR analyses (n=7 for each group). All the examined mRNAs (Hmox1, Cd44, C1qa, Gfap, and Fcrls) showed a significant increase in BDEVs from tMCAO mice compared to shams with a similar fold-increase as found in the nCounter® panels (Table 1).

Overrepresentation analysis of GO terms by using the 770 genes present in the nCounter® panel as background mRNA, revealed two main types of responses: on the one hand, these were "immune system process", and "response to stress", indicating that BDEVs carry mRNAs related to inflammatory processes. On the other hand, terms such as "anatomical structure development", "cell differentiation", "cell population differentiation", "anatomical structure formation involved in morphogenesis", or "extracellular matrix reorganization", were also overrepresented, suggesting that certain recovery processes are already taking place at 72 h after tMCAO with BDEVs participating in these events (Fig. 4B and Table 2). To assess the origin of the highest upregulated mRNAs carried in BDEVs after tMCAO (log2FC≥2) we generated a heat map based on data from the Cell Types Database: RNAseq Data from the Allen Brain Map. This revealed that several mRNAs (13 out of 21 with an assigned cell type) were originating from either microglia or perivascular macrophages (Fig. 4C).

Finally, we designed PCR primers to qualitatively assess whether the mRNA of six of the top ten candidates present in BDEVs was full length. We used primers allowing for the assessment of the open reading frame (ORF) as an indicator of intact mRNAs. Although the amounts were very variable between the samples, mRNAs for Hmox1, Gfap, C1qa, C1qb, and C1qc, were all present in BDEVs as full-length based on their expected size (Fig. 4D).

Oligodendrocytic-EVs are upregulated in the total BDEVs pool at 72 h after tMCAO.

We have demonstrated earlier that the main EVs population contributing to the total BDEVs pool under physiological conditions originated from microglia. This situation changed 24 h after tMCAO when astrocytic EVs were found significantly upregulated[32]. Considering our aforementioned finding of a predominantly microglial origin of mRNAs in BDEVs obtained at 72 h after stroke (Fig. 4C), we wondered whether this would also reflect an increased contribution of this cell type to the total EV pool in stroked brains at this time-point. Therefore, by applying the same methodology as in our previous study (i.e., biochemical assessment of two typical markers per brain cell type), we compared

BDEVs from tMCAO (n=5) and sham (n=5) mice at 72 h after stroke. For neurons, we detected the Neural Cell Adhesion Molecule 1 (NCAM1) as it was present in the mass spectroscopy analysis from BDEVs in our previous study, and Synapsin 1 as used before[32]. As astrocyte-specific markers we assessed the Excitatory Amino Acids Transporter 1 and 2 (EAAT1, EAAT2)[39]; and for microglia, we used the G-protein coupled P2Y receptor 12 (P2Y12) as well as CD40, present in activated microglia and macrophages[40]. Lastly, for oligodendrocytes, we detected the proteolipid protein (PLP, a major component of the myelin sheath) and 2'-3'-Cyclicnucleotide 3'-phosphodiesterase (CNP) [41]. The quantification was done by first referring the band intensity of the marker protein to the total protein staining serving a loading control, and the mean values between sham and tMCAOs were then compared. As shown in the western blots of Fig. 5A, all marker proteins were present in BDEVs. An obvious increase in both markers for oligodendrocytes (i.e., PLP and CNP1, significantly upregulated in tMCAO **p=0.0079 and *p=0.0317, respectively) was observed. This increase was specific for BDEVs as brain homogenates showed no differences between shams and strokes (Suppl. Fig. 2). Surprisingly, although most of the mRNA present in BDEVs in our study is characteristic of microglial origin, both microglial markers used for immunoblotting did not show any increase in the tMCAO samples compared to shams. The neuronal markers NCAM1 and Syn1 were upregulated but only the increase in NCAM1 reached significance (**p=0.0079), indicating that neurons could significantly contribute to the BDEVs pool 72 h after stroke. Again, as for PLP and CNP1, the increase in NCAM was specific for BDEVs and not paralleled in brain homogenates (Suppl. Fig. 2). Finally, although Gfap was one of the mRNAs with highest fold-change in our analysis, we did not observe a significant increase in BDEVs from astrocytes. This is in contrast to what we have previously found at 24 h after tMCAO using the same protein markers[32] and may highlight the transient nature of successive inflammatory and repair processes after stroke with the relative contributions from different cell types changing over time.

DISCUSSION

In the present study, we have used the Nanostring nCounter® panels to demonstrate that, after inducing stroke in mice followed by 72 h reperfusion, BDEVs increased their content in mRNAs related to immune, inflammatory, and defense responses as well as recovery processes. The mRNAs present a full-length ORF in BDEVs, at least for the most upregulated genes in tMCAO compared to shams. The top five most upregulated genes shared by all panels detected here are Hmox1, Cd44, C1q (composed by C1qa, C1qb, and C1qc), Gfap, and Fcrls. Hmox1 encodes for the inducible Heme Oxygenase (HO1), which has been implicated in neuroprotection after stroke and is considered a possible therapeutic target[42]. CD44 protein is important for synaptic plasticity and axon guidance, among other functions, in the central nervous system (CNS). Under pathological conditions such as multiple sclerosis (MS) and its respective experimental model in rodents (Experimental Autoimmune Encephalomyelitis, EAE), CD44 has immunomodulatory properties and protects from the breakage of the BBB[43]. After stroke, CD44 seems to be upregulated in neural stem/progenitor cells (NSPCs) and microglia/macrophages at the penumbra area[44]. C1q, the recognition molecule complex that initiates the classical pathway of the complement cascade, is secreted by macrophages and exerts important functions in the brain such as tagging unwanted synapses for elimination[45,46]. In stroke, early activation of the complement system leads to inflammation, but at later time-points, C1q might also play a role in regenerative processes[47]. Gfap encodes for the Glial Fibrillary Acidic Protein (GFAP) which is mainly expressed by astrocytes. Its expression increases when astrocytes become reactive and when they form the glial scar which limits inflammation and promotes repair[48-50]. Fcrls encodes for the Fc Receptor-like S, a scavenger receptor expressed specifically by microglia[51] but only in mice, rats, and dogs[52]. Scavenger receptors bind ligands that are non-self or self-altered molecules and remove them by phagocytosis

82

(among other mechanisms) leading to the elimination of degraded or harmful substances[53]. Thus, at 72 h after tMCAO, BDEVs contain mRNAs encoding for proteins involved in inflammatory and defense responses but which may also participate in the reconstruction and repair of the affected area.

Because microglia and astrocytes are reactive and proliferate upon stroke, one question is whether an increase of mRNAs such as Gfap or C1qs in BDEVs is just a consequence of the increased amount of these mRNAs in the parental cells. While with the present study we cannot rule out this possibility (as one would have to assess the amount of mRNA in the cells of origin), the fact that Hmox1, C1q, Cd44, and Fcrls showed in general rather low counts in BDEVs from tMCAO mice (although with a significant fold increase compared to sham), our findings would speak in favor of a specific loading of these mRNAs into EVs as a reaction to hypoxic ischemia.

It has been shown that different types of EVs contain different RNA profiles, for instance, with apoptotic bodies being richer in ribosomal RNA (rRNA) when compared to microvesicles and exosomes[54]. Interestingly, we did not detect major differences in relative amounts of mRNAs between filtered and non-filtered samples (the latter presenting a larger average diameter[32]). Although we cannot rule out that an increased amount of protein (since the RNA was not isolated, and bigger EVs probably contain relatively more amount of proteins) could increase the background (overall fewer mRNAs were detected compared to the "NI+F" panel), it could also imply that sEVs (≤ 200nm) carry the majority of the EV-associated mRNAs. Crescitelli et al. showed that in two out of three investigated cell lines, most of the RNA was present in exosomes (which fall into the category of sEVs)[54]. Although the type of sample and the isolation methods impact the RNA yield and size distribution[55], and though the protocols differ between that and our study, the finding could indicate a general lack (or at least relatively reduced presence) of mRNA in larger EVs. Notably, in our previous study[32] we showed that sBDEVs were enriched in ribosomal proteins when compared to BDEVs that were not filtered and, in fact, ribosomal proteins are commonly found in BDEVs even when using different isolation protocols[56]. Even though it has been shown that EVs do not have the appropriate machinery to translate mRNA directly within the vesicles (at least in cultured cell lines[10]), it could be hypothesized that they could deliver most of the translation machinery plus the mRNA onto recipient cells, particularly as tRNA have also been found in BDEVs[57].

Previously, we observed a significant increase in astrocytic BDEVs in the total brain pool of tMCAO mice compared to shams at 24 h after stroke[32]. In the present study investigating the time-point of 72 h after tMCAO, EVs from oligodendrocytes are the most upregulated species as judged by two protein markers in western blot analyses. This came as a surprise considering that much of the BDEVs mRNA was found to be significantly upregulated at this time-point after tMCAO could be ascribed to microglia. However, given the fact that our analyses only investigated relative changes upon stroke and not absolute contributions by cell types, both findings are not necessarily conflictive as microglia derived-EVs could still make up a large part of the total pool. Of note, oligodendrocytes, the myelinating cells of the CNS, play a currently understudied role in stroke. They are highly susceptible to ischemic conditions, and the remyelination process starts through the proliferation of oligodendrocyte progenitor cells (OPCs) within the penumbra area[58]. Apart from axonal myelination oligodendrocytes can have an influence on neuronal survival after stroke. For instance, in vitro studies show that upon certain neuronal signals, oligodendrocytes release EVs that rescue primary neurons subjected to oxygen-glucose deprivation (OGD, an in vitro model of stroke)[29,30]. Oligodendrocyte-derived EVs also influence axonal transport in physiological conditions, an effect that is enhanced when neurons are nutrient-deprived, helping neurons to survive through the delivery of stress-protective macromolecules such as heat shock proteins[28]. Microglia-to-oligodendrocyte communication is another axis that should be considered. Oligodendrocytes can release chemokines and other factors (presumably through EVs) that, under stress conditions, promote microglial phagocytosis[59]. In a model of demyelination in mice, microglia and macrophages turn to anti-

inflammatory/immunoregulatory (M2) states and promote the differentiation of OPCs into oligodendrocytes[60]. Thus, by the fact that we also observe an increase in oligodendrocytic-derived EVs at 72 h after tMCAO (a time-point when recovery processes start to take place), it seems plausible that EVs of this particular origin not only play a role in the neuronal remyelination after injury but also in supporting neuronal survival and debris clearance, possibly through communication with microglia. From a technical point of view, we here present that the Nanostring nCounter® panels are useful tools to study the mRNA composition in BDEVs. We chose this technology because while RNA-seq is a very sensitive method and can detect a wide range of RNAs in a given sample, the nCounter® technology offers the advantage that the starting material can be of low amounts and that no further steps (such as reverse transcription, which can introduce certain biases) are necessary to analyze the mRNA content[61]. We show that even when the RNA was not extracted from BDEVs, similar results (although differing in absolute amounts) were obtained compared to samples that underwent the additional RNA isolation step. This is a clear advantage, as one of the problems when assessing EV-derived mRNA, and a considerable challenge for this field is the use of different methodologies to isolate EVs´ RNA[62]. Moreover, the approach presented here reduces steps in sample preparation and probably increases the chances to detect some species that otherwise would be lost during mRNA isolation. In our case, we were able to detect more significantly downregulated RNA species. It has recently been described that nCounter® panels are also useful and sensitive to analyze EVs isolated from human plasma samples and supernatants of cell cultures. However, in these studies, the amount of EVs obtained was too low to run the samples directly , and intermediate steps such as RNA retro-transcription and cDNA amplification had to be introduced[63,64]. These studies confirmed that even when RNA extracted from EVs is present in low amounts, it can still be used for analysis with the nCounter® panel. Our present report on BDEVs, to the best of our knowledge, is the first to show the suitability of these arrays for analysing the mRNA content of EVs obtained from complex tissues such as brain.

Some papers described the presence of mRNA in exosomes that could be translated in recipient cells[10,14,65], while in other instances mRNA in EVs was found mainly to be fragmented, as in the case of EVs from human glioblastoma stem cells[3,66]. A recent study using EVs isolated from human blood and performing RNAseq, found that a substantial amount of the total RNA detected in EVs was full-length with a mean size of around 2.800 nucleotides, but also containing very large mRNAs (e.g., KMT2D with more than 19.000 bp)[67]. In our study, we have explicitly checked by PCR if we could amplify the full open reading frame (ORF) of six of the top upregulated candidates. We confirmed that they were all present as full-length in BDEVs, and therefore have at least the potential to be translated in the recipient cells. However, studying the biological relevance of the mRNA content (and other RNA cargoes) in EVs and proving their functionality in the recipient cells is very challenging[68]. It has been shown in EVs of human glioblastoma stem cells that the number of mRNAs is substantially low, as it was estimated to be 1 copy in 1,000 EVs for the most abundant mRNA, and for others less than 1 copy every 10,000 to 100,000, or even 1 copy in a million EVs for some RNA species. However, related to miRNA and despite the low numbers, the authors of this study observed an effect of miR21 in recipient cells[3]. We have also made some rough calculations on the possible number of EVs containing mRNA detected in our system: for the NI-samples (where, in general, the amounts of mRNA counts were higher), we loaded 2.8 µg of sample which approximately corresponds to 6.6×10^{10} EVs (calculation based on the mean of 6 NTA measurements and previous micro-BCA assays). If we take Gfap (for which we confirmed presence in full length, and which showed the highest counts among the significantly upregulated BDEV mRNAs in stroke), the ratio would be approx. 1 mRNA copy per 19,000,000 EVs. Thus, the biological significance of mRNAs present in BDEVs in these relatively low amounts is difficult to judge with the current knowledge and tools. We have attempted to incubate BDEVs with several cell lines to assess any putative transfer and translation of Gfap and Hmox1 in recipient cells by employing immunocytochemistry and confocal microscopy to no avail (data not shown). However,

several variables could have played a role in our negative results. In the scenario where EVs were delivered and the mRNA translated, it is plausible to think that either confocal microscopy was not sensitive enough to detect newly translated proteins or the time points we chose to assess protein translation (24 h and 48 h) were not appropriate.

An important question in the EV field is how the cargo is delivered to the cytosol, especially in the case of RNAs that presumably have to reach this compartment in the recipient cell to exert their function/be translated to proteins[68]. Direct fusion of EVs with the target cell's plasma membrane would be the most plausible mechanism to deliver RNA and the EV luminal content to the cytosol of recipient cells. However, in only a few instances fusion of EVs with recipient cells has been demonstrated until now[69-71], and most of the experiments point to endocytosis as the main take-up mechanism. This implies fusion with late endosomal membranes as a mechanism of endocytic escape for the content of EVs to eventually reach the cytosol[72-74].

In conclusion, we demonstrate here that nCounter® panels are a useful tool for the targeted study of mRNAs contained in EVs derived from brain tissue. Investigations of the EVs content and alterations therein after cerebral ischemia will surely contribute to increasing our knowledge of this complex pathophysiology and may provide novel therapeutic tools to rescue neurons at the penumbra soon after hypoxic insults.

ACKNOWLEDGMENTS

CONFLICTS OF INTEREST

The authors declare no conflict of interest.

REFERENCES

1   Maas, S. L. N., Breakefield, X. O. & Weaver, A. M. Extracellular vesicles: unique intercellular delivery vehicles. *Trends in cell biology* **27**, 172-188, doi:10.1016/j.tcb.2016.11.003 (2017).

2   Lo Cicero, A., Stahl, P. D. & Raposo, G. Extracellular vesicles shuffling intercellular messages: for good or for bad. *Current Opinion in Cell Biology* **35**, 69-77, doi:https://doi.org/10.1016/j.ceb.2015.04.013 (2015).

3   Wei, Z. *et al.* Coding and noncoding landscape of extracellular RNA released by human glioma stem cells. *Nature communications* **8**, 1145-1145, doi:10.1038/s41467-017-01196-x (2017).

4   Fanale, D., Taverna, S., Russo, A. & Bazan, V. in *Circular RNAs: Biogenesis and Functions* (ed Junjie Xiao) 109-117 (Springer Singapore, 2018).

5   Eldh, M. *et al.* Exosomes communicate protective messages during oxidative stress; possible role of exosomal shuttle RNA. *PloS one* **5**, e15353-e15353, doi:10.1371/journal.pone.0015353 (2010).

6   Nolte-'t Hoen, E. N. M. *et al.* Deep sequencing of RNA from immune cell-derived vesicles uncovers the selective incorporation of small non-coding RNA biotypes with potential regulatory functions. *Nucleic acids research* **40**, 9272-9285, doi:10.1093/nar/gks658 (2012).

7   Lunavat, T. R. *et al.* Small RNA deep sequencing discriminates subsets of extracellular vesicles released by melanoma cells – Evidence of unique microRNA cargos. *RNA Biol* **12**, 810-823, doi:10.1080/15476286.2015.1056975 (2015).

8   Palma, J. *et al.* MicroRNAs are exported from malignant cells in customized particles. *Nucleic Acids Res* **40**, 9125-9138, doi:10.1093/nar/gks656 (2012).

9   Lässer, C. *et al.* Two distinct extracellular RNA signatures released by a single cell type identified by microarray and next-generation sequencing. *RNA Biol* **14**, 58-72, doi:10.1080/15476286.2016.1249092 (2016).

10   Valadi, H. *et al.* Exosome-mediated transfer of mRNAs and microRNAs is a novel mechanism of genetic exchange between cells. *Nature Cell Biology* **9**, 654, doi:10.1038/ncb1596 (2007).

11   Ratajczak, J. *et al.* Embryonic stem cell-derived microvesicles reprogram hematopoietic progenitors: evidence for horizontal transfer of mRNA and protein delivery. *Leukemia* **20**, 847-856, doi:10.1038/sj.leu.2404132 (2006).

12   Ridder, K. *et al.* Extracellular Vesicle-Mediated Transfer of Genetic Information between the Hematopoietic System and the Brain in Response to Inflammation. *PLOS Biology* **12**, e1001874, doi:10.1371/journal.pbio.1001874 (2014).

13   Deregibus, M. C. *et al.* Endothelial progenitor cell–derived microvesicles activate an angiogenic program in endothelial cells by a horizontal transfer of mRNA. *Blood* **110**, 2440-2448, doi:10.1182/blood-2007-03-078709 (2007).

14   Skog, J. *et al.* Glioblastoma microvesicles transport RNA and proteins that promote tumour growth and provide diagnostic biomarkers. *Nature Cell Biology* **10**, 1470-1476, doi:10.1038/ncb1800 (2008).

15   D'Asti, E., Chennakrishnaiah, S., Lee, T. H. & Rak, J. Extracellular Vesicles in Brain Tumor Progression. *Cellular and Molecular Neurobiology* **36**, 383-407, doi:10.1007/s10571-015-0296-1 (2016).

16   Li, K. *et al.* Advances, challenges, and opportunities in extracellular RNA biology: insights from the NIH exRNA Strategic Workshop. *JCI Insight* **3**, e98942, doi:10.1172/jci.insight.98942 (2018).

17   Yokoi, A. *et al.* Malignant extracellular vesicles carrying MMP1 mRNA facilitate peritoneal dissemination in ovarian cancer. *Nature Communications* **8**, 14470, doi:10.1038/ncomms14470 (2017).

18   Vu, L. T., Gong, J., Pham, T. T., Kim, Y. & Le, M. T. N. microRNA exchange via extracellular vesicles in cancer. *Cell Proliferation* **53**, e12877, doi:https://doi.org/10.1111/cpr.12877 (2020).

19   Gelderblom, M. *et al.* Temporal and Spatial Dynamics of Cerebral Immune Cell Accumulation in Stroke. *Stroke* **40**, 1849-1857, doi:10.1161/strokeaha.108.534503 (2009).

20   Puig, B., Brenna, S. & Magnus, T. Molecular Communication of a Dying Neuron in Stroke. *International Journal of Molecular Sciences* **19**, 2834 (2018).

21   Dirnagl, U., Iadecola, C. & Moskowitz, M. A. Pathobiology of ischaemic stroke: an integrated view. *Trends in Neurosciences* **22**, 391-397, doi:https://doi.org/10.1016/S0166-2236(99)01401-0 (1999).

22   Kim, S. M., Kwon, S. U., Kim, J. S. & Kang, D.-W. Early infarct growth predicts long-term clinical outcome in ischemic stroke. *Journal of the Neurological Sciences* **347**, 205-209, doi:https://doi.org/10.1016/j.jns.2014.09.048 (2014).

23   Lo, E. H. A new penumbra: transitioning from injury into repair after stroke. *Nat Med* **14**, 497-500, doi:10.1038/nm1735 (2008).

24   Drago, F. *et al.* ATP Modifies the Proteome of Extracellular Vesicles Released by Microglia and Influences Their Action on Astrocytes. *Frontiers in Pharmacology* **8**, 910, doi:10.3389/fphar.2017.00910 (2017).

25   Bianco, F. *et al.* Astrocyte-Derived ATP Induces Vesicle Shedding and IL-1β Release from Microglia. *The Journal of Immunology* **174**, 7268-7277, doi:10.4049/jimmunol.174.11.7268 (2005).

26   Turola, E., Furlan, R., Bianco, F., Matteoli, M. & Verderio, C. Microglial microvesicle secretion and intercellular signaling. *Frontiers in physiology* **3**, 149-149, doi:10.3389/fphys.2012.00149 (2012).

27   Guitart, K. *et al.* Improvement of neuronal cell survival by astrocyte-derived exosomes under hypoxic and ischemic conditions depends on prion protein. *Glia* **64**, 896-910, doi:10.1002/glia.22963 (2016).

28   Frühbeis, C. *et al.* Oligodendrocytes support axonal transport and maintenance via exosome secretion. *PLOS Biology* **18**, e3000621, doi:10.1371/journal.pbio.3000621 (2020).

29   Fröhlich, D. *et al.* Multifaceted effects of oligodendroglial exosomes on neurons: impact on neuronal firing rate, signal transduction and gene regulation. *Philosophical Transactions of the Royal Society B: Biological Sciences* **369**, doi:10.1098/rstb.2013.0510 (2014).

30   Frühbeis, C. *et al.* Neurotransmitter-Triggered Transfer of Exosomes Mediates Oligodendrocyte–Neuron Communication. *PLOS Biology* **11**, e1001604, doi:10.1371/journal.pbio.1001604 (2013).

31   Yang, J. *et al.* Neuronal extracellular vesicle derived miR-98 prevents salvageable neurons from microglial phagocytosis in acute ischemic stroke. *Cell Death Dis* **12**, 23, doi:10.1038/s41419-020-03310-2 (2021).

32   Brenna, S. *et al.* Characterization of brain-derived extracellular vesicles reveals changes in cellular origin after stroke and enrichment of the prion protein with a potential role in cellular uptake. *Journal of Extracellular Vesicles* **9**, 1809065, doi:10.1080/20013078.2020.1809065 (2020).

33   Love, M. I., Huber, W. & Anders, S. Moderated estimation of fold change and dispersion for RNA-seq data with DESeq2. *Genome Biology* **15**, 550, doi:10.1186/s13059-014-0550-8 (2014).

34   Wu, T. *et al.* clusterProfiler 4.0: A universal enrichment tool for interpreting omics data. *The Innovation* **2**, 100141, doi:https://doi.org/10.1016/j.xinn.2021.100141 (2021).

35   Mi, H., Muruganujan, A., Ebert, D., Huang, X. & Thomas, P. D. PANTHER version 14: more genomes, a new PANTHER GO-slim and improvements in enrichment analysis tools. *Nucleic Acids Res* **47**, D419-d426, doi:10.1093/nar/gky1038 (2019).

36   Lein, E. S. *et al.* Genome-wide atlas of gene expression in the adult mouse brain. *Nature* **445**, 168-176, doi:10.1038/nature05453 (2007).

37   Théry, C. *et al.* Minimal information for studies of extracellular vesicles 2018 (MISEV2018): a position statement of the International Society for Extracellular Vesicles and update of the MISEV2014 guidelines. *J Extracell Vesicles* **7**, 1535750, doi:10.1080/20013078.2018.1535750 (2018).

38   Geiss, G. K. *et al.* Direct multiplexed measurement of gene expression with color-coded probe pairs. *Nat Biotechnol* **26**, 317-325, doi:10.1038/nbt1385 (2008).

39   Kanai, Y., Smith, C. P. & Hediger, M. A. A new family of neurotransmitter transporters: the high-affinity glutamate transporters. *The FASEB Journal* **7**, 1450-1459, doi:10.1096/fasebj.7.15.7903261 (1993).

40   Ponomarev, E. D., Shriver, L. P. & Dittel, B. N. CD40 Expression by Microglial Cells Is Required for Their Completion of a Two-Step Activation Process during Central Nervous System Autoimmune Inflammation. *The Journal of Immunology* **176**, 1402-1410, doi:10.4049/jimmunol.176.3.1402 (2006).

41   Bradl, M. & Lassmann, H. Oligodendrocytes: biology and pathology. *Acta neuropathologica* **119**, 37-53, doi:10.1007/s00401-009-0601-5 (2010).

42   Bereczki, D., Jr., Balla, J. & Bereczki, D. Heme Oxygenase-1: Clinical Relevance in Ischemic Stroke. *Current pharmaceutical design* **24**, 2229-2235, doi:10.2174/1381612824666180717101104 (2018).

43   Dzwonek, J. & Wilczynski, G. M. CD44: molecular interactions, signaling and functions in the nervous system. *Frontiers in cellular neuroscience* **9**, 175-175, doi:10.3389/fncel.2015.00175 (2015).

44   Sawada, R., Nakano-Doi, A., Matsuyama, T., Nakagomi, N. & Nakagomi, T. CD44 expression in stem cells and niche microglia/macrophages following ischemic stroke. *Stem Cell Investig* **7**, 4-4, doi:10.21037/sci.2020.02.02 (2020).

45   Stevens, B. *et al.* The Classical Complement Cascade Mediates CNS Synapse Elimination. *Cell* **131**, 1164-1178, doi:https://doi.org/10.1016/j.cell.2007.10.036 (2007).

46   Lu, J. H. *et al.* The classical and regulatory functions of C1q in immunity and autoimmunity. *Cellular & molecular immunology* **5**, 9-21, doi:10.1038/cmi.2008.2 (2008).

47   Alawieh, A., Elvington, A. & Tomlinson, S. Complement in the Homeostatic and Ischemic Brain. *Front Immunol* **6**, 417, doi:10.3389/fimmu.2015.00417 (2015).

48   Anderson, M. A. *et al.* Astrocyte scar formation aids central nervous system axon regeneration. *Nature* **532**, 195-200, doi:10.1038/nature17623 (2016).

49   Liddelow, S. A. *et al.* Neurotoxic reactive astrocytes are induced by activated microglia. *Nature* **541**, 481-487, doi:10.1038/nature21029 (2017).

50   Cekanaviciute, E. & Buckwalter, M. S. Astrocytes: Integrative Regulators of Neuroinflammation in Stroke and Other Neurological Diseases. *Neurotherapeutics* **13**, 685-701, doi:10.1007/s13311-016-0477-8 (2016).

51   Butovsky, O. *et al.* Identification of a unique TGF-β–dependent molecular and functional signature in microglia. *Nature Neuroscience* **17**, 131-143, doi:10.1038/nn.3599 (2014).

52   Matos, M. C., Pinheiro, A., Melo-Ferreira, J., Davis, R. S. & Esteves, P. J. Evolution of Fc Receptor-Like Scavenger in Mammals. *Front Immunol* **11**, 590280, doi:10.3389/fimmu.2020.590280 (2020).

53   PrabhuDas, M. R. *et al.* A Consensus Definitive Classification of Scavenger Receptors and Their Roles in Health and Disease. *The Journal of Immunology* **198**, 3775-3789, doi:10.4049/jimmunol.1700373 (2017).

54   Crescitelli, R. *et al.* Distinct RNA profiles in subpopulations of extracellular vesicles: apoptotic bodies, microvesicles and exosomes. *Journal of Extracellular Vesicles* **2**, 10.3402/jev.v3402i3400.20677, doi:10.3402/jev.v2i0.20677 (2013).

55   Srinivasan, S. *et al.* Small RNA Sequencing across Diverse Biofluids Identifies Optimal Methods for exRNA Isolation. *Cell* **177**, 446-462.e416, doi:10.1016/j.cell.2019.03.024 (2019).

56   Brenna, S., Krisp, C., Altmeppen, H. C., Magnus, T. & Puig, B. Brain-Derived Extracellular Vesicles in Health and Disease: A Methodological Perspective. *International Journal of Molecular Sciences* **22**, 1365 (2021).

57   Cheng, L. *et al.* Small RNA fingerprinting of Alzheimer's disease frontal cortex extracellular vesicles and their comparison with peripheral extracellular vesicles. *Journal of extracellular vesicles* **9**, 1766822-1766822, doi:10.1080/20013078.2020.1766822 (2020).

58   Zhang, R., Chopp, M. & Zhang, Z. G. Oligodendrogenesis after cerebral ischemia. *Frontiers in Cellular Neuroscience* **7**, doi:10.3389/fncel.2013.00201 (2013).

59   Peferoen, L., Kipp, M., van der Valk, P., van Noort, J. M. & Amor, S. Oligodendrocyte-microglia cross-talk in the central nervous system. *Immunology* **141**, 302-313, doi:https://doi.org/10.1111/imm.12163 (2014).

60   Miron, V. E. *et al.* M2 microglia and macrophages drive oligodendrocyte differentiation during CNS remyelination. *Nature Neuroscience* **16**, 1211-1218, doi:10.1038/nn.3469 (2013).

61   Zhang, W. *et al.* A large-scale comparative study of isoform expressions measured on four platforms. *BMC Genomics* **21**, 272, doi:10.1186/s12864-020-6643-8 (2020).

62   Van Deun, J. *et al.* The impact of disparate isolation methods for extracellular vesicles on downstream RNA profiling. *Journal of Extracellular Vesicles* **3**, 10.3402/jev.v3403.24858, doi:10.3402/jev.v3.24858 (2014).

63   Bracht, J. W. P. *et al.* Analysis of extracellular vesicle mRNA derived from plasma using the nCounter platform. *Scientific Reports* **11**, 3712, doi:10.1038/s41598-021-83132-0 (2021).

64   Dong, L. *et al.* High-Throughput Simultaneous mRNA Profiling Using nCounter Technology Demonstrates That Extracellular Vesicles Contain Different mRNA Transcripts Than Their Parental Prostate Cancer Cells. *Anal Chem* **93**, 3717-3725, doi:10.1021/acs.analchem.0c03185 (2021).

65   Lässer, C. *et al.* Human saliva, plasma and breast milk exosomes contain RNA: uptake by macrophages. *Journal of translational medicine* **9**, 9-9, doi:10.1186/1479-5876-9-9 (2011).

66   Batagov, A. O. & Kurochkin, I. V. Exosomes secreted by human cells transport largely mRNA fragments that are enriched in the 3'-untranslated regions. *Biol Direct* **8**, 12-12, doi:10.1186/1745-6150-8-12 (2013).

67   Li, Y. *et al.* Extracellular Vesicles Long RNA Sequencing Reveals Abundant mRNA, circRNA, and lncRNA in Human Blood as Potential Biomarkers for Cancer Diagnosis. *Clinical Chemistry* **65**, 798-808, doi:10.1373/clinchem.2018.301291 (2019).

68   Somiya, M. Where does the cargo go?: Solutions to provide experimental support for the "extracellular vesicle cargo transfer hypothesis". *J Cell Commun Signal* **14**, 135-146, doi:10.1007/s12079-020-00552-9 (2020).

69   Montecalvo, A. *et al.* Mechanism of transfer of functional microRNAs between mouse dendritic cells via exosomes. *Blood* **119**, 756-766, doi:10.1182/blood-2011-02-338004 (2012).

70   Prada, I. & Meldolesi, J. Binding and Fusion of Extracellular Vesicles to the Plasma Membrane of Their Cell Targets. *International journal of molecular sciences* **17**, 1296, doi:10.3390/ijms17081296 (2016).

71   Parolini, I. *et al.* Microenvironmental pH Is a Key Factor for Exosome Traffic in Tumor Cells **. *Journal of Biological Chemistry* **284**, 34211-34222, doi:10.1074/jbc.M109.041152 (2009).

72   Somiya, M. & Kuroda, S. i. Real-Time Luminescence Assay for Cytoplasmic Cargo Delivery of Extracellular Vesicles. *Anal Chem* **93**, 5612-5620, doi:10.1021/acs.analchem.1c00339 (2021).

73   Mulcahy, L. A., Pink, R. C. & Carter, D. R. F. Routes and mechanisms of extracellular vesicle uptake. *Journal of Extracellular Vesicles* **3**, 24641, doi:10.3402/jev.v3.24641 (2014).

74   Christianson, H. C., Svensson, K. J. & Belting, M. Exosome and microvesicle mediated phene transfer in mammalian cells. *Seminars in Cancer Biology* **28**, 31-38, doi:https://doi.org/10.1016/j.semcancer.2014.04.007 (2014).

TABLES

Table 1.- Comparison between upregulated (log2FC≥2) and downregulated mRNAs in isolated vs non-isolated and non-filtered mRNAs from BDEVs in tMCAO compared to shams.

Mean counts, and log2FC for each group are provided. Samples with isolated mRNAs and a filtration step (column 1, I+F samples) are taken as the paradigm. The mRNAs of the other samples are compared to column 1 (and therefore the FC is not in decreasing order). In light grey is the fold change that is less than 2 for the mRNAs than in the I+F samples have a log2FC≥2. In blue, mRNAs that did not satisfy the criteria of FDR≤0.1 but are included in the list for comparison. In violet, mRNAs that were found increased with a log2FC≥2 in the NI+F samples which are then compared with the other two columns. No specific mRNA was found in the NI+NF samples. Downregulated mRNAs are shown in dark blue. None of the downregulated mRNAs were observed with a log2F ≤-2, and therefore, the FC is in grey. CxCl16 and Lrcc25 are not present in all columns as, in these instances, they did not satisfy the premises stablished for the background.

Table 2.- List of GO terms.

FIGURE LEGENDS

Figure 1.- BDEVs characterization and mRNA isolation. (A) Overview of the research strategy and experimental workflow followed in the present study. Different cell types, including neurons (N, green), oligodendrocytes (OD, orange), astrocytes (A, pink), microglia (MG, blue), and others (X, grey) contribute to the EV pool in brain. EVs were purified from the brains of mice 72 hours after experimental stroke (tMCAO) or a control procedure (sham). Small brain-derived EVs (sBDEVs) were obtained upon filtration (F) and characterized. The mRNA content of sBDEVs was assessed in detail for stroke and sham samples and compared with (I) or without (NI) a previous RNA isolation step. Moreover, a comparison was performed between filtered (F, sBDEVs) and non-filtered (NF) BDEVs (with the latter population also containing larger EV species). Lastly, changes in the relative contribution of different cell types to the EV pool upon stroke were assessed. (B) Western blot characterization of the six fractions obtained after sucrose gradient centrifugation. Fractions 2 and 3 are labeled with antibodies against EV markers flotillin, CD81, and 14-3-3 indicating enrichment of EVs. Moreover, presence in the same fractions of Alix and mature (m) ADAM10 indicates enrichment in exosomes. CD81 and flotillin are also found in fraction 4, therefore fractions 2, 3, and 4 were pooled for the subsequent experiments. The Golgi protein GM130 is absent in the BDEVs fractions indicating a lack of contamination with intracellular organelles. TS is total protein staining. TH is a total brain homogenate used for comparison purposes. (C) Nanoparticle tracking analysis (NTA) of pooled BDEVs fractions (n=6). Values are given in the main text. (D) Electron microscopy of BDEVs. Arrowheads point towards BDEVs, whereas the white asterisks mark structures that, for the shape, are not assignable to EVs and most likely represent some minor contamination by cell membrane fragments. The scale bar is 500 nm, 100 nm on the insert. (E) Example of the BDEVs-RNA profile obtained with the Bioanalyzer. Most of the RNA is under 1,000 nt in both, tMCAO and sham BDEVs. CL is a cell lysate, used for comparison purposes as it shows the two main rRNAs (18S and 28S), which are mostly absent in BDEVs. (F) Representative electropherogram obtained with the Bioanalyzer showing the fluorescent units (FU) on the Y-axis and the migration time (in seconds, s) on the X-axis.

Figure 2.- No major differences for the highest upregulated mRNAs in tMCAO sBDEVs compared to shams are observed with and without mRNA isolation. (A) Heat map showing the significantly up- (log2FC≥1) and downregulated (log2FC≤-1) mRNAs found in tMCAO mice compared to shams (n=3 mice per group) using the nCounter® Neuropathology panel with previous mRNA isolation (I) from sBDEVs. (B) Volcano plot for the same results as in (A) displaying the names of the ten significantly differentially expressed mRNAs with the highest log2FC in sBDEVs in tMCAO mice compared to shams. On the X-axis the log2FC is plotted while in the Y-axis shows the -log10 FDR. (C) Heat map showing the significantly up- and downregulated (absolut log2FC≥ 1) mRNAs in BDEVs from tMCAO compared to shams (n=3 per group) using the nCounter® panel without mRNA isolation. (D) Volcano plot for the same mRNAs as in (C) displaying the names of the ten significantly differentially expressed mRNAs in sBDEVs in tMCAO mice compared to shams. The X-axis shows the log2FC, the Y-axis the -log10 FDR. (E) Overview of the most up- and downregulated mRNAs (absolut log2FC≥2) with both types of preparations (i.e., with mRNA isolation (I) and without mRNA isolation (NI)) displayed in a Venn diagram showing the number of the commonly shared and unique mRNAs for each panel. (F) Venn diagram for the different sample conditions as in (E) but with a cut-off of absolut log2FC≥1.

Figure 3.- Non-filtered BDEVs show no major differences compared to the filtered ones in mRNA content after tMCAO. (A) Heat map of the up- and downregulated mRNAs (absolut log2FC≥1) in BDEVs

of tMCAO compared to shams (n=3 mice per group). (B) Volcano plot for the same mRNAs as in (A) displaying the names of the ten significantly differentially expressed mRNAs in BDEVs from tMCAO mice compared to shams. (C) Overview of the most up and downregulated mRNAs (absolut log2FC≥2) in each panel displayed in a Venn diagram showing the number of the commonly shared and the unique mRNAs for each studied condition: F= BDEV samples were filtrated during preparation (sBDEVs); NF= BDEVs samples were non-filtrated during preparation; I= the mRNA was isolated from BDEVs; NI= the mRNA was not isolated before running the nCounter® panel. (D) Venn diagram for the different sample conditions as in (C) but with a cut-off of absolut log2FC ≥1.

Figure 4.- Small BDEVs after tMCAO are enriched in mRNAs related to inflammation, defense response, and recovery processes, mainly derived from microglia, and PCR confirms that sBDEVs contain full-length mRNAs. (A) Dot plots of the RT-qPCR results of 5 of the top upregulated mRNAs in sBDEVs after tMCAO compared to shams. Every dot represents the log2FC calculated from the ΔΔCT value obtained for each mice (n=7 per group). (B) Enriched GO terms dot plot showing the processes related to the most upregulated SBDEV-derived mRNAs (log2FC≥2) in tMCAO compared to shams. The size of the dots is proportional to the number of mRNAs included in each process whereas the color indicates the *p adjusted* value. The list and the full names of the GO terms can be found in Table 2. (C) Heat map adapted from the transcriptomics data of the Allen Brain Atlas. EC: endothelial cells; A: astrocytes; N: Neurons; P: perivascular macrophages; MG: microglia. (D) Agarose gel images of the PCR products for the six most upregulated mRNAs in sBDEVs from tMCAO brains compared to shams. The results are only qualitative as the cDNA used for the PCR was not measured before the PCR (i.e., the cDNA was added to the reaction by volume). Note that all mRNAs tested present a full-length ORF when compared to the cDNA of wild-type mouse brains used as positive controls (+). (-) is the negative control, where all the procedure was performed without cDNA.

Figure 5.- The contribution of oligodendrocytes to the BDEVs pool is significantly upregulated at 72 h after tMCAO. (A) Western blots of sBDEVs samples from tMCAO and shams (n=5 per group) blotted for cell-type-specific markers: PLP and CNP1 are used as protein markers for oligodendrocytes (orange frame); synapsin1 (Syn1) and NCAM as markers for neurons (green); EAAT1 and EAAT2 as protein markers for astrocytes (pink) and P2Y12 and CD40 as markers for microglia/macrophages (blue). TH is a total mouse brain homogenate loaded in parallel for comparison purposes. TS is a representative total protein staining of the nitrocellulose membranes (TSs of all blots used for these analyses are provided in Suppl. Fig. 3). (B) Quantifications of the western blot intensities. For the quantification, each band intensity was first referred to the corresponding lanes of the total protein staining. Both markers for oligodendrocytes were found significantly increased upon stroke. Regarding neuronal markers, NCAM was significantly increased while Syn1 only showed a tendency to be elevated. Exact p- values are given in the main text.

Figure 6.- Summarizing scheme of the main findings and open questions. This study assessed alterations in the brain EV pool and the mRNA composition of BDEVs 72 hours after experimental stroke (tMCAO) and reperfusion in mice. Neurons (N), microglia (MG), oligodendrocytes (OD), astrocytes (A), and several other cell types (X) contribute to the EV pool in brain (box on the left). Focussing on small BDEVs, we found an upregulated (↑) contribution by ODs to the latter at this time point after stroke (①). Comparing samples with (I) and without RNA isolation, our multiplexed mRNA arrays revealed similar results regarding mRNA upregulated candidates, and our comparison of filtered and non-filtered BDEVs indicated that mRNAs may be predominantly contained in small BDEVs (②). Though OD showed an increased contribution to the overall EV pool, mRNAs assessed in BDEVs were mainly of MG origin (③). Consistent top hits showing an increased abundance in BDEVs after stroke included mRNAs for Hmox1, Gfap, Cd44, C1q proteins, and Fcrls (④), and predominant GO

terms derived from our mRNA findings could largely be linked with the aspects of inflammatory/immune and regenerative/repair regulation (⑤), thus fitting to processes expected to be initiated and to take place at this time point after stroke. Notably, we confirmed the presence of 'intact' mRNAs (as judged by a full-length (fl) ORF) for 6 top candidates upregulated in BDEVs upon stroke (⑥). Whether these mRNAs also contain important elements such as the 5' cap structure or the 3' poly-A tail and, importantly, if these mRNAs are successfully taken up and possibly even translated in recipient cells to elicit (fast) biological responses (e.g., in the context of post-stroke regeneration) remains to be studied further.

Table 1

UPREGULATED

	I+F-samples panel				NI+F-samples panel		
mRNA	avg sh	avg str	log2FC	mRNA	avg sh	avg str	log2FC
Hmox1	19.32	256.41	3.73	Hmox1	33.92	217.27	2.67
Cd44	17.83	176.82	3.30	Cd44	42.46	258.88	2.58
C1qb	35.31	318.21	3.16	C1qb	58.67	539.21	3.18
Gfap	397.09	3440.43	3.12	Gfap	438.58	3094.39	2.81
Fcrls	9.41	75.63	3.00	Fcrls	30.59	167.40	2.40
C1qa	24.68	189.18	2.93	C1qa	39.67	337.19	3.08
C1qc	25.76	196.33	2.93	C1qc	53.60	458.66	3.09
Cd68	28.88	215.43	2.89	Cd68	43.10	346.21	3.02
Ncf1	22.21	165.84	2.89	Ncf1	49.08	297.31	2.60
Nes	21.19	155.21	2.87	Nes	32.92	193.10	2.57
Ccl12	6.17	45.32	2.86	Ccl12	6.40	52.94	3.13
Il4ra	22.17	148.71	2.74	Il4ra	52.97	281.12	2.40
Ccr5	17.14	112.90	2.72	Ccr5	32.80	157.71	2.30
Tgfb1	16.53	108.81	2.70	Tgfb1	44.24	153.51	1.80
Tnc	22.50	146.39	2.70	Tnc	45.25	178.00	2.02
Tspo	9.19	56.83	2.65	Tspo	19.86	69.93	1.87
Itga5	8.86	53.37	2.57	Itga5	30.81	104.68	1.83
Casp8	7.59	44.62	2.54	Casp8	17.11	83.21	2.26
Cxcl16	12.45	71.08	2.49	Cxcl16	26.64	90.64	1.81
Psmb8	18.01	99.90	2.49	Psmb8	26.52	129.89	2.28
Msn	17.85	99.26	2.46	Msn	34.65	170.30	2.25
Ccr2	11.83	60.81	2.36	Ccr2	25.64	67.86	1.48
Itgam	24.30	124.13	2.35	Itgam	35.77	221.01	2.63
Spi1	11.97	59.62	2.33	Spi1	24.27	79.24	1.67
Tcirg1	28.69	137.19	2.25	Tcirg1	92.94	391.44	2.07
Fn1	45.10	197.11	2.14	Fn1	84.35	356.93	2.10
Osmr	10.04	43.05	2.11	Osmr	16.36	76.86	2.22
Grn	42.20	176.64	2.08	Grn	114.64	415.28	1.85
Stab1	12.06	50.81	2.07	Stab1	29.61	118.54	2.02
Trem2	23.97	101.00	2.06	Trem2	42.24	246.00	2.56
Hpgds	43.10	174.04	2.01	Hpgds	62.93	239.64	1.96
Csf2rb	12.00	37.08	1.62	Csf2rb	10.63	66.42	2.78
Tnfrsf1b	29.55	104.16	1.81	Tnfrsf1b	34.74	176.52	2.32
Bcas1	120.95	410.12	1.76	Bcas1	180.46	813.48	2.18
Lrrc25	-	-	-	Lrrc25	12.08	49.01	2.11
Tnfrsf1a	25.14	92.85	1.90	Tnfrsf1a	40.99	164.08	2.00

DOWNREGULATED

	I+F-samples panel				NI+F-samples panel		
mRNA	avg sh	avg str	log2FC	mRNA	avg sh	avg str	log2FC
Adora2a	73.23	21.39	-1.81	Adora2a	182.73	53.59	-1.75
Cd4	45.73	14.61	-1.66	Cd4	67.26	22.74	-1.54
Camk4	674.92	287.14	-1.24	CamK4	1379.95	816.96	-0.76

93

Bdnf	172.22	60.13	-1.52
Gabra4	754.17	299.96	-1.33
Drd2	326.13	131.88	-1.29
Arc	829.20	353.56	-1.23
Egr2	30.15	13.22	-1.18
Ppp3ca	7825.61	3541.84	-1.14
Homer1	1179.36	549.72	-1.10
Egr1	1726.43	850.26	-1.02

NI+NF-samples panel

mRNA	avg sh	avg str	log2FC
Hmox1	32.35	242.43	2.91
Cd44	30.82	159.37	2.37
C1qb	65.80	362.41	2.46
Gfap	337.06	2928.32	3.12
Fcrls	23.59	114.55	2.27
C1qa	38.47	224.20	2.54
C1qc	41.97	262.46	2.64
Cd68	46.07	234.75	2.35
Ncf1	37.23	191.94	2.37
Nes	29.41	141.39	2.27
Ccl12	10.32	39.30	1.96
Il4ra	38.55	164.61	2.09
Ccr5	34.44	103.34	1.58
Tgfb1	20.38	118.75	2.54
Tnc	52.13	177.97	1.77
Tspo	19.91	64.25	1.71
Itga5	19.86	92.11	2.20
Casp8	18.59	50.85	1.45
Cxcl16	-	-	-
Psmb8	26.51	106.12	2.01
Msn	28.70	132.50	2.21
Ccr2	23.59	114.55	2.27
Itgam	37.63	154.85	2.04
Spi1	23.91	62.24	1.40
Tcirg1	80.20	298.46	1.90
Fn1	73.62	367.47	2.32
Osmr	21.79	65.10	1.59
Grn	69.67	242.72	1.80
Stab1	25.20	59.83	1.25
Trem2	34.50	154.24	2.16
Hpgds	64.96	161.40	1.31
Csf2rb	10.82	53.79	2.34
Tnfrsf1b	25.24	127.96	2.33
Bcas1	223.39	680.18	1.61
Lrrc25	-	-	-
Tnfrsf1a	24.84	109.94	2.16

NI+NF-samples panel

mRNA	avg sh	avg str	log2FC
Adora2a	145.29	94.47	-0.62
Cd4	62.21	38.39	-0.70
CamK4	1173.19	695.38	-0.75

GO term	
GO:0048856	Anatomical structure development
GO:0006950	Response to stress
GO:0030154	Cell differentiation
GO:0007165	Signal transduction
GO:0002376	Immune system process
GO:0008283	Cell population proliferation
GO:0040011	Locomotion
GO:0048870	Cell motility
GO:0048646	Anatomical structure formation involved in morphogenesis
GO:0007155	Cell adhesion
GO:0030198	Extracellular matrix organization
GO:0044403	Symbiotic process

Table 2

Figure 1
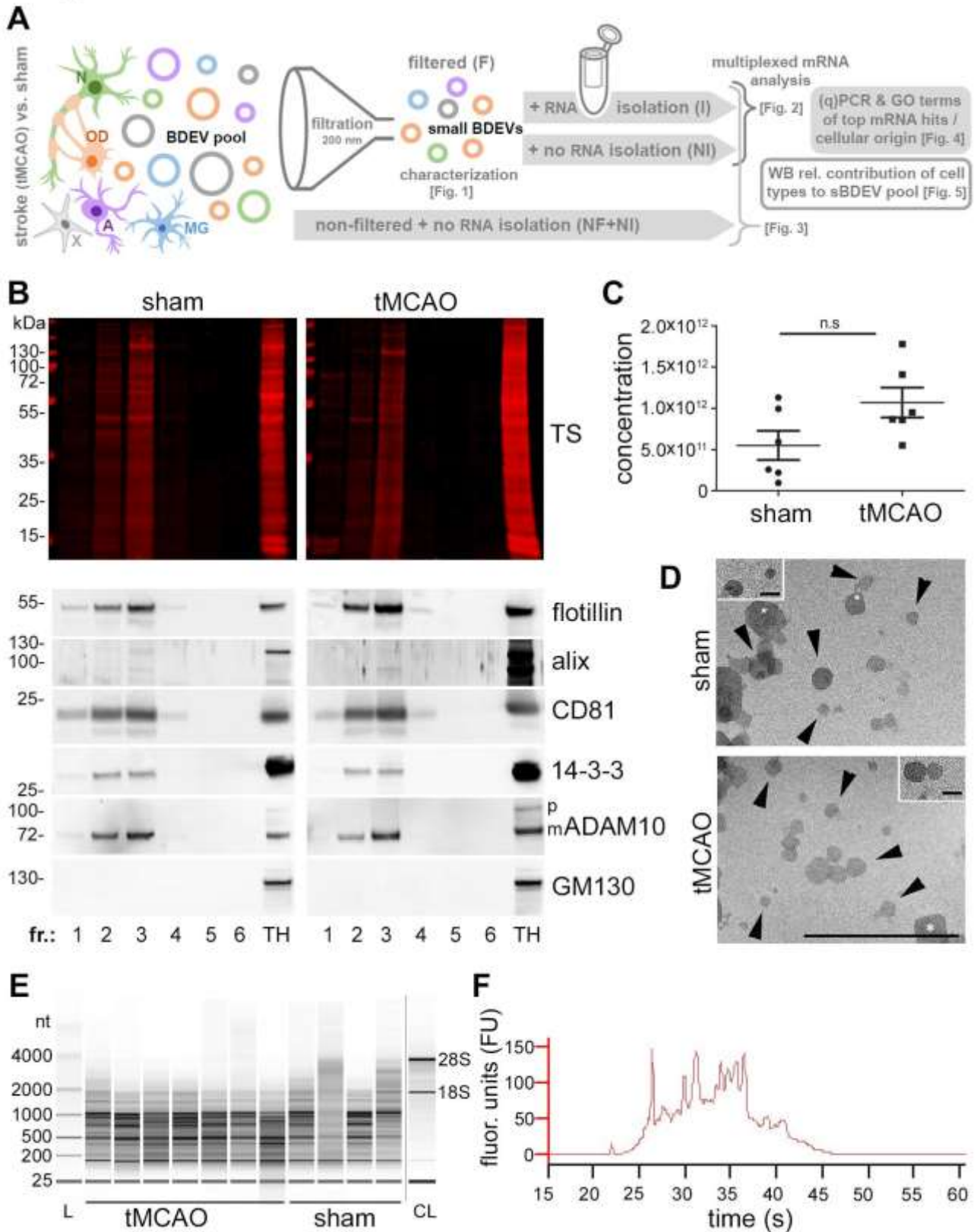
Figure 2

Figure 3

Figure 4

A

B

C

D
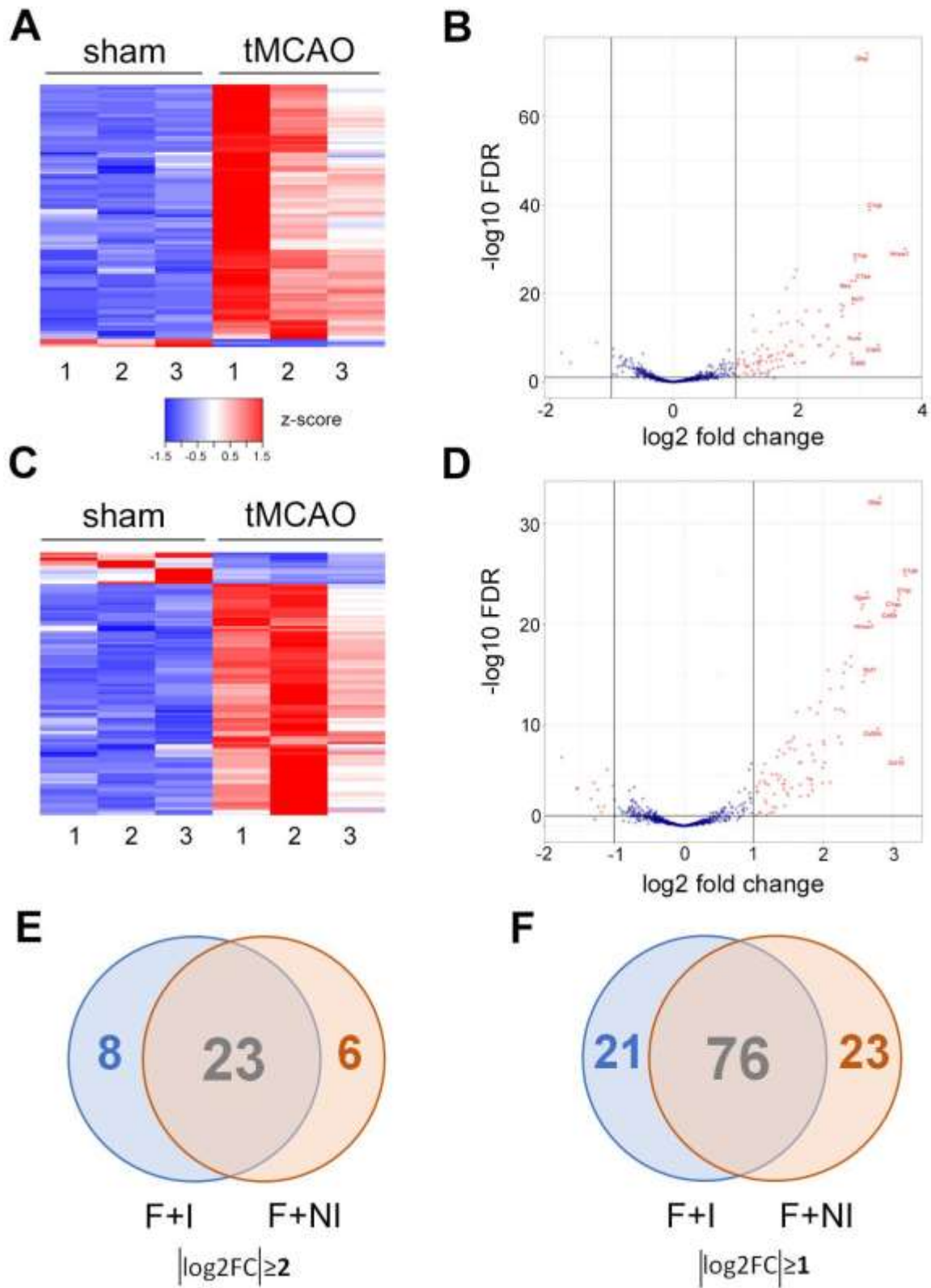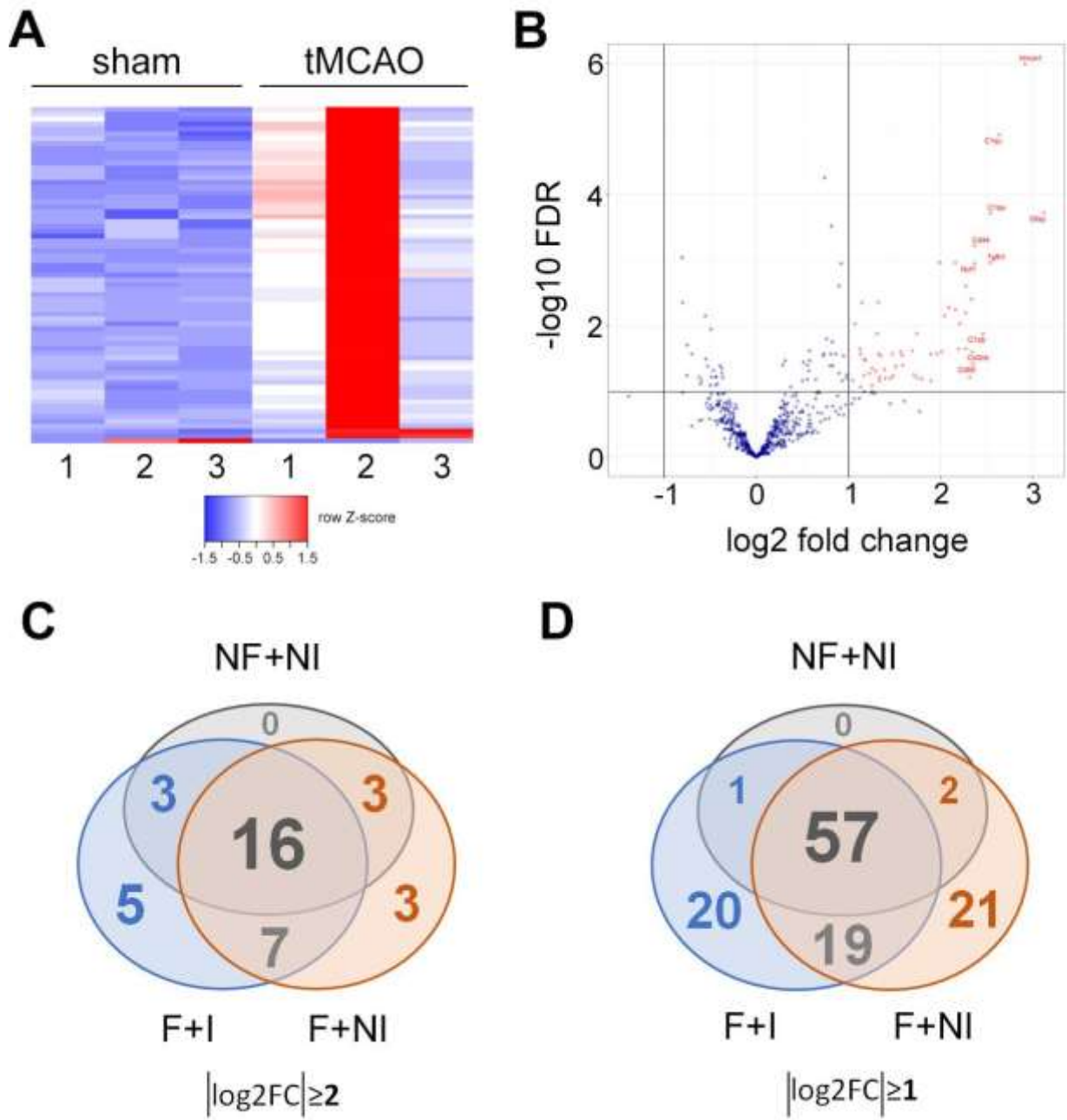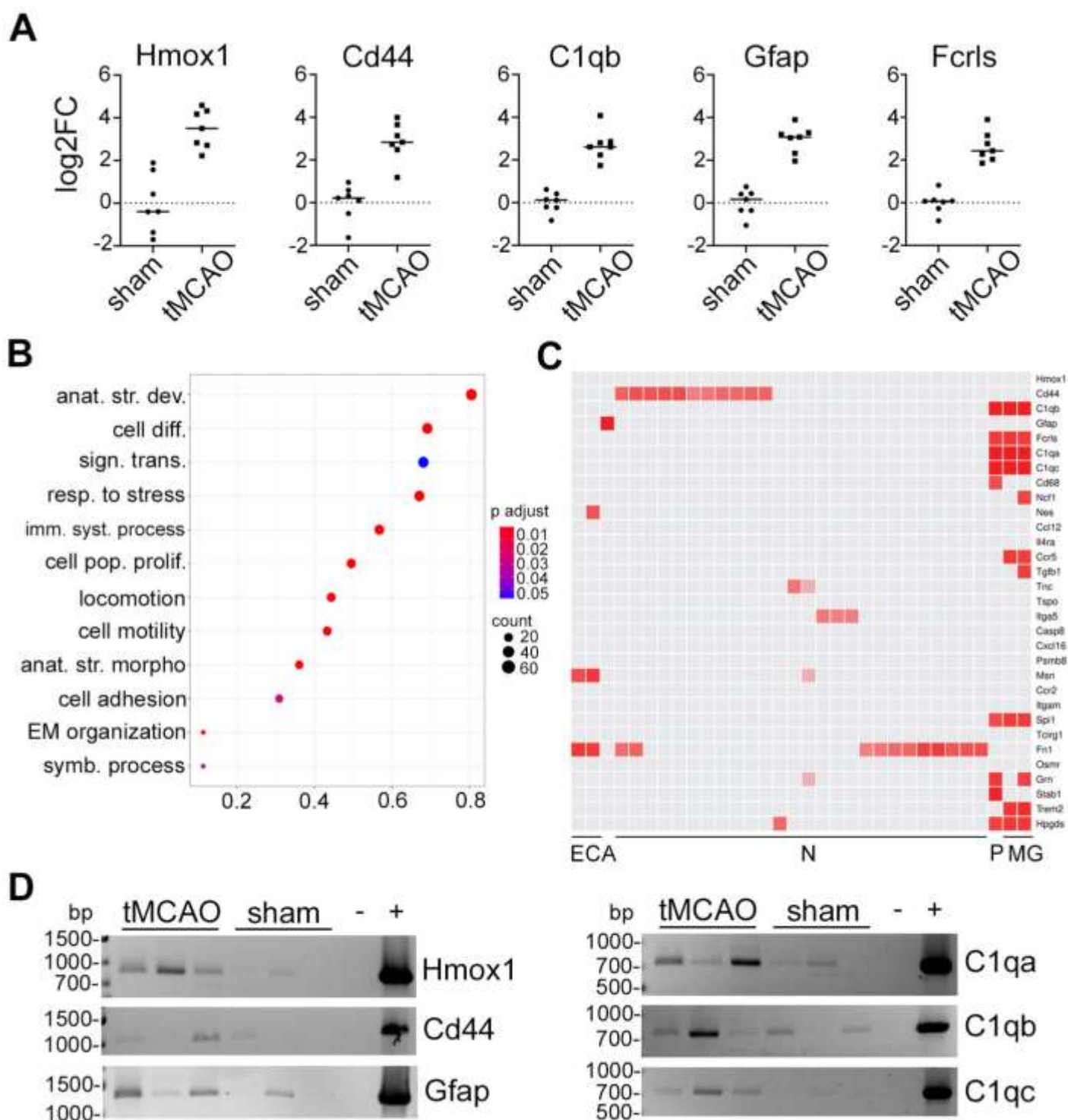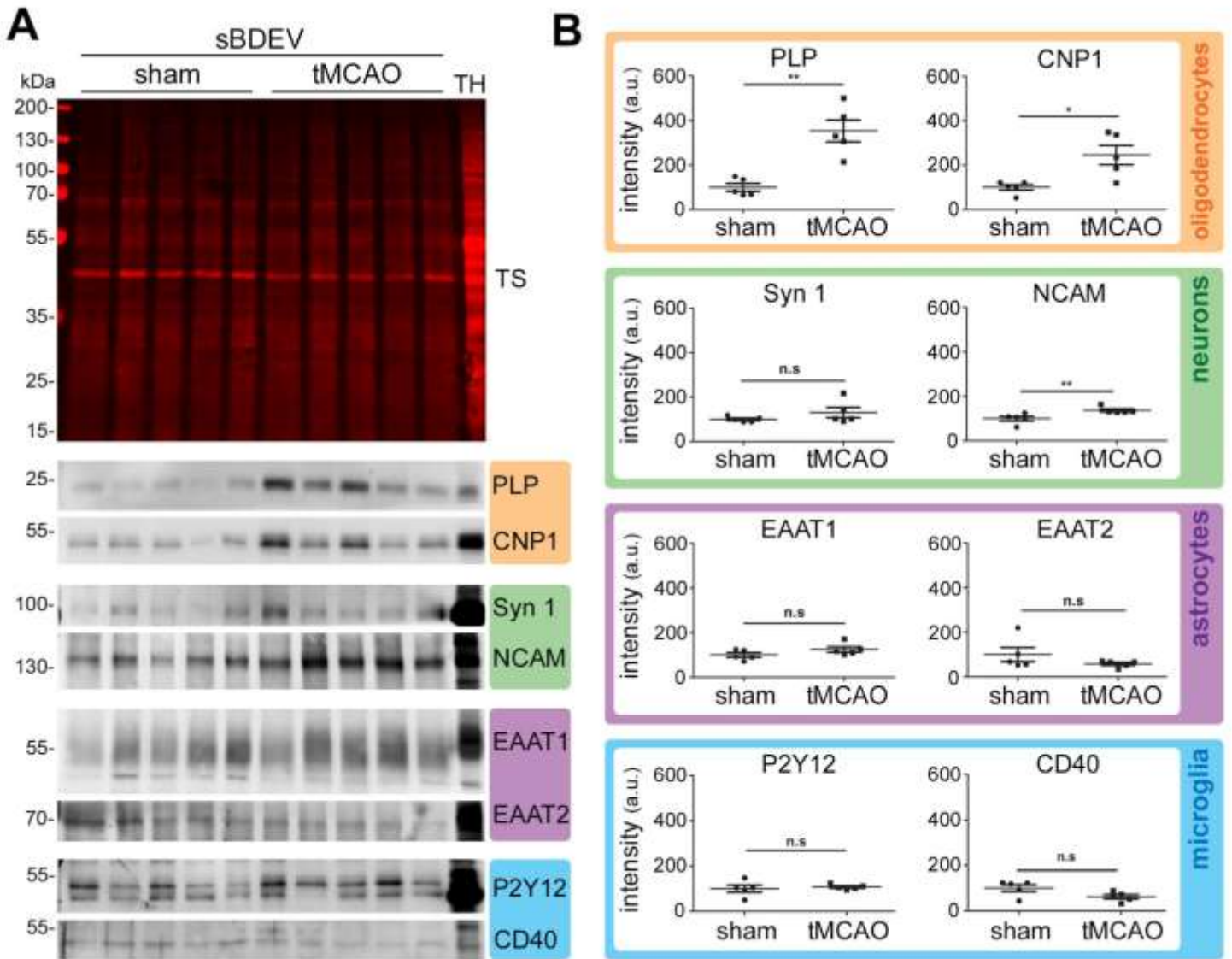
Figure 5

Figure 6
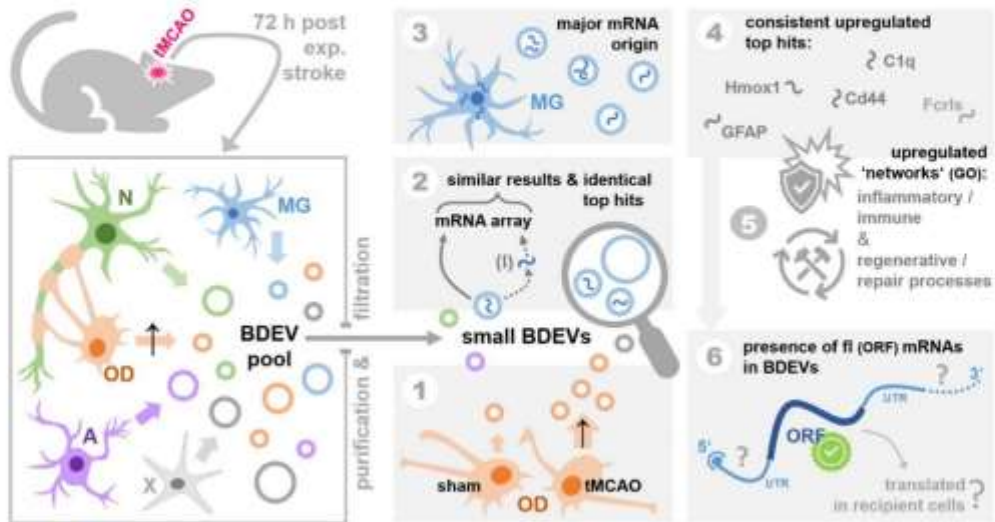
Review

Brain-Derived Extracellular Vesicles in Health and Disease: A Methodological Perspective

Santra Brenna [1], Christoph Krisp [2], Hermann Clemens Altmeppen [3], Tim Magnus [1] and Berta Puig [1,*]

[1] Neurology Department, Experimental Research in Stroke and Inflammation (ERSI), University Medical Center Hamburg-Eppendorf, 20246 Hamburg, Germany; s.brenna@uke.de (S.B.); t.magnus@uke.de (T.M.)

[2] Institute of Clinical Chemistry and Laboratory Medicine, Mass Spectrometric Proteomics University Medical Center Hamburg-Eppendorf, 20246 Hamburg, Germany; c.krisp@uke.de

[3] Institute of Neuropathology, University Medical Center Hamburg-Eppendorf, 20246 Hamburg, Germany; h.altmeppen@uke.de

* Correspondence: b.puig-martorell@uke.de; Fax: +49-(40)-7410-55591

Abstract: Extracellular vesicles (EVs) are double membrane structures released by presumably all cell types that transport and deliver lipids, proteins, and genetic material to near or distant recipient cells, thereby affecting their phenotype. The basic knowledge of their functions in healthy and diseased brain is still murky and many questions about their biology are unsolved. In neurological diseases, EVs are regarded as attractive biomarkers and as therapeutic tools due to their ability to cross the blood–brain barrier (BBB). EVs have been successfully isolated from conditioned media of primary brain cells and cerebrospinal fluid (CSF), but protocols allowing for the direct study of pathophysiological events mediated or influenced by EVs isolated from brain have only recently been published. This review aims to give a brief overview of the current knowledge of EVs' functions in the central nervous system (CNS) and the current protocols to isolate brain-derived EVs (BDEVs) used in different publications. By comparing the proteomic analysis of some of these publications, we also assess the influence of the isolation method on the protein content of BDEVs.

Keywords: extracellular vesicles; BDEVs; brain; isolation protocol; sucrose gradient; mass spectrometry; central nervous system; proteomics; intercellular communication

1. Introduction

1.1. Brief History of EVs

Since the 1960s, several studies reported evidence of the existence of extracellular vesicles-shaped membranous structures present in different tissues and organisms [1–5]. In 1967, Wolf et al. described minute lipid particles derived from platelets recovered after ultracentrifugation from serum and plasma, which showed "platelet-like" activity, thus confirming earlier observations made by Chargaff and West in 1946 [6,7]. They initially named this lipidic material "platelet dust", and later changed it to microparticles. The term "extracellular vesicle" (EV) was first used in 1971 by Aaronson et al. to describe the secreted membranous structures they observed in *Ochronomas Danica*, the golden alga [8]. These EVs of different sizes were visualized using electron microscopy with and without fixation, excluding the possibility of just being an artifact. In the late 1970s, Ronquist and colleagues described extracellular vesicles (later named "prostasomes" [9]) with ATPase activity, secreted from prostate epithelial cells that functionally affected sperm cells [10]. In 1981, Trams and colleagues observed that shed "microvesicles" harvested from conditioned media of glioblastoma cell lines had a special membrane composition originating from certain plasma membrane microdomains [11]. These shed vesicles also induced an effect in recipient cells, a fact that had already been observed in cancer cells by others [12].

They proposed the term "exosomes" (as opposed to intracellular endosomes) for this type of shed extracellular vesicles [11]. In 1983, by studying the maturation of reticulocytes to erythrocytes, two papers published in parallel demonstrated that the elimination of the transferrin receptor was mediated by the extracellular release of vesicles originating from the endocytic compartment by fusion of multivesicular bodies (MVB) with the plasma membrane. The term "exosome" was later used for these types of vesicles (i.e., intraluminal vesicles, ILVs, released to the extracellular space) [13–16].

However, at that point, there was rather broad scepticism about specific EV functions, and exosomes were widely regarded as garbage bags produced by cells to discard obsolete, superfluous proteins [17]. In 1996, Raposo and colleagues, in a seminal paper, could show that antigen-presenting exosomes derived from B lymphocytes were capable of specifically stimulating T cells, bestowing functionality to exosomes [18]. Further work showed that the release of functional exosomes was a general mechanism for several types of cells, related or not to the immune response, such as dendritic cells [19], mast cells [20], platelets [21], and intestinal epithelial cells [22], among others [23]. As the interest for exosomes was growing, they were starting to be more thoroughly characterized [24] and differentiated from other types of released EVs such as apoptotic blebs [25]. As already observed by Trams et al. (although at that point named exosomes), vesicles shed from the plasma membrane in a regulated process were also recognised as a communication tool and named microvesicles, ectosomes, shed vesicles, and microparticles [26–30]. Another important milestone in the research of EVs as a means of intercellular communication was the proof that they contain genetic material that can be transferred to and translated within the recipient cell [31–34].

Related to neurodegenerative diseases, several amyloidogenic and pathogenic proteins such as amyloid β (Aβ), prion protein, tau, and α-synuclein utilize EVs for spreading throughout the brain, thus contributing to disease progression [35,36].

The interest for EVs has grown exponentially over the last years and different protocols for their isolation, characterization, and, more recently, for EVs extraction from tissues such as brain have been published. Despite many advances, current protocols and protein markers used for their characterization cannot specifically differentiate between exosomes (of endosomal origin) and ectosomes/microvesicles (shed from the plasma membrane). The International Society of Extracellular Vesicles (ISEV, founded in 2011) has since 2012 published position papers, with the arduous task of standardizing the nomenclature, protocols, and techniques for their characterization [37–39] and increasing experimental reproducibility. At present, if no specific proof of the origin of exosomes/ectosomes is available, the agreement is to name them EVs. They can be further grouped by sizes (i.e., small EVs ($\leq$200 nm) or medium/large EVs ($\geq$200 nm)), by their density, or by their biochemical composition [37].

The aim of this review is to give an overview of the studies published so far that isolated BDEVs and to analyze different protocols used to purify them, highlighting their major differences. Finally, we also compare published proteomic data obtained with different isolation protocols from mouse and human tissue to assess the influence of the isolation procedure on the analysis of the BDEVs content.

1.2. EVs in Central Nervous System (CNS) Physiology

It has been proven that all CNS cells release EVs, which are involved in numerous physiological and pathological processes [39–43]. In steady-state conditions, EVs from human-induced pluripotent stem cells (hPSC)-derived neurons increase neurogenesis, cell proliferation, and neuronal differentiation when incubated with human primary neurons. Similarly, EVs isolated from rat neuronal primary cultures and injected into the lateral ventricle of postnatal day 4 (P4) mice, lead to hippocampal neurogenesis, highlighting the importance of EVs in the development of neuronal circuits [44]. In neurons, the release of EVs carrying the α-amino-3-hydroxy-5-methyl-4-isoxazolepropionic acid (AMPA) receptor subunit GluR2 is regulated by calcium influx and glutamatergic synaptic activity,

suggesting the involvement of EVs in synaptic transmission [45]. Glutamate can also stimulate vesicles release from oligodendrocytes [46], and these EVs are then taken up by neurons as support in stress conditions [47]. Moreover, EVs released by oligodendrocytes regulate myelin sheath formation in close coordination with neurons [48]. EVs released from astrocytes can regulate dendritic complexity in neurons via miR-26a-5p [49] and, conversely, EVs of neuronal origin containing miRNA 124a are taken up by astrocytes, leading to increased expression of excitatory amino acid transporter 2 (EAAT2) [50]. EVs released from microglia, on the other hand, can modulate neuronal activity in different ways: by stimulating the synaptic activity via enhanced sphingolipid metabolism [51], and by inhibiting the γ-aminobutyric acid (GABA)-ergic transmission via signaling of the endocannabinoid N-arachidonoylethanolamine (AEA) [52]. Moreover, the platelet-derived growth factor-BB (PDGF-BB)/PDGF receptor beta (PDGFRβ) signaling stimulates the release of EVs from pericytes carrying growth factors implicated in neuroprotection [42]. Lastly, EVs from brain endothelial cells promote oligodendrocyte precursor cell survival, motility, and proliferation [53].

1.3. EVs in CNS Pathologies

In pathological conditions, such as inflammation, extracellular astrocyte-derived ATP binds to the purinergic P2X7 receptor (P2X7R), activating microglia that then massively release EVs carrying IL-1β, thus further propagating the inflammatory response [40]. However, EVs released from ATP-stimulated microglia also contain a unique set of proteins that in turn impact astrocyte activation, showing then a protective role towards neurons [41]. Inflammatory microglia deliver EVs-associated microRNA 146-a-5p to neurons that negatively influence spine and synaptic density and strength [42]. As observed for microglia, astrocytes also increase EVs release when ATP activates the P2X7 receptors, and this process is associated with the release of the proinflammatory cytokine IL-1β [43].

Furthermore, it has been shown that EVs are involved in neurodegenerative diseases such as Alzheimer's disease (AD), Parkinson's disease (PD), and Creutzfeldt-Jakob disease (CJD). These diseases are characterized by the aggregation, deposition, and spread of specific misfolded proteins in particular regions of the brain: Aβ and hyperphosphorylated Tau for AD, α-synuclein for PD, and the pathogenic form of the prion protein (PrP^{Sc}) for CJD [44]. For AD, it has been shown that EVs isolated from neuronal cells contain not only Aβ [45] but also the full-length amyloid precursor protein (APP, from which the Aβ fragment is generated by two subsequent proteolytic cleavages) and other APP-derived proteolytic fragments [46]. Moreover, one of the typical neuropathological features of AD, the extracellular amyloid plaques, are enriched in the exosomal marker protein Alix [45], pointing to a possible role for EVs in plaque formation. Tau is also released in association with EVs [47], with consequences to the cerebral spread of Tau pathology [48–50]. Cells overexpressing cytoplasmic α-synuclein release EVs containing this protein in a calcium-dependent manner and are toxic to primary neurons [47,51,52]. Lastly, both the cellular form of the prion protein (PrP^C) and its infectious counterpart (PrP^{Sc}), the key pathological molecule underlying all transmissible prion diseases in humans and animals, are found on EVs purified from prion-infected neuronal cell lines [53] and are capable to transmit the toxic prion conformation to other cells in culture [54]. However, it is still not clear if, in humans (where neurodegenerative diseases last for years), EVs are relevant disease propagators or rather represent a failed mechanism of clearing misfolded proteins, such as Aβ [55], or whether both aspects hold true to some degree [35]. Of note, EVs in the context of neurodegenerative diseases have also been extensively studied and discussed as potential biomarkers [36,56,57].

In other neurological conditions, such as ischemic stroke (IS) and traumatic brain injury (TBI), where initial localized damage (either by the blockage of a main brain artery or by a blow, bump, jolt or a penetrating object to the head) is followed by neuroinflammation, breakage of the blood–brain barrier (BBB), and infiltration of peripheral immune cells, the role of EVs in the disease outcome is much more complex (reviewed in [58–62]).

In this context, it seems clear that EVs detected in CSF, plasma or blood could be valuable biomarkers of disease prognosis [63,64]. Moreover, treatment with EVs derived from mesenchymal stem cells (MSCs) shows promising results in improving the neurological outcome in animal models of stroke [65], and TBI, through a not-yet well-defined mechanism. Thus, therapeutical treatment with EVs is foreseeable in these acquired neurological disorders [66–69].

In a mouse model for Multiple Sclerosis (MS), an autoimmune disease characterized by demyelination and axonal injury in the CNS, myeloid microvesicles are significantly increased in the CSF compared to controls, and these EVs are capable to spread inflammatory signals both in vitro and in vivo [70]. Moreover, myeloid exosomes are increased in the CSF of patients with relapsing-remitting MS (RRMS) in comparison to healthy controls [70]. Plasma levels of endothelial EVs are increased in MS patients during the clinical relapse phase compared to the remission phase, pointing out a possible role for endothelial EVs as disease state biomarkers [71].

CNS-EVs in brain tumors have been intensively studied (reviewed in [72]). Cell lines of glioblastoma (GBM), an aggressive tumor of glial origin, secrete EVs with high immunogenic potential in mice and humans [73,74]. Serum EVs from patients suffering GBM are capable to polarize monocytes towards the anti-inflammatory phenotype M2, enhancing tumor growth in vitro [74]. Remarkably, astrocytes in the brain tumor microenvironment (TME) release EVs containing miR-19a, downregulating the tumor suppressor PTEN in tumor metastatic cells, thus contributing to their growth. When these cells exit the brain TME, PTEN function is restored [75].

Most of the above-mentioned studies were performed under in vitro conditions, or by isolating EVs from fluids. They have greatly helped to characterize the EV content and to the understanding of basic CNS-EVs functions. However, there is a clear need to retrieve and analyse EVs directly from brain tissue, to have a better picture of the whole physiological and pathological processes, including all cellular players. In 2012 the first paper isolating EVs from brain was published [76]. In the following years, modifications of this protocol and completely new protocols isolating BDEVs from both, healthy and diseased conditions, have been reported [49,77–82]. In the next paragraphs, we will analyse similarities and differences between the isolation methods and, for the sake of conciseness, we will only focus on protocols used for EVs isolation from brain. We will also re-examine and compare published proteomic analyses obtained by different isolation methods, to evaluate their efficiency and comparability in retrieving EVs from brain tissue.

2. BDEVs: Comparison of Current Protocols

As mentioned above, for over three decades EVs have been successfully isolated from cell culture media and body fluids (e.g., CSF, blood, urine, sperm, breast milk) [83]. Different protocols for EVs isolation from body fluids or conditioned media have been established, such as ultracentrifugation, immunoprecipitation, ultracentrifugation, size exclusion chromatography, or filtration-based concentration among others [84–87]. Notably, body fluids are generally more viscous than culture media as they contain numerous non-EV structures, such as lipidic components in plasma and serum, fat-containing vesicles in milk, and surfactant in bronchoalveolar lavage. For each type of body fluid, specific precautions have to be taken into account, as all of these non-EVs structures might be isolated together with EVs and interfere with the analyses [39,83]. An even more challenging procedure is to isolate EVs from complex tissues. To liberate the EVs from the extracellular matrix (ECM), the frozen or fresh tissue first must suffer an initial mechanical disruption (i.e., the tissue being cut into small pieces), generally followed by enzymatic digestion to disrupt the network of glycosaminoglycans, proteoglycans, glycoproteins, and fibrous proteins that compose the ECM. In the first protocol published in 2012 [76] and in later variations of this protocol [82,88], the enzyme of choice was papain, a cysteine protease found in papaya and often used, e.g., to prepare primary neuronal cultures. Another enzyme widely used is collagenase, which breaks the collagen peptide bonds of

the ECM [77–79,81,89]. During this disruption procedure, the creation of artifacts, such as synaptosome-like vesicles formation, membrane damage, or contamination with intracellular vesicles, seems unavoidable, and therefore, apart from several rounds of centrifugation, further purification steps, such as membrane pore filtration (e.g., using a 0.2 μm filter) and density gradients, are applied. The final washed pellet from the fractions generated through the density gradient is enriched in BDEVs. Variations of this protocol include the enzymatic dissociation of the tissue together with automatized disruption [90].

The whole procedure is very time consuming and difficult to automate. Therefore, other protocols have also been optimized for BDEVs isolation such as size exclusion chromatography (SEC) [81], avoiding the density gradient step, or precipitation with organic solvents methods such as the PROSPR method, which avoids enzymatic digestion, ultracentrifugation, and density gradients ultracentrifugation [80]. Even though PROSPR has already been used to isolate EVs from plasma [91,92], to purify BDEVs it so far was the chosen and published method by one group only [80].

To evaluate the comparability of BDEVs isolated with different protocols, we have compared available proteomics data from different studies. For mouse brain, we have compared a paper recently published from our lab [78], a paper from Silverman et al. [93], and the mouse data published by Gallart-Palau et al. [80]. For human BDEVs, we have compared the proteomic data of Vella et al. [77], Huang et al. [81], and the human data from the paper of Gallart-Palau et al. [80].

Figure 1 shows the major steps of the protocols used in these studies, but for in-depth details, we of course suggest the reader refers to the original papers. Except for Gallart-Palau et al., all these studies included short tissue slicing and incubation with collagenase type III for not longer than 20 min at 37°. In the study from Gallart-Palau et al., they used a mechanical approach, consisting of a bullet blender homogenizer with metallic beads to disrupt the tissue.
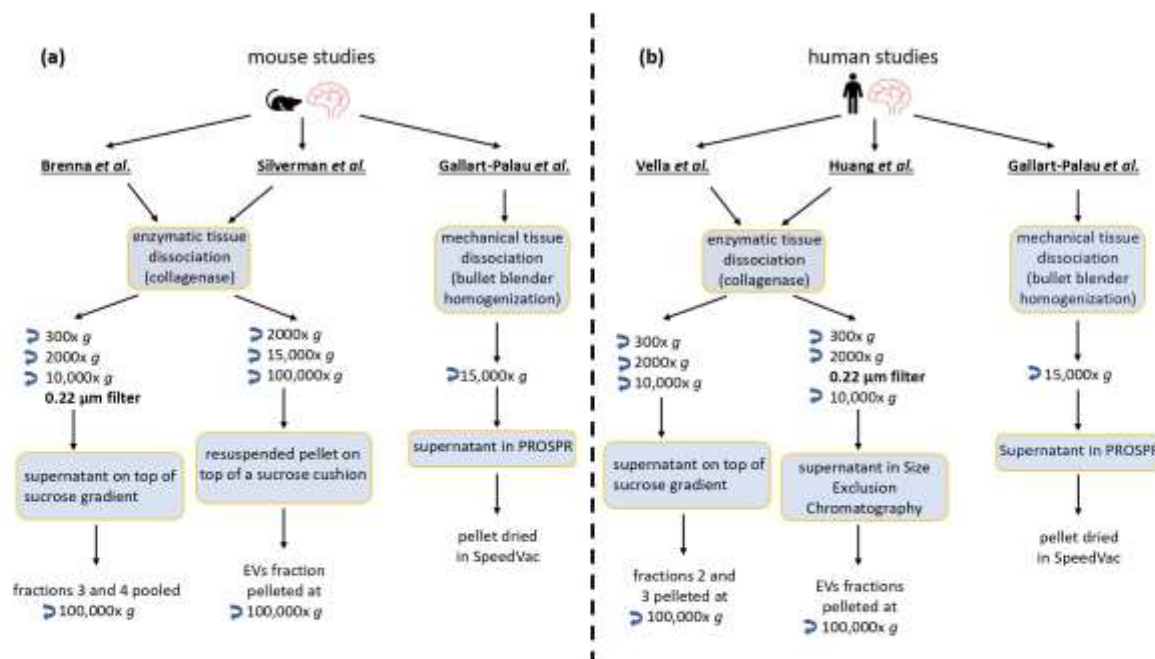
Figure 1. Summarizing scheme comparing protocols used for the proteomics analysis of BDEVs. (a) Schematic workflow of the protocols used in the mouse studies. (b) Schematic workflow of the protocols used in human studies.

After the dissociation step, low speed centrifugations ($300\times g$ and $2000\times g$), to clear cells, tissue fragments, and other debris are performed in Silverman et al., Huang et al., Vella et al., and Brenna et al. protocols, as depicted in Figure 1. Higher-speed centrifugations

(10,000× *g* and 15,000× *g*) were used in all considered studies to further discard debris and/or larger vesicles. An additional filtration step (0.22 μm filter) is introduced either before the 10,000× *g* centrifugation (in Huang et al.) or after this centrifugation step (in Brenna et al.) to eliminate large EVs (≥200 nm). In the latter study, it was assessed that this filtration step was indeed discriminating between different EV populations as the filtered preparation was specifically enriched in different proteins (e.g., ribosomal proteins) compared to the unfiltered, as revealed by mass spectrometry [78].

In the protocols of Brenna et al. and Vella et al. the 10,000× *g* supernatant (filtered or not) is then overlayed on top of a sucrose gradient, centrifuged at 180,000× *g*, and designated fractions containing EVs were collected. Differently, in Silverman et al. the 10,000× *g* supernatant is first pelleted at 100,000× *g*, then resuspended, placed on top of a sucrose cushion, and centrifuged at 150,000× *g*. In the study of Huang et al., the supernatant collected after the 10,000× *g* centrifugation is further processed by SEC and the EVs are collected in specific eluate fractions. Gallart-Palau et al. isolate EVs with a solvent-based precipitation method coupled with low-speed centrifugation (PRotein Organic Solvent Precipitation, PROSPR), and the supernatant containing the EVs is dried in a SpeedVac.

Except for Gallart-Palau et al., all the other studies (EVs collected either from the sucrose gradient or from SEC) lastly pelleted the EVs at 100,000× *g* for further analyses.

3. Mass Spectrometry Analysis-Based Comparison between Different BDEVs Isolation Protocols

3.1. Methods

Mouse BDEVs proteomic data: as most raw data were not publicly available, the protein identification lists provided in the publications were used for our comparison. For the data sets of Gallart-Palau et al. and Silverman et al. the protein sequence database searches were performed with a combination of reviewed and non-reviewed protein sequence databases and, to better compare the studies, gene names were used and converted to Uniprot-reviewed protein accessions (www.uniprot.org). Proteins that were identified in at least one of the replicates per study were used for the analysis.

Human BDEVs proteomic data: Mass spectrometry raw data were either downloaded from the specified online repository or requested from the authors. In the case of Vella et al., the already processed protein list provided in the original publication was used.

Raw data were re-processed using the Andromeda algorithm in MaxQuant 1.6.3.4 (Max Planck Institute for Biochemistry, Martinsried, Germany) setting with carbamidomethylation of cysteines as a fixed modification and the oxidation of methionine as a variable modification. A reviewed human protein sequence database downloaded from Uniprot (EMBL, released in September 2020, 20,387 sequence entries) was used. Proteins with a protein and peptide false discovery rate of <0.01 percent were accepted as being present in the data set.

The representative Uniprot accession for each protein group was taken and Venn diagrams were generated using Venny 2.1 (https://bioinfogp.cnb.csic.es/tools/venny/index.html).

Cellular Component enrichment analysis based on Gene Ontology (GOCC) was performed using DAVID Bioinformatics Resources (DOI: 10.1038/nprot.2008.211). Ranking based on enrichment significance (*p*-value) was used. For comparison, the fifteen most significant enrichments across all data sets were used.

3.2. Results

Regarding mouse BDEVs, Silverman et al. identified 1191 proteins in BDEVs, Gallart-Palau et al. found 444 proteins, and Brenna et al. 1518 proteins (Table 1). To better compare such different studies, we decided to not consider the absolute number of proteins detected in each study but their specific GO Cellular Component enrichments (GOCC) using the DAVID program. As depicted in Figure 2, the top 15 GOCC enrichments of the three data sets identified with DAVID and ranked by *p*-value include the GO term "extracellular

exosome" (GO:0070062), highly enriched (over 40%) in all three mouse studies. Another largely represented GO term is "membrane" (GO:0016020) accounting for around 70% of proteins in Brenna et al. and Silverman et al., and 50% for Gallart-Palau et al. "Cytoplasm" (GO:0005737) accounts for 50% of the identified proteins in Brenna et al., around 45% in Silvermann et al., and almost 60% in Gallart-Palau et al. The terms "cytosol" (GO:0005829) and "mitochondrion" (GO:0005739) are around 20% of the identified proteins, whereas "focal adhesion" (GO:0005925) and "synapse" (GO:0045202) accounts for almost 10% of the proteins in all three studies. Even though all mouse data sets share similarities, the study of Gallart-Palau et al. shows a total absence of ribosomal components (i.e., "ribosome" (GO:0005840) and "intracellular ribonucleoprotein complex" (GO:0030529)) which in the other two studies account for around 5–7% of the identified proteins. A similar absence is observed for "endoplasmic reticulum" (GO:0005783), accounting for almost 20% in the Silverman et al. and Brenna et al. studies. On the other hand, the presence of "myelin sheath" (GO:0043209) is increased in the Gallart-Palau et al. study, accounting for more than 20% of the identified proteins. The differences are noticeable in the Venn diagram (Figure 3), where Silverman et al. and Brenna et al. share 36.9% of the detected proteins while the PROSPR study shares with them roughly 9.3%.

Table 1. Total protein IDs identified in human and mouse studies. Note that there is a slight difference in protein numbers published in the referred papers and in Table 1. This is due to our strategy to use gene names and convert them to Uniprot-reviewed accessions as described in Material and Methods.

Human		Mouse	
Study	Proteins	Study	Proteins
Gallart-Palau et al.	3056	Silverman et al.	1191
Huang et al.	714	Gallart-Palau et al.	444
Vella et al. F2	1144	Brenna et al.	1518
Vella et al. F3	815		
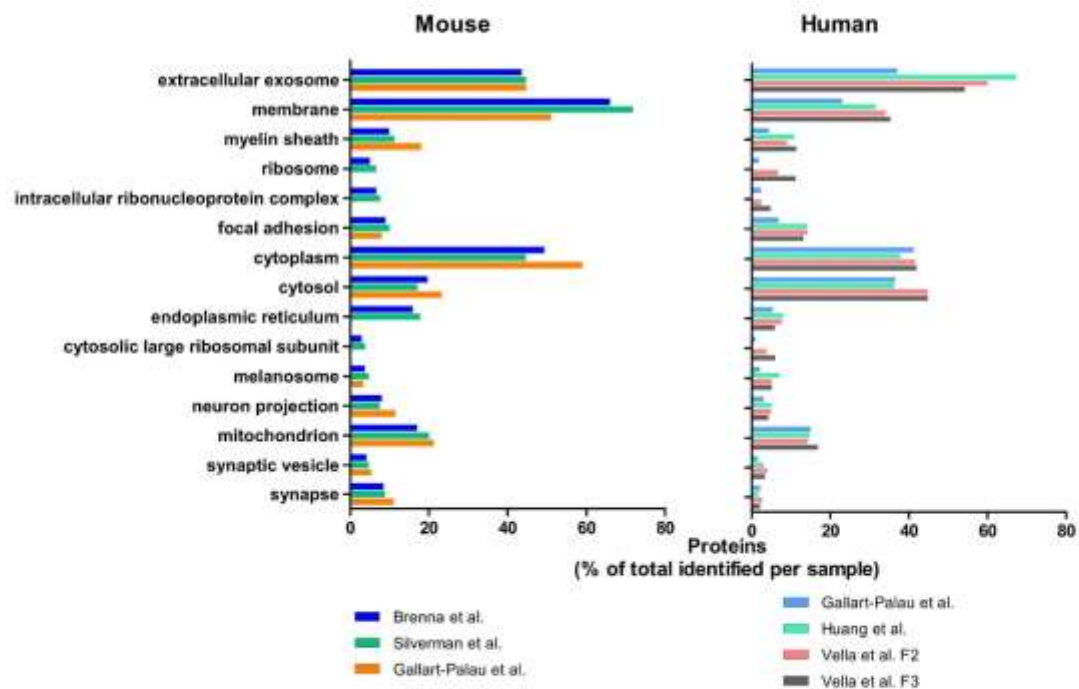
Figure 2. Bar charts of the 15 most enriched GO Cellular Components (GOCCs) in the mouse and human studies. The graph shows the top 15 GOCC detected with DAVID in the mouse studies (on the left) and the human studies (on the right).
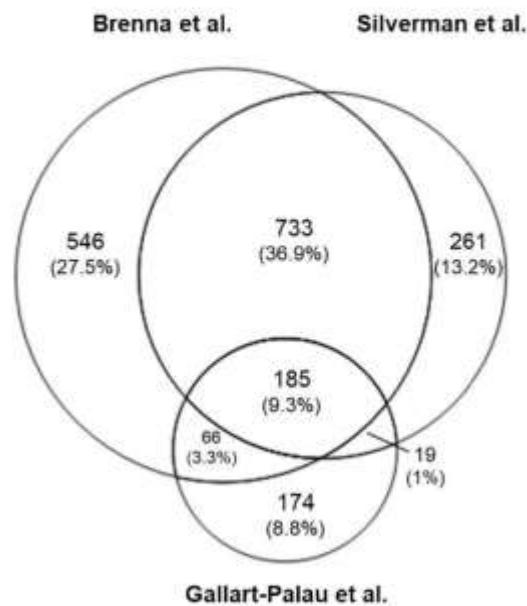
Figure 3. Venn diagram of all proteins detected in mouse studies. The data set from Brenna et al. detected 27.5% of proteins as unique, sharing 36.9% of proteins with the data set from Silverman et al. and 3.3% with Gallart-Palau et al. Silverman et al. detected 13.2% of proteins as unique, sharing with Gallart-Palau et al. 1% of proteins. Gallart-Palau et al. present 8.8% of proteins as unique. 9.3% of all proteins are shared among all three studies.

Regarding human BDEVS, Huang et al. identified 714 proteins, Gallart-Palau et al. 3056 proteins, while Vella et al. detected 1144 proteins in Fraction 2 and 815 in Fraction 3 (Table 1). For the latter study, we here analyze the two fractions most enriched with EV markers as described in the paper [77].

As shown in Figure 2, in all three human studies, coinciding with the mouse studies, the most enriched GO term is "extracellular exosome", accounting for nearly 70% identified proteins in Huang et al., 60% in Vella et al. (Fraction 2), and for 54% in Fraction 3, while in Gallart-Palau et al., this term accounts for 37% of the identified proteins. The GO term "membrane" is also highly enriched in all three studies, accounting for 38% (F2) and 37% (F3) in Vella et al., 35% in Huang et al., and around 23% in Gallart-Palau et al. "Cytoplasm" accounts for almost 40% of all the proteins in all three studies, and the same is observed for the term "cytosol" with 45% of the proteins identified falling on this term in F2 and F3 of Vella et al., and around 37% in Huang et al. and Gallart-Palau et al. Additionally, in all the human data sets "mitochondrion" is around 15% and "endoplasmic reticulum" between 5 and 8%. The GO term "focal adhesion" accounts for 7% in the PROSPR study and 14% of the total identified proteins in all the other human studies. Conspicuously, the human data of Gallart-Palau and colleagues, contrary to their own mouse study, retrieves proteins related to the terms "ribosome", "intracellular ribonucleoprotein complex" and "cytosolic large ribosomal subunit". In this case, the data set from Huang et al. does not identify proteins for these terms. The Venn diagram (Figure 4) shows that the number of identified proteins shared by Gallart-Palau et al. and Vella et al. are higher than in Huang et al. compared either to Vella et al. and Gallart-Palau et al. This is in contrast to the mouse studies where the PROSPR method of Gallart-Palau et al. was the least similar to the other two studies.
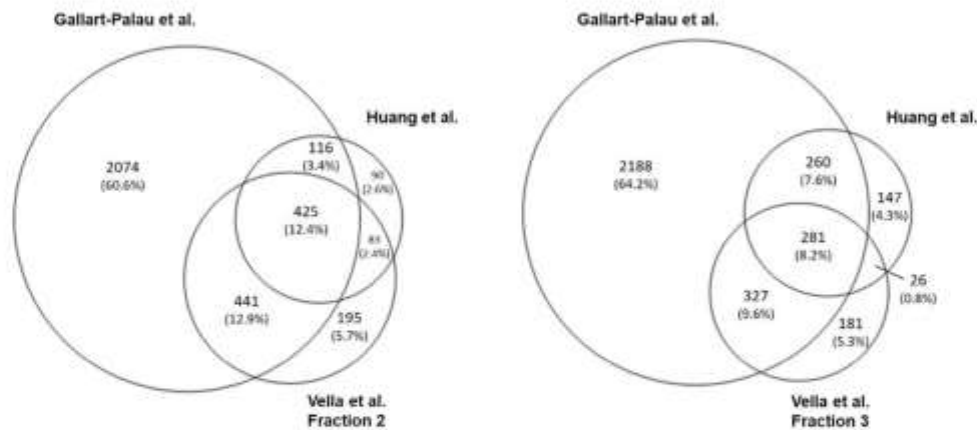
Figure 4. Venn diagram of all proteins detected in human studies. On the left, the Venn diagram for human studies including Vella et al. fraction 2. On the right, including Vella et al. fraction 3. Gallart-Palau et al. detected 60.6% of proteins as unique, sharing 12.9% of proteins with the data set of fraction 2 from Vella et al., and 3.4% with Huang et al. The latter detected 2.6% of proteins as unique while sharing with Vella's fraction 2 the 2.4% of detected proteins. Fraction 2 from Vella et al. accounts the 5.7% of proteins as unique. 12.4% of all proteins are shared among the three studies. When considering Vella's fraction 3, Gallart-Palau et al. detected 64.2% of proteins as unique, sharing 9.6% of proteins with the data set of fraction 3 from Vella et al., and 7.6% with Huang et al. The latter detected 4.3% of proteins as unique, sharing with Vella et al. fraction 3 0.8% of proteins detected. Fraction 3 from Vella et al. presents 5.3% of proteins as unique. 8.2% of all proteins are shared among the three studies.

Overall, the graph in Figure 2 shows that the terms "exosome", "membrane", "cytoplasm" and "cytosol" followed by "mitochondrion" are the most enriched GO terms in the mouse and human proteomic studies compared herein, regardless of the method, implying a real enrichment of BDEVs in all of them. Nevertheless, we could observe some differences between the methods. Of note, it must be considered that all studies included in this review had different aims in terms of protein identification and quantification, and thus, they used different mass spectrometric strategies such as fractionation and proteome analysis applications. Moreover, different generations of mass spectrometers were used: Orbitrap Elite (Thermo Scientific) in Gallart-Palau et al., Orbitrap Fusion (Thermo Scientific in Brenna et al., Q Exactive Plus (Thermo Scientific) in Vella et al., Q Exactive HF (Thermo Scientific) in Huang et al. and Impact II Q-TOF (Bruker) in Silverman et al. Important to consider is also the overall quality of the tissue sample, in terms of post-mortem time and storage conditions, especially for the human brains [39].

However, by using the same MS strategy, the PROSPR method of Gallart-Palau et al. detected the highest number of proteins in the human brain, but the lowest in the mouse brain. It is hard to say if the method is indeed more effective in human brain than in mouse samples, as several variables can account for this discrepancy. For example, the amount of tissue used for the extraction was differing very much among the two experiments (40 mg of mouse brain tissue versus 150 mg of human brain tissue, as reported in the publication), thus introducing a potential source of variability. This could also be an explanation for why the authors did not find enrichment for ribosomal proteins in mouse brain but human. Still, as Huang et al. already pointed out in their study, the same method applied to human, macaque, and mouse tissue produces different results and yields. As the authors indicate, this could also be a consequence of either inter-species differences in tissue fragility or the processing of different brain areas with a different cellular composition [81]. Another possible source of variability can be the exact brain area used, especially in human studies (parietal cortex in Huang et al. versus frontal cortex in Vella et al. versus temporal lobe in Gallart-Palau et al.).

Brenna et al., Silverman et al., and Vella et al. found ribosomal-related proteins in the mass spectrometry analysis, whereas, as discussed, the PROSPR method only found

these in humans, and in Huang et al. they were not detected at all. The first three studies share major steps in the EVs isolation protocols, suggesting that density gradients isolate BDEVs with similar characteristics and/or contaminants. Thus, the current methods used for BDEVs isolation show that some proteins are differentially enriched, or diverse unique proteins are identified, when the isolation is made by SEC or by chemical separation such as PROSPR, compared with density gradients and ultracentrifugation methods. However, as mentioned above, the amounts of tissue used in the studies were different, and the amount of protein evaluated in MS was not always reported, making any comparison difficult when certain proteins are not identified.

More recently, gradients using iodixanol with upwards floatation (instead of overlaying the sample) have been implemented in the isolation of EVs [79,94] which can help to minimize contamination and to yield the highest purity for BDEVs (our unpublished observations).

Finally, we would like to mention that, in the papers reviewed herein, the enzyme of choice was collagenase. However, papain has also been very successfully applied in several BDEVs isolation protocols [76,95,96]. From our own experience (unpublished observations) and that of others [97], when using papain it is important to consider the accuracy in incubation time and proper inhibition of the enzyme.

4. Future Perspectives

The study of BDEVs can significantly help to understand complex and multicellular physiological and pathological processes in the brain, which is simply not possible in in vitro studies.

Since the publication of the first protocol for isolation of BDEVs [76], the number of publications on this topic is increasing, with the first group of those publications reviewed in reference [98]. Since then, regarding neurodegenerative diseases such as AD, it has been shown that during the preclinical stage the expression of MHC class I markers in BDEVs is significantly upregulated [99] and that EVs isolated from murine brain are enriched with C-terminal fragments of APP (APP-CTFs), actively produced on the vesicles [76,100]. Furthermore, brain-derived EVs isolated both from early AD subjects and BCAS (bilateral common carotid stenosis) mice carry proteins involved in hypoxia such as EFEMP1, downstream activator of HIFs [101], highlighting the role of EVs in the hypoperfusion in human dementias. In a mouse model of PD, the inhibition of glucocerebrosidase (GCase) activity increased the amounts of BDEVs-associated α-synuclein oligomers [102]. Furthermore, another study showed that, when injected into mouse brains, EVs isolated from patients with Lewy Body Disease (LBD) were capable to induce α-synuclein aggregation [103]. In our lab, we recently demonstrated in mice that, under physiological conditions, microglia are the main source of small EVs (sEVs; <200 nm) in the brain sEV pool and that 24 h after experimental stroke, astrocyte-derived sEVs are significantly increased. Moreover, in the same study, we were able to describe a role for the prion protein (PrP^C) and its proteolytically truncated C1 fragment in the uptake of sEVs by recipient cells [78]. Additionally, a recent study demonstrated enrichment of TDP-43 C-terminal fragments in BDEVs isolated from the motor cortex of ALS patients [104]. Lastly, it has been shown that EVs from different organs (e.g., brain, lung, heart) have specific markers, specifically synaptophysin (SYP) for brain-derived EVs, which are enriched also in other synaptic membrane proteins and receptors [105].

All in all, BDEVs are a particularly important tool for studying EVs-mediated intercellular communication in the brain in steady-state and relevant alterations in various disease conditions. It is difficult to draw clear conclusions on whether one isolation technique is better than another, at least by comparing proteomic analysis as we did here. All methods included in this review can successfully isolate BDEVs and differences in the proteomic analysis seem to be more dependent on other aspects, such as the amount and area of tissue used for isolation, and, for the proteomic analysis, the mass spectrometric strategy and analysis, and the employed mass spectrometer itself. As the field advances very rapidly, and as highlighted in this review, there is an obvious need for exact reporting standards

(e.g., protein amounts, tissue regions) to make studies more comparable with reliable and reproducible results.

References

1. Mercer, E.H.; Shaffer, B.M. Electron Microscopy of Solitary and Aggregated Slime Mould Cells. *J. Biophys. Biochem. Cytol.* **1960**, 7, 353–356. [CrossRef] [PubMed]
2. Vickerman, K. Patterns of cellular organisation in Limax amoebae. An electron microscope study. *Exp. Cell Res.* **1962**, 26, 497–519. [PubMed]
3. Sun, C.N. Lattice structures and osmiophilic bodies in the developing respiratory tissue of rats. *J. Ultrastruct. Res.* **1966**, 15, 380–388. [CrossRef] [PubMed]
4. Bonucci, E. Fine structure of early cartilage calcification. *J. Ultrastruct. Res.* **1967**, 20, 33–50. [CrossRef]
5. Anderson, H.C. Vesicles associated with calcification in the matrix of epiphyseal cartilage. *J. Cell Biol.* **1969**, 41, 59–72. [CrossRef]
6. Wolf, P. The nature and significance of platelet products in human plasma. *Br. J. Haematol.* **1967**, 13, 269–288. [CrossRef]
7. Chargaff, E.; West, R. The biological significance of the thromboplastic protein of blood. *J. Biol. Chem.* **1946**, 166, 189–197. [CrossRef]
8. Aaronson, S.; Behrens, U.; Orner, R.; Haines, T.H. Ultrastructure of intracellular and extracellular vesicles, membranes, and myelin figures produced by Ochromonas danica. *J. Ultrastruct. Res.* **1971**, 35, 418–430. [CrossRef]
9. Ronquist, G.; Brody, I. The prostasome: Its secretion and function in man. *Biochim. Biophys. Acta* **1985**, 822, 203–218. [CrossRef]
10. Ronquist, G.; Hedström, M. Restoration of detergent-inactivated adenosine triphosphatase activity of human prostatic fluid with concanavalin A. *Biochim. Biophys. Acta* **1977**, 483, 483–486. [CrossRef]
11. Trams, E.G.; Lauter, C.J.; Salem, N.; Heine, U. Exfoliation of membrane ecto-enzymes in the form of micro-vesicles. *Biochim. Biophys. Acta* **1981**, 645, 63–70. [CrossRef]
12. Poste, G.; Nicolson, G.L. Arrest and metastasis of blood-borne tumor cells are modified by fusion of plasma membrane vesicles from highly metastatic cells. *Proc. Natl. Acad. Sci. USA* **1980**, 77, 399–403. [CrossRef] [PubMed]
13. Pan, B.T.; Johnstone, R.M. Fate of the transferrin receptor during maturation of sheep reticulocytes in vitro: Selective externalization of the receptor. *Cell* **1983**, 33, 967–978. [CrossRef]
14. Harding, C.; Heuser, J.; Stahl, P. Receptor-mediated endocytosis of transferrin and recycling of the transferrin receptor in rat reticulocytes. *J. Cell Biol.* **1983**, 97, 329–339. [CrossRef]
15. Harding, C.V.; Heuser, J.E.; Stahl, P.D. Exosomes: Looking back three decades and into the future. *J. Cell Biol.* **2013**, 200, 367–371. [CrossRef]
16. Johnstone, R.M.; Adam, M.; Hammond, J.R.; Orr, L.; Turbide, C. Vesicle formation during reticulocyte maturation. Association of plasma membrane activities with released vesicles (exosomes). *J. Biol. Chem.* **1987**, 262, 9412–9420. [CrossRef]
17. Johnstone, R.M.; Mathew, A.; Mason, A.B.; Teng, K. Exosome formation during maturation of mammalian and avian reticulocytes: Evidence that exosome release is a major route for externalization of obsolete membrane proteins. *J. Cell. Physiol.* **1991**, 147, 27–36. [CrossRef]
18. Raposo, G.; Nijman, H.W.; Stoorvogel, W.; Liejendekker, R.; Harding, C.V.; Melief, C.J.; Geuze, H.J. B lymphocytes secrete antigen-presenting vesicles. *J. Exp. Med.* **1996**, 183, 1161–1172. [CrossRef]
19. Zitvogel, L.; Regnault, A.; Lozier, A.; Wolfers, J.; Flament, C.; Tenza, D.; Ricciardi-Castagnoli, P.; Raposo, G.; Amigorena, S. Eradication of established murine tumors using a novel cell-free vaccine: Dendritic cell-derived exosomes. *Nat. Med.* **1998**, 4, 594–600. [CrossRef]
20. Raposo, G.; Tenza, D.; Mecheri, S.; Peronet, R.; Bonnerot, C.; Desaymard, C. Accumulation of major histocompatibility complex class II molecules in mast cell secretory granules and their release upon degranulation. *Mol. Biol. Cell* **1997**, 8, 2631–2645. [CrossRef]

21. Heijnen, H.F.; Schiel, A.E.; Fijnheer, R.; Geuze, H.J.; Sixma, J.J. Activated platelets release two types of membrane vesicles: Microvesicles by surface shedding and exosomes derived from exocytosis of multivesicular bodies and alpha-granules. *Blood* **1999**, *94*, 3791–3799. [CrossRef] [PubMed]

22. Van Niel, G.; Raposo, G.; Candalh, C.; Boussac, M.; Hershberg, R.; Cerf-Bensussan, N.; Heyman, M. Intestinal epithelial cells secrete exosome-like vesicles. *Gastroenterology* **2001**, *121*, 337–349. [CrossRef] [PubMed]

23. Colombo, M.; Raposo, G.; Théry, C. Biogenesis, secretion, and intercellular interactions of exosomes and other extracellular vesicles. *Annu. Rev. Cell Dev. Biol.* **2014**, *30*, 255–289. [CrossRef] [PubMed]

24. Escola, J.-M.; Kleijmeer, M.J.; Stoorvogel, W.; Griffith, J.M.; Yoshie, O.; Geuze, H.J. Selective enrichment of tetraspan proteins on the internal vesicles of multivesicular endosomes and on exosomes secreted by human B-lymphocytes. *J. Biol. Chem.* **1998**, *273*, 20121–20127. [CrossRef]

25. Théry, C.; Boussac, M.; Véron, P.; Ricciardi-Castagnoli, P.; Raposo, G.; Garin, J.; Amigorena, S. Proteomic analysis of dendritic cell-derived exosomes: A secreted subcellular compartment distinct from apoptotic vesicles. *J. Immunol.* **2001**, *166*, 7309–7318. [CrossRef]

26. Stein, J.M.; Luzio, J.P. Ectocytosis caused by sublytic autologous complement attack on human neutrophils. The sorting of endogenous plasma-membrane proteins and lipids into shed vesicles. *Biochem. J.* **1991**, *274 Pt 2*, 381–386. [CrossRef]

27. Hess, C.; Sadallah, S.; Hefti, A.; Landmann, R.; Schifferli, J.A. Ectosomes released by human neutrophils are specialized functional units. *J. Immunol.* **1999**, *163*, 4564–4573. [CrossRef]

28. Mause, S.F.; Ritzel, E.; Liehn, E.A.; Hristov, M.; Bidzhekov, K.; Müller-Newen, G.; Soehnlein, O.; Weber, C. Platelet microparticles enhance the vasoregenerative potential of angiogenic early outgrowth cells after vascular injury. *Circulation* **2010**, *122*, 495–506. [CrossRef]

29. Cocucci, E.; Racchetti, G.; Meldolesi, J. Shedding microvesicles: Artefacts no more. *Trends Cell Biol.* **2009**, *19*, 43–51. [CrossRef]

30. Bastida, E.; Ordinas, A.; Escolar, G.; Jamieson, G.A. Tissue factor in microvesicles shed from U87MG human glioblastoma cells induces coagulation, platelet aggregation, and thrombogenesis. *Blood* **1984**, *64*, 177–184. [CrossRef]

31. Lotvall, J.; Valadi, H. Cell to cell signalling via exosomes through esRNA. *Cell Adhes. Migr.* **2007**, *1*, 156–158. [CrossRef] [PubMed]

32. Valadi, H.; Ekström, K.; Bossios, A.; Sjöstrand, M.; Lee, J.J.; Tvall, J.O.L.O. Exosome-mediated transfer of mRNAs and microRNAs is a novel mechanism of genetic exchange between cells. *Nat. Cell Biol.* **2007**, *9*, 654–659. [CrossRef] [PubMed]

33. Ramachandran, S.; Palanisamy, V. Horizontal transfer of RNAs: Exosomes as mediators of intercellular communication. *Wiley Interdiscip. Rev. RNA* **2012**, *3*, 286–293. [PubMed]

34. El Andaloussi, S.; Lakhal, S.; Mäger, I.; Wood, M.J. Exosomes for targeted siRNA delivery across biological barriers. *Adv. Drug Deliv. Rev.* **2013**, *65*, 391–397. [CrossRef] [PubMed]

35. Hill, A.F. Extracellular Vesicles and Neurodegenerative Diseases. *J. Neurosci.* **2019**, *39*, 9269–9273. [CrossRef] [PubMed]

36. Vassileff, N.; Cheng, L.; Hill, A.F. Extracellular vesicles-propagators of neuropathology and sources of potential biomarkers and therapeutics for neurodegenerative diseases. *J. Cell Sci.* **2020**, *133*. [CrossRef]

37. Gould, S.J.; Raposo, G. As we wait: Coping with an imperfect nomenclature for extracellular vesicles. *J. Extracell. Vesicles* **2013**, *2*, 20389. [CrossRef]

38. Lötvall, J.; Hill, A.F.; Hochberg, F.; Buzás, E.I.; Di Vizio, D.; Gardiner, C.; Gho, Y.S.; Kurochkin, I.V.; Mathivanan, S.; Quesenberry, P.; et al. Minimal experimental requirements for definition of extracellular vesicles and their functions: A position statement from the International Society for Extracellular Vesicles. *J. Extracell. Vesicles* **2014**, *3*, 26913. [CrossRef]

39. Théry, C.; Witwer, K.W.; Aikawa, E.; Alcaraz, M.J.; Anderson, J.D.; Andriantsitohaina, R.; Antoniou, A.; Arab, T.; Archer, F.; Atkin-Smith, G.K.; et al. Minimal information for studies of extracellular vesicles 2018 (MISEV2018): A position statement of the International Society for Extracellular Vesicles and update of the MISEV2014 guidelines. *J. Extracell. Vesicles* **2018**, *7*, 1535750. [CrossRef]

40. Bianco, F.; Pravettoni, E.; Colombo, A.; Schenk, U.; Möller, T.; Matteoli, M.; Verderio, C. Astrocyte-derived ATP induces vesicle shedding and IL-1 beta release from microglia. *J. Immunol.* **2005**, *174*, 7268–7277.

41. Drago, F.; Lombardi, M.; Prada, I.; Gabrielli, M.; Joshi, P.; Cojoc, D.; Franck, J.; Fournier, I.; Vizioli, J.; Verderio, C. ATP Modifies the Proteome of Extracellular Vesicles Released by Microglia and Influences Their Action on Astrocytes. *Front. Pharmacol.* **2017**, *8*, 910. [CrossRef] [PubMed]

42. Prada, I.; Gabrielli, M.; Turola, E.; Iorio, A.; D'Arrigo, G.; Parolisi, R.; De Luca, M.; Pacifici, M.; Bastoni, M.; Lombardi, M.; et al. Glia-to-neuron transfer of miRNAs via extracellular vesicles: A new mechanism underlying inflammation-induced synaptic alterations. *Acta Neuropathol.* **2018**, *135*, 529–550. [CrossRef] [PubMed]

43. Bianco, F.; Perrotta, C.; Novellino, L.; Francolini, M.; Riganti, L.; Menna, E.; Saglietti, L.; Schuchman, E.H.; Furlan, R.; Clementi, E.; et al. Acid sphingomyelinase activity triggers microparticle release from glial cells. *EMBO J.* **2009**, *28*, 1043–1054. [CrossRef] [PubMed]

44. Dugger, B.N.; Dickson, D.W. Pathology of Neurodegenerative Diseases. *Cold Spring Harb. Perspect Biol.* **2017**, *9*, a028035. [CrossRef] [PubMed]

45. Rajendran, L.; Honsho, M.; Zahn, T.R.; Keller, P.; Geiger, K.D.; Verkade, P.; Simons, K. Alzheimer's disease beta-amyloid peptides are released in association with exosomes. *Proc. Natl. Acad. Sci. USA* **2006**, *103*, 11172–11177. [CrossRef]

46. Vingtdeux, V.; Hamdane, M.; Loyens, A.; Gelé, P.; Drobeck, H.; Bégard, S.; Galas, M.-C.; Delacourte, A.; Beauvillain, J.-C.; Buée, L.; et al. Alkalizing drugs induce accumulation of amyloid precursor protein by-products in luminal vesicles of multivesicular bodies. *J. Biol. Chem.* **2007**, *282*, 18197–18205. [CrossRef]

47. Saman, S.; Kim, W.; Raya, M.; Visnick, Y.; Miro, S.; Saman, S.; Jackson, B.; McKee, A.C.; Alvarez, V.E.; Lee, N.C.Y.; et al. Exosome-associated tau is secreted in tauopathy models and is selectively phosphorylated in cerebrospinal fluid in early Alzheimer disease. *J. Biol. Chem.* **2012**, *287*, 3842–3849. [CrossRef]

48. Baker, S.; Polanco, J.C.; Götz, J. Extracellular Vesicles Containing P301L Mutant Tau Accelerate Pathological Tau Phosphorylation and Oligomer Formation but Do Not Seed Mature Neurofibrillary Tangles in ALZ17 Mice. *J. Alzheimer's Dis.* **2016**, *54*, 1207–1217. [CrossRef]

49. Polanco, J.C.; Scicluna, B.J.; Hill, A.F.; Götz, J. Extracellular Vesicles Isolated from the Brains of rTg4510 Mice Seed Tau Protein Aggregation in a Threshold-dependent Manner. *J. Biol. Chem.* **2016**, *291*, 12445–12466. [CrossRef]

50. Wang, Y.; Balaji, V.; Kaniyappan, S.; Krüger, L.; Irsen, S.; Tepper, K.; Chandupatla, R.; Maetzler, W.; Schneider, A.; Mandelkow, E.; et al. The release and trans-synaptic transmission of Tau via exosomes. *Mol. Neurodegener.* **2017**, *12*, 5. [CrossRef]

51. Emmanouilidou, E.; Melachroinou, K.; Roumeliotis, T.; Garbis, SD.; Ntzouni, M.; Margaritis, LH.; Stefanis, L.; Vekrellis, K. Cell-produced alpha-synuclein is secreted in a calcium-dependent manner by exosomes and impacts neuronal survival. *J. Neurosci.* **2010**, *30*, 6838–6851. [CrossRef] [PubMed]

52. Danzer, K.M.; Kranich, L.R.; Ruf, W.P.; Cagsal-Getkin, O.; Winslow, AR.; Zhu, L.; Vanderburg, CR.; McLean, PJ. Exosomal cell-to-cell transmission of alpha synuclein oligomers. *Mol. Neurodegener.* **2012**, *7*, 42. [CrossRef] [PubMed]

53. Fevrier, B.; Vilette, D.; Archer, F.; Loew, D.; Faigle, W.; Vidal, M.; Laude, H.; Raposo, G. Cells release prions in association with exosomes. *Proc. Natl. Acad. Sci. USA* **2004**, *101*, 9683–9688. [CrossRef] [PubMed]

54. Vella, L.J.; Sharples, R.A.; Lawson, V.A.; Masters, C.L.; Cappai, R.; Hill, A.F. Packaging of prions into exosomes is associated with a novel pathway of PrP processing. *J. Pathol.* **2007**, *211*, 582–590. [CrossRef]

55. Falker, C.; Hartmann, A.; Guett, I.; Dohler, F.; Altmeppen, H.; Betzel, C.; Schubert, R.; Thurm, D.; Wegwitz, F.; Joshi, P.; et al. Exosomal cellular prion protein drives fibrillization of amyloid beta and counteracts amyloid beta-mediated neurotoxicity. *J. Neurochem.* **2015**, *137*, 88–100. [CrossRef]

56. Soares Martins, T.; Trindade, D.; Vaz, M.; Campelo, I.; Almeida, M.; Trigo, G.; da Cruz E Silva, O.A.B.; Henriques, A.G. Diagnostic and therapeutic potential of exosomes in Alzheimer's disease. *J. Neurochem.* **2020**. [CrossRef]

57. VandenDriessche, C.; Bruggeman, A.; Van Cauwenberghe, C.; Vandenbroucke, R.E. Extracellular Vesicles in Alzheimer's and Parkinson's Disease: Small Entities with Large Consequences. *Cells* **2020**, *9*, 2485. [CrossRef]

58. Puig, B.; Brenna, S.; Magnus, T. Molecular Communication of a Dying Neuron in Stroke. *Int. J. Mol. Sci.* **2018**, *19*, 2834. [CrossRef]

59. Wang, M.-M.; Feng, Y.-S.; Tan, Z.-X.; Xing, Y.; Dong, F.; Zhang, F. The role of exosomes in stroke. *Mol. Biol. Rep.* **2020**, *47*, 6217–6228. [CrossRef]

60. Zhang, Z.G.; Chopp, M. Exosomes in stroke pathogenesis and therapy. *J. Clin. Investig.* **2016**, *126*, 1190–1197.

61. Yates, A.G.; Anthony, D.C.; Ruitenberg, M.J.; Couch, Y. Systemic Immune Response to Traumatic CNS Injuries-Are Extracellular Vesicles the Missing Link? *Front. Immunol.* **2019**, *10*, 2723. [CrossRef] [PubMed]

62. Osier, N.; Motamedi, V.; Edwards, K.; Puccio, A.; Diaz-Arrastia, R.; Kenney, K.; Gill, J. Exosomes in Acquired Neurological Disorders: New Insights into Pathophysiology and Treatment. *Mol. Neurobiol.* **2018**, *55*, 9280–9293. [CrossRef] [PubMed]

63. SStenz, K.T.; Just, J.; Blauenfeldt, R.A.; Drasbek, K.R. Extracellular Vesicles in Acute Stroke Diagnostics. *Biomedicines* **2020**, *8*, 248. [CrossRef] [PubMed]

64. Guedes, V.A.; Devoto, C.; Leete, J.; Sass, D.; Acott, JD.; Mithani, S.; Gill, JM. Extracellular Vesicle Proteins and MicroRNAs as Biomarkers for Traumatic Brain Injury. *Front. Neurol.* **2020**, *11*, 663. [CrossRef]

65. Doeppner, T.R.; Herz, J.; Görgens, A.; Schlechter, J.; Ludwig, A.K.; Radtke, S.; de Miroschedji, K.; Horn, P.A.; Giebel, B.; Hermann, D.M. Extracellular Vesicles Improve Post-Stroke Neuroregeneration and Prevent Postischemic Immunosuppression. *Stem Cells Transl. Med.* **2015**, *4*, 1131–1143. [CrossRef]

66. Doeppner, T.R.; Bähr, M.; Hermann, D.M.; Giebel, B. Concise Review: Extracellular Vesicles Overcoming Limitations of Cell Therapies in Ischemic Stroke. *Stem Cells Transl. Med.* **2017**, *6*, 2044–2052. [CrossRef]

67. Zhang, Z.G.; Chopp, M. Promoting brain remodeling to aid in stroke recovery. *Trends Mol. Med.* **2015**, *21*, 543–548. [CrossRef]

68. Zhang, H.; Wu, J.; Fan, Q.; Zhou, J.; Wu, J.; Liu, S.; Zang, J.; Ye, J.; Xiao, M.; Tian, T.; et al. Exosome-mediated targeted delivery of miR-210 for angiogenic therapy after cerebral ischemia in mice. *J. Nanobiotechnol.* **2019**, *17*, 1–13. [CrossRef]

69. Yuan, J.; Botchway, B.O.A.; Zhang, Y.; Wang, X.; Liu, X. Combined bioscaffold with stem cells and exosomes can improve traumatic brain injury. *Stem Cell Rev. Rep.* **2019**, *16*, 323–334. [CrossRef]

70. Verderio, C.; Muzio, L.; Turola, E.; Bergami, A.; Novellino, L.; Ruffini, F.; Riganti, L.; Corradini, I.; Francolini, M.; Garzetti, L.; et al. Myeloid microvesicles are a marker and therapeutic target for neuroinflammation. *Ann. Neurol.* **2012**, *72*, 610–624. [CrossRef]

71. Jimenez, J.; Jy, W.; Mauro, L.M.; Horstman, LL.; Ahn, ER.; Ahn, YS.; Minagar, A. Elevated endothelial microparticle-monocyte complexes induced by multiple sclerosis plasma and the inhibitory effects of interferon-beta 1b on release of endothelial microparticles, formation and transendothelial migration of monocyte-endothelial complexes. *Mult. Scler. J.* **2005**, *11*, 310–315.

72. Ciregia, F.; Urbani, A.; Palmisano, G. Extracellular Vesicles in Brain Tumors and Neurodegenerative Diseases. *Front. Mol. Neurosci.* **2017**, *10*, 276. [CrossRef] [PubMed]

73. Harshyne, L.A.; Hooper, K.M.; Andrews, E.G.; Nasca, B.J.; Kenyon, L.C.; Andrews, D.W.; Hooper, D.C. Glioblastoma exosomes and IGF-1R/AS-ODN are immunogenic stimuli in a translational research immunotherapy paradigm. *Cancer Immunol. Immunother.* **2014**, *64*, 299–309. [CrossRef] [PubMed]

74. Harshyne, L.A.; Nasca, B.J.; Kenyon, L.C.; Andrews, D.W.; Hooper, D.C. Serum exosomes and cytokines promote a T-helper cell type 2 environment in the peripheral blood of glioblastoma patients. *Neuro Oncol.* **2015**, *18*, 206–215. [CrossRef]

75. Zhang, L.; Zhang, S.; Yao, J.; Lowery, F.J.; Zhang, Q.; Huang, W.C.; Li, P.; Li, M.; Wang, X.; Zhang, C.; et al. Microenvironment-induced PTEN loss by exosomal microRNA primes brain metastasis outgrowth. *Nature* **2015**, *527*, 100–104. [CrossRef]

76. Perez-Gonzalez, R.; Gauthier, S.A.; Kumar, A.; Levy, E. The exosome secretory pathway transports amyloid precursor protein carboxyl-terminal fragments from the cell into the brain extracellular space. *J. Biol. Chem.* **2012**, *287*, 43108–43115. [CrossRef]

77. Vella, L.J.; Scicluna, B.J.; Cheng, L.; Bawden, E.G.; Masters, C.L.; Ang, C.S.; Willamson, N.; McLean, C.; Barnham, K.L.; Hill, A.F. A rigorous method to enrich for exosomes from brain tissue. *J. Extracell. Vesicles* **2017**, *6*, 1348885. [CrossRef]

78. Brenna, S.; Altmeppen, H.C.; Mohammadi, B.; Rissiek, B.; Schlink, F.; Ludewig, P.; Krisp, C.; Schlüter, H.; Failla, A.V.; Schneider, C.; et al. Characterization of brain-derived extracellular vesicles reveals changes in cellular origin after stroke and enrichment of the prion protein with a potential role in cellular uptake. *J. Extracell. Vesicles* **2020**, *9*, 1809065. [CrossRef]

79. Jeppesen, D.K.; Fenix, A.M.; Franklin, J.L.; Higginbotham, J.N.; Zhang, Q.; Coffey, R.J. Reassessment of Exosome Composition. *Tumor Biology* **2019**, *177*, 428–445.e418. [CrossRef]

80. Gallart-Palau, X.; Serra, A.; Sze, S.K. Enrichment of extracellular vesicles from tissues of the central nervous system by PROSPR. *Mol. Neurodegener.* **2016**, *11*, 1–13. [CrossRef]

81. Huang, Y.; Cheng, L.; Turchinovich, A.; Mahairaki, V.; Troncoso, J.C.; Pletniková, O.; Haughey, N.J.; Vella, L.J.; Hill, A.F.; Zheng, L.; et al. Influence of species and processing parameters on recovery and content of brain tissue-derived extracellular vesicles. *J. Extracell. Vesicles* **2020**, *9*, 1785746. [CrossRef] [PubMed]

82. Asai, H.; Ikezu, S.; Tsunoda, S.; Medalla, M.; Luebke, J.; Haydar, T.; Wolozin, B.; Butovsky, O.; Kügler, S.; Ikezu, T. Depletion of microglia and inhibition of exosome synthesis halt tau propagation. *Nat. Neurosci.* **2015**, *18*, 1584–1593. [CrossRef] [PubMed]

83. Witwer, K.W.; Buzás, E.I.; Bemis, L.T.; Bora, A.; Lässer, C.; Lötvall, J.; Hoen, E.N.N.; Piper, M.G.; Sivaraman, S.; Skog, J.; et al. Standardization of sample collection, isolation and analysis methods in extracellular vesicle research. *J. Extracell. Vesicles* **2013**, *2*. [CrossRef] [PubMed]

84. Royo, F.; Théry, C.; Falcon-Perez, J.M.; Nieuwland, R.; Witwer, K.W. Methods for Separation and Characterization of Extracellular Vesicles: Results of a Worldwide Survey Performed by the ISEV Rigor and Standardization Subcommittee. *Cells* **2020**, *9*, 1955. [CrossRef] [PubMed]

85. Cocozza, F.; Grisard, E.; Martin-Jaular, L.; Mathieu, M.; Théry, C. SnapShot: Extracellular Vesicles. *Cell* **2020**, *182*, 262–262.e1. [CrossRef] [PubMed]

86. Brennan, K.; Martin, K.; FitzGerald, S.P.; O'Sullivan, J.; Wu, Y.; Blanco, A.; Richardson, C.; Mc Gee, M.M. A comparison of methods for the isolation and separation of extracellular vesicles from protein and lipid particles in human serum. *Sci. Rep.* **2020**, *10*, 1–13. [CrossRef] [PubMed]

87. Dash, M.; Palaniyandi, K.; Ramalingam, S.; Sahabudeen, S.; Raja, N. Exosomes isolated from two different cell lines using three different isolation techniques show variation in physical and molecular characteristics. *Biochim. Biophys. Acta BBA Biomembr.* **2021**, *1863*, 183490. [CrossRef]

88. Pérez-González, R.; Gauthier, S.A.; Kumar, A.; Saito, M.; Saito, M.; Levy, E. A Method for Isolation of Extracellular Vesicles and Characterization of Exosomes from Brain Extracellular Space. *Methods Mol. Biol.* **2017**, *1545*, 139–151. [CrossRef]

89. Polanco, J.C.; Li, C.; Durisic, N.; Sullivan, R.; Götz, J. Exosomes taken up by neurons hijack the endosomal pathway to spread to interconnected neurons. *Acta Neuropathol. Commun.* **2018**, *6*, 1–14. [CrossRef]

90. Dagur, R.S.; Liao, K.; Sil, S.; Niu, F.; Sun, Z.; Lyubchenko, Y.L.; Peeples, E.S.; Hu, G.; Bucha, S. Neuronal-derived extracellular vesicles are enriched in the brain and serum of HIV-1 transgenic rats. *J. Extracell. Vesicles* **2020**, *9*, 1703249. [CrossRef]

91. Gallart-Palau, X.; Serra, A.; Wong, A.S.; Sandin, S.; Lai, M.K.P.; Chen, C.P.; Kon, O.L.; Sze, S.K. Extracellular vesicles are rapidly purified from human plasma by PRotein Organic Solvent PRecipitation (PROSPR). *Sci. Rep.* **2015**, *5*, 14664. [CrossRef] [PubMed]

92. Ruf, J.; Vairo, D.; Paganelli, F.; Guieu, R. Extracellular vesicles with ubiquitinated adenosine A. *J. Cell. Mol. Med.* **2019**, *23*, 6805–6811. [CrossRef]

93. Silverman, J.M.; Christy, D.; Shyu, C.C.; Moon, K.-M.; Fernando, S.; Gidden, Z.; Cowan, C.M.; Ban, Y.; Stacey, R.G.; Grad, L.I.; et al. CNS-derived extracellular vesicles from superoxide dismutase 1 (SOD1). *J. Biol. Chem.* **2019**, *294*, 3744–3759. [CrossRef] [PubMed]

94. Kowal, J.; Arras, G.; Colombo, M.; Jouve, M.; Morath, J.P.; Primdal-Bengtson, B.; Dingli, F.; Loew, D.; Tkach, M.; Théry, C. Proteomic comparison defines novel markers to characterize heterogeneous populations of extracellular vesicle subtypes. *Proc. Natl. Acad. Sci. USA* **2016**, *113*, E968–E977. [CrossRef]

95. Yelamanchili, S.V.; Lamberty, B.G.; Rennard, D.A.; Morsey, B.M.; Hochfelder, C.G.; Meays, B.M.; Levy, E.; Fox, H.S. MiR-21 in Extracellular Vesicles Leads to Neurotoxicity via TLR7 Signaling in SIV Neurological Disease. *PLoS Pathog.* **2015**, *11*, e1005032.

96. Shahjin, F.; Guda, R.S.; Schaal, V.L.; Odegaard, K.; Clark, A.; Gowen, A.; Xiao, P.; Lisco, S.J.; Pendyala, G.; Yelamanchili, S.V. Brain-Derived Extracellular Vesicle microRNA Signatures Associated with In Utero and Postnatal Oxycodone Exposure. *Cells* **2019**, *9*, 21. [CrossRef]

97. Volovitz, I.; Shapira, N.; Ezer, H.; Gafni, A.; Lustgarten, M.; Alter, T.; Ben-Horin, I.; Barzilai, O.; Shahar, T.; Kanner, A.; et al. A non-aggressive, highly efficient, enzymatic method for dissociation of human brain-tumors and brain-tissues to viable single-cells. *BMC Neurosci.* **2016**, *17*, 1–10. [CrossRef] [PubMed]

98. Levy, E. Exosomes in the Diseased Brain: First Insights from. *Front. Neurosci.* **2017**, *11*, 142. [CrossRef]

99. Gallart-Palau, X.; Guo, X.; Serra, A.; Sze, S.K. Alzheimer's disease progression characterized by alterations in the molecular profiles and biogenesis of brain extracellular vesicles. *Alzheimer's Res. Ther.* **2020**, *12*, 54. [CrossRef]

100. Pérez-González, R.; Kim, Y.; Miller, C.; Pacheco-Quinto, J.; Eckman, E.A.; Levy, E. Extracellular vesicles: Where the amyloid precursor protein carboxyl-terminal fragments accumulate and amyloid-β oligomerizes. *FASEB J.* **2020**, *34*, 12922–12931. [CrossRef]

101. Gallart-Palau, X.; Serra, A.; Hase, Y.; Tan, C.F.; Chen, C.P.; Kalaria, R.N.; Sze, S.K. Brain-derived and circulating vesicle profiles indicate neurovascular unit dysfunction in early Alzheimer's disease. *Brain Pathol.* **2019**, *29*, 593–605. [CrossRef] [PubMed]

102. Papadopoulos, V.E.; Nikolopoulou, G.; Antoniadou, I.; Karachaliou, A.; Arianoglou, G.; Emmanouilidou, E.; Sardi, S.P.; Stefanis, L.; Vekrellis, K. Modulation of β-glucocerebrosidase increases α-synuclein secretion and exosome release in mouse models of Parkinson's disease. *Hum. Mol. Genet.* **2018**, *27*, 1696–1710. [CrossRef] [PubMed]

103. Ngolab, J.; Trinh, I.; Rockenstein, E.; Mante, M.; Florio, J.; Trejo, M.; Masliah, D.; Adame, A.; Masliah, E.; Rissman, R.A. Brain-derived exosomes from dementia with Lewy bodies propagate α-synuclein pathology. *Acta Neuropathol. Commun.* **2017**, *5*, 1–10. [CrossRef] [PubMed]

104. Vassileff, N.; Vella, L.J.; Rajapaksha, H.; Shambrook, M.; Kenari, A.N.; McLean, C.; Hill, A.F.; Cheng, L. Revealing the Proteome of Motor Cortex Derived Extracellular Vesicles Isolated from Amyotrophic Lateral Sclerosis Human Postmortem Tissues. *Cells* **2020**, *9*, 1709. [CrossRef] [PubMed]

105. Chand, S.; Jo, A.; Vellichirammal, N.N.; Gowen, A.; Guda, C.; Schaal, V.; Odegaard, K.; Lee, H.; Pendyala, G.; Yelamanchili, SV. Comprehensive Characterization of Nanosized Extracellular Vesicles from Central and Peripheral Organs: Implications for Preclinical and Clinical Applications. *ACS Appl. Nano Mater.* **2020**, *3*, 8906–8919. [CrossRef] [PubMed]

117

ARTICLE

CD73-mediated adenosine production by CD8 T cell-derived extracellular vesicles constitutes an intrinsic mechanism of immune suppression

Enja Schneider [1,15], Riekje Winzer [1,15✉], Anne Rissiek[1], Isabell Ricklefs[2,3], Catherine Meyer-Schwesinger[4], Franz L. Ricklefs [5], Andreas Bauche[6], Jochen Behrends [7], Rudolph Reimer[8], Santra Brenna [9], Hauke Wasielewski [1], Melchior Lauten [10], Björn Rissiek [9], Berta Puig [9], Filippo Cortesi [11,12], Tim Magnus [9], Ralf Fliegert[6], Christa E. Müller [13], Nicola Gagliani [11,12,14] & Eva Tolosa [1✉]

Immune cells at sites of inflammation are continuously activated by local antigens and cytokines, and regulatory mechanisms must be enacted to control inflammation. The stepwise hydrolysis of extracellular ATP by ectonucleotidases CD39 and CD73 generates adenosine, a potent immune suppressor. Here we report that human effector CD8 T cells contribute to adenosine production by releasing CD73-containing extracellular vesicles upon activation. These extracellular vesicles have AMPase activity, and the resulting adenosine mediates immune suppression independently of regulatory T cells. In addition, we show that extracellular vesicles isolated from the synovial fluid of patients with juvenile idiopathic arthritis contribute to T cell suppression in a CD73-dependent manner. Our results suggest that the generation of adenosine upon T cell activation is an intrinsic mechanism of human effector T cells that complements regulatory T cell-mediated suppression in the inflamed tissue. Finally, our data underscore the role of immune cell-derived extracellular vesicles in the control of immune responses.

[1] Department of Immunology, University Medical Center Hamburg-Eppendorf, 20246 Hamburg, Germany. [2] Division of Pediatric Pneumology & Allergology, University Medical Center Schleswig-Holstein, 23538 Lübeck, Germany. [3] Airway Research Center North, Member of the German Center for Lung Research, Lübeck, Germany. [4] Department of Cellular and Integrative Physiology, University Medical Center Hamburg-Eppendorf, 20246 Hamburg, Germany. [5] Department of Neurosurgery, University Medical Center Hamburg-Eppendorf, 20246 Hamburg, Germany. [6] Department of Biochemistry and Molecular Cell Biology, University Medical Center Hamburg-Eppendorf, 20246 Hamburg, Germany. [7] Core Facility Fluorescence Cytometry, Research Center Borstel, 23845 Borstel, Germany. [8] Technology Platform Microscopy and Image Analysis, Heinrich Pette Institute/Leibniz Institute for Experimental Virology, 20251 Hamburg, Germany. [9] Department of Neurology, University Medical Center Hamburg-Eppendorf, 20246 Hamburg, Germany. [10] Department of Pediatrics and Adolescent Medicine, University of Lübeck, 23538 Lübeck, Germany. [11] I. Department of Medicine, University Medical Center Hamburg-Eppendorf, 20246 Hamburg, Germany. [12] Department of General, Visceral and Thoracic Surgery, University Medical Center Hamburg-Eppendorf, 20246 Hamburg, Germany. [13] Department of Pharmaceutical & Medicinal Chemistry, University of Bonn, 53121 Bonn, Germany. [14] Immunology and Allergy Unit, Department of Medicine, Solna, Karolinska Institute and University Hospital, Stockholm, Sweden. [15] These authors contributed equally: Enja Schneider, Riekje Winzer. ✉email: r.winzer@uke.de; etolosa@uke.de

Immune cell activation, cellular stress, or metabolic changes during inflammation favor the release of ATP into the extracellular space. High extracellular ATP is a danger signal for immune cells and is swiftly metabolized by ATP-degrading enzymes. Among them, the ectonucleotidase CD39 dephosphorylates ATP and ADP to AMP, which is subsequently converted to adenosine by Ecto-5′-nucleotidase (CD73)[1]. The amount of available extracellular adenosine is further determined by the rate of adenosine deaminase (ADA)-mediated degradation, and by cellular uptake through nucleoside transporters. Activation of the adenosine receptor subtype A$_{2A}$, the predominantly expressed adenosine receptor in T cells (ImmGen database consortium[2]), results in a rise of intracellular cAMP, leading to decreased T cell activation and effector function[3,4].

Increased adenosine signaling limits mucosal inflammation[5] and improves disease in several animal models of autoimmunity[6,7]. Deletion of the A$_{2A}$ receptor enhances gastritis in *Helicobacter*-infected mice[8] and exacerbates inflammation in the early stages of experimental autoimmune encephalomyelitis[9]. In humans, high ADA activity has been documented in the serum of patients with autoimmune diseases[7,10]. Consequently, the adenosine-generating enzyme CD73 plays a protective role in the animal models of arthritis[11] and colitis[12].

The control of immune responses is crucial to prevent inflammation-induced damage to healthy tissue. FOXP3+ regulatory T cells (Tregs) are essential to maintain peripheral tolerance to self-antigens and play a pivotal role in terminating an immune response by inhibiting T cell proliferation and effector function. Tregs use an array of suppressive mechanisms to restore immune homeostasis, including the production of anti-inflammatory cytokines, engagement of co-inhibitory receptors, and the modulation of effector T cell metabolism[13]. Murine Tregs express CD39 and high levels of CD73 on the cell surface to degrade ATP and produce adenosine, which in turn has a dual effect; inhibiting effector T cells[14] and enhancing the suppressive capacity of Tregs[15]. In the human T cell compartment, however, CD73 is expressed on the surface of most naïve CD8 T cells and in a small proportion of mature CD4 and CD8 memory T cells, but it is almost absent on Tregs[16–18]. Therefore, co-expression of CD73 with CD39 on Tregs is a rare event[17,19], challenging the concept of adenosine generation as a suppression mechanism used by Tregs in humans. While several studies demonstrate the importance of CD39 expression on human Tregs for their suppressive capacity[17,20,21], the evidence for an essential role of CD73 on Tregs is controversial[22–24].

Considering the low expression of CD73 on human Tregs, the question arises of how immunosuppressive adenosine is generated in the human system under conditions of inflammation. Our data reveal that CD73 contained in extracellular vesicles (EVs) derived from activated CD8 T cells is sufficient to degrade AMP and dampen T cell proliferation and function. This T cell-intrinsic mechanism, in concerted action with a high ATPase activity of Tregs, mediates the production of adenosine from ATP, and warrants sufficient immune suppression. Moreover, we find that EVs isolated from the synovial fluid (SF) of patients with juvenile idiopathic arthritis (JIA) induce T cell suppression in a CD73-dependent manner, underscoring the relevance of CD73 on EVs in the control of inflammation.

Results

Human regulatory T cells do not generate sufficient adenosine to suppress T cell proliferation and function. The concentration of pericellular ATP increases upon T cell activation[25] and ATP is quickly metabolized to adenosine by the ectonucleotidases CD39 and CD73. Activation of A$_2$ receptors on immune cells increases intracellular cAMP levels, resulting in decreased T cell activation, and effector function[4] (Fig. 1a). To assess the effect of adenosine receptor activation in human primary T cells, we first added EHNA, an inhibitor of ADA that prevents the degradation of adenosine. In the presence of EHNA, we observed a 20% reduction in T cell proliferation compared to the untreated control (Fig. 1b). Similarly, the metabolically stable, nonselective adenosine analogs 5′-N-ethylcarboxamidoadenosine (NECA) and 2-chloroadenosine (CADO) led to a concentration-dependent decrease in activation (measured as a percentage of CD25+ cells out of CD4 T cells) and proliferation (Fig. 1c, d), demonstrating the suppressive effect of adenosine receptor activation on human T cells.

Adenosine is generated from ATP by the concerted action of CD39 and CD73, and co-expression of these ectonucleotidases is a hallmark of murine Foxp3+ Tregs and allows them to generate immunosuppressive adenosine[14]. Even though this pathway is widely accepted to be valid also in the human system, gene expression data from the Human Protein Atlas[26,27] and the ImmGen project[2,28] show that the expression of NT5E, the gene encoding CD73, is divergent in different immune cell compartments of the two species. According to gene expression data, all murine T cell subpopulations express Nt5e, while in the human peripheral T cell compartment CD8 T cells have a high NT5E expression and the expression in Tregs is much lower. Our data confirm that nearly all peripheral Tregs in mice express high levels of CD73 on the cell surface, and two-thirds of the cells co-express CD39 (Supplementary Fig. 1), fulfilling the enzymatic requirements for adenosine generation. To systematically explore CD39 and CD73 expression on human peripheral T cells, we measured cell surface expression of these two ectonucleotidases by flow cytometry (Fig. 1e, f). We found that only a minimal frequency of human peripheral Tregs express CD73 (average of 3%, ranging from 0.8 to 6%, Fig. 1f). CD39 is expressed on 10 to 70% of Tregs, depending on the genotype of the donor[17,29], and on around 5% of nonactivated conventional CD4 (CD4con, defined as non-Treg CD4 T cells) and CD8 T cells. CD73, in contrast, is expressed on ~20 to 60% of the CD8 T cells, and on less than 20% of CD4con T cells. Given the low frequency of Tregs expressing CD73, co-expression of both ectoenzymes is a rare event even in donors with high CD39 expression (Fig. 1e, f), questioning the relevance of Treg-derived adenosine for immune suppression in the human system. To address this point experimentally, we performed an in vitro suppression assay using different ratios of CD4con T cells:Treg (Fig. 1g), considering that the physiological proportion of Tregs is around 10% of CD4 T cells[30]. As responder cells, we used sorted CD73− CD4con T cells to prevent the production of adenosine by CD73+ cells other than Tregs (Supplementary Fig. 2). In these specific conditions, we did not observe an effect of Tregs on suppression at any ratio. When we added ATP to mimic the inflammatory milieu, we observed maximal suppression of T cell activation, proliferation, and IFNγ production at a high Treg ratio (1:0.5 CD4con T cells to Tregs, fivefold the physiological concentration). The addition of recombinant CD73 had no further suppressive effect, indicating that there was enough CD73 in the system (in this donor in particular 2% of Tregs were CD73+) to produce adenosine. At a low Treg ratio (1:0.125 CD4con T cells to Tregs, similar to physiological conditions), Tregs could only induce partial suppression in the presence of ATP. In combination with recombinant CD73, though, expression of CD25 was reduced to the minimum, and proliferation and IFNγ production were completely abolished (Fig. 1g). These data indicate that at a physiological CD4con:Treg ratio, there is not enough Treg-derived AMPase activity to generate adenosine that mediates significant suppression.
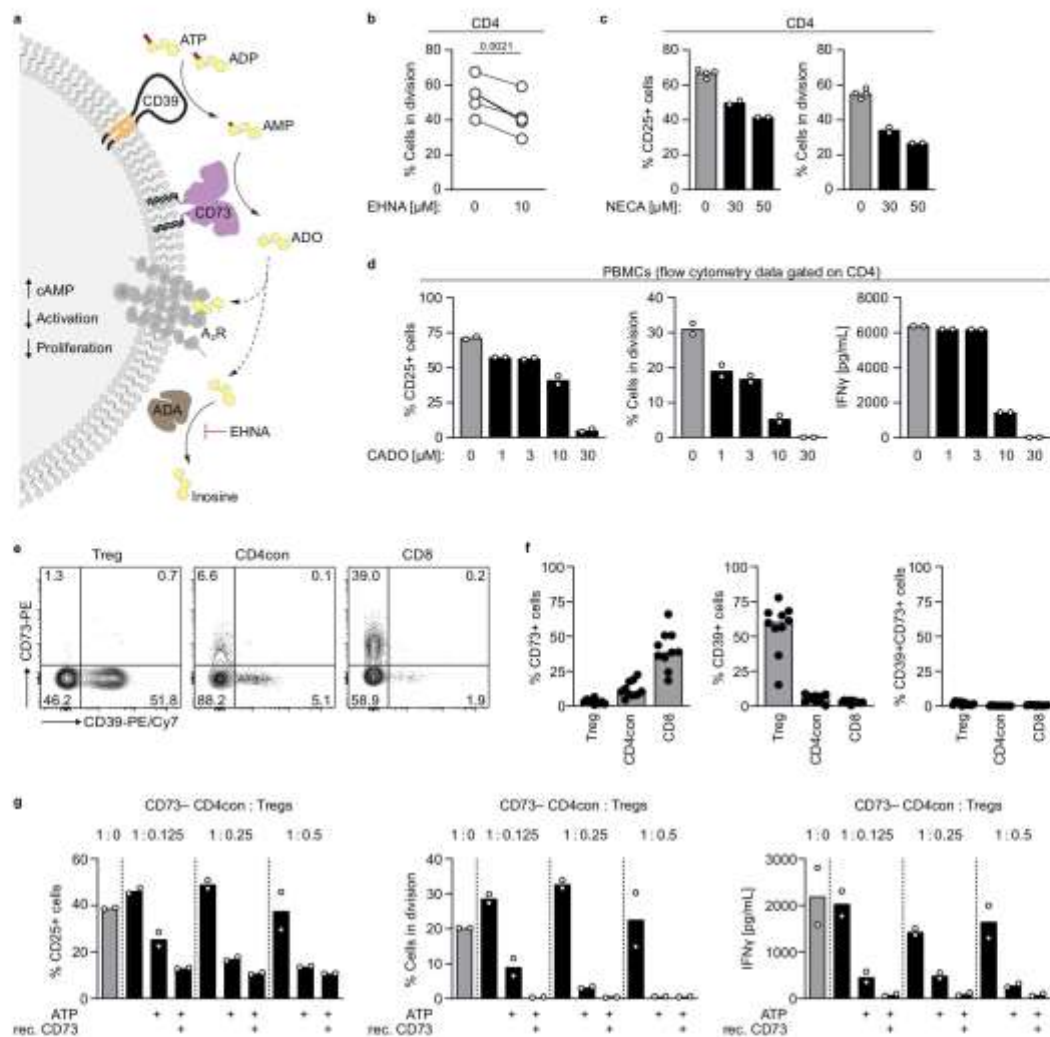
Fig. 1 Adenosine generated in the course of T cell activation prevents an exacerbated T cell response. a Schematic representation for the degradation of ATP to adenosine by the ectonucleotidases CD39 and CD73. **b–d** PBMCs or CD4 T cells were stimulated with αCD3/αCD28 and treated with **b** the ADA inhibitor EHNA or different concentrations of adenosine receptor agonists **c** NECA, and **d** CADO. CD25 expression and proliferation were measured after 3 to 4 days by flow cytometry. Data were shown for **b** five donors or **c**, **d** one representative donor (mean of technical replicates). **e**, **f** CD73 and CD39 expression on human T cell subsets in **e** representative dot plots and **f** as a summary for ten donors (median). **g** CD73⁻ CD4con T cells were stimulated with αCD3/αCD28 in the presence of the ADA inhibitor EHNA (10 μM) and incubated with Tregs, ATP (50 μM) and recombinant CD73 (15 ng/mL) as indicated. The ratios of CD4con T cells to Tregs were 1:0.125 to 1:0.5. CD25 expression and proliferation were measured after 4 days by flow cytometry. IFNγ production was determined by ELISA in the cell culture supernatant on day 4. Data were shown for one representative donor out of four analyzed (mean of technical duplicates). A two-tailed paired t-test was used to compare untreated and treated samples in **b**.

CD73-mediated AMPase activity by Tregs is dispensable for the control of CD4 T cell proliferation and function. In humans, CD73 expression is less frequent in Tregs than in CD4con and CD8 T cells (Fig. 1f). We hypothesized that AMPase activity derived from nonregulatory T cells contributes to adenosine production and immune suppression. To test this, we stimulated CD4con T cells and added Tregs at different ratios. As expected, the addition of Tregs at a very high CD4con:Treg ratio (1:2) resulted in a decrease of T cell activation, and proliferation by 30 to 50%, respectively. We observed a dramatic reduction when exogenous AMP was added to the cell culture to ensure an equal amount of substrate for CD73 in all conditions. Importantly, this effect was independent of the Treg-derived AMPase activity (Fig. 2a). We reasoned that the likely source of AMPase activity in our system could be CD73 from the responder T cells themselves. To test this, we sorted CD4con T cells into CD73⁻

and CD73⁺ and stimulated them in the presence of AMP, but without Tregs (Fig. 2b). As predicted, CD73⁺-sorted cells were less activated and proliferated at lower levels after incubation with AMP, and this effect was reversed by adding the specific CD73 inhibitor PSB-14685. Importantly, the addition of AMP to CD73⁻-sorted CD4con T cells did not have any suppressive effect on activation or proliferation (Fig. 2b), indicating that CD73 on the responder T cells is necessary for the production of adenosine. Addition of recombinant CD73 to AMP-treated CD73⁻ CD4con T cells reestablished the suppressive effect, demonstrating that exogenous CD73 functionally compensates the lack of CD73 in the responder cells (Fig. 2c). Of note, recombinant CD73 was able to induce T cell suppression of CD73⁻ CD4con T cells at a concentration as low as 0.15 ng/mL of the enzyme when the substrate AMP was provided (Fig. 2d). IFNγ production followed the same pattern as CD25 expression and proliferation in the

120
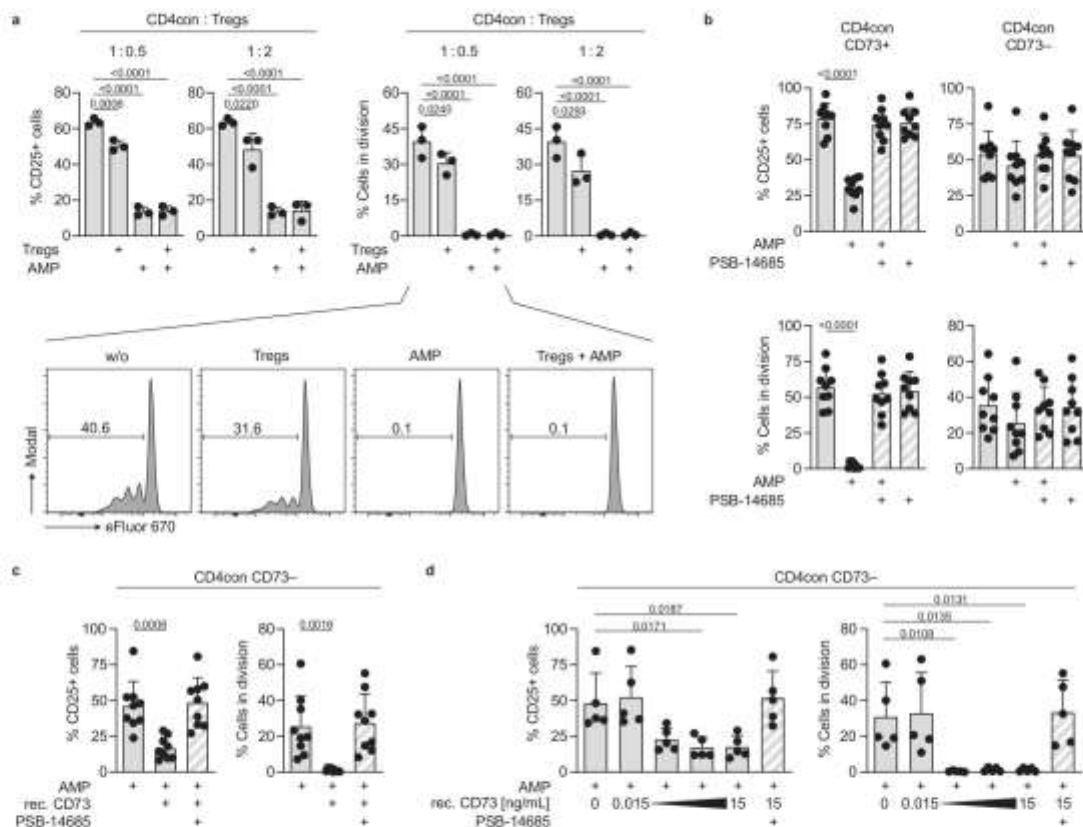
Fig. 2 Treg-derived CD73 is not essential for adenosine-mediated suppression of conventional CD4 T cells. a–d CD4 responder T cells were stimulated with αCD3/αCD28 in the presence of the ADA inhibitor EHNA (10 μM). CD25 expression and proliferation were measured after 4 days by flow cytometry. **a** CD4con T cells were stimulated and incubated with AMP (50 μM) and Tregs in the indicated ratio. **b** CD4con T cells were sorted into CD73− and CD73+, the cells were incubated with AMP (50 μM) and the specific CD73 inhibitor PSB-14685 (10 μM). **c** CD4con CD73− T cells were incubated with AMP (50 μM), the specific CD73 inhibitor PSB-14685 (10 μM), and recombinant CD73 (15 ng/mL). **d** CD4con CD73− T cells were incubated with AMP (50 μM) and different concentrations of soluble recombinant CD73 (three tenfold serial dilutions starting with 15 ng/mL). PSB-14685 was used to block the highest concentration of recombinant CD73. Data were shown for **a** three, **b**, **c** nine and **d** five donors (mean ± SD). Ordinary one-way ANOVA with Dunnett's multiple comparisons test was used to compare all conditions to cells treated with EHNA or EHNA and AMP (first bar).

experiments shown in Fig. 2a–d (Supplementary Fig. 3a–d). We conclude that CD73-mediated production of adenosine constitutes an intrinsic mechanism of conventional T cells to control ongoing activation.

Enzymatically active CD73 is released from the T cell membrane upon activation. In human peripheral blood (PB) T cells, CD73 is predominantly expressed on CD8 T cells (Fig. 1f), and we have previously shown that activated T cells lose the membrane expression of CD73[31]. We hypothesized that the CD73 released from activated cells plays a role in adenosine generation. To address this point, we first investigated the time point of release in peripheral blood mononuclear cells (PBMCs) during activation. We observed a peak of CD73 expression on CD8 T cells 1 day after stimulation, followed by a marked decrease 2 or 3 days after stimulation (Fig. 3a). The loss of CD73 from the cell membrane was also detected in CD4 T cells. CD39 was upregulated in both T cell populations. Even though the loss of CD73 from the cell membrane was a general phenomenon, we observed interindividual variability both in the timing and extend of CD73 loss, and also in the level of CD39 upregulation.

Next, we investigated the fate of the released form of CD73. CD73 is a GPI-anchored protein that can be found as an enzymatically active soluble form, and CD73-specific AMPase activity is present in human plasma[32,33]. We implemented a sensitive, HPLC-based assay

with improved signal-to-noise sensitivity using fluorescent 1,N⁶-etheno-AMP (eAMP) as a substrate to measure AMPase activity in cells and cell culture supernatants (Fig. 3b). As a proof of principle, we forced shedding of cell surface CD73 on CD8 T cells using phosphatidylinositol-specific phospholipase C (PI-PLC) (Fig. 3c, left) and observed lower AMPase activity of the PI-PLC-treated cells compared to untreated cells (Fig. 3c, middle). In contrast, the supernatants from PI-PLC treated cells converted more eAMP to 1,N⁶-etheno-adenosine (eADO), in line with a higher amount of CD73 present in the supernatant (Fig. 3c, right). The CD73-specific inhibitor PSB-14685 completely blocked eAMP degradation, verifying the specificity of the AMPase activity. Activated T cells that had lost CD73 expression (Fig. 3d, left), showed lower AMPase activity than unstimulated cells (Fig. 3d, middle). This decrease in activity in the cell-bound compartment was paralleled by increased generation of eADO in the cell culture supernatant of activated cells and accompanied by an increase in the concentration of soluble CD73 detected by ELISA (Fig. 3d, right). These data demonstrate that CD73 is released in the cell culture supernatant upon T cell activation and retains its enzymatic activity.

EVs are the major source of AMPase activity in CD8 T cell culture supernatants and mediate suppression of responder T cells. We next sought to decipher the mechanism of CD73 release from the membrane. We first considered enzyme-
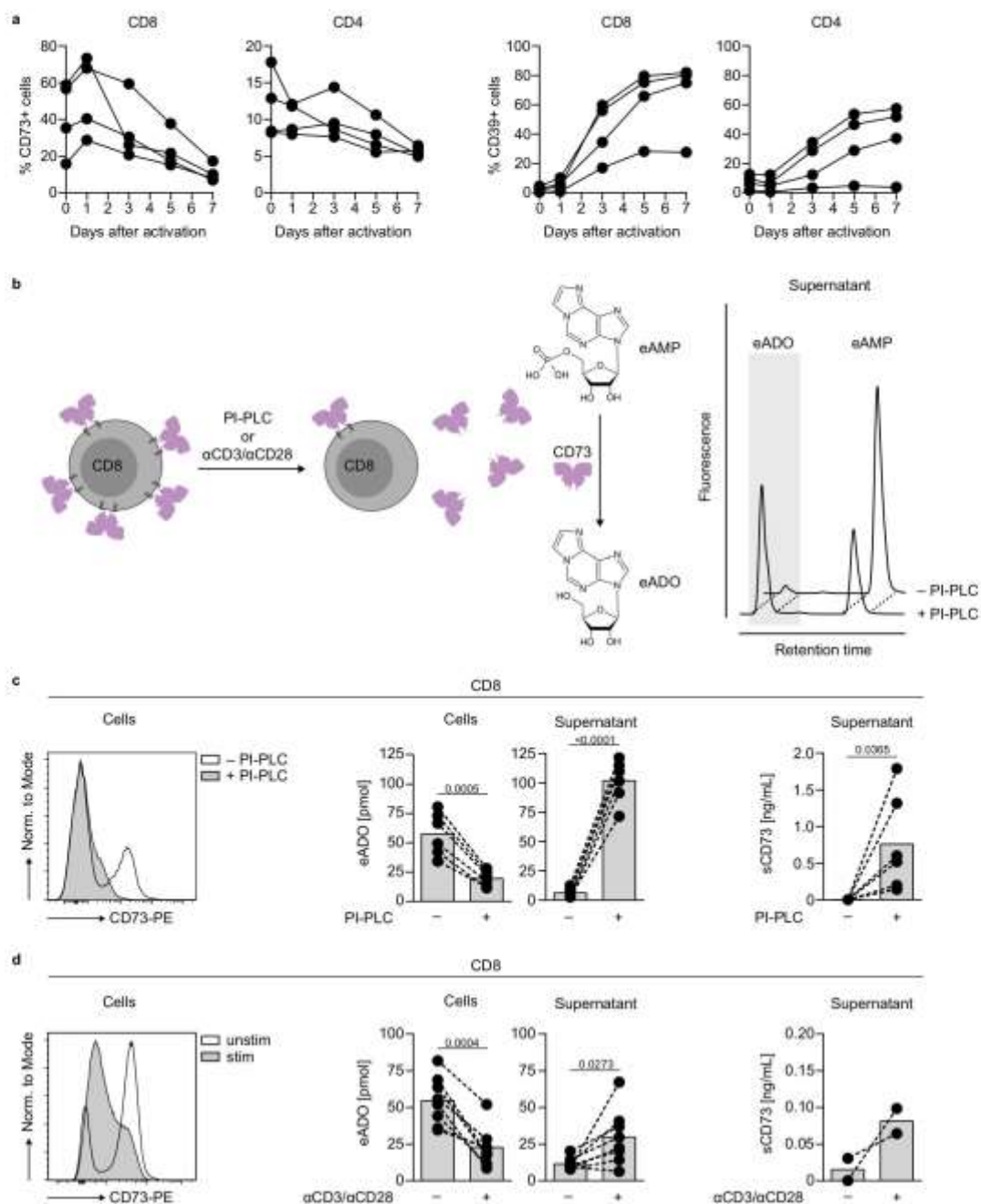
Fig. 3 CD8 T cells release enzymatically active CD73 upon activation. a Flow cytometric analysis of CD73 and CD39 expression on CD8 and CD4 T cells after activation of PBMCs (measurement on five time points from day 0 to day 7). Data were shown for four donors. **b** Schematic representation of CD73 released from CD8 T cells after PI-PLC treatment or activation. AMPase activity is measured by the conversion of 1,N^6-etheno-AMP (eAMP) to 1,N^6-etheno-ADO (eADO). **c, d** Determination of the AMPase activity of CD8 T cells and supernatants. 0.2×10^6 CD8 T cells were treated with **c** PI-PLC (0.5 U/mL) or **d** stimulated with αCD3/αCD28 for 4 days. Histograms show CD73 expression of the cells at the time of eAMP incubation for one selected donor. The cells and supernatants were incubated with eAMP and degradation of eAMP to eADO was determined by HPLC (middle panel, mean of **c** six donors and **d** eight donors). The amount of soluble CD73 (sCD73) was measured by ELISA (right panel, mean of **c** six donors and **d** two donors). A two-tailed paired t-test was used to compare untreated and treated samples in **c, d**.

mediated shedding; however, neither specific inhibition of phospholipase D nor inhibition of metalloproteinases prevented loss of CD73 from the cell surface (Supplementary Fig. 4). CD73 is enriched in lipid rafts of T cells after activation, suggesting that the release might occur in form of vesicles, as it has been described in tumor cells[34]. Using differential centrifugation of cell culture supernatants, we observed a stepwise reduction in the

AMPase activity in the supernatants of stimulated CD8 T cells after $10,000 \times g$ (large vesicles and apoptotic bodies are pelleted) and $110,000 \times g$ centrifugation (small vesicles are pelleted), indicating that CD73 is, indeed, present on vesicles (Fig. 4a). To verify the specificity of the CD73-mediated enzymatic activity on these vesicles, supernatants from activated CD73$^-$ and CD73$^+$-sorted CD8 T cells were subjected to differential centrifugation and
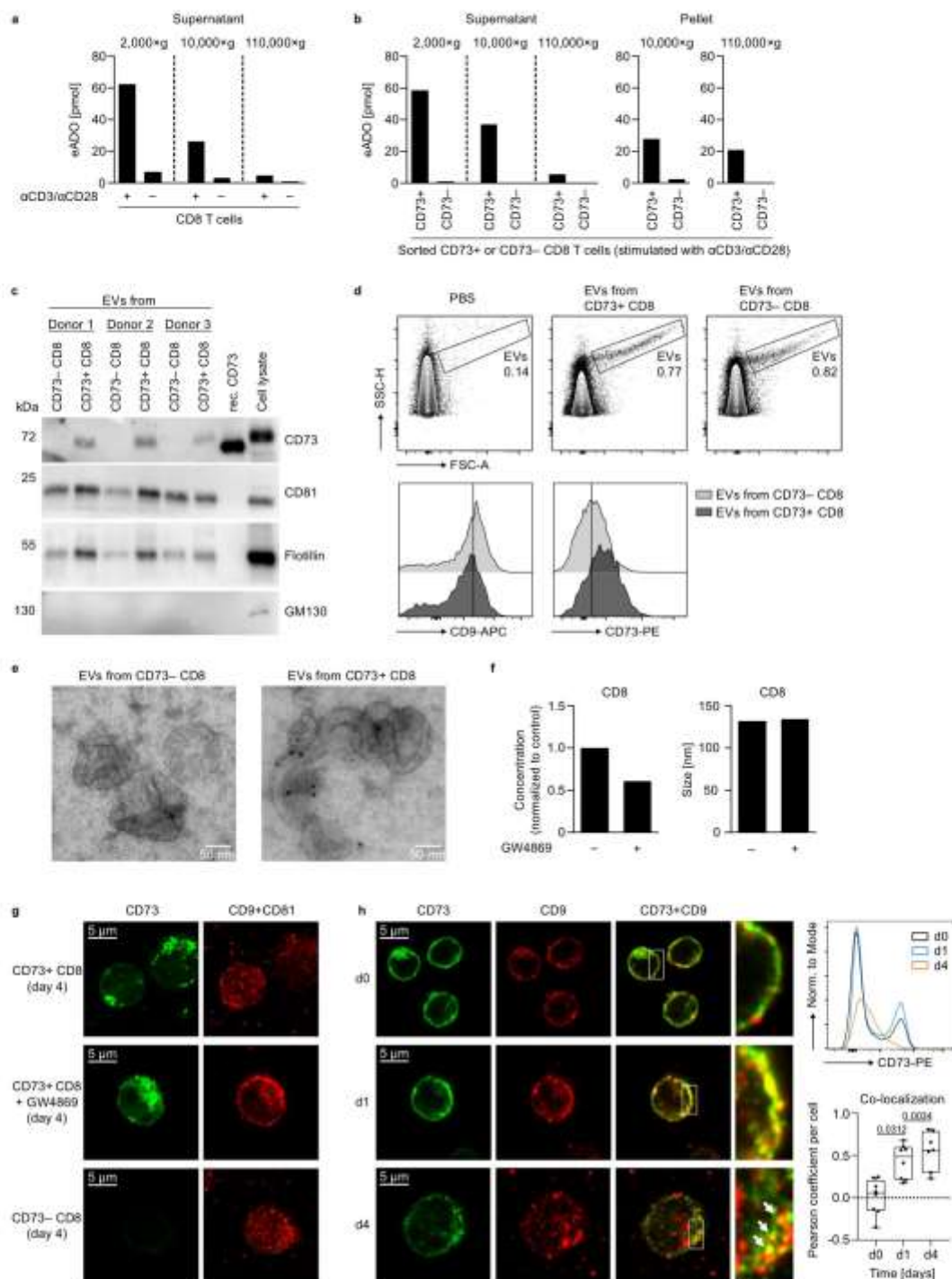
AMPase activity was measured in the obtained fractions. The cell culture supernatants of CD73$^+$ CD8 T cells displayed AMPase activity after 2000 × g centrifugation (removal of cell debris), but ultracentrifugation heavily reduced eADO generation. Remarkably, the EV-enriched pellets derived from 110,000×g centrifugation (hereinafter named EVs) showed substantial AMPase activity (Fig. 4b). Supernatants from CD73$^-$ CD8 T cells did not have AMPase activity, demonstrating the specificity of CD73 for the enzymatic degradation of AMP in these samples.

Nanoparticle tracking analysis (NTA) of CD8 T cell EVs revealed a size of around 100 nm for the majority of the isolated

CD8 T cell vesicles (Supplementary Fig. 5). The presence of EV markers CD81 and flotillin, as well as the absence of the Golgi protein GM130 confirmed the EV nature and purity of our samples. In addition, CD73 protein was detected in EVs derived from CD73$^+$ CD8 T cells, but not in those from CD73$^-$ CD8 T cells (Fig. 4c). Even though the small size of the EVs limits precise analysis by conventional flow cytometry, particles gated by forward vs. side scatter showed increased staining intensity of CD73 in vesicles derived from CD73$^+$ CD8 T cells compared to those derived from CD73$^-$ CD8 T cells, while expression of tetraspanin CD9 was comparable (Fig. 4d). Electron microscopy

Fig. 4 Extracellular vesicles are the major source of AMPase activity in human CD8 T cell culture supernatants. a, b CD8 T cells were stimulated with αCD3/αCD28 and kept in culture for 4 days. Analysis of AMPase activity in **a** cell culture supernatants of stimulated or unstimulated total CD8 T cells and **b** supernatants and EVs of sorted CD8 CD73+ or CD8 CD73− T cells after differential centrifugation. The conversion of eAMP to eADO was measured by HPLC. **c–e** Analysis of CD73 and EV markers on EVs derived from stimulated cell culture supernatants of CD73+ or CD73− CD8 T cells by **c** western blot, **d** flow cytometry, and **e** electron microscopy with immunogold labeling. Recombinant CD73 or cell lysate from stimulated CD8 T cells served as positive controls. **f** EVs were isolated from CD8 T cells stimulated with αCD3/αCD28 for 3 days in the presence or absence of GW4869 (10 μM), and particle concentration and size were measured by NTA. **g** Microscopy analysis of CD73, CD9, and CD81 expression in sorted CD73+ or CD73− CD8 T cells after 4 days of stimulation with αCD3/αCD28. GW4869 (10 μM) was added at day 0. **h** Microscopy analysis of CD73 and CD9 expression in CD8 T cells before and after activation. Pearson coefficient was determined to quantify the co-localization of CD73 and CD9. Data were analyzed from seven (d4) or eight (d0, d1) high power fields (center line: median, box limits: 25th to 75th percentiles, whiskers: min to max). Donors analyzed: **a, b** three donors in three independent experiments; **c** six donors in three independent experiments; **d–f** three donors; **g, h** samples from three donors processed independently. Each figure panel shows a representative donor/experiment. Kruskal–Wallis test with Dunn's multiple comparisons test was used to compare Pearson coefficients of co-localization in **h**.

of the purified vesicles revealed the characteristic cup-shaped morphology with sizes between 50 to 200 nm. Immunogold labeling further confirmed the presence of CD73 in EVs derived from CD73+ CD8 T cells (Fig. 4e). To investigate the vesicular release of CD73, we treated T cells with GW4869, a pharmacological compound that blocks the generation of a specific type of EVs called exosomes[35]. The addition of GW4869 to the cell culture reduced the amount of generated EVs whereas the size was not affected (Fig. 4f). It also prevented the loss of tetraspanins CD9 and CD81 from the cell (Fig. 4g). High-resolution fluorescence microscopy of CD8 T cells showed the reduction of CD73 surface expression after 4 days of stimulation (Fig. 4h) consistent with the results obtained by flow cytometry (Fig. 4h upper right panel and Fig. 3a). Overlay of CD73 with tetraspanins CD9 and CD81 revealed significant co-localization of CD73 with vesicle markers at day 1 and day 4 after activation (Fig. 4h lower right panel and Supplementary Fig. 6). Altogether, these data show that CD73 is released with EVs upon T cell activation and that these EVs comprise the majority of AMPase activity in T cell culture supernatants.

We wondered if CD73-containing EVs isolated from T cell culture supernatants functionally compensate the lack of membrane-bound CD73 in the control of T cell activation and proliferation as we have shown for recombinant CD73 (Fig. 2c). To test if EVs, a natural source of non-cell-bound CD73, can suppress T cell function, we activated CD73− CD4con T cells (to prevent any effect of residual membrane-bound CD73 on the responder T cells) in the presence of AMP. Addition of recombinant CD73 or EVs isolated from the supernatant of CD73+ CD8 T cells induced strong suppression, which was dose-dependent and could be blocked by the CD73 inhibitor PSB-14685 (Fig. 5a, b and Supplementary Fig. 7). Importantly, EVs isolated from the supernatant of CD73− CD8 T cells did not suppress activation and proliferation of the responder T cells, and neither did the pelleted material after ultracentrifugation of cell culture medium (Fig. 5 and Supplementary Fig. 8), indicating that the observed suppressive effect is CD73-specific and not due to contaminants in the EV preparation. In summary, we show that enzymatically active CD73 is released from activated CD8 T cells with EVs, and that EVs derived from activated CD73+ T cells are highly suppressive.

T cell-derived EVs released during immune cell activation cooperate with regulatory T cells for the efficient suppression of effector T cells. In our previous experiments, we exogenously provided AMP, the substrate for CD73. AMP is generated from ATP by the enzymatic activity of CD39. In contrast to conventional T cells, a substantial proportion of Tregs constitutively express CD39 in humans (Fig. 1f). Therefore, Tregs are likely to be superior at degrading ATP than conventional T cells. We used

the sensitive HPLC-based assay to compare the ATPase activity of purified Tregs, CD4con, and CD8 T cells after activation. Using 1,N6-etheno-ATP (eATP) as substrate, we found that Tregs had the highest ATPase activity of all tested T cell subsets (Fig. 6a), and this was more pronounced in donors with substantial basal CD39 expression on Tregs (Fig. 6a, left panel) than in donors with low frequency of CD39-expressing Tregs (Fig. 6a, right panel). Notably, CD8 T cells were the second most efficient cell type in degrading ATP, while CD4con T cells showed the least ATPase activity, in agreement with the percentage of cells upregulating CD39 after activation (Fig. 3a).

We suspected that the high ATPase activity of Tregs combines with CD73-containing EVs to mediate maximum immune suppression. We performed a suppression assay, using CD73− CD4con T cells as responder T cells, and added different ratios of Tregs. With a ratio of CD4con T cells to Tregs close to the physiological situation (1:0.125), Tregs could only induce partial suppression. The addition of EVs from CD73+ CD8 T cells, a natural source of non-cell-bound CD73, reduced CD25 expression, and completely suppressed proliferation and IFNy production of effector T cells (Fig. 6b). Importantly, EVs derived from CD73− CD8 T cells had no additional effect on the suppression of responder T cells, revealing that they do not cooperate with Tregs to generate immunosuppressive adenosine. We conclude that Tregs are the main providers of ATPase activity in our system, and the concerted action between Treg-derived ATPase activity and effector cell-derived AMPase activity in form of EVs ensures the best conditions for immune suppression.

EVs isolated from the synovial fluid of patients with juvenile idiopathic arthritis are immunosuppressive. An interesting question to address is the relevance of non-cell-bound CD73 in the context of inflammation. The SF of patients with autoimmune arthritis offers an ideal chance to analyze an inflammatory compartment in the human system because we can access disease-relevant infiltrating immune cells. Flow cytometric analyses of the cellular composition of the SF from eight children with JIA (Fig. 7a) revealed that T cells constitute the main cell population, and that CD8 T cells are enriched in the SF compared to PB in most cases. B cells, the only other prominent CD73-expressing cell type in the human immune compartment[2,28], are clearly underrepresented in the SF compared to PB in all patients. We next compared the expression of CD73 and CD39 on the T cells from PB and SF (Fig. 7b). In agreement with published data[36,37], we found increased expression of CD39 on CD4 T cells and Tregs and decreased CD73 expression on CD8 T cells in the synovial T cell subsets compared to their peripheral counterparts. In analogy to our in vitro findings after activation, we suspected that CD73 has been lost from the cell membrane. Indeed, we detected moderate to high concentrations of soluble CD73 in the
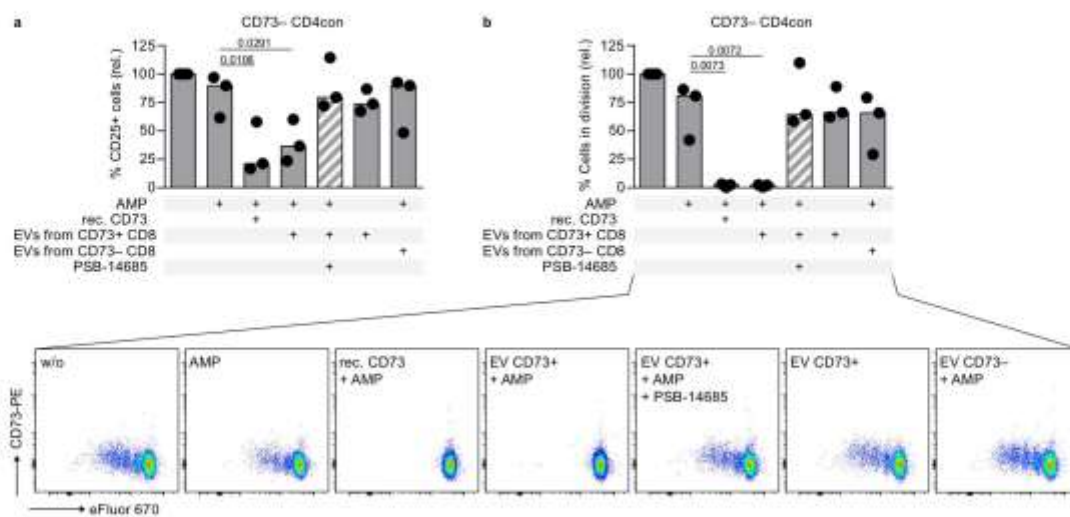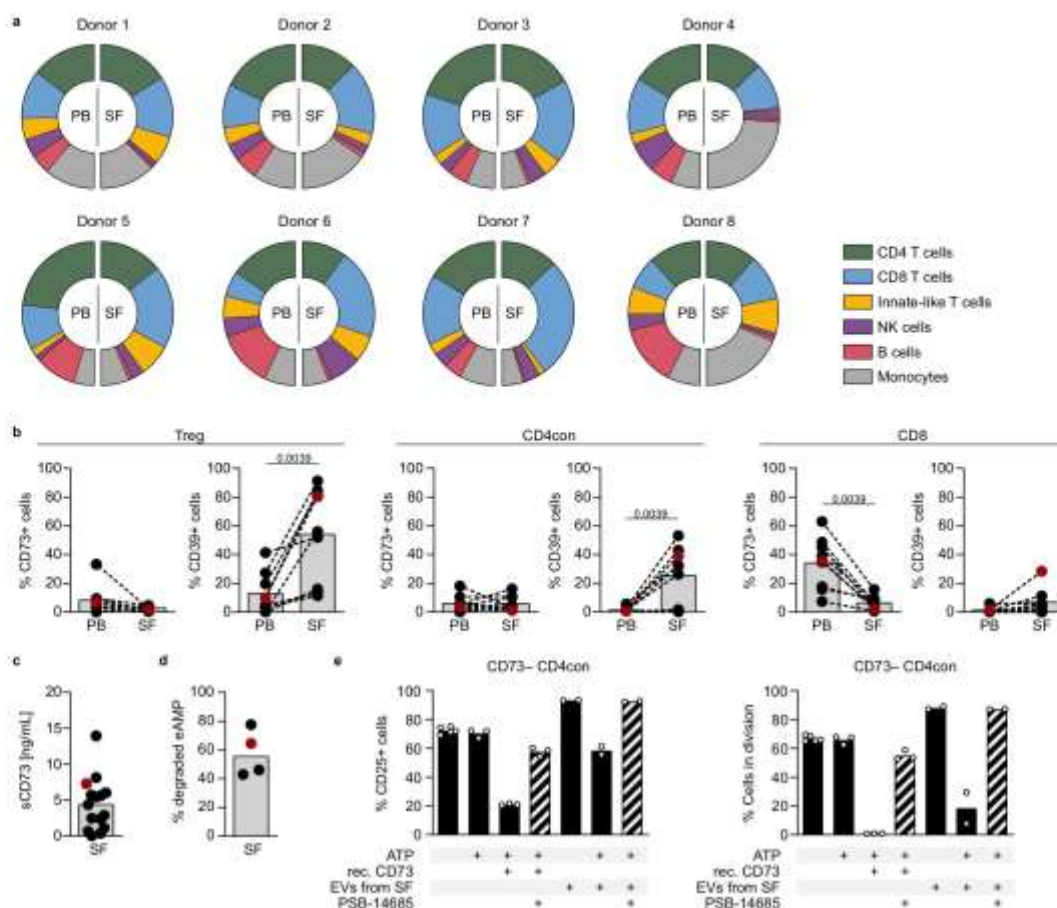
Fig. 5 Extracellular vesicles isolated from the cell culture supernatant of activated CD73$^+$ CD8 T cells are immunosuppressive. CD73$^-$ CD4con T cells were stimulated with αCD3/αCD28 in the presence of the ADA inhibitor EHNA (10 µM) and incubated with AMP (50 µM), recombinant CD73 (15 ng/mL), EVs and PSB-14685 (10 µM) as indicated. **a** CD25 expression and **b** proliferation were measured after 4 days by flow cytometry. Data were shown as a median of three donors from independent experiments. For each donor, CD25 expression and proliferation were set in relation to cells only treated with EHNA. Repeated measures one-way ANOVA with Dunnett's multiple comparisons test was used to compare all conditions to cells treated with EHNA and AMP (second bar).
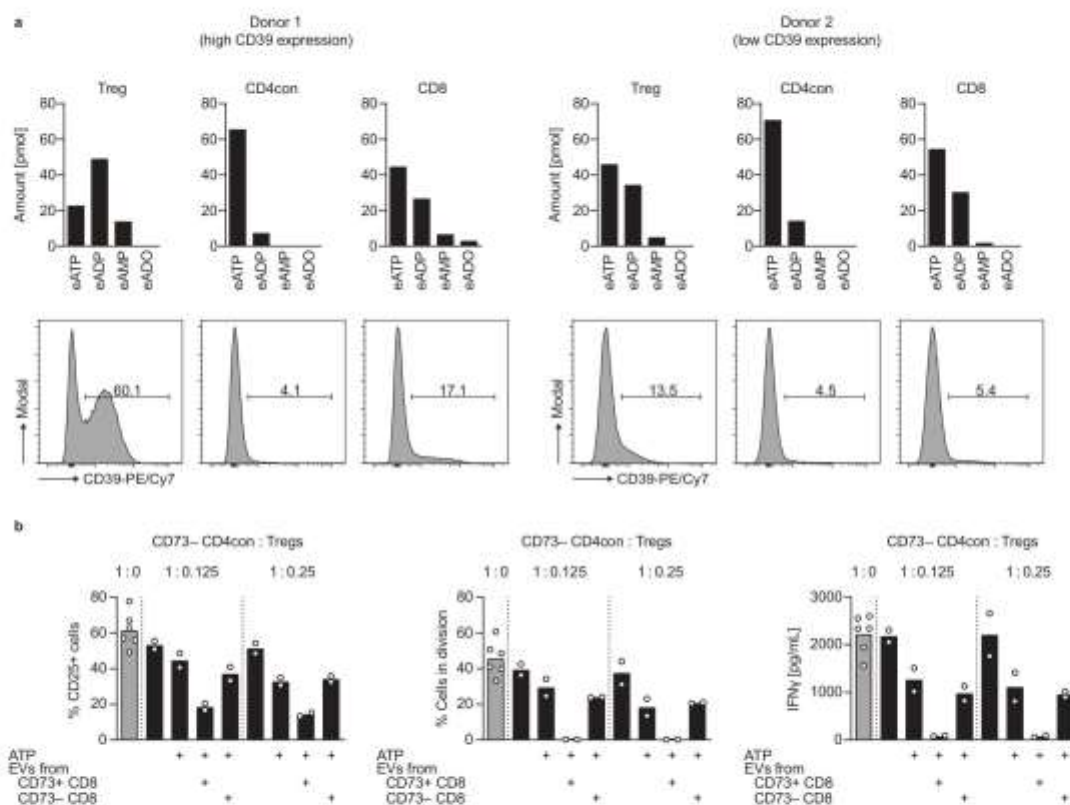
Fig. 6 The combined activities of Treg-derived CD39 and vesicular CD73 result in optimal suppression of T cell function. a Analysis of ATPase activity in sorted T cell subsets of two donors by HPLC. Activated cells (αCD3/αCD28, 3 days) were incubated with 1,N^6-etheno-ATP (eATP) and degradation of etheno-nucleotides was determined by HPLC. Histograms show CD39 expression on the cells at the time of eATP incubation. **b** CD73$^-$ CD4con T cells were stimulated with αCD3/αCD28 in the presence of the ADA inhibitor EHNA (10 µM) and incubated with Tregs, ATP (50 µM), and EVs from cell culture supernatants of sorted and activated CD8 T cells as indicated. CD25 expression and proliferation were measured after 4 days by flow cytometry. IFNγ production was determined by ELISA in the cell culture supernatant harvested on day 4. Data were shown for one representative donor out of four analyzed (mean of technical replicates).

125

Fig. 7 Extracellular vesicles isolated from synovial fluid of patients with juvenile idiopathic arthritis are immunosuppressive. a, b Flow cytometric analysis of **a** immune cell subsets and **b** CD73 and CD39 expression in SF and PB of JIA patients. **c** CD73 in the cell-free moiety of SF was measured by ELISA. **d** SF was incubated with eAMP and degradation of eAMP was determined by HPLC. **e** CD73$^-$ CD4con T cells were stimulated with αCD3/αCD28 in the presence of the ADA inhibitor EHNA (10 μM) and incubated with ATP (50 μM), recombinant CD73 (15 ng/mL), EVs (3.1 × 10^8 particles), and PSB-14685 (10 μM) as indicated. CD25 expression and proliferation were measured after 4 days by flow cytometry. Data were shown for **a** eight individual donors, as mean of **b** nine, **c** fifteen, and **d** four donors indicated by dots, or for **e** a representative donor out of three analyzed (mean of technical replicates), marked as a red dot in **b**–**d**. A two-tailed Wilcoxon test was used to compare ectonucleotidase expression in PB and SF in **b**.

SF of nearly all patients tested (Fig. 7c) and confirmed AMPase activity in the samples measured (Fig. 7d). We next isolated EVs from the SF and verified their EV nature by electron microscopy and western blot. The EV markers flotillin and CD81 could be detected in all EV samples along with CD73 (Supplementary Fig. 9a, b). We also assessed for the presence of protein contamination and found rests of albumin, as previously reported when using differential ultracentrifugation for EV isolation[38], but not of apolipoproteins (Supplementary Fig. 8b).

Among other cell types, T cells clearly contributed to the cellular sources of EVs in the SF (Supplementary Fig. 9c), and we could show co-expression of CD8 and CD73 on these EVs by conventional flow cytometry (Supplementary Fig. 9d). We assessed if SF-derived EVs suppress CD73$^-$ CD4con T cells. As observed before, the addition of recombinant CD73 and ATP to the responder T cells resulted in reduced T cell activation and completely abolished proliferation. When SF-derived EVs were added to the culture in the absence of ATP, we observed an increase in activation and cell proliferation. Importantly, in the presence of ATP, this increase was abrogated, and a clear reduction in cell proliferation was induced, which was reversed by the addition of the CD73-specific inhibitor PSB-14685 (Fig. 7e). Of note, SF-derived EVs decreased the activation and

proliferation of responder T cells in a dose-dependent manner (Supplementary Fig. 9e). In summary, we show here that EVs from the SF of JIA patients degrade AMP, generating adenosine and suppressing T cell proliferation and function.

Discussion

Adenosine is a potent regulator of inflammation generated in the extracellular space by the sequential hydrolysis of ATP by ectonucleotidases CD39 and CD73. We show here that activated human CD8 T cells release CD73-containing EVs that generate adenosine, contributing substantially to immune suppression.

The degradation of ATP and generation of adenosine is a well-described mechanism of suppression in murine Foxp3$^+$ Tregs, which express both CD39 and CD73 on their cell surface[14]. However, very few human FOXP3$^+$ Tregs express CD73, and they are not particularly adept at adenosine generation. We describe here how CD73-mediated generation of adenosine is mostly independent from Tregs in the human system, and propose a coordinated effort involving CD39 on Tregs for the degradation of ATP to AMP, and CD73 on T cell-derived EVs that provide the necessary AMPase activity to generate adenosine. We have shown the release of CD73-containing EVs from activated CD8 T cells. However, CD4 T cells also lose CD73 from the

cell membrane upon activation, suggesting a parallel mechanism for CD4 T cells.

Intracellular ATP functions as an essential energy source. Once released into the extracellular space, ATP becomes a biologically active signaling molecule[39]. Conditions such as cellular activation and stress, inflammation, ischemia, or hypoxia promote ATP release and raise the pericellular concentration of ATP sufficiently to activate P2 receptors and support inflammation[25,40,41]. Extracellular ATP is rapidly hydrolyzed by ectonucleotidases in a stepwise manner to yield adenosine, a potent immune suppressor upon binding to P1 receptors A_{2A} and A_{2B} on immune cells. The degradation of adenosine by ADA further regulates the availability of adenosine for signaling. Thus, a complex network of purinergic enzymes and receptors controls the duration and magnitude of purinergic signaling and regulates the immune response[42]. Remarkably, the affinity of purinergic molecules for its receptors and the outcome after receptor activation are cell- and species-specific[43]. Adenosine signaling supports the expansion and suppressive function of murine Tregs[15] while inhibiting effector T cells. In humans, adenosine inhibits both Tregs and effector T cells[44]. Not only the response to extracellular adenine nucleotides is different between mice and humans, but also the expression and regulation of ectonucleotidases CD39 and CD73. The co-expression of both enzymes on murine Tregs secures the production of adenosine, and this metabolic path is important for their suppressive function[14,45]. In contrast, very few circulating human Tregs express CD73 and they are still suppressive. This poses the question of whether human Tregs rely on adenosine generation or rather favor other mechanisms of immune suppression. The absence of CD73 on the membrane of human Tregs could be an evolutionary advantage to avoid the production of pericellular adenosine that inhibits their function[44]. Further, human Tregs do not express CD26, a docking site for ADA at the cell membrane[46], lacking a mechanism for efficient degradation of pericellular adenosine.

CD73, as a GPI-anchored protein, clusters at the plasma membrane in lipid rafts that are poised for EV formation[47,48]. We found that CD73 diminished drastically from the surface of T cells 3 to 4 days after activation, concomitant to the loss of AMPase activity in the cellular compartment. In parallel, enzymatic activity increased in the cell culture supernatants. Importantly, the capacity to produce adenosine found in the cell culture supernatants was lost after ultracentrifugation, indicating that it was contained in EVs and not present as a soluble protein. Part of the AMPase activity was already lost after $10,000 \times g$ centrifugation, which we attribute to CD73 on apoptotic bodies or larger EVs. Even though CD73 has higher enzymatic activity in its soluble form compared to the membrane-bound variant[49], we speculate that the vesicular form has advantages, such as an extended half-life, and better distribution through body fluids. It is not yet known how far EVs can travel in human body fluids, but murine EVs can rapidly traffic to the spleen and liver before elimination 6 h after intravenous injection[50]. The generation of EVs poses the question of how the cells recover the membrane loss. A possibility would be the fusion with foreign EVs, which would permit a very dynamic exchange of membrane components between cells and the acquisition of new functions[51,52].

The exact contribution of EV- and T cell-derived adenosine to immune suppression in vivo is difficult to predict due to the multiple levels of regulation that influence the availability of adenine nucleotides during an immune response. Contributing factors include the rapid generation and degradation of signaling-relevant molecules, local differences in nucleotide concentrations, potential feed-forward inhibition mechanisms, and alternative degrading enzymes. In our in vitro experiments with human T cells, we used different substrates and specific inhibitors to overcome these difficulties. By blocking the degradation of adenosine with an ADA inhibitor, we emphasized the role of the purinergic cascade in immune suppression. The addition of exogenous ATP at a moderate concentration (50 μM) served to mimic local increases of ATP as it has been reported in different settings of inflammation and ischemia[53]. In the absence of Tregs, we added AMP to ensure the availability of enough substrate for CD73, because conventional T cells are much less efficient than Tregs in producing AMP. Furthermore, adding AMP as substrate bypasses a potential feed-forward inhibition of CD73 by ATP or ADP[54]. Although CD73 is the main AMP-degrading enzyme, adenosine is still generated by tissue-nonspecific alkaline phosphatase (TNAP) when CD73 is absent, as shown in CD73 knockout mice[55,56] and in cells from patients with CD73 deficiency[57]. In our experiments, we could completely abolish AMPase activity with a specific CD73 inhibitor[58,59], indicating that TNAP activity is negligible in our system. The observed ATPase activity is likely CD39-mediated, but we cannot exclude a contribution of other enzymes, such as ENPP1 (ectonucleotide pyrophosphatase/phosphodiesterase-1) or other members of this family of pyrophosphatases[60]. Of note, the expression, regulation, and activity of ENPP1 on T cells has not been explored. The detection of ADP as an intermediate product in our assays indicates a stepwise degradation of ATP, favoring the role of ectonucleoside triphosphate diphosphohydrolases (ENTPDases) like CD39, but not pyrophosphatases.

Both CD39 and CD73 are expressed in distinct immune cell types. In humans, apart from T cells, B cells express both ecto-nucleotidases, while monocytes and dendritic cells express mostly CD39. Also, endothelial cells and mesenchymal cells express CD73, and all these cell types contribute to ATP metabolism in vivo. EVs containing CD39 or CD73 have been isolated from mesenchymal stem cells, B cells, and Tregs[24,61,62]. These EVs have immunoregulatory properties[63] and their modulatory role has been reported in cancer[34,62]. We have not addressed here the contribution of other ectonucleotidases present in T cell-derived EVs to ATP metabolism, but it has been shown that Treg-derived EVs contain CD39 and inhibit T cell proliferation[24]. Further work will be required to dissect the role of cellular and EV-associated ectonucleotidases in immune suppression.

We had the unique chance to isolate EVs from a human site of inflammation, the SF of JIA patients. The SF contains predominantly monocytes and memory T cells that produce inflammatory cytokines, sustaining inflammation in the affected joints[64,65]. In agreement with previous reports, we found increased CD39 and negligible expression of CD73 in the T cells of the SF. While SF-infiltrating cells show ATPase activity, AMPase activity is decreased in the cellular fraction[36,37]. Our analysis revealed that CD73 is present in the cell-free fraction of the SF, including EVs. The cellular source for these EVs are T cells, monocytes/macrophages, and endothelial and mesenchymal stem cells. Because human monocytes do not express CD73[26,27], we concluded that activated T cells are a relevant source of vesicular CD73. This was confirmed by the co-expression of CD73 and CD8 on SF-derived EVs. The endothelial cells in the synovial lining and mesenchymal stem cells, both expressing CD73, are also plausible sources for CD73$^+$ SF EVs. This finding deserves further investigation. Our in vitro experiments showed that SF-derived EVs promote T cell activation and proliferation, probably due to cytokines and growth factors contained in these EVs[66]. However, by strengthening the purinergic signaling cascade with the addition of ADA inhibitor EHNA and ATP, we turned the outcome around, and EVs became immunosuppressive, as it has been shown for CD73-containing EVs produced by tumor cells[34]. Therefore, in an ATP-rich environment, as it is at sites of inflammation and ischemia or

127

in the intestine, the purinergic signaling cascade becomes highly relevant for immune regulation[67].

We conclude that abundant CD39 expression on Tregs secures the hydrolysis of ATP to ADP and AMP, but that the AMPase activity of CD73 is provided by CD8 T cells, and mostly contained in EVs. We propose that adenosine generation by conventional (nonregulatory) T cells is a built-in mechanism of immune suppression necessary to restrain ongoing inflammation, contesting the common paradigm that Tregs must provide the whole machinery for adenosine production. Finally, our results highlight the role of EVs in the control of immune responses and support the prospect of modulating the purinergic axis for the treatment of local inflammation.

Methods

Origin of samples and isolation of human mononuclear cells. Buffy coats were obtained from the blood bank of the University Medical Center Hamburg-Eppendorf (UKE). PB was drawn from healthy volunteers visiting the UKE. Blood and SF of patients with JIA, specifically oligo- and polyarthritis, were obtained from children visiting the UKE, the Altona Children's Hospital, the University Medical Center Schleswig-Holstein (campus Lübeck), or the Medical Center Bad Bramstedt. SF was obtained from joint puncture for diagnostic or therapeutic reasons. All samples were handled according to corresponding ethics protocols (Ethics Committee of the Hamburg Chamber of Physicians, protocols PV5139 for samples from healthy donors, and PV3746 for samples from JIA patients), and informed consent was obtained from all donors. Mononuclear cells (MC) were isolated from blood and SF by Biocoll density gradient centrifugation (Merck). Isolated immune cells were used for flow cytometric analyses or further isolation of T cell subsets.

Isolation of murine splenocytes. All mouse experiments were performed in accordance with national and institutional guidelines on animal care (Hamburg Authority for Health and Consumer Protection, Veterinary Affairs/Food Safety, protocol ORG983). Lymphocytes were isolated from the spleen of C57BL/6 mice housed in the animal facility at the UKE. Single-cell suspensions were prepared by processing the spleen through a 70 μm strainer. After erythrocyte lysis, splenocytes were used for the analysis of surface markers by flow cytometry.

Flow cytometry and fluorescence-activated cell sorting (FACS). Human and murine immune cells were preincubated with immunoglobulins to block unspecific binding and stained with fluorescence-labeled antibodies for 30 min at 4 °C. All antibodies were titrated prior to use. The following fluorochrome-conjugated anti-human antibodies were used: anti-CD3 (clone UCHT1 and clone OKT3), anti-CD4 (clone RPA-T4, clone SK3, and clone OKT4), anti-CD8α (clone RPA-T8 and clone HIT8a), anti-CD9 (clone HI9a), anti-CD16 (clone 3G8), anti-CD19 (clone HIB19), anti-CD25 (clone BC96), anti-CD39 (clone A1), anti-CD73 (clone AD2), anti-CD127 (clone HCD127 and clone A019D5) (all BioLegend), anti-CD14 (clone M5E2), anti-CD25 (clone 2A3), anti-CD45 (clone HI30), anti-TCRγδ (clone 11F2) (all BD Biosciences), anti-CD56 (clone N901) (Beckman Coulter). The following fluorochrome-conjugated anti-mouse antibodies were used: anti-CD3 (clone 17A2), anti-CD4 (clone RM4-5), anti-CD25 (clone PC61), anti-CD73 (clone TY/11.8) (all BioLegend), anti-CD8 (clone 53-6.7), anti-CD19 (clone 1D3), and anti-CD39 (clone 24DMS1) (all eBioscience). For dead cell exclusion, a live/dead dye (Thermo Fisher Scientific) was included. The staining cocktails were designed to minimize the effects of spectral overlap. Prior to analysis, a compensation matrix was calculated after single color staining of human PBMCs, as described[68]. Samples were measured at FACSCanto II, FACSCelesta, or LSR-Fortessa (BD Biosciences) using FACSDiva software for data acquisition (BD Biosciences) and analyzed using FlowJo software (BD). For isolation of specific T cell subpopulations by FACS, cells were stained as described above and sorted at FACSAria IIIU (BD Biosciences).

Preparation and stimulation of human T cells. CD8 or CD4 T cells were isolated from PBMCs by negative selection using the EasySep Human T Cell Enrichment Kit (Stemcell Technologies). The purity of the isolated cells was assessed by flow cytometry. For indicated assays, Tregs (defined as CD4+ CD25high CD127low) and conventional CD4 T cells (CD4con, defined as non-Treg CD4 T cells) were obtained by FACS. CD4con T cells were additionally sorted with regard to their CD73 expression if indicated. To assess proliferation in T cell assays, responder cells were labeled with 2 μM eFluor 670 (Thermo Fisher Scientific).

Purified T cells were stimulated with 1 μg/mL coated αCD3 (OKT3) and 5 μg/mL soluble αCD28 (CD28.2) (both BioLegend) and cultured in serum-free X-VIVO 15 medium (Lonza). PBMCs were activated with 0.5 μg/mL soluble αCD3 in RPMI containing 1% penicillin-streptomycin, 1% L-glutamine (all Thermo Fisher Scientific), and 10% FBS (Biochrom). If not otherwise stated, cells were seeded at a density of 1×10^6 cells/mL.

Isolation of EVs. EVs were isolated from cell culture supernatants, X-VIVO 15 medium, and SF by differential centrifugation at 4 °C. Samples were centrifuged at $450 \times g$ for 5 min, followed by centrifugation at $2000 \times g$ for 10 min. After centrifugation at $10,000 \times g$ for 30 min, the supernatant was subjected to ultracentrifugation ($110,000 \times g$, 70 min, in an SW 60 Ti swinging-bucket rotor, Beckman Coulter). The EV-enriched pellet (hereinafter named EVs) was washed and resuspended in PBS. Particle concentration and size were determined using the NTA instrument NanoSight LM14 (Malvern Panalytical) equipped with a 638 nm laser and a Marlin F-033B IRF camera (Allied Vision Technologies), operated with NTA 3.0 software.

Characterization of EVs

Western blot. The EVs were characterized according to the ISEV guidelines[69]. For western blot analysis, EVs were incubated with RIPA buffer (50 mM Tris-HCl pH 7.4, 150 mM NaCl, 1% NP40, 0.5% Na-deoxycholate, and 0.1% SDS) in the presence of protease and phosphatase inhibitors (Roche). The protein content of EVs was assessed with a Micro BCA Protein assay kit (Thermo Scientific). Samples (3.5 μg per EV sample, 15 ng recombinant CD73, 10 μg cell lysate, 2 μL pure SF, 15 μL X-VIVO 15 medium, or 15 μL of EV ultracentrifugation pellet corresponding to 2 mL X-VIVO 15 medium) were mixed with 4X loading buffer (250 mM Tris-HCl, 8% SDS, 40% glycerol, 20% β-mercaptoethanol, 0.008% Bromophenol Blue, pH 6.8), boiled for 5 min at 95 °C and subjected to electrophoresis on a 10% Bis-Tris gel (Invitrogen) under denaturing conditions. The gel was electroblotted onto a nitrocellulose membrane (LI-COR) and stained with the Revert Total Protein Stain (LI-COR). After blocking for 60 min with Roti-Block (Carl Roth), membranes were incubated overnight with the following primary antibodies diluted in Roti-Block: anti-CD73 (clone D7F9A, Cell Signaling, 1:1000), anti-CD81 (clone D3N2D, Cell Signaling, 1:1000), anti-Flotillin-1 (clone 18/Flotillin-1, BD Biosciences, 1:1000), anti-GM130 (clone 35/GM130, BD Biosciences, 1:500), anti-Albumin (clone F-10, Santa Cruz, 1:1000), anti-apoA-1 (clone E-20, Santa Cruz, 1:500), or anti-apoB (polyclonal, Acris, 1:1000). After washing with TBST, the membranes were incubated for 60 min with anti-rabbit-HRP-conjugated secondary antibody (Cell Signaling, 1:1000), or anti-mouse-HRP-conjugated secondary antibody (Cell Signaling, 1:1000), or anti-goat-HRP-conjugated secondary antibody (Jackson ImmunoResearch Laboratories, 1:5000). Membranes were developed with SuperSignal West Femto Maximum Sensitivity Substrate (Thermo Fisher Scientific), and images were taken on a ChemiDoc Imaging System (Bio-Rad) using the Quantity One software.

Electron microscopy. For electron microscopy with immunogold labeling, EVs were adsorbed to carbon-coated grids for 20 min, washed with PBS, quenched in glycine, and blocked with blocking solution for goat gold conjugates (Aurion)[70]. After 30 min incubation with the primary anti-CD73 antibody (clone AD2, BioLegend, 5 μg/mL), the grids were incubated for 20 min with the anti-mouse IgG 10 nm gold conjugate (Sigma, 1:20), fixed in 2.5% glutaraldehyde, washed with water, and transferred onto methyl cellulose/uranyl acetate mixture drops on ice for 10 min. Grids were looped out, air-dried, and analyzed by transmission electron microscopy. Electron microscopy was performed at 80 kV in an FEI Tecnai G20 microscope equipped with an SIS Veleta camera.

Flow cytometry. For phenotypical single EV analysis by conventional flow cytometry, the EV suspension was extensively diluted in 400 μL filtered PBS and stained for 30 min with anti-CD8-BV421 (clone RPA-T8, 1:500), anti-CD73-PE (clone AD2, 1:300), and anti-CD9-APC (clone HI9a, 1:200) antibodies as indicated. After extensive washing of the fluidics system of the cytometer, ApogeeMix (Apogee Flow Systems, silica and latex beads) and Megamix-Plus SSC (BioCytex, latex/polystyrene beads) heterogenous fluorescent beads were used to set up the system. Samples were measured at the FACSAria IIIU (BD Biosciences) for 1 min at a flow rate of 1.0 at 4 °C. Controls included buffer alone, buffer with single and combined antibodies, EVs with buffer, and EVs with fluorescence minus one (FMO) stainings for each fluorochrome. To confirm the nature of the EVs, the samples were incubated with 0.5% NP40 for 45 min and reanalyzed for 1 min (lysis control).

For the phenotypical characterization of SF EVs, we used the MACSPlex Exosome kit (Miltenyi). This bead-based assay allows the simultaneous detection of 37 surface markers to determine the cellular origin of the EVs. In brief, EVs were incubated overnight with antibody-coated capture beads, washed, and incubated with tetraspanin CD9/CD81/CD63 antibodies provided in the kit. The measurements were done at FACSCanto II (BD Biosciences).

T cell assays. T cells were stimulated as described above and cultured at a density of $0.25-0.5 \times 10^6$ cells/mL in serum-free X-VIVO 15 medium (Lonza) for 3 to 4 days at 37 °C, 5% CO_2 in the presence of ADA inhibitor EHNA (10 μM, Tocris). In Treg suppression assays, responder T cells were cocultured with Tregs at different ratios. When indicated, AMP (50 μM, Sigma-Aldrich), ATP (50 μM, Sigma-Aldrich), the CD73-specific inhibitor 2-chloro-N^6-o-chlorobenzyl-α,β-methylene-ADP (PSB-14685, 10 μM)[59], recombinant CD73 (15 ng/mL, unless otherwise noted, Sino Biological) or EVs (equivalent to 150 μL of cell culture supernatant of activated CD8 T cells, if not stated otherwise) were added. At the time of harvest, the cell membrane expression of the activation marker CD25, and the dilution of

128

eFluor 670 as a measure of proliferation were assessed by flow cytometry. IFNγ was determined in cell culture supernatants by ELISA (BioLegend), measured with a Victor[3] 1240 plate reader equipped with Wallac 1240 Manager software (PerkinElmer).

Phospholipase C treatment. Forced shedding of CD73 was achieved by incubating 0.2×10^6 CD8 T cells with 0.5 U/mL bacterial phosphatidylinositol-specific phospholipase C (PI-PLC, Thermo Fisher Scientific) for 30 min at 37 °C. Cells and supernatants after PI-PLC treatment were subsequently used for the determination of AMPase activity by high-performance liquid chromatography (HPLC).

Analysis of ATPase and AMPase activities by HPLC. AMPase and ATPase activity of cells, cell culture supernatants, EVs, and SF were analyzed by assessing the degradation of $1,N^6$-etheno-AMP (eAMP) or $1,N^6$-etheno-ATP (eATP), respectively. For this, 0.2×10^6 T cells, 150 μL cell culture supernatant, EVs (equivalent to 150 μL of supernatant), or 20 μL SF were incubated with 1 μM eAMP or eATP (Biolog) for 30 min (cells) or 60 min (cell culture supernatants, EVs and SF) at 37 °C. After the incubation, cells were removed by centrifugation ($450 \times g$, 5 min, 4 °C) and all samples were directly frozen and stored at −20 °C until HPLC analysis. The analysis of etheno-nucleotides was conducted by ion pair reversed-phase HPLC on a 1260 Infinity system (Agilent Technologies). Before measurement, samples were passed through 10 kDa size exclusion filters to remove proteins (10 min, $10,000 \times g$, 4 °C, Sartorius). A volume corresponding to starting amount of 85 pmol eAMP or eATP was loaded on the HPLC. For quantification of nucleotides in the sample, different amounts of commercially available etheno-nucleotides (Biolog) were analyzed under the same conditions. The separation was performed on a 250 mm × 4.6 mm C-18 BDS Multohyp 5 μm column (CS Chromatographie Service) with a C-18 security guard cartridge (Phenomenex). The mobile phase was composed of HPLC buffer A (20 mM KH_2PO_4, 5 mM TBAHP, pH 6.0) and HPLC buffer B (50% buffer A and 50% methanol) with the following gradient: 0.0 min (30.0% buffer B), 3.5 min (30.0% buffer B), 11.0 min (62.5% buffer B), 15.0 min (62.5% buffer B), 25.0 min (100.0% buffer B), 27.0 min (100.0% buffer B), 29.0 min (30.0% buffer B), and 38.0 min (30.0% buffer B). The injection volume was 100 μL and the flow rate was 0.8 mL/min. The temperature of the column compartment was 20 °C and the autosampler was kept at 8 °C. The signals were detected by the fluorescence detector (excitation 230 nm and emission 410 nm) of the system. Peak integration was performed using ChemStation Software (Agilent Technologies).

Detection of non-cell-bound CD73. Non-cell-bound CD73 was determined in cell culture supernatants and in SF by ELISA (Abcam).

Fluorescence microscopy. Human CD73^{+} and CD73^{−} CD8 T cells or total CD8 T cells were stimulated as described above. At the day of harvest, cells were plated on poly-L-lysine coated cytoslides (Thermo Fisher Scientific) at a density of 0.2×10^6 cells/cytoslide using a cytospin centrifuge (Shandon Elliott). In some experiments, exocytosis was blocked with 10 μM GW4869 (Cayman Chemical). Cells were fixed for 10 min at room temperature (RT) with 4% PFA (EMSciences) and washed with PBS. For immunofluorescent localization of CD73, unspecific binding was blocked with 5% normal horse serum (Vector) diluted in 0.05% Triton X-100 (Merck) in PBS. The cytoslides were incubated overnight with unconjugated anti-CD73 (clone AD2, 1:10, Biolegend) in blocking buffer at 4 °C and detected using a Cy2 anti-mouse antibody (1:200, Jackson ImmunoResearch Laboratories) for 30 min at RT. After washing, cells were further incubated with APC anti-CD9 (clone HI9A, 1:10) or/and anti-CD81 (clone 5A6, 1:10) (both BioLegend) for 60 min at RT. An LSM800 confocal microscope with airyscan and the ZENblue software (all ZEISS) were used for analysis. Pearson's coefficient of co-localization was determined in seven to ten randomly chosen high power fields (630X) per condition (three individual cells/high power field).

Statistical analysis. Prism 8 (GraphPad) was used to perform statistical analyses, detailed information are provided in the figure legends. In brief, data were analyzed for normal distribution. When they passed the normality test, they were analyzed by two-tailed Student's t-test (two groups, paired), ordinary one-way ANOVA (multiple groups, unpaired), or repeated measures (RM) one-way ANOVA (multiple groups, paired). When data did not pass the normality test, they were analyzed by a two-tailed Wilcoxon test (two groups, paired) or Kruskal–Wallis test (multiple groups, unpaired). When multiple groups were compared, post hoc tests were performed to correct for multiple comparisons. Dunnett's multiple comparisons test was used when all groups were compared to the same control condition. Dunn's multiple comparisons test was performed to compare the mean ranks of not normally distributed data. p values < 0.05 were considered to indicate statistical significance. Non-significant differences were not annotated.

References

1. Zimmermann, H., Zebisch, M. & Sträter, N. Cellular function and molecular structure of ecto-nucleotidases. *Purinergic Signal* **8**, 437–502 (2012).
2. Heng, T. S. P. et al. The Immunological Genome Project: networks of gene expression in immune cells. *Nat. Immunol.* **9**, 1091–1094 (2008).
3. Huang, S., Apasov, S., Koshiba, M. & Sitkovsky, M. Role of A2a extracellular adenosine receptor-mediated signaling in adenosine-mediated inhibition of T-cell activation and expansion. *Blood* **90**, 1600–1610 (1997).
4. Linden, J. & Cekic, C. Regulation of lymphocyte function by adenosine. *Arterioscler. Thromb. Vasc. Biol.* **32**, 2097–2103 (2012).
5. Aherne, C. M. et al. Coordination of ENT2-dependent adenosine transport and signaling dampens mucosal inflammation. *JCI Insight* **3**, e121521 (2018).
6. Naganuma, M. et al. Cutting edge: critical role for A2A adenosine receptors in the T cell-mediated regulation of colitis. *J. Immunol.* **177**, 2765–2769 (2006).
7. Dong, K., Gao, Z. & Zhang, H. The role of adenosinergic pathway in human autoimmune diseases. *Immunol. Res.* **64**, 1133–1141 (2016).
8. Alam, M. S. et al. A2A adenosine receptor (AR) activation inhibits pro-inflammatory cytokine production by human CD4+ helper T cells and regulates Helicobacter-induced gastritis and bacterial persistence. *Mucosal Immunol.* **2**, 232–242 (2009).
9. Ingwersen, J. et al. Dual roles of the adenosine A2a receptor in autoimmune neuroinflammation. *J. Neuroinflammation* **13**, 48 (2016).
10. Gao, Z.-W. et al. Serum adenosine deaminase activity is increased in systemic lupus erythematosus patients and correlated with disease activity. *Immunol. Res.* **66**, 299–304 (2018).
11. Chrobak, P. et al. CD73 plays a protective role in collagen-induced arthritis. *J. Immunol.* **194**, 2487–2492 (2015).
12. Louis, N. A. et al. Control of IFN-αA by CD73: implications for mucosal inflammation. *J. Immunol.* **180**, 4246–4255 (2008).
13. Sakaguchi, S., Miyara, M., Costantino, C. M. & Hafler, D. A. FOXP3+ regulatory T cells in the human immune system. *Nat. Rev. Immunol.* **10**, 490–500 (2010).
14. Deaglio, S. et al. Adenosine generation catalyzed by CD39 and CD73 expressed on regulatory T cells mediates immune suppression. *J. Exp. Med.* **204**, 1257–1265 (2007).
15. Ohta, A. et al. The development and immunosuppressive functions of CD4+ CD25+ FoxP3+ regulatory T cells are under influence of the adenosine-A2A adenosine receptor pathway. *Front. Immunol.* **3**, 190 (2012).
16. Dianzani, U. et al. Co-stimulatory signal delivered by CD73 molecule to human CD45RAhiCD45ROlo (naive) CD8+ T lymphocytes. *J. Immunol.* **151**, 3961–3970 (1993).
17. Rissiek, A. et al. The expression of CD39 on regulatory T cells is genetically driven and further upregulated at sites of inflammation. *J. Autoimmun.* **58**, 12–20 (2015).
18. Kling, L. et al. Changes in CD73, CD39 and CD26 expression on T-lymphocytes of ANCA-associated vasculitis patients suggest impairment in adenosine generation and turn-over. *Sci. Rep.* **7**, 11683 (2017).
19. Tóth, I. et al. Decreased frequency of CD73+ CD8+ T cells of HIV-infected patients correlates with immune activation and T cell exhaustion. *J. Leukoc. Biol.* **94**, 551–561 (2013).
20. Borsellino, G. et al. Expression of ectonucleotidase CD39 by Foxp3+ Treg cells: hydrolysis of extracellular ATP and immune suppression. *Blood* **110**, 1225–1232 (2007).
21. Fletcher, J. M. et al. CD39+ Foxp3+ regulatory T cells suppress pathogenic Th17 cells and are impaired in multiple sclerosis. *J. Immunol.* **183**, 7602–7610 (2009).
22. Alam, M. S. et al. CD73 is expressed by human regulatory T helper cells and suppresses proinflammatory cytokine production and Helicobacter felis-induced gastritis in mice. *J. Infect. Dis.* **199**, 494–504 (2009).
23. Gourdin, N. et al. Autocrine adenosine regulates tumor polyfunctional CD73+CD4+ effector T cells devoid of immune checkpoints. *Cancer Res.* **78**, 3604–3618 (2018).

ARTICLE

24. Tung, S. L. et al. Regulatory T cell extracellular vesicles modify T-effector cell cytokine production and protect against human skin allograft damage. *Front. Cell Dev. Biol.* **8**, 317 (2020).

25. Yip, L. et al. Autocrine regulation of T-cell activation by ATP release and P2X7 receptors. *FASEB J.* **23**, 1685–1693 (2009).

26. Uhlen, M. et al. A genome-wide transcriptomic analysis of protein-coding genes in human blood cells. *Science* **366**, eaax9198 (2019).

27. Blood atlas - NT5E - The Human Protein Atlas. https://www.proteinatlas.org/ENSG00000135318-NT5E/blood.

28. Shay, T. et al. Conservation and divergence in the transcriptional programs of the human and mouse immune systems. *Proc. Natl Acad. Sci. USA* **110**, 2946–2951 (2013).

29. Roederer, M. et al. The genetic architecture of the human immune system: a bioresource for autoimmunity and disease pathogenesis. *Cell* **161**, 387–403 (2015).

30. Hartigan-O'Connor, D. J., Poon, C., Sinclair, E. & McCune, J. M. Human CD4+ regulatory T cells express lower levels of the IL-7 receptor alpha chain (CD127), allowing consistent identification and sorting of live cells. *J. Immunol. Methods* **319**, 41–52 (2007).

31. Raczkowski, F. et al. CD39 is upregulated during activation of mouse and human T cells and attenuates the immune response to Listeria monocytogenes. *PLoS ONE* **13**, e0197151 (2018).

32. Pettengill, M. et al. Soluble ecto-5′-nucleotidase (5′-NT), alkaline phosphatase, and adenosine deaminase (ADA1) activities in neonatal blood favor elevated extracellular adenosine. *J. Biol. Chem.* **288**, 27315–27326 (2013).

33. Schneider, E. et al. Generation and function of non-cell-bound CD73 in inflammation. *Front. Immunol.* **10**, 1729 (2019).

34. Clayton, A., Al-Taei, S., Webber, J., Mason, M. D. & Tabi, Z. Cancer exosomes express CD39 and CD73, which suppress T cells through adenosine production. *J. Immunol.* **187**, 676–683 (2011).

35. Essandoh, K. et al. Blockade of exosome generation with GW4869 dampens the sepsis-induced inflammation and cardiac dysfunction. *Biochim. Biophys. Acta* **1852**, 2362–2371 (2015).

36. Moncrieffe, H. et al. High expression of the ectonucleotidase CD39 on T cells from the inflamed site identifies two distinct populations, one regulatory and one memory T cell population. *J. Immunol.* **185**, 134–143 (2010).

37. Botta Gordon-Smith, S., Ursu, S., Eaton, S., Moncrieffe, H. & Wedderburn, L. R. Correlation of low CD73 expression on synovial lymphocytes with reduced adenosine generation and higher disease severity in juvenile idiopathic arthritis. *Arthritis Rheumatol.* **67**, 545–554 (2015).

38. Foers, A. D. et al. Enrichment of extracellular vesicles from human synovial fluid using size exclusion chromatography. *J. Extracell. Vesicles* **7**, 1490145 (2018).

39. Khakh, B. S. & Burnstock, G. The double life of ATP. *Sci. Am.* **301**, 84–92 (2009).

40. Woehrle, T. et al. Pannexin-1 hemichannel-mediated ATP release together with P2X1 and P2X4 receptors regulate T-cell activation at the immune synapse. *Blood* **116**, 3475–3484 (2010).

41. Idzko, M., Ferrari, D. & Eltzschig, H. K. Nucleotide signalling during inflammation. *Nature* **509**, 310–317 (2014).

42. Junger, W. G. Immune cell regulation by autocrine purinergic signalling. *Nat. Rev. Immunol.* **11**, 201–212 (2011).

43. Sitkovsky, M. V. et al. Physiological control of immune response and inflammatory tissue damage by hypoxia-inducible factors and adenosine A2A receptors. *Annu. Rev. Immunol.* **22**, 657–682 (2004).

44. Baroja-Mazo, A. et al. Extracellular adenosine reversibly inhibits the activation of human regulatory T cells and negatively influences the achievement of the operational tolerance in liver transplantation. *Am. J. Transplant.* **19**, 48–61 (2019).

45. Smyth, L. A. et al. CD73 expression on extracellular vesicles derived from CD4+CD25+Foxp3+ T cells contributes to their regulatory function. *Eur. J. Immunol.* **43**, 2430–2440 (2013).

46. Salgado, F. J. et al. CD26: a negative selection marker for human Treg cells. *Cytom. Part A* **81**, 843–855 (2012).

47. De Gassart, A., Géminard, C., Février, B., Raposo, G. & Vidal, M. Lipid raft-associated protein sorting in exosomes. *Blood* **102**, 4336–4344 (2003).

48. López-Cobo, S., Campos-Silva, C. & Valés-Gómez, M. Glycosyl-phosphatidyl-inositol (GPI)-anchors and metalloproteases: their roles in the regulation of exosome composition and NKG2D-mediated immune recognition. *Front. Cell Dev. Biol.* **4**, 97 (2016).

49. Lehto, M. T. & Sharom, F. J. Release of the glycosylphosphatidylinositol-anchored enzyme ecto-5′-nucleotidase by phospholipase C: catalytic activation and modulation by the lipid bilayer. *Biochem. J.* **332**, 101–109 (1998).

50. Lai, C. P. et al. Dynamic biodistribution of extracellular vesicles in vivo using a multimodal imaging reporter. *ACS Nano* **8**, 483–494 (2014).

51. Prada, I. & Meldolesi, J. Binding and fusion of extracellular vesicles to the plasma membrane of their cell targets. *Int. J. Mol. Sci.* **17**, 1296 (2016).

52. Joly, E. & Hudrisier, D. What is trogocytosis and what is its purpose? *Nat. Immunol.* **4**, 815 (2003).

53. Dale, N. & Frenguelli, B. Release of adenosine and ATP during ischemia and epilepsy. *Curr. Neuropharmacol.* **7**, 160–179 (2009).

54. Vieira, C. et al. Feed-forward inhibition of CD73 and upregulation of adenosine deaminase contribute to the loss of adenosine neuromodulation in postinflammatory ileitis. *Mediators Inflamm.* **2014**, 254640 (2014).

55. Zhang, D. et al. Inhibition of hippocampal synaptic activity by ATP, hypoxia or oxygen-glucose deprivation does not require CD73. *PLoS ONE* **7**, e39772 (2012).

56. Jackson, E. K., Cheng, D., Verrier, J. D., Janesko-Feldman, K. & Kochanek, P. M. Interactive roles of CD73 and tissue nonspecific alkaline phosphatase in the renal vascular metabolism of 5′-AMP. *Am. J. Physiol. Renal Physiol.* **307**, F680–F685 (2014).

57. Jin, H. et al. Increased activity of TNAP compensates for reduced adenosine production and promotes ectopic calcification in the genetic disease ACDC. *Sci. Signal.* **9**, ra121 (2016).

58. Bhattarai, S. et al. X-ray Co-crystal structure guides the way to subnanomolar competitive ecto-5′-nucleotidase (CD73) inhibitors for cancer immunotherapy. *Adv. Ther.* **2**, 1900075 (2019).

59. Bhattarai, S. et al. 2-substituted α,β-methylene-ADP derivatives: potent competitive ecto-5′-nucleotidase (CD73) inhibitors with variable binding modes. *J. Med. Chem.* **63**, 2941–2957 (2020).

60. Horenstein, A. L. et al. A CD38/CD203a/CD73 ectoenzymatic pathway independent of CD39 drives a novel adenosinergic loop in human T lymphocytes. *Oncoimmunology* **2**, e26246 (2013).

61. Kerkelä, E. et al. Adenosinergic immunosuppression by human mesenchymal stromal cells requires co-operation with T cells. *Stem Cells* **34**, 781–790 (2016).

62. Zhang, F. et al. Specific decrease in B-cell-derived extracellular vesicles enhances post-chemotherapeutic CD8+ T cell responses. *Immunity* **50**, 738–750.e7 (2019).

63. Robbins, P. D. & Morelli, A. E. Regulation of immune responses by extracellular vesicles. *Nat. Rev. Immunol.* **14**, 195–208 (2014).

64. De Jager, W. et al. Blood and synovial fluid cytokine signatures in patients with juvenile idiopathic arthritis: a cross-sectional study. *Ann. Rheum. Dis.* **66**, 589–598 (2007).

65. Hunter, P. J. et al. Biologic predictors of extension of oligoarticular juvenile idiopathic arthritis as determined from synovial fluid cellular composition and gene expression. *Arthritis Rheum.* **62**, 896–907 (2010).

66. Fitzgerald, W. et al. A system of cytokines encapsulated in extraCellular vesicles. *Sci. Rep.* **8**, 8973 (2018).

67. Longhi, M. S., Moss, A., Jiang, Z. G. & Robson, S. C. Purinergic signaling during intestinal inflammation. *J. Mol. Med.* **95**, 915–925 (2017).

68. Bremer, S. J. et al. OMIP 073: analysis of human thymocyte development with a 14-color flow cytometry panel. *Cytom. Part A* **99**, 875–879 (2021).

69. Théry, C. et al. Minimal information for studies of extracellular vesicles 2018 (MISEV2018): a position statement of the International Society for Extracellular Vesicles and update of the MISEV2014 guidelines. *J. Extracell. Vesicles* **7**, 1535750 (2018).

70. Théry, C., Amigorena, S., Raposo, G. & Clayton, A. Isolation and characterization of exosomes from cell culture supernatants and biological fluids. *Curr. Protoc. Cell Biol.* **Chapter 3**, Unit 3.22 (2006).

Acknowledgements

Author contributions

Idea and design of research project: E.T., E.S., R.W., and N.G. Writing manuscript: R.W., E.S., and E.T. Supply of patient material: I.R. and M.L. Establishment of methods: E.S., R.W., A.R., J.B., A.B., R.F., B.P., B.R., and F.L.R. Experimental work: E.S., R.W., A.R., C.M.-S., R.R., J.B., S.B., and H.W. Data analysis and interpretation: E.S., R.W., A.R., and E.T. Scientific input and manuscript revision: A.R., C.M.-S., F.L.R., J.B., B.R., B.P., F.C., T.M., R.F., C.E.M., N.G.

Funding

Competing interests

C.E.M. has given scientific advice to Arcus Biosciences (Arcus Biosciences, Inc. is a publicly-traded biotechnology company working on CD73 inhibitor development). The remaining authors declare no competing interests.

13

130

Additional information

Supplementary information The online version contains supplementary material available at https://doi.org/10.1038/s41467-021-26134-w.

Correspondence and requests for materials should be addressed to Riekje Winzer or Eva Tolosa.

Peer review information *Nature Communications* thanks Lesley Smyth and the other, anonymous, reviewer(s) for their contribution to the peer review of this work. Peer reviewer reports are available.

Reprints and permission information is available at http://www.nature.com/reprints

Publisher's note Springer Nature remains neutral with regard to jurisdictional claims in published maps and institutional affiliations.

8. Summary in English and German

Extracellular vesicles (EVs) are lipid bilayer enclosed structures, formed via the endocytic pathway (exosomes) or shed from the plasma membrane (ectosomes/microvesicles). EVs are powerful communication tools, as they can be taken up by recipient cells, transferring their cargo composed by proteins, nucleic acids, and lipids. The cargo reflects the status of the cell of origin and, as EVs are found in body fluids, they are very promising biomarkers. EVs are involved in physiological and pathological processes in the Central Nervous System (CNS), playing a role in disease progression and recovery. To be studied, EVs are isolated either from cell-conditioned media, body fluids, and tissue.

Ischemic stroke occurs when a brain artery is occluded, causing a lack of blood flow and subsequent lack of oxygen and glucose supply in the affected area. The cells at the core of the infarct die immediately, while neurons in the surrounding area could be rescued, depending on the signals received in the next hours/days. The pathophysiology of stroke is complex, involving different brain and infiltrating cells, which are in close communication with each other, possibly also by EVs.

In this thesis, EVs isolated from the brain of mice subjected to transient Middle Cerebral Artery Occlusion (tMCAO, mouse model of stroke) and sham controls together with healthy mice, were analyzed at proteomic and transcriptomic levels. We reported that small brain-derived EVs (sBDEVs; ≤200nm) from healthy mice are enriched in ribosomal proteins, while large BDEVs (≥200nm) carry more proteins related to metabolic pathways. We confirmed the ribosomal protein enrichment also by re-analysing the proteome of BDEVs published in other studies using different isolation protocols. We saw that in steady-state conditions microglia are the main contributors to the BDEVs pool. 24h after stroke, astrocytes increase significantly their EVs release, possibly in relation to glial scar formation, neuronal survival, and/or microglial activation. Differently, there is a significant increase of oligodendrocyte-derived EVs 72h after stroke, a time when recovery processes such as remyelination start to take place. At a transcriptomic level, BDEVs isolated 72h after stroke carry mRNAs that are related mainly to inflammatory response and stress defense, but also to recovery processes. These mRNAs are mostly released by microglia. Moreover, we found that the most upregulated mRNAs after stroke are present in the EVs as full-length, and therefore potentially translatable in the recipient cells. How EVs reach the target cell and how they deliver their cargo are still unanswered questions. We saw that the presence of prion protein (PrP) on the surface of BDEVs influences their uptake by recipient cells, as EVs carrying PrP behaved differently to EVs lacking PrP. We demonstrated that PrP is significantly increased in BDEVs 24h after stroke/reperfusion, and we hypothesize a role for PrP in EVs' fusion with the plasma membrane of the recipient cells, which could influence stroke.

Lastly, we showed that activated human CD8T cells release EVs containing CD73, which has AMPase activity and activity and can degrade to adenosine the AMP resulting from ADP and ATP. This purinergic signaling cascade is fundamental for immune regulation during inflammation and ischemia, where the levels of extracellular ATP are critical and EVs seem pivotal for its degradation.

Extrazelluläre Vesikel (EV) sind von einer Lipiddoppelschicht umschlossene Strukturen, die entweder im endosomalen System gebildet (Exosomen) oder direkt von der Plasmamembran freigesetzt werden (Ektosomen/Mikrovesikel). EV gelten als wichtiges interzelluläres Kommunikationsmittel. Durch Aufnahme von Empfängerzellen kann ihre Ladung, bestehend aus Proteinen, Nukleinsäuren und Lipiden der Ursprungszelle, so weitergegeben werden. Da EV in Körperflüssigkeiten vorkommen, sind sie vielversprechende Biomarker verschiedener Erkrankungen. Sie sind an zahlreichen (patho-)physiologischen Prozessen im zentralen Nervensystem (ZNS) beteiligt. Um EV untersuchen zu können, müssen sie entweder aus Zellkulturüberständen oder Körperflüssigkeiten wie dem Liquor isoliert werden. Seit kurzem ist es außerdem möglich, EV aus Gehirnen aufzureinigen.

Ein ischämischer Schlaganfall tritt auf, wenn sich eine Hirnarterie verschließt und es durch den Mangel an Blutfluss folglich zu einer Minderversorgung mit Sauerstoff und Glukose im betroffenen Hirnareal kommt. Zellen im Zentrum des Infarktgebiets sterben sofort ab, während die Neuronen in der Umgebung (sog. Penumbra) abhängig von Signalen innerhalb der nächsten Stunden/Tagen, noch gerettet werden können. Die Pathophysiologie des Schlaganfalls umfasst sowohl hirnansässige als auch infiltrierende Zelltypen, die möglicherweise durch Übermittlung von Molekülen und Signalen via EV in enger Kommunikation miteinander stehen.

In dieser Arbeit wurden EV aus Gehirnen von Mäusen mit experimentellem Schlaganfall ("tMCAO"), zusammen mit EV aus Hirnen von Kontrolltieren auf proteomischer und transkriptomischer Ebene analysiert. Wir stellten fest, dass kleine hirnabgeleitete EV (sBDEVs; Durchmesser ≤200 nm) von gesunden Mäusen mit ribosomalen Proteinen angereichert sind, während große BDEVs (≥200 nm) in Abhängigkeit von bestimmten Stoffwechselwegen mehr Proteine enthalten. Wir bestätigten die Anreicherung ribosomaler Proteine auch durch Analyse des Proteoms von BDEV mit unterschiedlichen Isolierungsprotokollen anderer Studien. Es zeigte sich, dass Mikrogliazellen unter physiologischen Bedingungen den größten Beitrag zum gesamten BDEV-Pool leisten. 24 Stunden nach Schlaganfall im Mausmodell ist die EV Freisetzung aus Astrozyten signifikant erhöht, was mit der glialen Narbenbildung, dem neuronalen Überleben oder der Aktivierung von Mikroglia zusammenhängen könnte. Im Gegensatz dazu besteht ein signifikanter Anstieg der aus Oligodrendrozyten stammenden EV 72 Stunden nach Schlaganfall. Unsere Analysen ergaben, dass 72 Stunden nach Schlaganfall isolierte BDEV mRNA enthalten, die mit Entzündungsreaktionen, Stressabwehr und Genesungsprozessen in Zusammenhang stehen und hauptsächlich von Mikroglia stammen. Des Weiteren konnten wir zeigen, dass die am stärksten hochregulierten mRNAs nach Schlaganfall in den EV in voller Länge vorhanden sind und daher in Empfängerzellen translatierbar wären.

Wie EV die Zielzelle erreichen und wie (z.B. Fusion mit Plasmamembran oder endozytotische Aufnahme) sie ihre Ladung übertragen, ist noch unklar. Wir konnten zeigen, dass die Anwesenheit des Prionproteins (PrP) auf der Oberfläche von BDEV deren Aufnahme durch die Zielzellen deutlich beeinflusst. Da 24 Stunden nach Schlaganfall PrP auf BDEV signifikant erhöht ist, stellten wir die Hypothese auf, dass es eine wichtige modulatorische Rolle bei der Aufnahme durch, bzw. Fusion mit den Empfängerzellen und somit auch der Progredienz des Schlaganfalles spielt.

Schließlich haben wir gezeigt, dass aktivierte humane CD8 T-Zellen EV freisetzen, die das Protein CD73 enthalten, welches AMPase-Aktivität besitzt und ATP abbauen kann. Diese purinerge Signalkaskade ist von hoher Bedeutung für die Immunregulation bei Entzündungen und Ischämie, bei denen der Gehalt an extrazellulärem ATP kritisch ist und EV für dessen Abbau eine zentrale Rolle zu spielen scheinen.

9. Declaration of personal contribution to publications and manuscripts

Paper 1 (Original article, peer-reviewed and published)

<u>Title</u>: *Characterization of brain-derived extracellular vesicles reveals changes in cellular origin after stroke and enrichment of the prion protein with a potential role in cellular uptake*

<u>Authors</u>: **Santra Brenna**, Hermann C Altmeppen, Behnam Mohammadi, Björn Rissiek, Florence Schlink, Peter Ludewig, Christoph Krisp, Hartmut Schlüter, Antonio Virgilio Failla, Carola Schneider, Markus Glatzel, Berta Puig, Tim Magnus

<u>Date of publication, journal</u>: 27 August 2020, *Journal of Extracellular Vesicles*

<u>DOI</u>: 10.1080/20013078.2020.1809065

<u>IF</u>: 25.841 (2020)

<u>UKE Journal Score</u>: 57,26

<u>Contribution</u>: participated in the planning and scheduling of the project; performed all experiments (except mass spectrometry analysis and confocal and electron microscopy imaging); interpretation and analysis of data; correction and proof-reading of the manuscript.

Paper 2 (Original article, published online on bioRvix)

<u>Title</u>: *Multiplexed mRNA analysis of brain-derived extracellular vesicles upon experimental stroke in mice reveals increased mRNA content related to inflammation and recovery processes*

<u>Authors</u>: Annika Bub*, **Santra Brenna***, Malik Alawi, Paul Kügler, Yuqi Gui, Oliver Kretz, Hermann Altmeppen, Tim Magnus, Berta Puig
*equal contribution

<u>Date of publication</u>: 9 December 2021, bioRxiv

<u>DOI</u>: 10.1101/2021.12.09.471913

<u>Contribution</u>: participated in the planning and scheduling of the project; performed 50% of the experiments; interpretation and analysis of data; correction and proof-reading of the manuscript.

Paper 3 (Original article, peer-reviewed and published)

<u>Title</u>: *Brain-Derived Extracellular Vesicles in Health and Disease: A Methodological Perspective*

<u>Authors</u>: **Santra Brenna**, Christoph Krisp, Hermann Clemens Altmeppen, Tim Magnus, Berta Puig

<u>Date of publication, journal</u>: 29 January 2021, *International Journal of Molecular Sciences*

<u>DOI</u>: 10.3390/ijms22031365

Contribution: conception of the study; writing the manuscript; prepared figures; interpretation of data.

Paper 4 (Original article, peer-reviewed and published)

Title: *CD73-mediated adenosine production by CD8 T cell-derived extracellular vesicles constitutes an intrinsic mechanism of immune suppression*

Authors: Enja Schneider, Riekje Winzer, Anne Rissiek, Isabell Ricklefs, Catherine Meyer-Schwesinger, Franz L. Ricklefs, Andreas Bauche, Jochen Behrends, Rudolph Reimer, **Santra Brenna**, Hauke Wasielewski, Melchior Lauten, Björn Rissiek, Berta Puig, Filippo Cortesi, Tim Magnus, Ralf Fliegert, Christa E. Müller, Nicola Gagliani, Eva Tolosa

Contribution: performed experiments (western blot); interpretation and analysis data (western blot); proof-reading of the manuscript.

10. Acknowledgements

11. Resume

Lebenslauf wurde aus datenschutzrechtlichen Gründen entfernt.

12. Eidesstattliche Versicherung

Ich versichere ausdrücklich, dass ich die Arbeit selbständig und ohne fremde Hilfe verfasst, andere als die von mir angegebenen Quellen und Hilfsmittel nicht benutzt und die aus den benutzten Werken wörtlich oder inhaltlich entnommenen Stellen einzeln nach Ausgabe (Auflage und Jahr des Erscheinens), Band und Seite des benutzten Werkes kenntlich gemacht habe.

Ferner versichere ich, dass ich die Dissertation bisher nicht einem Fachvertreter an einer anderen Hochschule zur Überprüfung vorgelegt oder mich anderweitig um Zulassung zur Promotion beworben habe.

Ich erkläre mich einverstanden, dass meine Dissertation vom Dekanat der Medizinischen Fakultät mit einer gängigen Software zur Erkennung von Plagiaten überprüft werden kann.

Unterschrift: ....